DISSERTATION

"BIOFILMOMICS": FUNCTIONAL PROTEIN EXPRESSION IN BIOFILM BIOTECHNOLOGIES REVEALED BY QUANTITATIVE PROTEOMICS

Submitted by

Jeremy Chignell

Department of Chemical and Biological Engineering

In partial fulfillment of the requirements

For the degree of Doctor of Philosophy

Colorado State University

Fort Collins, Colorado

Spring 2020

Doctoral Committee:

Advisor: Kenneth Reardon
Co-Advisor: Susan De Long

Christie Peebles
Sybil Sharvelle

ABSTRACT

"BIOFILMOMICS": FUNCTIONAL PROTEIN EXPRESSION IN BIOFILM BIOTECHNOLOGIES REVEALED BY QUANTITATIVE PROTEOMICS

Microbial biotechnologies that utilize biofilms often exhibit superior performance compared with planktonic systems. Many details of biofilm metabolism that drive those improvements in performance remain unclear. Only recently have molecular tools emerged that can provide a holistic picture of life in a complex biosystem like a biofilm for the purposes of answering questions on a system level. The purpose of this work was to address four fundamental questions about protein expression in biofilms: what kind of protein expression is distinctive to biofilms? Which biofilm proteins are associated with a function of interest? How does co-culture with another species affect biofilm-related protein expression? When during multi-species biofilm development does a function of interest emerge and who in the community is responsible? Label-free quantitative proteomics was used in conjunction with physiological experimentation to address these four questions.

In the first study we found that *L. delbrueckii lactis* protein expression in flow-cell biofilms was 31% more diverse than in planktonic cultures, and proteins related to catalytic activity were significantly increased in biofilms at the expense of proteins for cell motility and replication. Roles for riboflavin and fatty acid metabolism suggested modulations in redox functions and membrane turnover during life in a biofilm. The second study compared protein expression by *S. onedensis* MR-1 in electricity-generating biofilms with that in aerobic biofilms from the same microbial fuel cell reactor. Three novel proteins associated with electricity

generation were identified, in addition to proteomic evidence of aerobic metabolism by anode biofilm cells. The latter result was shown to be consistent with kinetics of oxygen depletion and bulk cell growth in the MFC, suggesting operational conditions to reduce this bulk cell growth and thereby reduce fouling of the cathode and improve overall Coulombic efficiency of the single-chamber MFC system. In the third study, it was discovered through proteomic and physiological experiments that a virulent phenotype associated with biofilm formation was triggered in *P. putida* when co-cultured with *B. atrophaeus*. Dramatic shifts in protein expression at the initial trigger point of virulent biofilm formation by *P. putida* are described. Finally, a comparison of the meta-proteomes of microbial fuel cell biofilms at different stages of development indicated that proteins in metabolic pathways for carbon storage and competitive inhibition are differentially expressed when the biofilm becomes electrochemically active. Meta-proteomics and 16S rRNA gene sequencing agreed that it is possible for a microbial fuel cell community to maintain high diversity (and therefore potentially higher resilience) while generating electricity at levels comparable to a MFC community dominated by *Geobacter*. Each of these chapters was prepared as an independent manuscript, though the themes were integrated by the overall theme of quantifying differential protein expression in biofilms in order to reveal new details about their development and functionality.

Since the performance of many engineered biosystems—including those that employ biofilms—often can be controlled adequately at an operational level, an attitude persists that any additional molecular investigation is superfluous. The work presented here provides evidence for the opposite viewpoint: a rich understanding of the molecular mechanisms behind biofilm functionality can inform strategies for continuous system improvement and suggest new capabilities and biotechnological applications of biofilms.

ACKNOWLEDGMENTS

I thank my committee members—Dr. Ken Reardon, Dr. Susan De Long, Dr. Christie Peebles, and Dr. Sybil Sharvelle –for their feedback and encouragement. Throughout several detours and detailed investigations of rabbit holes, my co-advisors Ken Reardon and Susan DeLong consistently provided valuable guidance and support without steering too much.

Thanks to members of both the Reardon and De Long research lab groups, including Mona Mirsiaghi, Xingfeng Huang, Justin Sweeley, Tara Schumacher, Mario Aguilar, Scott Fulbright, Brian Heinze and Zeyu Sun. Special thanks to Dr. Seijin Park for his mentorship in LC-MS/MS technology. Thanks to Christin Schlegel and Prof. Roland Ulber for facilitating the collaborative effort that resulted in our *Lactobacillus* work. I am also grateful to members of other lab groups within CBE, including Steve Albers, Ian Cheah, Jiayi Sun and Lucas Johnson for conversation and friendship. Thanks to Kirsten Davis for her contributions to microbial fuel cell work as part of her undergraduate honors project. Special thanks to Barb Gibson for her support and friendship as part of the Multidisciplinary Approaches to Sustainable Bioenergy NSF IGERT program. Thanks to Dr. Ann Hess for her excellent course on data analysis for omics as well as her in-person advice on statistical analysis.

Thanks to the funding programs that provided support during my research program, including the NSF-IGERT program, the Jud and Pat Harper Endowment in the CSU Department of Chemical and Biological Engineering, the Colorado Center for Biorefining and Bioproducts, and the Sustainable Bioenergy Development Center. Thanks also to the CSU Biology Department for taking a chance on hiring a graduate student in engineering to teach biology labs.

Thanks to my family for their questions and support throughout my graduate school experience. Thanks to my mother-in-law for her interest and enthusiasm. Most of all, I thank my wife and sons for their patience and support throughout late nights, stress, disappointments and successes.

TABLE OF CONTENTS

CHAPTER 1: BACKGROUND AND RESEARCH OBJECTIVES

1.1 Biofilms: the ancient microbial preference

In nature, unlike in lab experiments, microbes rarely live as homogenously-dispersed cells in a planktonic culture. Rather, when given the opportunity, most microbes will attach to surfaces and self-aggregate into non-homogenous collections. These aggregations are encased in a secreted extracellular matrix (ECM) consisting of extracellular polysaccharide (EPS), extracellular nucleic acids (eDNA and eRNA) and proteins [Flemming et al. 2007]. The resulting structure, a biofilm, confers several advantages to bacterial cells compared with a planktonic mode of life. First, cells fixed in a biofilm need not expend energy to acquire nutrients, since nutrients diffuse passively to them through the biofilm. Second, biofilms offer protection from toxic or antimicrobial compounds in the environment, thereby increasing the survival of bacterial cells in the face of stresses such as desiccation, starvation, or pH fluctuations. Furthermore, cells grow to higher densities in biofilms, compared with planktonic cultures; the increased proximity of neighbor cells facilitates exchange of metabolites and horizontal gene transfer [Costerton et al. 1999]. Finally, some sessile consortia of bacteria are able to perform complex or specialized tasks comparable to multi-cellular organisms [Nikolaev and Plakunov 2007]. Biofilms in fact represent the oldest form of bacterial life in nature, and perhaps the oldest form of life on Earth [Karunakaran et al. 2011]. Reports on ancient biofilms suggests mechanisms by which biofilms allowed living cells to transition from aquatic environments to colonize terrestrial environments [Karunakaran et al. 2011.].

Despite the importance of a biofilm mode of life, the majority of laboratory experimentation on bacteria has focused on planktonic cultures. Biofilms first were reported more than 80 years ago [Henrici 1933; Zobell 1937], but their pervasiveness in the natural environment was described only 40 years ago [Geesey et al. 1977; Marshall et al. 1971]. While the phenomenon of bacterial aggregation in liquid cultures has been recognized for decades, notably in the context of bacterial flocculation during wastewater treatment or fermentation [Biggs and Lant 2000; Bauer et al. 2010], tools have become available only recently that allow detailed investigation of the structure of bacterial biofilms and the interactions between cells encased in them [Vanwonterghem et al. 2014].

The development of biofilms has been described in terms of successive stages observed in model species such as *P. aeruginosa*. These stages comprise (i) reversible attachment of early colonizers to a surface; (ii) irreversible attachment; (iii) maturation; (iv) detachment [Sauer et al. 2002]. Each of these stages of development entails unique physiochemical and molecular mechanisms [Dunne 2002]. One important physiochemical mechanism during the attachment stages is the assembly of ECM itself. Bacterial production of ECM material during adhesion is a metabolically expensive process, suggesting its importance during initial adhesion and aggregation. While comprising >90 wt% of the biofilm, ECM itself is poorly-characterized, and the interactions between the different components of ECM that result in a stable matrix remain undescribed [Branda et al. 2005; Stoodley et al. 2002]. Other studies have investigated physiochemical features of bacterial adhesion by using physical models for adhesion of colloidal particles to surfaces, emphasizing the effects of electrostatic

interactions and van der Waal's forces between the colloid and the surface during the attachment phase [Bos et al. 1999]. Earlier studies described bacterial adhesion in terms of the properties of the surface, such as hydrophobicity [Busscher and Weerkamp 1987], wettability [Pedersen et al. 1986], and surface charge [Van Loosdrecht et al. 1987]. Notably, these types of investigations treat bacteria as inert particles, when, in fact, bacteria conduct rapid and global molecular changes in protein and gene expression during all stages of biofilm development, the details of which have just started to be investigated using an array of powerful molecular tools [Khemiri et al. 2015; Karunakaran et al. 2011; Allegrucci et al. 2006; Vilain et al. 2004].

1.2 Biofilms in medical research

In addition to basic microbiological research, biofilms hold considerable interest for medical science and engineering. Since the ECM slows or prevents the diffusion of antibiotics or chemical toxins to bacterial cells in the matrix, biofilms on the surfaces of medical instruments such as catheters can allow pathogens to persist in a hospital environment, despite standard sterilization techniques [Poole et al. 2002]. Moreover, for many pathogenic bacterial species, a biofilm mode of life often is associated with active virulence [Seth et al. 2012; Phillips et al. 2012; Cotter et al. 2007]. The most well-studied example of this association is the development of *P. aeruginosa* biofilms in the lungs of cystic fibrosis patients. *P. aeruginosa* may persist in the lung environment for years without displaying a virulent phenotype; certain conditions such as iron depletion can trigger the formation of biofilms that eventually can obstruct the breathing of patients with fatal consequences [Kim et al. 2003]. Metabolic details behind this kind of shift to a

virulent phenotype have not been described in depth for non-model organisms or microbial consortia.

The medical relevance of bacterial biofilms also has been investigated in the context of chronic wound infections and oral bacterial communities. Formation of biofilms in wounds can result in chronic, debilitating infections that allow bacteria to resist immune responses and eventually to enter the bloodstream or colonize tissues and organs. Several studies have investigated the dynamics of interactions between species in model wound polyculture biofilms, in order to determine how life in an infectious community progresses and matures [Dalton et al. 2011; Dowd et al. 2008]. Likewise, the ecology of oral biofilm communities is relatively well-described: fermentative species such as *Streptococcus mutans* convert sucrose to dextran-based EPS. They ferment a range of carbohydrates to organic acids, generating localized acidic conditions that dissolve mineralized tooth enamel, accelerating tooth decay. The biofilm produced on teeth and gums by these species—"plaque"— allow acidic microniches to persist, despite chemical and mechanical treatments [Pitts et al. 2017].

1.3 Engineering applications of biofilms

In engineering contexts, biofilms have both negative and positive associations. For decades engineers have investigated biofilms in pipes [Donlan et al. 1994], in storage tanks [Characklis et al. 1981], on surfaces of machinery used for food processing [Chmielewski et al. 2003], on ship hulls [Tribou et al. 2010], and membranes for water treatment [Herzberg et al. 2007]. Most of this research concerns prevention of biofouling during equipment use; the focus of many of these studies has been to predictively describe the process of initial attachment to the surface [Busscher et al. 1995] or to test

the capability of surface modifications to prevent or slow bacterial attachment [Klueh et al. 2000]. Much of the available information on the effects of flow regimes on bacterial interactions with surfaces is derived from this type of research [Vrouwenvelder et al. 2010]. In addition to prevention of biofilms, many studies have investigated the effectiveness of different treatments to eradicate established biofilms from surfaces, e.g., chemical (e.g., detergents combined with increased pH or chlorination) or biochemical (enzymatic) treatments to dissolve EPS from surfaces and expose bacterial cells [Chen et al. 2000].

Biofilms also have a positive implication for engineers who use them to improve performance of bioreactor systems. Many studies have documented increases in productivity, conversion rates, and titers with fermentation reactor systems that utilize immobilized cells, compared with planktonic fermentations [Pflugmacher and Gottschalk 1994; Grote et al. 1980]. Self-produced biofilms have been used most extensively in biological wastewater treatment; mixed culture biofilm reactors have demonstrated improved specific rates of efficiency for the removal of organic [Li et al. 2003] and inorganic compounds such as nitrate [Villahermosa et al. 2016], sulfur [Huang et al. 2018], and heavy metal pollutants [Azizi et al. 2016]. Furthermore, biofilm wastewater microbial communities often display improved functional stability in response to perturbations, compared to planktonic cultures [Inaba et al. 2018; Wang et al. 2010]. For example, methanogenic communities, known for their high sensitivity to oxygen intrusion or substrate inhibition, generally tolerate these sorts of perturbations in biofilms with fewer catastrophic failures, compared with planktonic cultures [Gagliano et al. 2017; Brileya et al. 2014; Vanwonterghem et al. 2014].

In general, the improved performance of engineered systems using biofilms is attributed to physical features of the biofilm itself, or to the changes in physiology that occur in cells after immobilization in the biofilm. Physical features of a biofilm, such as thickness, homogeneity and cell density, can affect rates of mass transport and reaction [Beyenal and Lewandowski 2005], exposure to inhibitors [Stewart and Costerton 2001] and substrate inhibition [Jih and Huang 1994]. Moreover, from a process perspective, the physical immobilization of cells confers considerable advantages compared to continuous stirred tank reactor (CSTR) models. For batch systems, a new batch can be initiated in a biofilm reactor without consideration of preparing a new inoculum or re-starting the reactor, a benefit when using fastidious or slow-growing species for enrichment [Fernandez et al. 2008]. For continuous systems, hydraulic retention time for a biofilm reactor may be decreased to a low level with less concern for washing out cells from the reactor [Qureshi et al. 2005]. Moreover, cell attachment to a surface makes possible a range of alternative reactor designs that can increase productivity [McQuarrie and Boltz 2011].

In addition to advantages conferred by physical features of biofilms, immobilization confers physiological benefits to cells in biofilms. As noted above (Section 1.1), the opportunity to receive nutrients and other materials passively from the environment allows for re-direction of energy that would have been spent on motility to primary metabolic functions [Guttenplan and Kearns 2013]. Additional energy savings are derived from a decrease in cell replication rates in biofilms as compared with planktonic environments [Watnick and Kolter 2000]. Finally, the higher cell density in biofilms can increase the rate of conversion per unit bioreactor volume [Qureshi et al.

2005]. In mixed species biofilms, sharing of metabolites or functional genes in horizontal gene transfer between cells in close proximity can improve functionality or resilience of biofilm cells [Kreft 2004; Costerton et al. 1999]. While the metabolic requirements for successful adhesion and biofilm formation may entail slower initial start-up times, especially for anaerobic biofilm systems, once a mature biofilm is developed, process improvements may be achieved [Escudie et al. 2011].

1.4 Bioelectrochemical systems: a "current" biofilm application

Bioelectrochemical systems (BESs) are an emerging biofilm technology with an expanding array of applications, including wastewater treatment, bioenergy generation, and bioproduct synthesis. While many BES designs exist [Escapa et al. 2016; Logan et al. 2015], a defining feature of the BES platform is the formation of an electrochemically active bacterial biofilm on an electrode that can use the electrode as an electron donor or acceptor. In the most well-characterized BES, a microbial fuel cell (MFC), bacteria attach to the surface of an insoluble anode—constructed of conductive material such as carbon cloth, carbon paper, or metal—and utilize the anode as an electron acceptor in anaerobic respiration [Logan et al. 2006]. Organic materials in the bulk solution of the MFC reactor are degraded by biofilm bacteria and the electrons are transferred to the anode surface. The electrons travel through a circuit to a cathode, at which they reduce a chemical electron acceptor such as ferricyanide or oxygen. As the electrons travel through the circuit, they create an electrical current that may be used to power a device or for energy storage. The electrochemically active biofilms on the anode may be comprised of mixed cultures or pure cultures of bacteria; in BES systems relevant for functions such as wastewater treatment, endogenous organisms in the influent colonize

the electrode [Zhi et al. 2014; Logan 2009; Logan and Regan 2006]. Certain well-characterized, model bacterial species—e.g., species in genera *Shewanella* and *Geobacter*—have emerged as model species for BES systems, due to their high capacity for electricity generation and their well-described genetic systems for anaerobic respiration [Song et al. 2016; Ueki et al. 2016]. The mechanisms responsible for transfer of electrons from bacterial cells to the electrode surface in MFCs have been described in some detail for these model species. The general mechanisms of extracellular electron transfer include electron shuttling with soluble redox compounds [von Canstein et al. 2008; Marsili et al. 2008], direct electron transfer via outer membrane cytochrome proteins [Inoue et al. 2011; Shi et al. 2009], and longer-distance electron transfer through conductive pilin protein structures called "nanowires" [Gorby et al. 2006]. Recent studies report direct interspecies electron transfer between cells or to the biofilm itself, suggesting that the entire anode biofilm matrix is a conductive entity [Lovley 2017].

Much of the research into the mechanisms of electron transfer by model species in MFCs aims toward improving power generation or efficiencies. More recently, mechanisms of electron transfer have gained new interest as a critical step in microbial electrosynthesis. This application of BESs is like a MFC in reverse: electrons are fed from a solar cell or other electrical source to bacteria on an electrode that have been genetically modified to combine those electrons with CO_2 to produce useful organic compounds [Rabaey and Rozendal 2010; Nevin et al. 2010]. This process potentially offers a method to produce specialty compounds directly from solar energy, bypassing photosythetic biosynthesis of sugars. More detailed information behind the mechanisms

of electron transfer between bacteria and electrodes will enable improvements of BES functionality for electrobiosynthesis or other disruptive BES applications.

The use of mixed cultures in BES systems largely has targeted energy recovery during wastewater treatment. While power generation and efficiencies have improved by orders of magnitude due to optimization of reactor designs and materials [Logan et al. 2015; Logan 2010], limitations in maximum power densities suggest that new approaches are required for further scale-up. The potential for improvements in performance through design of the composition and metabolic capabilities of the mixed culture consortium remains largely unexplored. Many studies have described the community composition of MFC biofilms under different operational conditions, e.g., different carbon sources, but few studies have described the development of electron transfer capabilities by the community as a whole. Generally, descriptions of MFC communities have relied on 16S rRNA gene-dependent sequencing methods [Paitier et al. 2017; Zhi et al. 2014]. These studies have consistently suggested that, for many carbon sources, the dominant current-generating species in the consortium is *Geobacter*; for several carbon sources, however, *Geobacter* is not dominant in the community, suggesting that under certain conditions other species may outcompete *Geobacter*, despite its superior electron-transfer capabilities [Pant et al. 2010]. Interestingly, *Shewanella* species rarely are found as major components of mature, mixed culture MFC consortia [Pant et al. 2010], suggesting that they are outcompeted by *Geobacter* or other species in the mixed culture. The fact that mixed culture consortia are not necessarily dominated by well-characterized model species opens the door for research into mechanisms of electron transfer by non-model species or by microbial consortia as a whole. Since non-model species and

environmental consortia often lack sufficient genome sequence information (and annotation) and are under-described physiologically, traditional molecular tools to quantify gene or protein expression may be inadequate for this sort of research. Therefore, for these sorts of systems an experimental methodology is required that can take into account the totality of available sequence and annotation information and allow functional inferences from sequence or structural homology. As detailed below (Section 1.3), a proteomics approach offers such a methodology.

1.5 Challenges and limitations in biofilm research

1.5.1 Biomass limitations

The study of biofilms poses unique methodological challenges. First, in contrast to planktonic cultures that scale relatively easily, biofilm samples often are biomass-limited, especially thin biofilms, such as those in early stages of development or those enriched under anaerobic conditions. Biomass limitation is especially relevant for studies investigating quantitative expression of proteins in a biofilm, since, unlike DNA, proteins cannot be amplified. While mRNA may be amplified through RT-qPCR while obtaining quantitative information, the extraction and purification of mRNA from biofilms is notoriously difficult and raises questions about the representational accuracy of the sample [Cury and Koo 2007]. Moreover, in contrast to planktonic cultures in which sample sizes may be increased simply by growing a more dense culture or by scaling up the volume of the culture, increasing biofilm biomass may entail changes in structure, maturity, composition, or performance of the biofilm system. For example, in the case of MFC biofilms, performance suffers by simply scaling up the size of the anode, due to resistance across the reactor system and limitations on rates of electron transfer to the

anode surface [Fan et al. 2008; Logan et al. 2010; Janicek et al. 2014]. Furthermore, loss of biomass during sampling or due to incomplete separation from ECM will have a more pronounced effect on low-abundance molecules than on high-abundance molecules within the sample [Denef et al. 2010; Podar et al. 2007]. These methodological challenges decrease reproducibility of results, thereby complicating statistical analysis and decreasing confidence in conclusions.

1.5.2 Spatial Heterogeneity

A second difficulty unique to the investigation of biofilms concerns their defining feature: heterogeneity in spatial organization. While planktonic cultures in controlled experiments usually are considered well-mixed, biofilms are spatially complex in all three dimensions in ways that contribute to their unique metabolic features. A degree of spatial heterogeneity exists within the biofilm matrix due to interactions with the surface and dynamic porosity and multicellular structures that develop stochastically in response to changing flow regimes, chemical gradients, or cell viability [Tolker-Nielsen and Molin 2000]. This spatial complexity is especially pronounced in mixed culture biofilms, in which species composition and distribution within the biofilm affect chemical characteristics within the biofilm that then recursively affect species composition and distribution over time [Hansen et al. 2007]. Due to this spatial complexity, different cells in a biofilm interact with the surface, other cells, and their micro-environments in different ways. Understanding these dynamics requires analysis of functional gene or protein expression in addition to simple species identification.

Finally, heterogeneity of spatial structure results in a lack of experimental reproducibility from one biofilm to another, especially for multi-species biofilms, despite

rigorous cultivation strategies [Lewandowski et al. 2004; Beyenal et al. 2004; Jackson et al. 2001]. Complicating the experimental situation further, sampling a biofilm requires at least partial destruction of the biofilm that permanently alters the structure of the remaining biofilm. For biomass-limited biofilms, complete removal of the biofilm may be necessary in order to obtain enough sample for analysis, leaving little or no option for multiple samples from the same biofilm in, for example, a time-course study. Therefore, "replicate" biofilms must be cultivated, adding to the lack of reproducibility.

1.6 The potential of proteomics in biofilm research

1.6.1 "Biofilmomics" : a new approach to study an ancient form of life

The past two decades have seen a revolution in methodologies for investigating biological systems. In contrast to previous years in which gene and protein expression was quantified by methods that were restricted to a limited number of genes and proteins at a given time, the advent of omics methods allows for identification of thousands of transcripts or proteins in a single experiment [Gutleben et al. 2017; Franzosa et al. 2015]. Computational methods associating sequences with functional molecules allow for categorization and mapping not just of individual molecules but of entire metabolic pathways, according to curated databases such as the Gene Ontology (GO) project (www.geneontology.org) and KEGG (http://www.genome.jp/kegg/). By quantifying differential expression of functional molecules, particular biomarkers of a biological response may be identified and associated with a treatment condition. Conventional tools such as RT-qPCR, Western blot, or physiological growth studies may be used to corroborate conclusions and investigate new hypotheses generated from -omics results.

Genomics methods that describe and quantify the total set of protein-encoding genes are critical for annotation of genomes. Since genomics describes the DNA of the system, however, genomics studies are restricted to describing the genetic potential of the system, rather than quantifying dynamic responses of the cell. In contrast, transcriptomics approaches such as microarrays and RNA-seq attempt to determine functional responses to treatments by obtaining a "snapshot" of mRNA transcript abundance at a certain time. Microarrays depend on a well-curated genome to generate probes for hybridization, while in RNA-seq all transcript molecules are sequenced and their association with genes is computationally determined [Wang et al. 2009]. Differentially-expressed genes are identified according to different measures of abundance of transcripts associated with those genes [Garber et al. 2011]. Both transcriptomics methods suffer from the fact that mRNA transcript abundance does not necessarily correlate with abundance of proteins, the functional products of gene expression [Rogers et al. 2008]. Additionally, post-translational modifications of proteins, important for determining their ultimate function in the cell, are not detectable by a transcriptomics approach [Grangeasse et al. 2015].

1.6.2 Outlines of a Label-Free Quantitative Proteomics Workflow

In contrast to quantifying mRNA transcripts, quantitative proteomics identifies and quantifies proteins, the functional molecules responsible for an observable phenotype. Since there is no sequencing technology for proteins similar to that used for nucleic acids, a mass spectrometer (MS) is utilized. In a general proteomics workflow, proteins are extracted from a sample and cleaned up by some kind of precipitation (e.g., acetone) and/or by SDS-PAGE, which also serves to separate proteins by mass into

fractions. Proteins may also be separated by isoelectric point and mass by 2-D gel electrophoresis [Gygi and Aebersold 2000]. Proteins then are denatured, cysteine-alkylated, and digested with trypsin and/or another enzyme. The resulting mixture of peptides is separated by liquid chromatography (LC) at extremely low flow rates (nanoLC) prior to tandem mass spectrometry, using 1D (hydrophobicity/hydrophilicity) or 2D (e.g., cation exchange followed by reverse phase) separation [Zhang et al. 2010].

As peptides elute from the LC column, they are introduced to the MS through an inlet. Peptides in the sample are converted to ions (usually positive ions in proteomics) by the ionization source. Samples are most commonly ionized by protonation, in which a proton converts the molecule to a positively-charged ion. In electrospray ionization (ESI), an injection or infusion inlet generates a Taylor cone at the tip of the injection/infusion inlet needle that produces a plume containing a fine aerosol of the analyte and the aqueous-organic solvent. Droplet size is decreased by increasing the conductivity of the solution by adding formic acid, which also provides a source of protons for the ionization. The solvent evaporates by heating until the charged droplet becomes unstable and splits into smaller, more stable droplets. This process continues until charged ions emerge from the solvent droplets. Electrosprays operated at lower flow rates generally result in smaller droplets in the initial aerosol; chromatography setups that allow for nano-scale flow rates therefore generally have greater ionization efficiencies. Both ESI and matrix-assisted laser desorption/ionization (MALDI), another ionization technique, are “soft” ionization methods that ionize peptides with minimal fragmentation. The resulting ions have a hydrogen cation added $[M+H]^+$. Multiply-charged ions $[M + nH]^{n+}$ often are observed, which may complicate interpretation of the

spectrum, since a peak for an ion of a certain mass with multiple charges will not be distinguishable on the spectrum from a peak for an ion with a lower mass. The charge state and location of charge is driven by the basicity of residues in the peptide: positive charge is carried on the peptide N-terminus, on lysine side-chain amino groups, or on arginine guanidyl groups. For peptides that are longer than five amino acids, chelation of a proton by amide carbonyl functional groups can compete with the N-terminus for the location of charge. [Vidova and Spacil 2017; Liu et al. 2011; Huang et al. 2005]

Peptide ions are propelled to a mass analyzer that separates them according to mass/charge. Most mass analyzers achieve this separation by applying an electrical field. Only charged particles respond to an electric field, which is the reason why peptides are ionized prior to entering the mass analyzer. Several types of mass analyzer are available, including quadrupole, time-of-flight, ion trap, Fourier transform ion cyclotron resonance and Orbitrap, as well as hybrids of these types. A quadrupole is a group of four parallel metal rods across which a radio frequency voltage is applied, which allows for the passage only of ions with a mass/charge that is selected by the voltage applied. In the case of a triple quadrupole, the first quadrupole acts as a selective "filter" for ions with a chosen mass/charge. In a second quadrupole, the selected ions ("precursor" ions) are fragmented by collision-induced dissociation with an inert gas to "product" ions. The third quadrupole then can scan across the mass/charge range to allow different product ions to pass through to the detector. For the first and third quadrupoles, the "filtering" occurs by selectively separating different ions according to mass/charge. In the case of time-of-flight mass analyzers, the separation is effected by first accelerating all ions to the same kinetic energy (KE); the velocity of each ion is calculated using the known

length of the flight path. The equation KE= 1/2*m*v^2 allows calculation of each ion's mass (assuming a charge of +1). The detector then determines the intensity of each ion (considered correlated to the abundance of that ion). Alternatively, an ion trap mass analyzer "filters" ions by trapping the ions in oscillating electric fields. Ions are selectively released from the ion trap by changing the electric field such that ions of a chosen mass/charge become unstable and are released to the collision cell (MS/MS) or to the detector. In the case of a linear ion trap, a set of quadrupole rods are used as part of the ion trap in the radial direction. An Orbitrap is a hybrid mass analyzer that traps ions in a spindle-like electrode complex, in which the attraction of ions to an inner electrode on the axis of the spindle is offset by centrifugal forces. The ions also move axially along the spindle in a way that can be described mathematically by harmonic motion and is independent of all ion properties except mass/charge. By using Fourier transform methods to interpret the harmonic oscillation of ions in the Orbitrap, the mass/charge of the ions can be determined. [Haag 2016; Eliuk and Makarov 2015; Yates et al. 2009].

Finally, ions are selectively allowed to proceed to a detector that records the current induced when an ion passes by or hits a surface. Since the mass analyzer "filters" the ions that proceed to the detector based on mass/charge, the result is a mass spectrum of current (converted to a unit-less intensity value) as a function of mass/charge. Since the current produced by an ion is very small, usually an electron multiplier is required to generate a quantifiable electrical signal [Aebersold and Mann 2016; Yates et al. 2009].

In a proteomics pipeline, acquisition of tandem mass spectra is just the first step in identification of sample proteins (Figure 1).

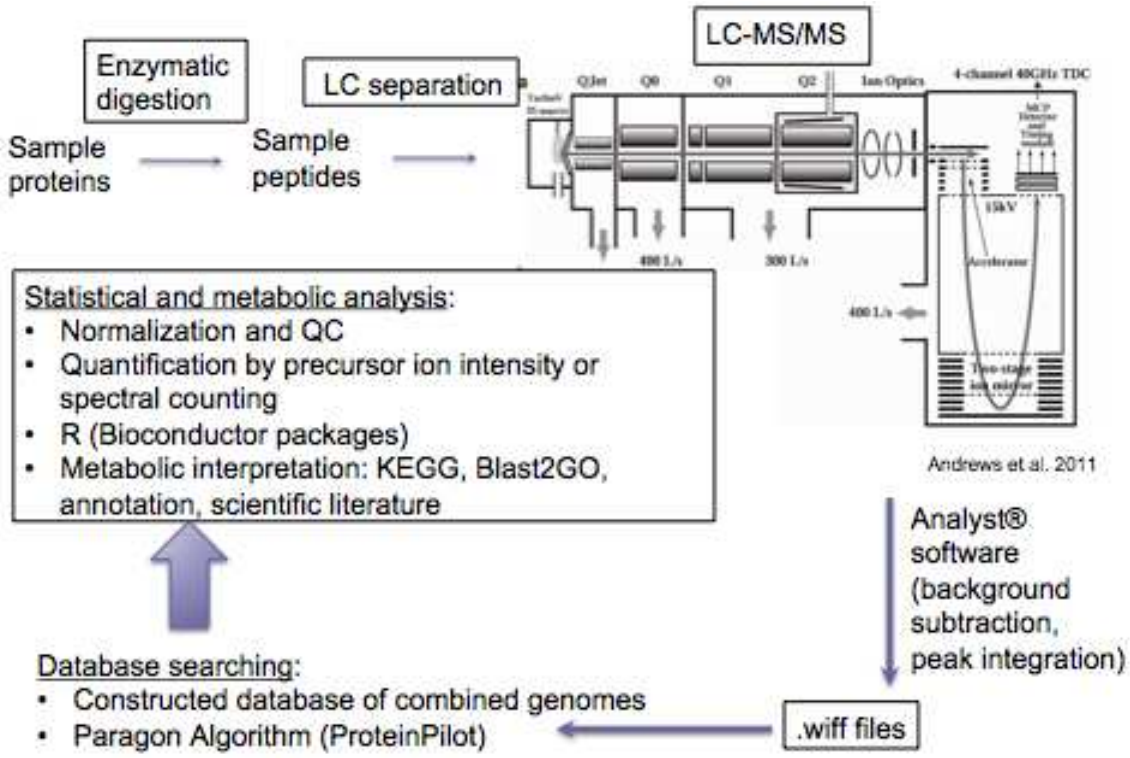

Figure 1: General workflow for label-free proteomics analysis with LC-MS/MS. Image of ABSciex TripleTOF LC-MS/MS is taken from Andrews et al. 2011.

After mass spectra are acquired, they are matched with peptide sequences by a peptide spectrum matching (PSM) algorithm. In PSM algorithms, observed tandem mass spectra are compared with a set of expected tandem mass spectra computed from an *in silico* enzymatic digest of all protein sequences given in a .fasta database. Best PSMs are determined according to some accuracy parameter that varies between different software programs. For example, in ProteinPilot—a proprietary software program available from ABSciex—the accuracy parameter of a PSM is an "Unused Score," which refers to the percentage of available tandem mass spectra explained by the given PSM that is not already explained by a higher ranking PSM. Therefore, in the case that a mass spectrum

is matched to multiple possible peptide sequences, the PSM with the highest Unused Score is the most rational choice, in order to avoid counting spectra as evidence for multiple peptides. An alternative method to PSM algorithms for identifying peptides is to "sequence" the peptide directly from the acquired tandem mass spectrum. In this *de novo* approach, the product ions that result from collision-induced dissociation of a peptide molecule at the second MS step are compiled and the original peptide sequence is pieced back together from the product ion fragments. The result is a list of all peptide sequences in the sample determined directly from the peptide molecules themselves, rather than through a PSM algorithm dependent upon pattern matching of expected and observed mass spectra. *De novo* sequencing is similar to conventional small-molecule tandem mass spectrometry in the sense that each amino acid in a product ion is identified individually in order to reconstruct the peptide sequence [Tran et al. 2017]. While *de novo* sequencing provides confident sequence identification, the process is more time-consuming than PSM algorithms and may result in loss of information due to errors or ambiguity in compilation of product ion mass spectra [Medzihradszky and Chalkley 2015].

In addition to matching spectra to peptides, peptides must be matched to proteins. Most proteomics software programs have an algorithm (often proprietary) for matching peptide sequences from tryptic or other enzymatic digestion to the proteins from which they are derived. These algorithms provide a score describing the accuracy of the match, e.g., Xcorr [Klammer et al. 2009]. After matching peptides to proteins, the end result is a list of spectra associated with each protein that is identified in the sample.

Quantification of protein abundance in a sample may be conducted in many ways. Concerns regarding the accuracy of measuring protein abundance by spot intensity in 2-DE gels were overcome by the emergence of sensitive techniques for isotope labeling of proteins or peptides during mass spectrometry. These labeling techniques included labeling proteins isotopically with isotope-coded affinity tags [ICAT], stable isotope labeling [SILAC], or $H_2{}^{18}O$ isotope exchange, and labeling peptides with isobaric tags for relative and absolute quantitation [iTRAQ]. In these labeling methods, the m/z of peptides labeled with different isotopes are easily distinguished from each other and from non-labeled peptides, allowing for simultaneous quantification of several conditions in a single sample of mixed peptides labeled with different isotopes [Rauniyar and Yates 2014]. While often highly precise for quantitation, labeling methods have several drawbacks including a restricted dynamic range, between-run variation in intensity signals, incomplete incorporation of labels into proteins or peptides, and high reagent costs [Rauniyar and Yates 2014]. Over the past 5-6 years, effort in the field has shifted to label-free quantitation methods. In label-free quantitation, the abundance of a protein in a sample may be correlated with either (i) integrated peak area intensities of a subset of ions associated with that protein that are measured either during the LC-MS step (precursor ions) or the LC-MS/MS step (precursor and peptide ions) [Simburger et al. 2016; Shalit et al. 2015; Griffin et al. 2010; Asara et al. 2008] or (ii) the total number of spectra in the sample that are associated with that protein [Lundgren et al. 2010]. Each label-free quantitation method has its advantages: quantitation by ion intensity may be more precise and sensitive than spectral counting, while spectral counting maintains accuracy over a greater dynamic range of peptides and may be more appropriate for large

datasets to avoid computational challenges of ion peak integration [Nahnsen et al. 2012; Milac et al. 2012].

Statistical analysis of label-free proteomics data entails unique challenges regarding data handling, transformation, normalization, and comparative testing between conditions. As in transcriptomics, proteomics datasets may be extremely large and complex, even after parsing raw LC-MS/MS data and association of spectra with peptides and proteins, making traditional spreadsheet analysis cumbersome. Moreover, pre-processing methods for either intensity-based or spectral counting-based proteomics data are not clear *a priori*. Since each peptide precursor ion intensity is a unitless, continuous value, algorithms developed over the past 20 years for statistical analysis of microarray intensity data or transcript counts may be appropriated in some cases for proteomics quantitation [Roxas and Li 2008; Pavelka et al. 2008]. Differences between proteomics and microarray data, however, have prompted numerous proteomics studies on the effects of data transformation and normalization on the accuracy of protein detection and quantitation with LC-MS intensity data [Rudnick et al. 2014; Karpievitch et al. 2012]. With regard to spectral counting, since this type of data entails counts associated with each peptide or protein, pre-processing for accurate statistical analysis can be more difficult. Numerous methods to transform spectral counts into appropriate values for statistical comparisons have been developed, including emPAI, various iterations of a normalized spectral abundance factor (NSAF), and a spectral index (SpI) that incorporates some intensity data into the spectral counting algorithm [Griffin et al. 2012; Zybailov et al. 2006; Ishihama et al. 2005]. Comparison studies have indicated that a distributed NSAF that accounts for multiple assignations of spectra to different peptides

is the most accurate for quantifying protein abundance [McIlwain et al. 2012]. Finally, a raft of methods for statistical comparison between conditions for both intensity-based and spectral counting data have been developed, partially due to the unknown distributional and variance characteristics of proteomics data [Zhu et al. 2010; Zhang et al. 2006]. Two of the most successful methods have been appropriated from transcriptomics technologies. Statistical analysis of microarrays (SAM) algorithm may be applied to intensity-based proteomics data after appropriate log2-transformation and normalization [Roxas and Li 2008]. For spectral counting, traditional hypothesis testing or regressions—e.g., the EdgeR program [Robinson et al. 2010]—may be used with ln-transformed NSAF values [Silva et al. 2006]. In all statistical comparison methodologies, multiple testing corrections must be applied to avoid dramatic increases in type II errors [Serang and Kall 2015; Noble 2009]. Statistical analysis of omics data remains a field of intense research interest and change, with the goal of improving confidence in the accuracy of quantitation of LC-MS/MS results.

1.6.3 Proteomics is a natural fit for biofilm research

Proteomics is a natural choice for broad-scale investigations of biofilms. First, there is the potential for generating rich datasets by differential extraction of proteins from the same sample. For example, subproteomes (e.g., membrane proteome, surface-associated proteome, extracellular proteome, and cytosolic proteome) may be distinguished and investigated separately by using established protein separation techniques such as differential enrichment, affinity purification, precipitation, compartmentalization, enrichment with detergents, fractionation, and biotinylation [Mangiapane et al. 2015; Wurpel et al. 2015; Olaya-Abril et al. 2014]. These methods of

protein enrichment allow for discovery of the involvement of the various structures of bacterial cells in each step of biofilm development, as detailed below.

During early biofilm stages (reversible and irreversible attachment), integral membrane proteins and surface-associated proteins are critical targets for analysis. Many of the unique proteins expressed during early attachment involve membrane proteins, including cell-binding proteins [Asakura et al. 2007] and fibrinogen-binding proteins [Resch et al. 2006]. Several studies have suggested that the nature of the substratum to which the biofilm adheres has a significant impact on protein expression [Schlisselberg et al. 2013; Chaturongkasumrit et al. 2011; Vilain et al. 2004]. In several *Pseudomonas* model species, proteins associated with reversible attachment include cell wall proteins and proteins involved with functions such as motility, antibiotic resistance, and virulence [Sauer et al. 2001]. Reversible attachment is associated with initial production of extracellular polymeric substances (EPS), lipopolysaccharides (LPS), and secreted proteins that are regulated by the BfiSR two-component system [Petrova et al. 2010; Hinsa et al. 2003].

In mature biofilms, the ECM itself includes an "exoproteome," proteins secreted or released by cells that are retained by or adsorbed to biofilm structural components. These exoproteome proteins include virulence factors [Gallaher et al. 2006], outer membrane proteins (OMPs), and proteins encapsulated in outer membrane vesicles (OMVs) that may be involved in transport of antibiotic resistance or pathogenic factors between individual cells [Schaar et al. 2011; Bauman et al. 2009]. Other studies have indicated a role for OMVs in secretion of biofilm matrix components [Altindis et al.

2014]. The mature ECM forms a part of each individual biofilm's unique proteome "signature" [Vilain et al. 2006].

In the final stage of the biofilm phenotype, detachment, bacterial protein expression includes modulation of expression of motility proteins such as FliC and PilA [Sauer et al. 2004]. Detachment may be induced by increases in availability of carbon [Sauer et al. 2004] or by carbon starvation mediated by the secondary messenger cAMP [Huynh et al. 2012]. Cells in the detachment phase have been shown in some species to have a unique phenotype distinct from biofilm cells and planktonic cells that have not yet attached [Vaysse et al. 2009; Vaysse et al. 2011]. In the case of *P. aeruginosa* and some other pathogenic species, proteomics studies showed that the low levels of cyclic di-GMP in cells dispersed from biofilms induced expression of virulence proteins and development of resistance to antimicrobial peptides [Duvel et al. 2012]. Moreover, in a phosphoproteomic study, *P. aeruginosa* cells exhibited an increase in Ser/Thr-phosphorylated proteins soon after nutrient-induced dispersion from a biofilm [Sauer et al. 2004]. In each of these studies, proteomics has been instrumental in describing the proteome of cells in the detachment phase as well as reasons for transition to the detachment phase, including regulation by quorum sensing [Solano et al. 2014].

A second reason proteomics is a natural fit for biofilm research is that the formation of a biofilm entails global changes in phenotype (cell morphology, metabolism, behavior). The analysis of global expression patterns of proteins, biomolecules closest to defining phenotype, seems highly appropriate. Since many unique features of biofilm life have just started to be described, it is likely that many proteins not previously associated with change to a biofilm lifestyle remain to be

identified. This fact is reflected in the high proportion of proteins identified as "uncharacterized" or "hypothetical" in many biofilm proteomics studies [Clark et al. 2012; Dharmaprakash et al. 2014]. From a medical perspective, identifying biomarkers for a shift to biofilm and the concomitant virulent phenotype may identify protein targets for antibiotics or inform design of drugs that prevent that virulent state. Moreover, a proteomics approach offers the possibility of distinguishing between bacterial and host protein expression, allowing simultaneous characterization of the activities of both the pathogen and the host [Kaakoush et al. 2015]. From an engineering perspective, distinguishing mechanisms during the various stages of bacterial attachment to surfaces may suggest surface modifications that will reduce biofouling of important surfaces or may suggest techniques to accelerate or improve the process of biofilm formation in a bioreactor system.

Finally, the methods of proteomics are uniquely suited to address many of the limitations of biofilm research detailed in sections above. For example, the very small quantity of protein necessary for proteomics analysis with contemporary LC-MS/MS instrumentation (~0.5 μg protein per LC-MS/MS run) may reduce difficulties with low biomass samples. Additionally, protein fractionation methods offer the possibility of enrichment of information acquired from any given sample. For example, localization of proteins to different parts of the cell (e.g., membrane vs. cytosol), which has special relevance for a biofilm system in which the bacterial cells interact with a surface, may be distinguished by differential protein extraction methods. The unique ability of proteomics to describe post-translational modifications (PTMs) is especially advantageous for investigating biofilm formation, during which PTMs play a

determinative role for many species [Richter et al. 2017; Zhang et al. 2016; Kiley et al. 2010] as well as for biofilms of microbial consortia [Li et al. 2014].

Despite the fact that a biofilm mode of life likely is the dominant form of bacterial life in nature, the vast majority of bacteriological studies over the past 200 years have concerned bacteria in planktonic cultures. Over the past 20 years, the development of microscopy tools has enabled detailed investigation of biofilm systems; the application of omics to biofilms so far has been limited. Proteomics in particular offers a powerful set of analysis tools especially appropriate to biofilm investigation that promises to uncover new details distinctive to the physiology of bacteria living in a biofilm. Considering the importance of biofilms for basic microbiological research, medicine, and engineering, and considering the emergence of proteomics as a mature technology for investigating complex systems, the application of proteomics tools to biofilms is a natural and promising development likely to yield useful information about this important form of bacterial life.

1.7 Research objectives

By relying on living organisms, engineered biosystems entail complexity and unpredictability not found in abiotic engineered systems. For that reason, the prospects for improving biosystems are limited unless new, useful information can be obtained about the organisms involved. Obtaining this kind of information is especially problematic for systems like biofilms that have multiple layers of complexity; an experimental approach is required that has the capacity to address multiple hypotheses simultaneously. In this work, system-wide protein expression was analyzed in four different biofilm systems, in order to answer four types of questions:

1. **What** protein expression is distinctive to biofilms, compared with planktonic cultures?

2. **Which** proteins are specific to a biofilm performing a certain function, compared with a biofilm not performing it?

3. **How** does co-culture with another species affect biofilm-related protein expression?

4. **When** during multi-species biofilm development does a function of interest emerge, and **who** in the community is involved?

The first question was addressed by comparing protein expression in biofilm and planktonic cells of *L. delbrueckii lactis* during lactic acid fermentation. The second question was addressed by comparing the proteomes of electricity-producing and aerobic biofilms of *S. oneidensis* MR-1. The third question was addressed by quantifying proteome shifts in *B. atrophaeus* and *P. putida* in response to growth together, compared with growth of each species as a pure culture. The last question was addressed by tracking consortium-wide protein expression in a mixed culture microbial fuel cell as the anode biofilm transitioned to becoming electrochemically active.

CHAPTER 1 REFERENCES

Aebersold R, Mann M. (2016) Mass-spectrometric exploration of proteome structure and function. Nature 537:347-355

Allegrucci M, Hu FZ, Shen K, Hayes J, Ehrlich GD, Post JC, Sauer K. (2006) Phenotypic characterization of Streptococcus pneumoniae biofilm development. J. Bacteriol. 188:2325-2335

Altindis E, Fu Y, Mekalanos JJ. (2014) Proteomic analysis of Vibrio cholerae outer membrane vesicles. Proc. Nat. Acad. Sci. 111:E1548-E1556

Andrews GL, Simons BL, Young JB, Hawkridge AM, Muddiman DC. (2011) Performance characteristics of a new hybrid quadrupole time-of-flight tandem mass spectrometer (TripleTOF 5600). Anal. Chem. 83:5442-5446

Asakura H, Yamasaki M, Yamamoto S, Igimi S. (2007) Deletion of *peb4* gene impairs cell adhesion and biofilm formation in *Campylobacter jejuni*. FEMS Microbiol. Lett. 278-285

Azizi S, Kamika I, Tekere M. (2016) Evaluation of heavy metal removal from wastewater in a modified packed bed biofilm reactor. PLoS One. 11(5):e0155462

Bauer FF, Govendar P, Bester MC. (2010) Yeast flocculation and its biotechnologies relevance. Appl. Microbiol. Biotechnol. 88:31-39.

Bauman SJ, Kuehn MJ. (2009) Pseudomonas aeruginosa vesicles associate with and are internalized by human lung epithelial cells. BMC Microbiol. 26: https://doi.org/10.1186/1471-2180-9-26

Beyenal H, Lewandowski Z, Harkin G. (2004a) Quantifying biofilm structure: facts and fiction. Biofouling. 20:1-23.

Beyenal H, Donovan C, Lewandowski Z, Harkin G. (2004b) Three-dimensional biofilm structure quantification. J. Microbiol. Meth. 59:395-413.

Beyenal H, Lewandowski Z. (2005) Modeling mass transport and microbial activity in stratified biofilms. Chem. Eng. Sci. 60:4337-4348

Biggs CA, Lant PA. (2000) Activated sludge flocculation: on-line determination of floc size and the effect of shear. Water Res. 34:2542-2550

Bos R, van der Mei HC, Busscher HJ. (1999) Physico-chemistry of initial microbial adhesive interactions – its mechanisms and methods for study. FEMS Microbiol. Rev. 23:179-230

Branda SS, Vik A, Friedman L, Kolter R. (2005) Biofilms: the matrix revisited. Trends Microbiol. 13:20-26

Brileya KA, Camilleri LB, Zane GM, Wall JD, Fields MW. (2014) Biofilm growth mode promotes maximum carrying capacity and community stability during product inhibition syntrophy. Front. Microbiol. 5: article 693

Busscher HJ, Weerkamp AH. (1987) Specific and non-specific interactions in bacterial adhesion to solid substrata. FEMS Microbiol. Rev. 3:165-173

Busscher HJ, Bos R, van Der Mei HC. (1995) Initial microbial adhesion is a determinant for the strength of biofilm adhesion. FEMS Microbiol. Lett. 128:229-234

Characklis WG. (1981) Bioengineering report: fouling biofilm development: a process analysis. Biotech. Bioeng. 23(9): https://doi.org/10.1002/bit.260230902

Chaturongkasumrit Y, Takahashi H, Keeratipibul S, Kuda T, Kimura B. (2011) The effect of polyesterurethane belt surface roughness on Listeria monocytogenes biofilm formation and its cleaning efficiency. Food Control 22:1893-1899

Chen X, Stewart PS. (2000) Biofilm removal caused by chemical treatments. Water Res. 34:4229-4233.

Chmielewski RAN, Frank JF. (2006) Biofilm formation and control in food processing facilities. Comp. Rev. Food Sci. Food Safety. 2(1): https://doi.org/10.1111/j.1541-4337.2003.tb00012.x

Clark ME, He Z, Redding AM, Joachimiak MP, Keasling JD, Zhou JZ, Arkin AP, Mukhopadhyay A, Fields MW. (2012) Transcriptomic and proteomic analyses of *Desulfovibrio vulgaris* biofilms: carbon and energy flow contribute to the distinct biofilm growth state. BMC Genomics 13: https://doi.org/10.1186/1471-2164-13-138

Costerton JW, Stewart PS, Greenberg EP. (1999) Bacterial biofilms: a common cause of persistent infections. Science 284:1318-1322

Cotter PA, Stibitz S. (2007) c-di-GMP-mediated regulation of virulence and biofilm formation. Curr. Opin. Microbiol. 10:17-23

Cury JA, Koo H. (2007) Extraction and purification of total RNA from Streptococcus mutans biofilms. Analytic. Biochem. 365:208-214

Dalton T, Dowd SE, Wolcott RD, Sun Y, Watters C, Griswold JA, Rumbaugh KP. An *in vivo* polymicrobial biofilm wound infection model to study interspecies interactions. PLoS One 6:e27317

Denef VJ, Mueller RS, Banfield JF. (2010) AMD biofilms: using model communities to study microbial evolution and ecological complexity in nature. ISME J. 4:599-610

Dharmaprakash A, Mutt E, Jaleel A, Ramanathan S, Thomas S. (2014) Proteome profile of a pandemic Vibrio parahaemolyticus SC192 strain in the planktonic and biofilm condition. Biofouling 30:729-739

Donlan RM, Pipes WO, Yohe TL. (1994) Biofilm formation on cast iron substrata in water distribution systems. Water Res. 28:1497-1503

Dowd SE, Wolcott RD, Sun Y, McKeehan T, Smith E, Rhoads D. (2008) Polymicrobial nature of chronic diabetic foot ulcer biofilm infections determined using bacterial tag encoded FLX amplicon pyrosequencing (bTEFAP). PLoS One 3:e3326

Dunne WM. (2002) Bacterial adhesion: seen any good biofilms lately? Microbiol. Rev. 15:155-166.

Duvel J, Berinetti D, Moller S, Schwede F, Morr M, Wissing J, Radamm L, Zimmermann B, Genieser H-G, Jansch L, Herberg FW, Haussler S. (2012) A chemical proteomics approach to identify c-di-GMP binding proteins in *Pseudomonas aeruginosa*. 88:229-236

Eliuk S. and Makarov A. (2015) Evolution of Orbitrap mass spectrometry instrumentation. Annu. Rev. Anal. Chem. 8:61-80

Escapa A, Mateos R, Martinez EJ, Blanes J. (2016) Microbial electrolysis cells: an emerging technology for wastewater treatment and energy recovery. From laboratory to pilot plant and beyond. Renew. Sust. Ener. Rev. 55:942-956

Escudie R, Cresson R, Delgenes J-P, Bernet N. (2011) Control of start-up and operation of anaerobic biofilm reactors: an overview of 15 years of research. Water Res. 45:1-10

Fan Y, Sharbrough E, Liu H. (2008) Quantification of the internal resistance distribution of microbial fuel cells. Environ. Sci. Technol. 42:8101-8107

Fernandez I, Vazquez-Padin JR, Mosquera-Corral A, Campos JF, Mendez R. (2008) Biofilm and granular systems to improve Anammox biomass retention. Biochem. Eng. J. 42:308-313

Flemming H-C, Neu TR, Wozniak DJ. (2007) The EPS matrix: the 'house of biofilm cells'. J. Bacteriol. 189: 7945-7947.

Franzosa EA, Hsu T, Sirota-Madi A, Shafquat A, Abu-Ali G, Morgan XC, Huttenhower C. (2015) Sequencing and beyond: integrating molecular 'omics' for microbial community profiling. Nat. Rev. Microbiol. 13:360-372

Gagliano MC, Ismail SB, Stams AJM, Plugge CM, Temmink H, Van Lier JB. (2017) Biofilm formation and granule properties in anaerobic digestion at high salinity. Water Res. 121:61-71

Gallaher TK, Wu S, Webster P, Aguilera R. (2006) Identification of biofilm proteins in non-typeable Haemaopilus influenzae. BMC Microbiol. 65: https://doi.org/10.1186/1471-2180-6-65

Garber M, Brabherr MG, Guttman M, Trapnell C. (2011) Computational methods for transcriptome annotation and quantification using RNA-seq. Nat. Meth. 8:469-477

Geesey GG, Richardson WT, Yeomans HG, Irvin RT, Costeron JW. (1977) Microscopic examination of natural sessile bacterial populations from an alpine stream. Can. J. Microbiol. 23:1733-36

Gorby YA, Yanina S, McLean JS, Rosso KM, Moyles D, Dohnalkova A et al. Electrically conductive bacterial nanowires produced by *Shewanella oneidensis* strain MR-1 and other microorganisms. PNAS 2006;103:11358-11363

Grangeasse C, Stulke J, Mijakovic I. (2015) Regulatory potential of poast-translational modifications in bacteria. Front. Microbiol. 6: https://doi.org/10.3389/fmicb.2015.00500

Grote W, Lee KJ, Rogers PL. (1980) Continuous ethanol production by immobilized cells of Zymomonas mobilis. Biotechnol. Lett. 2:481-486

Griffin NM, Yu J, Long F, Oh P, Shore S, Li Y, Koziol JA, Schnitzer JE. (2010) Label-free, normalized quantification of complex mass spectrometry data for proteomic analysis. Nat. Biotech. 28:83-89

Gutleben J, De Mares MC, van Elsas JD, Smidt H, Overmann J, Sipkema D. (2017) The multi-omics promise in context: from sequence to microbial isolate. 44:212-229

Guttenplan SB, Kearns DB. (2013) Regulation of flagellar motility during biofilm formation. FEMS Microbiol. Rev. FEMS

Gygi SP, Aebersold R. (2000) Mass spectrometry and proteomics. 4:489-494

Haag A.M. (2016) Mass Analyzers and Mass Spectrometers. In: Mirzaei H., Carrasco M. (eds) Modern Proteomics – Sample Preparation, Analysis and Practical Applications. Advances in Experimental Medicine and Biology, vol 919. Springer, Cham

Hansen SK, Rainey PB, Haagensen JAJ, Molin S. (2007) Evolution of species interactions in a biofilm community. 445:533-536

Henrici AT. (1933) Studies of freshwater bacteria. I. A direct microscopic technique. J. Bacteriol. 25:277-87

Herzberg M, Elimelech M. (2007) Biofouling of reverse osmosis membranes: role of biofilm-enhanced osmotic pressure. J. Memb. Sci. 295:11-20

Hinsa SM, Espinosa-Urgel M, Ramos JL, O'Toole GA. (2003) Transition from reversible to irreversible attachment during biofilm formation by Pseudomonas fluorescens WCS365 requires an ABC transporter and a large secreted protein. Molec. Microbiol. 49: https://doi.org/10.1046/j.1365-2958.2003.03615.x

Huang L, Harvie G, Feitelson JS, Gramatikoff K, Herold DA, Allen DL, Amunngama R, Hagler RA, Pisano MR, Zhang W-W, Xiangming F. (2005) Immunoaffinity separation of plasma proteins by IgY microbeads: meeting the needs of proteomics sample preparation and analysis. Proteomics 5:3314-3328

Huang C, Liu W-Z, Li Z-L, Zhang S-M, Chen F, Yu H-R, Shao S-L, Nan J, Wang A-J. (2018) High recycling efficiency and elemental sulfur purity achieved in a biofilm formed membrane filtration reactor. Water Res. 130:1-12

Huynh TT, McDougald D, Klebensberger J, Al Qarni B, Barraud N, Rice SA, Kjelleberg S, Schleheck D. (2012) Glucose starvation-induced dispersal of Pseudomonas aeruginosa biofilms is cAMP and Energy dependent. PLoS One 7:e42874

Inaba T, Hori T, Navarro RR, Ogata A, Hanajima D, Habe H. (2018) Revealing sludge and biofilm microbiomes in membrane bioreactor treating piggery wastewater by non-destructive microscopy and 16S rRNA gene sequencing. Chem. Eng. J. 331:75-83

Inoue K, Leang C, Franks AE, Woodard TL, Nevin KP, Lovley DR. (2011) Specific localization of the c-type cytochrome OmcZ at the anode surface in current-producing biofilms of Geobacter sulfurreducens. Environ. Microbiol. Rep. 3:211-217

Ishihama Y, Oda Y, Tabata T, Sato T, Nagasu T, Rappsilber J, Mann M. (2005) Exponentially modified protein abundance index (emPAI) for estimation of absolute protein amount in proteomics by the number of sequenced peptides per protein. Molec. Cell. Proteomics 4:1265-1272

Jackson CR, Churchill PF, Roden EE. (2001) Successional changes in bacterial assemblage structure during epilithic biofilm development. Ecology 82: https://doi.org/10.1890/0012-9658(2001)082[0555:SCIBAS]2.0.CO;2

Janicek A, Fan Y, Liu H. (2014) Design of microbial fuel cells for practical application: a review and analysis of scale-up studies. Biofuels 5:79-92

Jih C-G, Huang J-S. (1994) Effect of biofilm thickness distribution on substrate-inhibited kinetics. Water Res. 28:967-973

Kaakoush NO, Deshpande NP, Man SM, Burgos-Portugal JA, Khattak FA, Raftery MJ, Wilkins MR, Mitchel HM. (2014) Transcriptomic and proteomic analyses reveal key innate immune signatures in the host response to the gastrointestinal pathogen *Campylobacter concisus*. 83:832-845

Karpievitch YV, Dabney AR, Smith RD. (2012) Normalization and missing value imputation for label-free LC-MS analysis. BMC Bioinform. 13:55

Karunakaran E, Mukherjee J, Ramalingam B, Biggs CA. (2011) 'Biofilmology': a multidisciplinary review of the study of microbial biofilms. Appl. Microbiol. Biotechnol. 90:1869-1881

Khemiri A, Jouenne T, Cosette P. (2015) Proteomics dedicated to biofilmology: what have we learned from a decade of research? Med. Microgiol. Immunol. 205:1-19

Kim E-J, Sabra W, Zeng A-P. Iron deficiency leads to inhibition of oxygen transfer and enhanced formation of virulence factors in cultures of Pseudomonas aeruginosa PAO1. 149: 2627-2634

Kiley TB, Stanley-Wall NR. (2010) Post-translational control of Bacillus subtilis biofilm formation mediated tyrosine phosphorylation. Molec. Microbiol. 78:947-963

Klammer AA, Park CY, Noble WS. (2009) Statistical calibration of the SEQUEST XCorr function. J. Proteome Res. 8:2106-2113

Klueh U, Wagner V, Kelly S, Johnson A, Bryers JD. (2002) Efficacy of silver-coated fabric to prevent bacterial colonization and subsequent device-based biofilm formation. J. Biomed. Mat. Res. 53:621-631

Kreft J-U. (2004) Biofilms promote altruism. Microbiol. 150: 2751-2760

Lewandowski Z, Beyenal H, Stookey D. (2004) Reproducibility of biofilm processes and the meaning of steady state in biofilm reactors. Water Sci. Technol. 49:359-364

Li YM, Gu GW, Zhao JF, Yu HQ, Qiu YL, Peng YZ. (2003) Treatment of coke-plant wastewater by biofilm systems for removal of organic compounds and nitrogen. Chemosphere. 52:997-1005

Li Z, Wang Y, Yao Q, Justice NB, Ahn T-H, Xu D, Hettich RL, Banfield JF, Pan C. (2014) Diverse and divergent protein post-translational modifications in two growth stages of a natural microbial community. Nat. Commun. 5: https://doi.org/10.1038/ncomms5405

Logan BE. (2010) Scaling up microbial fuel cells and other bioelectrochemical systems. 85:1665-1671

Logan BE, Hamelers B, Rozendal R, Schroder U, Keller J, Freguia S, et al. (2006) Microbial fuel cells: Methodology and Technology. Environ. Sci. Technol. 40:5181-5192

Logan BE, Regan JM. (2006) Electricity-producing bacterial communities in microbial fuel cells. Trends Microbiol. 14:512-518

Logan BE, Wallack MJ, Kim K-Y, He W, Feng Y, Saikaly P. (2015) Assessment of microbial fuel cell configurations and power densities. *Environ. Sci. Technol. Lett*. 2:206-214.

Lovley DR. (2017) Syntrophy goes electric: direct interspecies electron transfer. Ann. Rev. Micobiol. 71:643-664.

Lundgren DH, Hwang S-I, Wu L, Han DK. (2010) Role of spectral counting in quantitative proteomics. Exp. Rev. Proteomics 7:39-53

Mangiapane E, Mazzoli R, Pessione A, Svensson B, Riedel K, Pessione E. (2015) Ten years of subproteome investigations in lactic acid bacteria: a key for food starter and probiotic typing. 127:332-339

Marshall KC, Stout R, Mitchell R. 1971. Mechanism of the initial events in the sorbtion of marine bacteria to surfaces. J. Gen. Microbiol. 68:337–48

Marsili E, Baron DB, Shikhare ID, Coursolle D, Gralnik J, Bond DR. (2008) Shewanella secretes flavins that mediate extracellular electron transfer. Proc. Nat. Acad. Sci. 105: 3968-3973.

McIlwain S, Mathews M, Bereman MS, Ruvel EW, MacCoss MJ, Noble WS. (2012) Estimating relative abundances of proteins from shotgun proteomics data. BMC Bioinform. 13:308

McQuarrie JP, Boltz JP. (2011) Moving bed biofilm reactor technology: process applications, design, and performance. Wat. Env. Res. 83: 560-575

Medzihradsky KF, Chalkley RJ. (2015) Lessons in de novo peptide sequencing by tandem mass spectrometry. Mass Spectrom. Rev. 34:43–63

Milac TI, Randolph TW, Wang P. (2012) Analyzing LC-MS/MS data by spectral count and ion abundance: two case studies. Stat Interface 5:75-87

Nahnsen S, Bielow C, Reinert K, Kohlbacher O. (2013) Tools for label-free peptide quantification. Molec. Cell. Proteomics 12:549-556

Nevin KP, Woodard TL, Franks AE, Summers AM, Lovley DR. (2010). Microbial electrosynthesis: feeding microbes electricity to convert carbon dioxide and water to multicarbon extracellular organic compounds. mBio 2010; doi:10.1128/mBio.00103-10

Nikolaev YA, Plakunov VK. (2007) Biofilm – 'City of microbes' or an analogue of multicellular organisms? Microbiol. 76:125-138

Noble WS. (2009) How does multiple testing correction work? Nat. Biotechnol. 27:1135-1137

Olaya-Abril A, Jimenez-Munguia I, Gomez-Gascon L, Rodriguez-Ortega MJ. (2014) Surfomics: shaving live organisms for a fast proteomic identification of surface proteomics. J. Proteomics 97:164-176

Paitier A, Godain A, Lyon D, Haddour N, Vogel TM, Monier J-M. (2017) Microbial fuel cell anodic microbial population dynamics during MFC start-up. Bioelectronics 92:357-363

Pant D, Van Bogaert G, Porto-Carrero C, Diels L, Vanbroekhoven K. (2010) A review of the substrates used in microbial fuel cells (MFCs) for sustainable energy production. Biores. Technol. 101:1533-1543

Pavelka N, Fournier ML, Swanson SK, Pelizzola M, Ricciardi-Castagnoli P, Florens L, Washburn MP. (2008) Statistical similarities between transcriptomics and quantitative shotgun proteomics data. Molec. Cell. Proteomics 7:631-644

Pederson K, Holmstrom C, Olsson A-K, Pedersen A. (1986) Statistic evaluation of the influence of species variation, culture conditions, surface wettability, and fluid shear on attachment and biofilm development of marine bacteria. Archives Microbiol. 145:1-8

Petrova OE, Sauer K. (2010) The novel two-component regulatory system BfiSR regulates biofilm development by controlling the small RNA *rsmZ* through CafA. J. Bacteriol. 192:5275-5288.

Phillips PL, Schultz GS. (2012) Molecular mechanisms of biofilm infection: biofilm virulence factors. Adv. Wound Care. 109-114

Pitts NB, Zero DT, Marsh PD, Ekstrand K, Weintraub JA, Ramos-Gomez F, Tagami J, Twetman S, Tsakos G, Ismail A. (2017) Dental caries. Nat. Rev. Dis. Primers. 3:17030

Pflugmacher U, Gottschalk G. (1994) Development of an immobilized cell reactor for the production of 1,3-propanediol by Citrobacter freundii. Appl. Microbiol. Biotechnol.

Podar M, Abulencia CB, Walcher M, Hutchison D, Zengler K, Garcia JA, Holland T, Cotton D, Hauser L, Keller M. (2007) Targeted access to the genomes of low-abundance organisms in complex microbial communities. Appl. Environ. Microbiol. 73: 3205–3214.

Poole K. (2002) Mechanisms of bacterial biocide and antibiotic resistance. J. Appl. Microbiol. 92:55S-64S

Rauniyar N, Yates JR. (2014) Isobaric labeling-based relative quantification in shotgun proteomics. J. Proteome Res. 13:5293-5309

Resch A, Leicht S, Saric M, Pasztor L, Jakob A, Gotz F, Nordheim A. (2006) Comparative proteome analysis of Staphylococcus aureus biofilm and planktonic cells and correlation with transcriptome profiling. Proteomics 6: https://doi.org/10.1002/pmic.200500531

Richter K, Van den Driessche F, Coenye T. (2017) Innovative approaches to treat Staphylococcus aureus biofilm-related infections. Essays Biochem. 61:61-70

Rogers S, Girolami M, Kolch W, Waters KM, Liu T, Thrall B, Wiley HS. (2008) Investigating the correspondence between transcriptomic and proteomic expression profiles using couples cluster models. Bioinformatics24:2894-2900

Roxas BAP, Li Q (2008) Significance analysis of microarray for relative quantitation of LC/MS data in proteomics. BMC Bioinform 9:187. doi: 10.1186/1471-2105-9-187

Rudnick PA, Wang X, Yan X, Sedranski N, Stein SE. (2014) Improved normalization of systematic biases affecting ion current measurements in label-free proteomics data. Molec. Cell. Proteomics 13:1341-1351

Qureshi N, Annous BA, Ezeji TC, Karcher P, Maddox IS. (2005) Biofilm reactors for industrial bioconversion processes: employing potential of enhanced reaction rates. Microb. Cell Fact. 4:24

Sauer K, Camper AK, Ehrlich GD, Costerton JW, Davies DG. (2002) Pseudomonas aeruginosa displays multiple phenotypes during development as a biofilm. J. Bacteriol. 184:1140-1154.

Schlisselberg DB, Yaron S. (2013) The effects of stainless stell finish on Salmonella Typhimurium attachment, biofilm formation and sensitivity to chlorine. Food Microbiol. 35:65-72

Shalit T, Elinger D, Savidor A, Gabashvili A, Levin Y. (2015) MS-based label-free proteomics using a quadrupole orbitrap mass spectrometer. J. Proteome Res. 14:1979-1986

Shi L, Richardson DJ, Wang Z, Kerisit SN, Rosso KM, Zachara JM, Frederickson JK. (2009) The roles of outer membrane cytochromes of Shewanella and Geobacter in extracellular electron transfer. Environ. Microbiol. Rep. 1:220-227

Simburger JMB, Dettmer K, Oefner P, Reinders J. (2016) Optimizing the SWATH-MS workflow for label-free proteomics. J. Proteomics. 145:137-140

Solano C, Echeverz M, Lasa I. (2014) Biofilm dispersion and quorum sensing. Curr. Opin. Microbiol. 18:96-104

Tolker-Nielsen T, Molin S. (2000) Spatial organization of microbial biofilm communities. Microb. Ecology 40:75-84

Rabaey K, Rozendal RA. (2010) Microbial electrosynthesis – revisiting the electrical route for microbial production. Nat. Rev. Microbiol. 8: 706-716

Robinson MD, McCarthy DJ, Smyth GK. (2010) edgeR:a Bioconductor package for differential expression analysis of digital gene expression data. Bioinformatics 26:139-140

Sauer K and Camper AK. (2001) Characterization of phenotypic changes in *Pseudomonas putida* in response to surface-associated growth. J. Bacteriol. 183:6579-6589

Sauer K, Cullen MC, Rickard AH, Zeef LAH, Davies DG, Gilbert P. (2004) Characterization of nutrient-induced dispersion in Pseudomonas aeruginosa PAO1 biofilm. J. Bacteriol. 186:7312-7326

Schaar V, Nordstrom T, Morgelin M, Riesbeck K. (2011) Moraxella catarrhalis outer membrane vesicles carry β-lactamase and promote survival of *Streptococcus pneumoniae* and *Haemophilus influenzae* by inactivating amoxicillin. Antimicrob. Agents Chemother. 55:3845-3853

Serang O, Kall L. (2015) Solution to statistical challenges in proteomics is more statistics, not less. J. Proteome Res. 14:4099-4103

Seth AK, Geringer MR, Hong SJ, Leung KP, Mustoe TA, Galiano RD. (2012) In vivo modeling of biofilm-infected wounds: a review. J. Surg. Res. 178:330-338

Silva JC, Gorenstein MV, Li G-Z, Vissers JPC, Geromanos SJ. (2006) Absolute quantification of proteins by LCMS^{E}

Song J, Sasaki D, Sasaki K, Kato S, Kondo A, Hashimoto K, Nakanishi S. (2016) Comprehensive metabolomic analysis of anode-respiring Geobacter Sulfurreducens cells:

the impact of anode-respiration activity on intracellular metabolite levels. Process Biochem. 51:34-38

Stewart PS, Costerton JW. (2001) Antibiotic resistance of bacteria to biofilms. The Lancet. 358:135-138

Stoodley P, Sauer K, Davies DG, Costerton JW. Biofilms as complex differentiated communities. Annu. Rev. Micobiol. 56:187-209

Tran NH, Zhang X, Xin L, Shan B, Li M. (2017) De novo peptide sequencing by deep learning. Proc. Nat. Acad. Sci. 114:8247-8252

Tribou M, Swain G. Grooming using rotating brushes as a proactive method to control ship hull fouling. J. Bioadhes. Biofilm Res. 31:309-319.

Ueki T, Nevin KP, Woodard TL, Lovley DR. (2016) Genetic switches and related tools for controlling gene expression and electrical outputs of Geobacter sulfurreducens. J. Ind. Microbiol. Biotechnol. 43:1561-1575

Van Loosdrecht MCM, Lyklema J, Norde W, Schraa G, Zehnder AJB. (1987) The role of bacterial cell wall hydrophobicity in adhesion. Appl. Env. Microbiol. 53:1893-1897

Vanwonterghem I, Jensen PD, Ho DP, Batstone DJ, Tyson GW. (2014) Linking microbial community structure, interactions and function in anaerobic digesters using new molecular techniques. Curr. Opin. Biotechnol. 27:55-64

Vaysse P-J, Prat L, Mangenot S, Cruveiller S, Goulas P, Grimaud R. (2009) Proteomic analysis of Marinobacter hydrocarbonoclasticus SP17 biofilm formation at the alkane-

water interface reveals novel proteins and cellular processes involved in hexadecane assimilation. 160:829-837

Vaysse P-J, Sivadon P, Goulas P, Grimaud R. (2011) Cells dispersed from Marinobacter hydrocarbonoclasticus SP17 biofilm exhibit a specific protein profile associated with a higher ability to reinitiate biofilm development at the hexadecane-water interface. Environ. Microbiol. 13:737-746

Vidova V. and Spacil Z. (2017) A review on mass spectrometry-based quantitative proteomics: targeted and data independent acquisition. Analy. Chim. Acta 964:7-23

Villahermosa D, Corzo A, Garcia-Robledo E, Gonzalez JM, Papaspyrou S. (2016) Kinetics of indigenous nitrate reducing sulfide oxidizing activity in microaerophilic wastewater biofilms. PLoS One 11(2):e0149096

Vilain S, Cosette P, Zimmerlin I, Dupont J-P, Junter G-A, Jouenne T. (2004) Biofilm proteome: homogeneity or versatility? J. Proteome Res.

Vilain S and Brozel VS. (2006) Multivariate approach to comparing whole-cell proteomes of Bacillus cereus indicates a biofilm-specific proteome. J. Proteome Res. 5:1924-1930

von Canstein H, Ogawa J, Shimizu S, Lloyd JR. (2007) Secretion of flavins by Shewanella species and their role in extracellular electron transfer. Appl. Environ. Microbiol. 74:615-623.

Vrouwenvelder JS, Buiter J, Riviere M, van der Meer WGJ, van Loosdrecht MCM, Kruithof JC. (2010) Impact of flow regime on pressure drop increase and biomass accumulation and morphology in membrane systems. Water Res. 44:698-702.

Wang X, Wen X, Criddle C, Wells G, Zhang J, Zhao Y. (2010) Community analysis of ammonia-oxidizing bacteria in activated sludge of eight wastewater treatment systems. J. Environ. Sci. 22:627-634

Wang Z, Gerstein M, Snyder M. RNA-seq: a revolutionary tool for transcriptomics. Nat. Rev. Gen. 10:57-63

Watnick P, Kolter R. (2000) Biofilm, city of microbes. J. Bacteriol. 182:2675-2679

Wurpel DJ, Totsika M, Allsopp LP, Webb RI, Moriel DG, Schembri MA. (2015) Comparative proteomics of uropathogenic Escherichia coli during growth in human urine identify UCA-like (UCL) fimbriae as an adherence factor involved in biofilm formation and binding to uroepithelial cells. J. Proteomics 131:177-189

Xie F, Liu T, Qian W-J, Petyuk VA, Smith RD. (2011) Liquid chromatography-mass spectrometery-based quantitative proteomics. J. Biol. Chem. 286:25443-25449

Yates JR, Ruse CI, Nakorchevsky A. (2009) Proteomics by mass spectrometry: approaches, advances, and applications. Ann. Rev. Biomed. Eng. 11:49-79

Zhang B, VerBerkmoes NC, Langston MA, Uberbacher E, Hettich RL, Samatova NF. (2006) Detecting differential and correlated protein expression in label-free shotgun proteomics. 5:2909-2918

Zhang C, Li B, Huang X, Ni Y, Feng X-Q. (2016) Morphomechanics of bacterial biofils undergoing anisotropic differential growth. Appl. Phys. Lett. 109: https://doi.org/10.1063/1.4963780

Zhang Y, Wen Z, Washburn MP, Florens L. (2010) Refinements to label free proteome quantitation: how to deal with peptides shared by multiple proteins. Anal. Chem. 82:2272-2281

Zhi W, Ge Z, He Z, Zhang H. (2014) Methods for understanding microbial community structures and functions in microbial fuel cells: a review. Biores. Technol. 171:461-468

Zhu W, Smith JW., Huang C-M. (2009) Mass spectrometry-based label-free quantitative proteomics. J. Biomed. Biotechnol. 2010: doi:10.1155/2010/840518

Zobell CE. (1937) The influence of solid surfaces upon the physiological activities of bacteria in sea water. J. Bacteriol. 33:86

Zybailov B, Mosley AL, Sardiu ME, Coleman MK, Florens L, Washburn MP. (2006) 5:2339-2347

CHAPTER 2: MODULATION IN PROTEIN EXPRESSION ASSOCIATED WITH CATALYTIC ACTIVITY AND METABOLIC DIVERSITY IN *LACTOBACILLUS DELBRUECKII* BIOFILMS, QUANTIFIED BY LABEL-FREE PROTEOMICS[1]

2.1 Introduction

Lactic acid is a valuable organic acid with multiple uses, including use as a food additive and as a precursor compound for the production of biodegradable plastics [Abdel-Rahman et al. 2013]. While it is possible to produce lactic acid by chemical synthesis, biological production through fermentation offers efficiency and cost advantages [Litchfield 1996]. Moreover, lactic acid may be produced from fermentation of renewable or waste sources of sugar, e.g., derived from cellulosic biomass [John et al. 2007], thereby improving the sustainability of production [Ghaffar et al. 2014]. Lactic acid bacteria in the genus *Lactobacillus* include some of the most promising strains for industrial production of lactic acid. Optimization of the growth and productivity of *Lactobacillus* strains generating lactic acid represent a significant portion of commercial efforts to improve the efficiency of fermentative production of this commodity chemical [Martinez et al. 2013].

One option for improving lactic acid fermentation is the use of immobilized cells. Cell immobilization offers several advantages over batch fermentations that can improve process performance by increasing cell density, reducing concerns about contamination, and reducing inhibition by product or other metabolites [Karunakaran et al. 2011].

[1] The text and results presented in this chapter were published previously in Chignell et al. 2018 (Chapter 2 References)

Moreover, unlike stirred tank reactors that use planktonic cells, continuous-feed reactors that use immobilized cells may be operated at dilution rates greater than the specific growth rate of the organisms, thereby increasing productivity and increasing process flexibility. Numerous studies have reported increases in productivity, yield, and titer using cells immobilized by entrapment, e.g., in alginate beads [Sirisansaneeyakul et al. 2007; Reardon and Bailey 1989; Kumar et al. 2014]. Biofilms, aggregates of bacterial cells on surfaces encased in a matrix of extracellular polysaccharides and other biomolecules that is produced by the cells themselves, represent an alternative form of immobilization. Biofilms are self-assembling, result in high cell concentrations, and can increase the operational lifetime of a reactor by obviating the need to re-start the reactor. Numerous applications of biofilm reactors have been successful in wastewater treatment [Boltz et al. 2017; Nicolella et al. 2000]. Several studies have reported improvements in productivity and yield using biofilms for fermentative production of commodity chemicals [Cheng et al. 2010; Quereshi et al. 2005], including, for example, up to 400% improvement in lactic acid productivity using a repeated batch biofilm system [Demirci et al. 1995].

A biofilm mode of life entails fundamental changes in the physiology of the immobilized bacterial cells, compared to a planktonic lifestyle [Karunakaran et al. 2011; Pulido et al. 2016]. Investigating this sort of large-scale change in physiology requires a technology that can quantify changes across the entire suite of expressed genes. Recently, several studies using "-omics" approaches have compared transcript or protein abundance between biofilm and non-biofilm bacterial phenotypes [Park et al. 2014; Resch et al. 2006; Booth et al. 2011]. In contrast to alternative -omics technologies,

proteomics is especially applicable to biofilms: DNA and RNA are both comprised as extracellular components of the physical biofilm matrix [Montanaro 2011] and mRNA is difficult to extract from biofilms in adequate amounts [Franca et al. 2011]. While few -omics studies, however, have examined biofilms relevant to industrial processes, and none have addressed lactic acid production by lactic acid bacteria. The goal of this study was to obtain information about the physiological changes in bacterial species during a biofilm mode of life that are associated with improvements in lactic acid production performance, in an industrial context. We applied a quantitative proteomics approach to compare the physiology of *Lactobacillus delbrueckii* ssp. *lactis*, during lactic acid production in a biofilm compared to that during planktonic growth. This strain is used industrially in dairy fermentation processes [Hebert et al. 2004; Forsman et al. 1991], including processes that use biofilms as starters [Licitra et al. 2007] or biofilm molecules as a texturant [Duboc et al. 2001]. This strain has been shown in previous work to generate lactic acid with high yield, titer, and productivity, including in immobilized and biofilm reactor systems [Rangaswamy and Ramakrishna 2001; Idiris and Suzana 2006; Bai et al. 2003]. Insights from this comparison will shed light on protein expression that enables higher metabolic rates—and therefore more efficient production of lactic acid—in biofilms compared with planktonic cells.

2.2 Experimental Procedures

2.2.1 Bacterial strains, maintenance and culture

The homofermentative lactic acid bacterium *Lactobacillus delbrueckii* subsp. *lactis* DSM 20073 (ATCC 14933) was cultivated routinely on a modified de Man-Rogosa-Sharpe (MRS) growth medium that consisted of 20 g/L glucose, 10 g/L peptone,

10 g/L meat extract, 5 g/L yeast extract, 5 g/L sodium acetate, 2 g/L dipotassium phosphate, 2 g/L ammonium citrate, 1 g/L Tween 80, 0.2 g/L $MgSO_4 \cdot 7H_2O$, 0.05 g/L $MnSO_4 \cdot H_2O$ in deionized water, with initial pH adjusted to 7.0 [de Man et al. 1960]. A pre-culture was grown in this MRS medium in a 100-mL Schott bottle by adding the contents of a glycerol stock at 1% (v/v). Pre-cultures were grown for 24 h prior to connecting to the flow cell (see Flow-Cell Design, Construction and Operation below) or inoculated (5 mL) into a Schott bottle containing 100 mL of MRS medium as a planktonic control. These planktonic control cultures were grown at 45 °C with shaking at 120 rpm and harvested at the same time as the biofilm samples.

2.2.2 Flow-cell design, construction, and operation

All flow-cell design parameters and operational settings were identical to those described previously [Schlegel et al. 2017]. Briefly, flow cells were constructed with a flow channel volume of 8.75 mL and either a smooth (S) or micro-etched (ME) bottom surface as a substrate for the attachment of cells and development of a biofilm. Micro-etching of the flow cell surface was conducted in response to previous results indicating that micro-etched surfaces promoted the development of *L. delbrueckii lactis* biofilm [Schlegel et al. 2017]. During biofilm cultivation, each flow cell (ME and S) was run in a continuous loop to a separate reservoir (MRS medium, pH 7.0, 45 °C) for 24 h at a flow rate of 5 mL/min in intervals of 15 min on and 60 min off. After biofilm formation on the bottom surface of each flow cell, the influent flow rate was changed to 0.3 mL/min, resulting in a dilution rate (D) of 2.06/h. Setting D higher than the specific growth rate (μ = 0.57/h) increased the likelihood that cells detached from the biofilm would be washed

out of the reactor and therefore not contribute to lactic acid production measured in the flow cell effluent.

2.2.3 Biofilm sampling and protein extraction

After 10-14 h growth, when OD_{600} of the planktonic control culture had indicated that late log phase had been reached, the entire biofilm flow cell setup and planktonic culture were transferred to an anaerobic tent flooded with N_2. Samples (~12 mL) from the planktonic control culture and the suspension reservoir from each flow cell were collected in Falcon tubes, while biofilm samples were collected by rinsing the surface of the flow cell three times with 0.09% NaCl buffer into a collection tube, resulting in a total of five samples. All samples were centrifuged (4217 x g, 5 min, 4 °C), the supernatant was removed, and the pellets were washed by re-suspending in 5 mL sterile 0.9% NaCl buffer. The pellets were centrifuged again as before the supernatant was discarded, and the tubes with the pellets were immersed into liquid nitrogen and stored at -80 °C This entire process was repeated four times, generating a total of 20 samples for downstream analysis.

2.2.4 Protein precipitation, digestion, and peptide preparation

Proteins were prepared for analysis by two methods, distinguished primarily by whether a precipitation step was used. Preparation of peptides from non-precipitated protein samples followed previous work that developed the method in order to reduce losses of proteins in sample-limited situations [Proc et al. 2010]. The cell pellet was thawed on ice and resuspended in sterile lysis buffer (50 mM ammonium bicarbonate with 1% sodium deoxycholate (SDC), pH 8.2). Cells were sonicated (Fisher Scientific

Sonic Dismembrator F550) for 2-4 min at 50% duty cycle and the resulting solution was centrifuged (10,000 x g, 30 min, 4 °C) to isolate cell debris. The supernatant was removed to a low-bind tube and the protein concentration was quantified by BCA assay (Pierce Thermo Scientific, Waltham, MA). An appropriate volume for 100 µg of protein was denatured at 98 °C for 2 min followed by an additional 30 min at 65 °C in the presence of 9.1 mM dithiothreitol (DTT). Five µL of 375 mM iodoacetamide (IAA) were added to each sample for cysteine alkylation at room temperature in the dark for 30 min. Then 1 µL of 50 mM $CaCl_2$ was added, along with 5 µg of Promega Gold mass spectrometry grade trypsin (Promega, Fitchburg, WI). Acetonitrile (ACN) was added to result in a final concentration of 9 mM ACN. Digestion reactions progressed at 38 °C for 12 h, after which double digestion with 2 µg additional trypsin was conducted for 4 h. Digestion reactions were stopped by adding 100% formic acid to decrease pH to ~2. Digestions were centrifuged (14,000 x g, 30 min) to collect SDC that precipitated with the drop in pH. A volume containing 20 µg peptides was evaporated and the resulting peptide pellets were resuspended in 20 µL equilibration solution and residual detergent and contaminants were removed with a C-18 spin column (Pierce Thermo Fisher, Madison, WI), following the manufacturer's instructions. Eluted peptides were evaporated to dryness and resuspended in 3% acetonitrile, 0.1% formic acid for LC-MS/MS analysis.

For preparation of peptides from precipitated proteins, proteins were precipitated with 80% (v/v) cold acetone added at 5X volume to the supernatant from samples after cell lysis and centrifugation. The mixture was centrifuged (25,000 x g, 30 min, 4 °C) and the supernatant was removed. The pellet was washed with 80% acetone and the mixture

was centrifuged again. After removal of the supernatant, the pellet was resuspended in a solution of 6 M urea and 2 M thiourea to denature proteins. Denatured proteins were reduced in 9.1 mM DTT and alkylated with IAA as described above. The solution was diluted by 50% to 4 M urea, 2 M thiourea and the sample was digested with LysC (37 °C) for additional C-terminal lysine cleavage, to reduce missed cleavages from trypsin digestion. The final peptide solution was diluted to 1 M urea, 0.5 M thiourea in preparation for trypsin digestion with 1:50 (w/w) trypsin (38 °C, 12 h). Double digestion was for 3 h with an additional 1:50 (w/w) trypsin. Digestion was stopped by decreasing pH to ~2 with trifluoroacetic acid and the peptides were desalted on a C-18 filter disk (Sigma-Aldrich St. Louis, MO), evaporated to dryness, and resuspended in LC-MS/MS buffer, as above.

2.2.5 Data-dependent ESI-LC-MS/MS

Two µg of resuspended peptides were loaded onto a C-18 trap (200 µm ID, 0.5 mm length, 120 Å, Eksigent Technologies). A 2–80% gradient of acetonitrile with 0.1% formic acid was used to elute the peptides from the trap and column (C18, 75 µm ID, 150 mm length, 120 Å, Eksigent Technologies) at a flow rate of 300 nL/min. Peptides were eluted into the electrospray ionization source of a TripleTOF 5600+ (ABSciex, Framingham, MA, USA). Up to 50 MS^2 scans followed each MS^1 scan, according to the order of intensity. Two technical replicate LC-MS/MS shots were run for each sample.

2.2.6 Protein identification, quantification, and statistical analysis

Acquired MS data (.wiff files from Analyst v.1.5 TR) were processed with ProteinPilot (v.4.5 beta), using a .fasta database consisting of the entire proteome of

Lactobacillus delbruekii lactis DSM 20072 (Uniprot downloaded October 2014, 2005 sequences). Both technical replicate .wiff files for each biological replicate sample were searched simultaneously in ProteinPilot using rapid search ID and no biological modifications. False discovery rate (FDR) was calculated with a decoy database consisting of reversed sequences from the target database, with FDR protein identification significance threshold ≤ 1%. The numbers of identified features for precipitated and non-precipitated samples were those reported by ProteinPilot as "Global FDR from Fit" with critical FDR of 1%, after a database search of both technical replicate LC-MS/MS datafiles simultaneously. For two of the 20 samples (two suspension cells from two replicates of S samples) insufficient protein was recovered after precipitation and downstream processing for accurate quantitation. Those samples were removed from subsequent analyses.

For relative quantification of proteins between selected conditions, the intensities of precursor ions for the top five peptides associated with each identified protein [Silva et al. 2006] were summed with a quantitation microapp (v. 1.0) in PeakView software (v. 1.1.1, ABSciex). Previous studies have noted linear correlation between the precursor ion intensities of the top peptides for a protein and the abundance of that protein in the original sample [Silva et al. 2006]. During relative quantification one technical replicate for one planktonic sample consistently generated unusually low precursor ion intensity values, despite multiple data processing attempts. Rather than remove this single technical replicate and retain the biological replicate, analysis proceeded instead with the three remaining biological replicate samples. Data normalization and assessment of summary statistics were conducted using R statistical package (v. 3.1.2). Each raw,

summed precursor ion intensity value were normalized to the sum of all intensities in the respective technical replicate. For each protein, the mean was calculated across technical replicates to generate an intensity value for that protein in each biological replicate. A correlation matrix for all technical replicates was constructed using the *cor()* function. The correlation coefficients (r-values) between technical replicates for each biological sample were used in a Student's t-test (two-tailed, assuming homoscedasticity) to compare biofilm and planktonic sample types with respect to technical replication of analysis by LC-MS/MS. Additionally, a mean r-value between biological replicates of the same sample type (biofilm or planktonic) was calculated by averaging all r-values within the same sample type, excluding comparisons of the two technical replicates for the same biological replicate. Then, for each protein, a Student's t-test between biofilm and planktonic samples was conducted across biological replicates, assuming homoscedasticity. Differentially abundant proteins (DAPs) ($p<0.05$) that were more or less abundant ($\log_2$-fold-change > 1 or < -1) in the biofilm sample were searched, mapped and annotated with Blast2GO software v.5.0 (www.blast2go.org). KEGG metabolic maps were obtained (http://www.genome.jp/kegg/pathway.html) and used to identify metabolic pathways containing more and less abundant proteins.

2.3 Results

2.3.1 ESI-LC-MS/MS feature identification with and without acetone precipitation

During the LC-MS/MS analysis, a total of 20 samples were analyzed. These were four biological replicates of each of the following sample types: biofilms from flow-cells with micro-etched surfaces ("ME biofilms"), biofilms from flow-cells with smooth surfaces ("S biofilms"), cells from the suspension of each flow-cell setup, and planktonic

cultures (P). The samples were analyzed in that order, with all replicates from ME biofilm samples analyzed first, then all replicates from S biofilm samples, etc. The same order was followed for samples prepared both with and without precipitation of proteins with 80% acetone prior to the protein digestion step. Two technical replicates were processed together to identify proteins for each sample. Two of the non-precipitated suspension samples resulted in errors during the LC-MS/MS analysis, likely owing to fouling of the instrument, and therefore were excluded from statistical comparison.

For samples that did not undergo acetone precipitation after extraction, identifications of proteins, peptides, and spectra decreased by 58.5%, 79.0%, and 90.2%, respectively, compared to the beginning of the sample set (Appendix SI 2.2: Figure S1A). In contrast, when the same protein samples were precipitated with 80% acetone after extraction, decreases of 9.0%, 12.0%, and 13.3%, respectively, were observed for those identifications over the course of the sample set (Appendix SI 2.2: Figure S1B). These data are summarized in terms of the percent difference between precipitated and non-precipitated samples (Appendix SI 2.2: Figure S2). The percent difference between identifications from non-precipitated and precipitated samples reached 74.9 ± 15.7%, 91.5 ± 5.6%, and 95.4 ± 3.1% (error bars represent standard deviation of percent differences across planktonic samples), for proteins, peptides, and spectra, respectively, by the end of the sample set (Appendix SI 2.2: Figure S2). Paired t-tests showed significant differences ($p<0.0001$) between precipitated and non-precipitated sample types with respect to each feature (Appendix SI 2.1: Table S1). Much of the decline in ESI-LC-MS/MS performance when processing non-precipitated samples occurred during the first four samples (ME biofilm): the percent difference between precipitated and non-

precipitated samples with respect to protein identifications increased linearly (R^2 = 0.9992) across the first four samples by nearly 10% (m = 9.989) for each sample (Appendix SI 2.2: Figure S3). Due to this decrease in ESI-LC-MS/MS performance, subsequent database searching and metabolic analysis was conducted only on results from samples that had undergone precipitation prior to processing for ESI-LC-MS/MS.

2.3.2 Identification and statistical assessment of proteome features

Identifications of spectra, peptides, and proteins for the samples from ME biofilms and planktonic control cultures are summarized in the Appendix (SI 2.1:Table S2). Processing two technical replicate ESI-LC-MS/MS runs simultaneously for each biological replicate resulted in identifications of 802 ± 33 proteins, 784 ± 19 proteins, and 772 ± 13 proteins from samples from ME biofilms, S biofilms, and planktonic samples, respectively (FDR < 1%). The peptide/protein ratio (an indicator of protein coverage) was 9.0 ± 1.2, 9.0 ± 0.3, and 9.5 ± 0.2 for ME biofilm, S biofilm, and planktonic sample types, respectively.

Since the focus of this study was on the unique proteome features of biofilms compared with planktonic cells, and because ME surfaces had been shown to develop biofilms of this strain more readily than smooth surfaces [Booth et al. 2011], the remainder of the proteomic study focused on the comparison of ME biofilm and planktonic conditions. When ME biofilm and planktonic results were processed simultaneously by ProteinPilot, a total of 886 proteins in common between these sample types were quantified as the sum of precursor ion intensities of the top five peptides. Although hypothesis testing on a per protein basis resulted in no proteins with a q-value [Storey 2002] less than 0.05, a histogram of p-values exhibited notable right skew

(Appendix SI 2.2: Figure S4), suggesting that relative quantification using a significance threshold with p-values and $\log_2$-fold-change would be appropriate [Pascovici et al. 2016]. Of 126 proteins with $p<0.05$, 48 proteins were found to be more abundant in ME biofilms than in planktonic samples ($\log_2FC > 1$). Likewise, 29 proteins were less abundant ($\log_2FC < -1$) in ME biofilms compared with planktonic samples (i.e., more abundant in planktonic). A complete list of these DAPs is provided in Table S3 (Appendix SI 2.1).

To evaluate the impact of using a 2-fold change threshold, the analysis was repeated with a 1.5-fold-change threshold. This resulted in identification of an additional 12 DAPs more abundant and 27 DAPs less abundant in ME biofilms, compared with planktonic samples. A complete list of DAPs at the 1.5-fold threshold is provided in Table S4 (Appendix SI 2.1). Since the 2-fold-change threshold, while arbitrary, is more commonly used than 1.5-fold, subsequent metabolic analysis focused on 2-fold-change DAPs.

The Pearson's correlation between LC-MS/MS technical replicate injections (Figure 2; Appendix SI 2.1: Table S5) was lower for biofilm samples ($r = 0.71 \pm 0.14$) than for planktonic samples ($r = 0.89 \pm 0.05$). However, this difference was not significant ($p > 0.05$, two-tailed t-test assuming equal variances), likely owing to the high variation between technical replicate injections for biofilm samples: relative standard deviation (RSD) was 20.2% between biofilm injection replicates, compared with RSD of 6.1% for planktonic samples. In both cases, RSD likely would have decreased with additional injection replicates. The higher RSD for biofilms compared with planktonic samples, however, suggests that, despite acetone precipitation, some interfering

compounds in the biofilm samples decreased the consistency of LC-MS/MS protein identification.

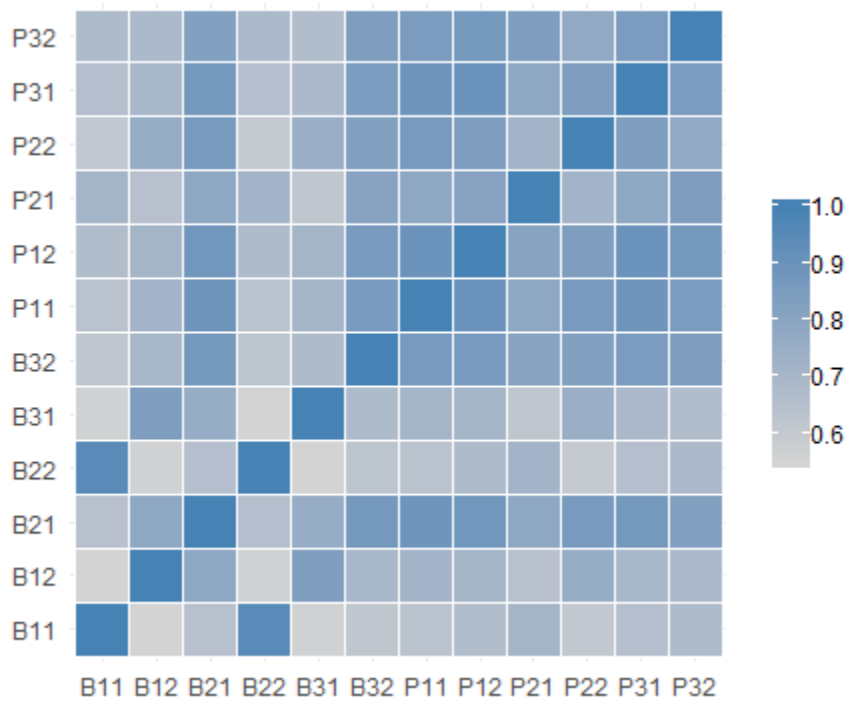

Figure 2: Correlation of protein relative abundances between biofilm and planktonic samples. Matrix of Pearson's correlations between relative abundance of proteins in ME biofilm ("B") and planktonic ("P") samples. Numerical designations of, e.g., "11" and "12" refer to the first and second technical replicates, respectively, of the first biological replicate sample. Protein abundance is quantified as $\log_2$-transformed, normalized intensity values summed for the top five peptides associated with a protein.

The overall correlation between ME biofilm samples and planktonic samples (r = 0.80 ± 0.10) was significantly ($p<0.001$, t-test assuming equal variances) less than that between replicate planktonic samples ($r = 0.90 \pm 0.05$), but not significantly less than that among the ME biofilm samples themselves ($r = 0.76 \pm 0.15$). That is, protein abundances from replicate ME biofilms were, overall, not significantly less correlated

with planktonic samples than with each other. Since the statistical comparison of biofilm and planktonic protein abundance was assessed on a per-protein basis, however, a low overall Pearson's correlation between biofilm samples does not entail that significant differences will not be found between biofilm and planktonic conditions for some individual proteins.

2.3.3 Biofilm vs. planktonic cells: Gene Ontology categorization of differentially-abundant proteins

DAPs were assigned to terms within the Gene Ontology (GO). The GO is a collaboratively curated gene annotation database that groups gene products into sub-categories associated with general categories of Biological Processes, Molecular Function, and Cellular Components. Level 3 Biological Process GO categorization indicated that the percentage of assignments to the GO category "biosynthetic process" for DAPs more abundant in ME biofilms (18.6%) was nearly double that (9.9%) for DAPs less abundant in ME biofilms (Figure 3). While "biosynthetic process" was the best represented category for ME biofilms, the three most abundant categories for planktonic samples were relevant to metabolic processes. DAPs less abundant in ME biofilms (i.e., more abundant in planktonic cultures) were categorized into six additional categories not applied to DAPs more abundant in ME biofilms, including categories associated with regulation, oxidation-reduction, response to stimulus, localization, and methylation.

In order to characterize DAPs in greater depth, a Fisher's Exact Test identified

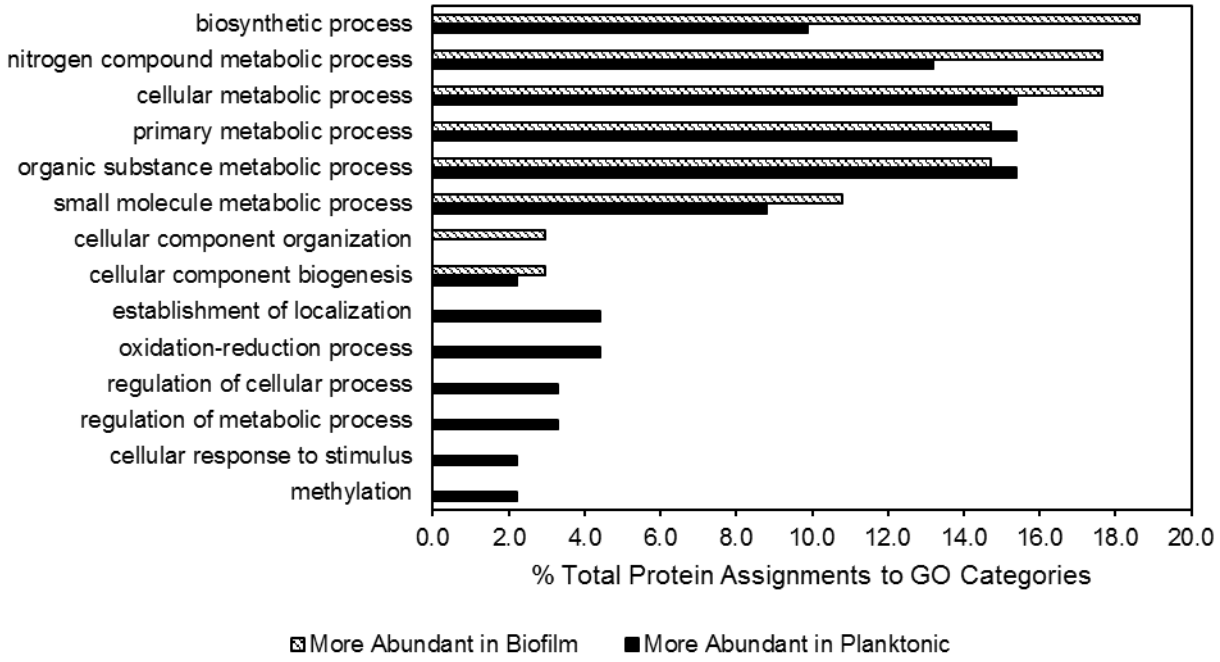

Figure 3: Comparison of Level 3 GO Biological Process categorization of DAPs between ME biofilms and planktonic cultures. DAPs were significantly ($p<0.05$, Student's t-test) more ($\log_2FC > 1$) or less ($\log_2FC < -1$) abundant in ME biofilms than in planktonic cultures. A total of 102 and 91 assignments of proteins to GO Biological Process categories were made, respectively, for proteins more and less abundant in ME biofilms.

GO categories that were enriched ($p<0.05$) among DAPs either more or less abundant in ME biofilms (relative to planktonic cells), compared with the set of remaining proteins (non-DAPs and DAPs less abundant in ME biofilms). A complete list of the enriched GO categories and the proteins associated with them are provided in Table S6 (Appendix SI 2.1). Of the 23 categories enriched in ME biofilms, only one, anion transmembrane transport, was represented by more than one protein (Appendix SI 2.2: Figure S5). Eight of the other 22 categories were related to metal ion homeostasis (two for iron ion homeostasis), all of which were redundant categorizations of a single protein, the DNA starvation/stationary phase protection protein Dps (F0HVV9). Similarly, six categories

were related to metabolism or biosynthesis of flavin adenine dinucleotide (FAD) or flavin mononucleotide (FMN). Each of these categories were redundant categorizations of riboflavin biosynthesis protein RibF (F0HTR3). Interestingly, the DAP with the greatest $\log_2$-fold-change (5.46) in ME biofilms compared with planktonic samples was a hypothetical protein; no non-hypothetical proteins were identified for this protein sequence by NCBI SmartBLAST (https://blast.ncbi.nlm.nih.gov) and no conserved domains were identified for this sequence either by NCBI BLAST or by structural analysis by the Protein Data Bank (www.pdb.org). In contrast, among DAPs less abundant in ME biofilms (more abundant in planktonic), significantly enriched Biological Process GO categories included metabolic process for sulfur compounds, terpenoids and carbohydrates (Appendix SI 2.2: Figure S6). Unexpectedly, categories for biosynthesis of carboxylic acids and adhesion were enriched among DAPs less abundant in biofilms.

For the GO Category of Molecular Function, a Level 3 GO comparison showed transferase activity and ion binding as the most well-represented categories for DAPs more abundant in ME biofilms (Figure 3). More Biological Process GO categories were represented among DAPs less abundant in biofilms (i.e., more abundant in planktonic cells); in this case, each of the additional categories represented a type of binding.

In addition to identifying enriched Biological Process categories, a Fisher's Exact Test also identified Molecular Function GO categories that were significantly ($p<0.05$) enriched in ME biofilm DAPs compared with remaining proteins. The GO Molecular Function category "catalytic activity" was the most well-represented among ME biofilm

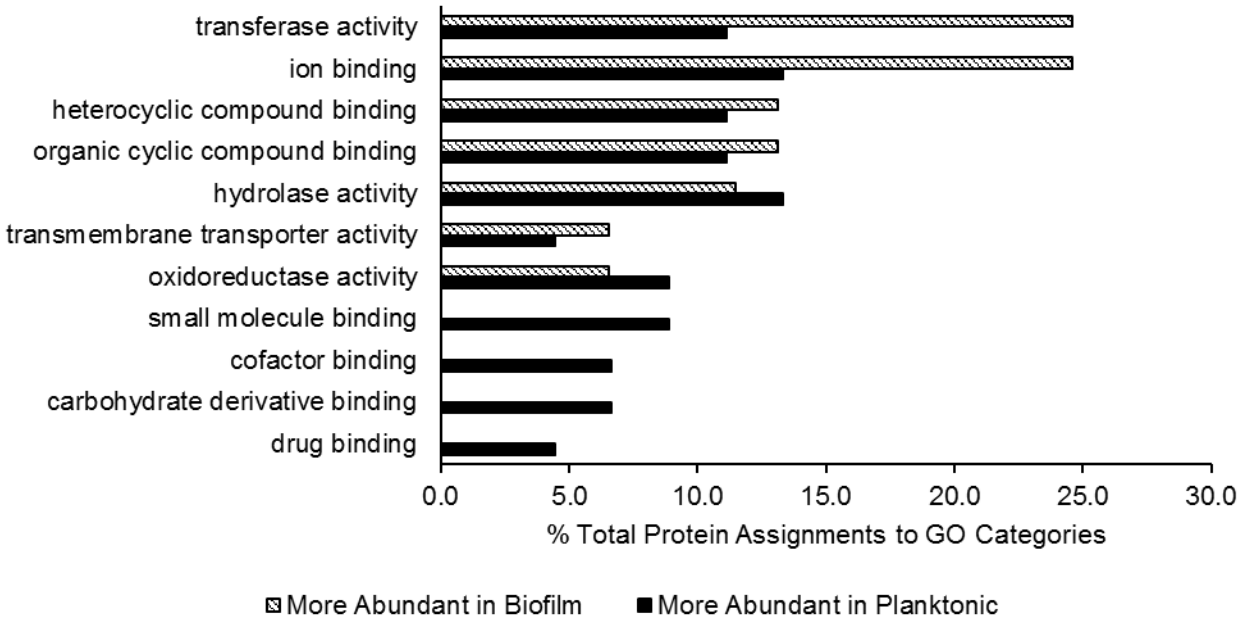

Figure 4: Comparison of Level 3 GO Molecular Function categorization of DAPs between ME biofilms and planktonic cultures. DAPs were significantly ($p<0.05$, Student's t-test) more abundant ($log2FC > 1$ or < -1) in ME biofilms or planktonic cultures. A total of 65 and 45 assignments of proteins to GO Molecular Function categories were made by Blast2GO, respectively, for proteins more abundant in biofilms or planktonic cultures.

DAPs, comprising 76.7% of biofilm DAPs, compared with 62.8% of the remaining proteins (Appendix SI 2.2: Figure S7). In the most general GO description, this category contains proteins involved in energy-consuming anabolic reactions transforming simple compounds into more complex compounds (www.amigo.geneontology.org). Enriched categories included those associated with biosynthesis of fatty acids, riboflavin metabolism, and metal ion binding or oxidation. Of the 35 enriched categories, 16 categories were related to transferase functionality, including five of the seven categories in which the percentage of "remaining proteins" was greater than zero. Four different proteins (F0HTR3, F0HTT9, F0HV15, and F0HYG1) were assigned non-exclusively into

11 of these 16 categories. In contrast, just two transferase categories were enriched among DAPs less abundant in ME biofilms (Appendix SI 2.2: Figure S8).

2.3.4 Biofilm vs. planktonic cells: KEGG pathway analysis of differentially-abundant proteins

2.3.4.1 Fatty acid metabolism

KEGG Pathway categorization of enzymes found among proteins differentially more abundant in ME biofilms compared with planktonic cultures is provided in Table 1. Four of these enzymes were associated with KEGG pathways for fatty acid biosynthesis. These included the alpha unit of acetyl-coA carboxylase (Acc-ase) (EC 6.4.1.2), a critical enzyme for fatty acid biosynthesis [Davis et al. 2000], which was 4.6 times more abundant in biofilm cells than in planktonic cells. Additionally, glycerol kinase (EC 2.7.1.30) – responsible for phosphorylation of glycerol during catabolism of that molecule – was the DEP with the fourth-highest relative abundance ($log_2FC = 3.84$).

2.3.4.2 Membrane and transport protein

DAPs associated with membrane functions included an integral membrane protein, a subunit of the protein translocation channel SecY, and OxaA2, a protein associated with assembly and insertion of proteins into the inner membrane [Preuss et al. 2005]. Additionally, there was modulation in the relative abundance of 10 proteins

Table 1: Categorization of enzymes found among proteins differentially more abundant in ME biofilms compared to the set of remaining proteins according to KEGG Pathways.

Pathway	**Pathway ID**	**#Enz in Pathway**	**Enzyme**

Phenylalanine metabolism	map00360	1	ec:3.5.1.4 - acylamidase
Aminoacyl-tRNA biosynthesis	map00970	1	ec:6.3.5.7 - synthase (glutamine-hydrolysing)
Tryptophan metabolism	map00380	1	ec:3.5.1.4 - acylamidase
Aminobenzoate degradation	map00627	2	ec:3.1.3.41 - nitrophenyl phosphatase, ec:3.5.1.4 - acylamidase
Pyruvate metabolism	map00620	1	ec:6.4.1.2 - carboxylase
Biotin metabolism	map00780	1	ec:1.1.1.100 - reductase
Riboflavin metabolism	map00740	2	ec:2.7.7.2 - synthetase, ec:2.7.1.26 - kinase
Lysine biosynthesis	map00300	1	ec:6.3.2.13 - ligase
Glycerophospholipid metabolism	map00564	1	ec:2.3.1.51 - O-acyltransferase
Biosynthesis of antibiotics	map01130	1	ec:6.4.1.2 - carboxylase
Thiamine metabolism	map00730	1	ec:3.6.1.15 - phosphatase
Nicotinate and nicotinamide metabolism	map00760	1	ec:2.7.1.23 - kinase
Carbon fixation pathways in prokaryotes	map00720	1	ec:6.4.1.2 - carboxylase

Purine metabolism	map00230	4	ec:3.6.1.3 - adenylpyrophosphatase, ec:3.6.1.15 - phosphatase, ec:4.6.1.1 - cyclase, ec:2.7.7.6 - RNA polymerase
Glycerolipid metabolism	map00561	2	ec:2.3.1.51 - O-acyltransferase, ec:2.7.1.30 - kinase
Styrene degradation	map00643	1	ec:3.5.1.4 - acylamidase
Th1 and Th2 cell differentiation	map04658	1	ec:3.1.3.16 - phosphatase
Fatty acid biosynthesis	map00061	4	ec:1.1.1.100 - reductase, ec:6.4.1.2 - carboxylase, ec:2.3.1.39 - S-malonyltransferase, ec:2.3.1.85 - synthase
T cell receptor signaling pathway	map04660	1	ec:3.1.3.16 - phosphatase
Peptidoglycan biosynthesis	map00550	1	ec:6.3.2.13 - ligase
Pyrimidine metabolism	map00240	1	ec:2.7.7.6 - RNA polymerase

Biosynthesis of unsaturated fatty acids	map01040	1	ec:1.1.1.100 - reductase
Arginine and proline metabolism	map00330	1	ec:3.5.1.4 - acylamidase
Aflatoxin biosynthesis	map00254	1	ec:6.4.1.2 - carboxylase
Isoquinoline alkaloid biosynthesis	map00950	1	ec:1.1.1.218 - 6-dehydrogenase
Propanoate metabolism	map00640	1	ec:6.4.1.2 - carboxylase

involved in transport. Five of these proteins were more abundant in ME biofilms compared with planktonic cultures, including ABC transporters for glutamine and phosphate ($log_2FC > 3$) as well as PTS transporters for maltose and mannose. Additionally, a HPr kinase/phosphorylase DAP more abundant in biofilms phosphorylates HPr, a protein that is part of a sugar transport and phosphorylation system, thereby serving as the sensor enzyme to initiate catabolite repression in gram-positive bacteria [Nessler et al. 2003]. Membrane transporter proteins significantly less abundant in biofilm cells compared with planktonic cells included two ABC transporters and an MFS family major facilitator transporter protein that exhibited the fourth-greatest negative fold change in abundance (log_2FC ~-2.3, or 4.9-fold less abundant in biofilms than in planktonic cultures).

2.3.4.3 Riboflavin metabolism and redox proteins

Several proteins in this dataset were associated with riboflavin metabolism, including the conversion of riboflavin to redox proteins. The alpha subunit of RibE, (riboflavin synthase), the enzyme responsible for catalyzing the final step of riboflavin biosynthesis, was more abundant in ME biofilms ($log_2FC = 2.2$) but was not a DAP ($p > 0.15$). RibF, riboflavin kinase, the enzyme responsible for converting riboflavin to FMN, and FMN to FAD, was a DAP ($log_2FC = 1.74$), more than three-fold more abundant in ME biofilms compared with planktonic cultures. Few additional DAPs more abundant in biofilm samples were associated with redox activities. Several DAPs less abundant in biofilm, however, had redox properties, including an FMN-binding protein and a Gfo/Ldh/MocA family oxidoreductase.

2.3.4.4 Adhesion and stress response

Several proteins associated with adhesion as well as stress or virulence were more abundant DAPs in biofilm samples, compared with planktonic samples. These included adherence and virulence protein A as well as a membrane surface-associated DAP LemA, previously associated with adhesion and biofilm formation in *Lactobacillus* [Malik et al. 2013]. A stress response was evident further by the greater abundance in biofilm samples of a cold-shock DeaD box that functions as a helicase to unwind double-stranded RNA under stress conditions [Jones et al. 1996]. Moreover, a Dps protein (F0HVV9) responsible for DNA protection during starvation or stationary phase was also the protein that had been binned into multiple GO categories associated with metal and cation homeostasis (Appendix SI 2.2: Figure S5). Additional DAPs more abundant in biofilm samples associated with a stress response included a chaperone protein DnaJ and an organophosphate reductase that had the second-highest fold-change ($log_2FC = 4.2$) of all

DAPs. The latter protein is a member of a protein superfamily that has been associated with metabolism of ketonic and aldehydic byproducts of the oxidation of lipids [Ellis 2002]. Finally, a NrdR protein more abundant in biofilms has been associated with global protein expression and reduced growth [Naveen and Hsiao 2016]. Several additional DAPs identified at the 1.5-fold-change threshold also were associated with adhesion or stress response. More abundant DAPs included a MOP superfamily polysaccharide flippase transporter [Hvorup et al. 2003], an Eps operon transcriptional regulator associated in other strains with EPS production and virulence [Huang and Schell 1995], and HtrA, a serine protease associated with survival under stress and with extracellular matrix adhesion proteins [Wessler et al. 2017]. Interestingly, DAPs at the 1.5-fold-change level that were less abundant in biofilms (i.e., more abundant in planktonic cultures) included cell division protein FtsA, a protein that, along with FtsZ, is essential for bacterial cytokinesis [Loose and Mitchison 2014], as well as DnaD [Bruand et al. 2005] and RecX [Drees et al. 2004], two proteins associated with DNA replication or repair.

2.4 Discussion

2.4.1 Impacts of protein precipitation on identification by ESI-LC-MS/MS

Methods for biofilm proteomics are still in development; only a few studies have investigated the effects of protein preparation methods on the identification of biofilm proteins using a proteomics workflow [Carvalhais et al. 2015; Leary et al. 2012]. Precipitation of proteins from cell lysate with acetone, the standard choice for proteomics, generally results in incomplete protein recovery [Crowell et al. 2013]. Moreover, the choice of precipitation method will have an impact on the types of proteins

are recovered, thereby influencing the character of the proteome that is quantified and analyzed [Feist and Hummon 2015]. This methodological concern is especially relevant for biofilm proteomics, since, for many biofilm types, the protein yield is already low [Ram et al. 2005]. Generally, a low protein recovery will increase the likelihood that proteins will be quantified inaccurately or, in the case of proteins present in low relative abundance, not identified at all during LC-MS/MS processing [Da Costa et al. 2017; Fonslow et al. 2014]. Thus, precipitation of proteins from biofilm samples will result in additional losses of proteins, especially low-abundance proteins. However, as shown in the present study, when a protein preparation method is used that avoids a precipitation step, the efficiency of ESI-LC-MS/MS feature identification is degraded over several runs (Appendix SI 2.2: Figure S1), perhaps due to fouling by extracellular polysaccharide retained in non-precipitated samples. Moreover, even after acetone precipitation, repeatability between LC-MS/MS injection replicates was worse for biofilm samples than for planktonic samples (Figure 2; Appendix SI 2.1: Table S5). Additional study is warranted to develop protein preparation methods that either (a) maximize recovery of protein during precipitation from biofilm samples or (b) avoid protein precipitation and thereby minimize protein losses, especially of low-abundance proteins. Additionally, future work could compare the type and abundance of proteins identified by LC-MS/MS after removal of biofilm impurities by different precipitation methods or other protein purification techniques. Since, as suggested by the present study, identification of proteins from non-precipitated biofilm samples by LC-MS/MS may be inaccurate or incomplete, alternative methods of protein identification may be required to compare protein profiles before and after precipitation.

2.4.2 Proteomic evidence for increased metabolic activity in biofilms

A biofilm lifestyle has a broad and comprehensive effect on protein expression by bacteria [Flemming et al. 2016]. Though the physical and chemical conditions under which two biofilms form may be identical, small differences in matrix structure can exert considerable influence on the "emergent properties" of the biofilm [Lewandowski et al. 2004]. Here the uniqueness of each biofilm expression was suggested by the lower overall correlation in protein abundance between biofilm samples, compared with a higher correlation among planktonic samples (Figure 2). As described above, the variation between technical replicate injections for each biofilm sample likely exacerbated the lack of overall correlation among biofilm samples. Future work should determine the extent to which variation in protein abundance between biofilm samples is a result of the biological uniqueness of each biofilm or due to the effects of biofilm sample preparation on the replicability of LC-MS/MS analysis.

Increased metabolic activity in biofilms, compared with planktonic cells, was suggested by significant enrichment in biosynthetic processes (Biological Process) and catalytic activity (Molecular Function) among DAPs in ME biofilms (Figure 3; Appendix SI 2.1: Table S6). The increase in catalytic activity is consistent with a previous report of modulation in abundance of metabolic proteins [De Angelis et al. 2015] as well as increased conversion of carbohydrate to lactic acid [De Angelis et al. 2015; Gross et al. 2007] when *Lactobacillus* are immobilized in biofilms, compared with planktonic cultures. The enrichment in several categories of transferase activity also is consistent with increased metabolic rates in biofilms, since transferases are responsible for critical metabolic functions in the cell (e.g., phosphorylation of glucose to G3P during

glycolysis). Immobilization likely allows cells to re-direct resources that in a planktonic culture would be spent on motility, sensing of changing environmental conditions (e.g., chemotaxis), or other diverse functions experienced in a dynamic environment, rather than on primary metabolic activities. Indeed, planktonic DAPs fell into a greater number of categories for both Biological Process (Figure 3) and Molecular Function (Figure 4), suggesting that in biofilms the attention of the cell may be less distracted by non-metabolic functions.

2.4.3 The role of riboflavin in L. delbrueckii *lactis biofilms*

Riboflavin has been identified as an important molecule during biofilm formation by some species [Tremblay et al. 2013; Mitra et al. 2012; De Vriendt et al. 2005]. Lactic acid bacteria (LAB) such as *Lactobacillus delbrueckii lactis* are known for their capabilities to produce riboflavin [Russo et al. 2014], but the role of riboflavin in LAB biofilms of has not been elucidated. An increase in riboflavin production by biofilm cells may simply be a function of the observed increase in overall metabolic rates in biofilms, compared with planktonic cultures, as discussed in the previous paragraph. Alternatively, the differential abundance of RibF may suggest that the production of riboflavin may perform some critical redox function in LAB biofilms as a precursor of FMN and FAD [Marsili et al. 2008]. A previous proteomics study showed that the abundance of several proteins associated with oxidation and reduction processes was modulated in response to biofilm growth of *L. plantarum* [De Angelis et al. 2015], perhaps in response to the aerobic culture conditions of biofilms in that study. In the present work only one DAP other than RibF was associated with redox activity: an FMN-binding protein (F0HWF9). A BLAST search (https://blast.ncbi.nlm.nih.gov) identified this protein sequence as

pyridoxamine-5'-phosphate oxidase, a protein that catalyzes the rate-limiting step of biosynthesis of pyridoxal 5'-phosphate, the active form of vitamin B6, an essential coenzyme factor [Zhao and Winkler 1995]. Pyridoxamine-5'-phosphate oxidase has a potential secondary function as an oxygen scavenger, consuming molecular oxygen and producing hydrogen peroxide. Similarly, the production of riboflavin, another B-vitamin (B2), in biofilms may also be related to detoxification by removal of molecular oxygen. An FMN reductase (F0HWG9) previously shown to use riboflavin instead of FMN to convert molecular oxygen to hydrogen peroxide in a related *Lactobacillus* species [Hertzberger et al. 2014] was close to differentially more abundant in ME biofilms (p = 0.07, $\log_2$-fold-change = 0.86). Production of peroxide by *L. delbrueckii lactis*, perhaps as an inhibitory mechanism against competing bacteria, has been described previously [Batdorj et al. 2007; Villegas and Gilliland 1998]. Modulation of proteins related to the production of riboflavin or other B-vitamins may form part of this strategy of competitive inhibition or part of a mechanism of detoxification in response to molecular O_2 that had accumulated in the medium or in the biofilm itself. This strategy may comprise part of the previously-observed Future study could quantify riboflavin and H_2O_2 during biofilm and planktonic growth to determine whether the production of these compounds is associated with growth in a biofilm of *L. delbrueckii lactis*.

2.4.4 Stress in a biofilm mode of life

A biofilm lifestyle has been associated in several -omics studies with a stress response [Rice et al. 2016; Stewart et al. 2015; O'Toole and Stewart 2005], including for *Lactobacillus* [De Angelis et al. 2015]. It is not always clear, however, the extent to which biofilm growth is a response to an external stress, or that life in the biofilm

involves its own types of stress, or that biofilm formation entails expression of stress response proteins as part of an overall strategy of cell protection. The response of many *Lactobacillus* strains to environmental stresses has been documented [De Angelis et al. 2004]. Here, several DAPs more abundant in *L. delbrueckii lactis* ssp. *lactis* biofilm samples were associated with stress — including organophosphate reductase, the DEP with the second-highest upward $\log_2$-fold change (4.22) — despite the lack of application of environmental stress factors, other than growth in the flow cell itself. Several of these DAPs are associated with stabilization of critical molecules, including DNA (DNA stationary phase protection protein Dps), RNA (cold-shock DeaD box protein A), and chaperone proteins (GrpE and DnaJ). Many studies have noted an association between biofilm formation with virulence and stress, especially in pathogenic species [Corehtash et al. 2015; Fattahi et al. 2015; Phillips et al. 2012; Naves et al. 2008]. Stress-response by biofilm-bound *Lactobacillus* species has been examined primarily in the context of survival in the gut of probiotic strains [Salas-Jara et al. 2016] or persistence of cells that results in food spoilage [Kubota et al. 2008]. The other DAPs identified in this study—including DAPs identified at the 1.5-fold-change threshold—suggest that life in the flow-cell biofilm may have included its own stresses, such as exposure to molecular oxygen or channeling of energy toward central metabolic pathways instead of cell replication. This kind of stress response is corroborated by changes in fatty acid metabolism suggesting accumulation of fatty acids under nitrogen stress, a response observed previously in some species of algae [Leyva et al. 2014], although modulation in fatty acid metabolism has been associated with a biofilm mode of life for *Lactobacillus* species as well [De Angelis et al. 2015].These types of stress response suggest the possibility of an effect on overall

metabolism of a biofilm mode of life that has an effect on the efficiency with which the biofilm generates lactic acid or other products of interest. Future work could quantify more precisely the stress impacts on the productivity of *L. delbrueckii lactis* biofilms and how those stresses could be prevented or relieved in order to maximize productivity and longevity of the biofilm for industrial applications.

2.5 Conclusions

The purpose of this study was to quantify changes in the proteome of *Lactobacillus delbrueckii* lactis during growth in a biofilm compared with planktonic culture. The advantage of protein precipitation during preparation of biofilm samples was demonstrated in the improvement in consistency of LC-MS/MS identification of spectra, peptides, and proteins across sample set. More diverse protein identification and categorization for biofilm samples as well as increases in proteins associated with catalysis suggested that growth in a biofilm stimulated the rate and variety of metabolic processes, compared with planktonic cultures. These changes in metabolism may have induced expression of proteins associated with stress that were observed in biofilms, including synthesis of riboflavin for detoxification. Future study would focus on these stress management functions in order to specify which of them may contribute to increases in lactic acid production by *L. lactis* biofilms, compared with planktonic cultures.

CHAPTER 2 REFERENCES

Abdel-Rahman MA, Tashiro Y, Sonomoto K. (2013) Recent advances in lactic acid production by microbial fermentation processes. Biotechnol. Adv. 31:877-902

Bai D-M, Wei Q, Yan Z-H, Zhao X-M, Li X-G, Xu S-M. Biotechnol. Lett. 2003;25:1833-1835.

Batdorj B, Trinetta V, Dalgalarrondo M, Prevost H, Dousset X, Ivanova I, Haertle T, Chobert J-M. (2007) Isolation, taxonomic identification and hydrogen peroxide production by Lactobacillus delbrueckii subsp. lactis T31, isolated from Mongolian yoghurt: inhibitory activity on food-borne pathogens. J. Appl. Microbiol. 103:584-593.

Boltz JP, Smets BF, Rittman BE, van Loosdrecht MCM, Morgenroth E, Daigger GT. (2017) From biofilm ecology to reactors: a focused review. Water Sci. Technol. 2017;75:1753-1760.

Booth SC, Workentine ML, Wen J, Shaykhutdinov R, Vogel HJ, Ceri H, Turner RJ, Weljie AM. (2011) Differences in metabolism between the biofilm and planktonic response to metal stress. J. Protome Res. 2011;10:3190-3199.

Bruand C, Velten M, McGovern S, Marsin S, Serena C, Ehrlich SD, Polard P. (2005) Functional interplay between the Bacillus subtilis DnaD and DnaB proteins essential for initiation and re-initiation of DNA replication. Mol. Microbiol. 2005; 55:1138-1150.

Carvalhais V, Cerca N, Vilanova M, Vitorino R. (2015) Proteomic profile of dormancy within Staphylococcus epidermidis biofilms using iTRAQ and label-free strategies. Appl.Microbiol. Biotechnol. 99:2751-2762.

Cheng K-C, Demirci A, Catchmark JM. (2010) Advances in biofilm reactors for production of value-added products. Appl Microbiol. Biotechnol. 87:445-456.

Chignell JF, Schlegel C, Ulber R, Reardon KF. (2018) Quantitative proteomic analysis of Lactobacillus delbrueckii ssp. lactis biofilms. AiChE J. 64:4341-4350.

Corehtash ZG, Khorshidi A, Firoozeh F, Akbari H, Aznaveh AM. (2015) Biofilm formation and virulence factors among *Pseudomonas aeruginosa* isolated from burn patients. Jundishapur J. Microbiol. 8:e22345

Crowell AMJ, Wall MJ, Doucette AA. (2013) Maximizing recovery of water-soluble proteins through acetone precipitation. Anal. Chim. Acta. 796:48-54.

Da Costa JP, Santos PSM, Vitorino R, Rocha-Santos T, Duarte AC. (2017) How low can you go? A current perspective on low-abundance proteomics. TrAC Trends Anal. Chem. 93:171-182.

Davis M, Solbiati J, Cronan JE. (2000) Overproduction of acetyl-coA carboxylase activity increases the rate of fatty acid biosynthesis in *Escherichia coli.* J. Biol. Chem. 275:28593-28598.

De Angelis M, Gobbetti M. (2004) Environmental stress response in *Lactobacillus*: A review. Proteomics 4:106-122.

De Angelis M, Siragusa S, Campanella D, Di Cagno R, Gobbetti M. (2015) Comparative proteomic analysis of biofilm and planktonic cells of *Lactobacillus plantarum* DB200. Proteomics 15:2244-2257.

de Man, JD, Rogosa M, Sharpe ME. (1960) A Medium for the Cultivation of Lactobacilli. J Appl Bact. 23:130–135.

Demirci A, Pometto AL. (1995) Repeated-batch fermentation in biofilm reactors with plastic composite supports for lactic acid production. Appl. Microbiol. Biotechnol. 1995;43:585-589.

De Vriendt K, Theunissen S, Carpentier W, De Smet L, Devreese B, Beeumen JV. (2005) Proteomics of *Shewanella oneidensis* MR-1 biofilm reveals differentially expressed proteins, including AggA and RibB. Proteomics 5:1308-1316.

Drees JC, Lusetti SL, Chitteni-Pattu S, Inman RB, Cox MM. (2004) A RecA filament capping mechanism for RecX protein. Molec. Cell.15:789-798.

Duboc P, Mollet B. (2001) Applications of exopolysaccharides in the dairy industry. Int Dairy J. 11:759-768.

Ellis EM. (2002) Microbial aldo-keto reductases. FEMS Microbiol. Lett. 2002;216:123-131.

Naveen V, Hsiao C-D. (2016) NrdR Transcription Regulation: Global Proteome Analysis and Its Role in *Escherichia coli* Viability and Virulence. PLoS ONE 11(6):e0157165.

Fattahi S, Kafil HS, Nahai MR, Asgharzadeh M, Nori R, Aghazadeh M. (2015) Relationship of biofilm formation and different virulence genes in uropathogenic *Escherichia coli* isolates from northwest Iran. GMS Hyg. Infect. Control 10:Doc11.

Feist P, Hummon AB. (2015) Proteomic challenges: sample preparation techniques for microgram-quantity protein analysis from biological samples. Int. J. Mol. Sci. 16:3537-3563.

Flemming H-C, Wingender J, Szewzyk U, Steinberg P, Rice SA, Kjelleberg S. (2016) Biofilms: an emergent form of bacterial life. Nat. Rev. Microbiol. 14:563-575.

Fonslow BR, Stein BD, Webb KJ, Xu T, Choi J, Park SK, Yates JR. (2014) Addendum:

Digestion and depletion of abundant proteins improves proteomic coverage. Nat. Methods 11:347-348.

Forsman P, Alatossava T. (1991) Genetic variation of Lactobacillus delbrueckii subsp. Lactis bacteriophages isolated from chees processing plants in Finland. App. Environ. Microbiol. 57:1805-1812.

Franca A, Melo LDR, Cerca N. (2011) Comparison of RNA extraction methods from biofilm samples of *Staphylococcus epidermidis*. BMC Res. Notes 4: 572.

Ghaffar T, Irshad M, Anwar Z, Aqil T, Zulifqar Z, Tariq A. (2014) Recent trends in lactic acid biotechnology: a brief review on production to purification. J. Rad. Res. Appl. Sci. 7:222-229.

Gross R, Hauer B, Otto K, Schmid A. (2007) Microbial biofilms: new catalysts for maximizing productivity of long-term biotransformations. Biotechnol. Bioeng. 98:1123-1134.

Hebert EM, Raya RR, de Giori GS. (2004) Nutritional requirements of *Lactobacillus delbrueckii* subsp. lactis in a chemically defined medium. Curr. Microbiol. 49:341-345.

Hertzberger R, Arents J, Dekker HL, Pridmore RD, Gysler C, Kleerebezem M, de Mattos MJT. (2014) H_2O_2 production in species of the *Lactobacillus acidophilus* group: a central role for a novel NADH-dependent flavin reductase. Appl. Environ. Microbiol. 80:2229-2239.

Huang J, Schell M. (1995) Molecular characterization of the eps gene cluster of *Pseudomonas solanacearum* and its transcriptional regulation at a single promoter. Mol. Microbiol.16:977-989.

Hvorup RN, Winnen B, Chang AB, Jiang Y, Zhou XF, Saier MH. (2003) The

multidrug/oligosaccharidyl-lipid/polysaccharide (MOP) exporter superfamily. Eur J Biochem. 270:799-813.

Idris A, Suzana W. (2006) Effect of sodium alginate concentration, bead diameter, initial pH and temperature on lactic acid production from pineapple waste using immobilized Lactobacillus delbrueckii. Process Biochemistry 41:1117-1123.

John RP, Nampoothiri KM, Pandey A. (2007) Fermentative production of lactic acid from biomass: an overview on process developments and future perspectives. Appl. Microbiol. Biotechnol. 74:524-534.

Jones PG, Mitta M, Kim Y, Jiang W, Inouye M. (1996) Cold shock induces a major ribosomal associated protein that unwinds double-stranded RNA in *Escherichia coli.* Proc. Nat. Acad. Sci. 93:76-80.

Karunakaran E, Mukherjee J, Ramalingam B, Biggs CA. (2011) 'Biofilmology': a multidisciplinary review of the study of microbial biofilms. Appl. Microbiol. Biotechnol. 90:1869-1881.

Kubota H, Senda S, Nomura N, Tokuda H, Uchiyama H. (2008) Biofilm formation by lactic acid bacteria and resistance to environmental stress. J. Biosci. Bioengin. 106:381-386

Kumar MN, Gialleli A-I, Masson JB, Kandylis P, Bekatorou A, Koutinas AA, Kanellaki M. (2014) Lactic acid fermentation by cells immobilized on various porous cellulosic materials and their alginate/poly-lactic acid composites. Biores. Technol. 165:332-335.

Leary DH, Hervey WJ, Li RW, Deschamps JR, Kusterveck AW, Vora GJ. (2012) Method development for metaproteomic analyses of marine biofilms. Anal. Chem. 84:4006-4013.

Lewandowski Z, Beyenal H, Stookey D. (2004) Reproducibility of biofilm processes and the meaning of steady state in biofilm reactors. Water Sci Technol. 49:359-364.

Leyva LA, Bashan Y, Mendoza A, de-Bashan LE. (2014) Accumulation of fatty acids in *Chlorella vulgaris* under heterotrophic conditions in relation to activity of acetyl-CoA carboxylase, temperature, and co-immobilization with *Azospirillum brasilense*. Naturwissenschaften 101:819-830.

Litchfield JH. (1996) Microbiological production of lactic acid. Adv. Appl. Microbiol. 42:45

Licitra G, Ogier JC, Parayre S, Pediliggieri C, Carnemolla TM, Falentin H, Madec MN, Carpino S, Lortal S. (2007) Variability of bacterial biofilms of the "Tina" wood vats used in the ragusano cheese-making process. Appl. Environ. Microbiol. 2007;73:6980-6987.

Loose M, Mitchison TJ. (2014) The bacterial cell division proteins FtsA and FtsZ self-organize into dynamic cytoskeletal patterns. Nat. Cell Bio. 16:38-46.

Malik S, Petrova MI, Claes IJJ, Verhoeven TLA, Busschaert P, Vaneechoutte M, Lievens B, Lambrichts I, Siezen RJ, Balzarini J, Vanderleyden J, and Lebeer S. (2013) The highly autoaggregative and adhesive phenotype of the vaginal *Lactobacillus plantarum* strain CMPG5300 is sortase dependent. Appl. Environ. Microbiol. 79:4576-4585.

Marsili E, Baron DB, Shikhare ID, Coursolle D, Gralnick JA, Bond DR. (2008) *Shewanella* secretes flavins that mediate extracellular electron transfer. Proc. Nat. Acad. Sci. 105:3968-3973.

Martinez FAC, Balciunas EM, Salgado JM, Gonzalez JMD, Converti A, Oliveira RPS. (2013) Lactic acid properties, applications and production: a review. Trends Food Sci. Technol. 30:70-83.

Mitra S, Thawrani D, Banerjee P, Gachhui R, Mukherjee J. (2012) Induced biofilm cultivation enhances riboflavin production by an intertidally derived *Candida famata*. Appl. Biochem. Biotechnol. 166:1991-2006.

Montanaro L, Poggi A, Visai L, Ravaioli S, Campoccia D, Speziale P, Arciola CR. (2011) Extracellular DNA in biofilms. Int. J Artif. Org. 34:824-831.

Naves P, del Prado G, Huelves L, Gracia M, Ruiz V, Blanco J, Ponte Mdel C, Soriano F. (2008) Correlation between virulence factors and in vitro biofilm formation by *Escherichia coli* strains. Microb. Pathog. 45:86-91.

Nessler S, Fieulaine S, Poncet S, Galinier A, Deutscher J, and Janin J. (2003) HPr Kinase/Phosphorylase, the Sensor Enzyme of Catabolite Repression in Gram-Positive Bacteria: Structural Aspects of the Enzyme and the Complex with Its Protein Substrate. J. Bacteriol. 185:14 4003-4010.

Nicolella C, van Loosdrecht MCM, Heijnen JJ. (2000) Wastewater treatment with particulate biofilm reactors. J Biotechnol 80:1-33

O'Toole GA, Stewart PS. (2005) Biofilms strike back. Nat. Biotechnol. 23:1378-1379.

Park AJ, Murphy K, Krieger JR, Brewer D, Taylor P, Habash M, Khursigara CM. (2014) A temporal examination of the planktonic and biofilm proteome of whole cell *Pseudomonas aeruginosa* PAO1 using quantitative mass spectrometry. Molec. Cell. Proteom. 13:1095-1105.

Pascovici D, Handler DCL, Wu JX, Haynes PA. (2016) Multiple testing corrections in

quantitative proteomics: a useful but blunt tool. Proteomics. 16:2448-2453

Phillips AJ, Lauchnor E, Eldring J, Esposito R, Mitchell AC, Gerlach R, Cunningham AB, Spangler LH. (2012) Potential CO_2 leakage reduction through biofilm-induced calcium carbonate precipitation. Environ. Sci. Technol. 47:142-149.

Preuss M, Ott M, Funes S, Luirink J, Herrmann JM. (2005) Evolution of mitochondrial Oxa proteins from bacterial YidC: inherited and acquired functions of a conserved protein insertion machinery. J. Biol. Chem. 280:13004-13011.

Proc JL, Kuzyk MA, Hardie DB, Yung J, Smith DS, Jackson AM, Parker CE, Borchers CH. (2010) A quantitative study of the effects of chaotropic agents, surfactants, and solvents on the digestion efficiency of human plasma proteins by trypsin. J. Proteome Res. 9:5422-5437.

Pulido MR, Garcia-Quintanilla M, Gil-Marques ML, McConnell MJ. (2016) Identifying targets for antibiotic development using omics technologies. Drug Disc. Tod. 21:465-472.

Qureshi N, Annous BA, Ezeji TC, Karcher P, Maddox IS. (2005) Biofilm reactors for industrial bioconversion processes: employing potential of enhanced reaction rates. Microb. Cell Fac. 4:24.

Ram RJ, VerBerkmoes NC, Thelen MP, Tyson GW, Baker BJ, Blake RC, Shah M, Hettich RL, Banfield JF. (2005) Community proteomics of a natural microbial biofilm. Science 308:1915-1920.

Rangaswamy V, Ramakrishna SV. (2008) Lactic acid production by Lactobacillus delbrueckii in a dual reactor system using packed bed biofilm reactor. Appl. Microbiol. 46:661-666.

Reardon KF and Bailey JE. (1989) Effects of pH and Added Metabolites on Bioconversions by Immobilized Non-Growing *Clostridium acetobutylicum*. Biotechnol. Bioeng.1989;34:825-837.

Resch A, Leicht S, Saric M, Pasztor L, Jakob A, Gotz F, Nordheim A. (2006) Comparative proteome analysis of *Staphylococcus aureus* biofilm and planktonic cells and correlation with transcriptome profiling. Proteomics 6:1867-1877.

Rice SA, Wuertz S, Kjelleberg S. (2016) Next-generation studies of microbial biofilm communities. Microb. Biotechnol. 9:677-680.

Russo P, Capozzi V, Arena MP, Spadaccino G, Duenas MT, Lopez P, Fiocco D, Spano G. (2014) Riboflavin-overproducing strains of *Lactobacillus fermentum* for riboflavin-enriched bread. Appl. Microbiol. Biotechnol. 98:3691-3700.

Salas-Jara MJ, Ilabaca A, Vega M, Garcia A. (2016) Biofilm-forming *Lactobacillus*: new challenges for the development of probiotics. Microorganisms 2016;4(3):35.

Schlegel C, Chodorski J, Huster M, Davoudi N, Huttenlochner K, Bohley M, Reichenbach I, Buhl S, Breuninger P, Müller-Renno C, Ziegler C, Aurich J, Antonyuk S, and Ulber R. (2017) Analyzing the influence of microstructured surfaces on the lactic acid production of *Lactobacillus delbrueckii lactis* in a flow-through cell system. Eng. Life Sci. 17:865-873.

Sirisansaneeyakul S, Luangpipat T, Vanichsriratana W, Srinophakun T, Chen HH, Chisti Y. (2007) Optimization of lactic acid production by immobilized *Lactococcus lactis* IO-1. J. Ind. Microbiol. Biotechnol. 2007;34:381

Silva JC, Gorenstein MV, Li G-Z, Vissers JPC, Geromanos SJ. (2006) Absolute quantification of proteins by LCMSE: A virtue of parallel MS acquisition. Molec. Cell. Proteomics. 5:144-156.

Stewart EJ, Ganesan M, Younger JG, Soloman MJ. (2015) Artificial biofilms establish the role of matrix interactions in staphylococcal biofilm assembly and disassembly. Sci. 2015;5:13081.

Storey JD. (2002) A direct approach to false discovery rates. RSS Series B Statist. Method. 64:479-498.

Tremblay YDN, Deslandes V, Jacques M. (2013) *Actinobacillus pleuropneumoniae* genes expression in biofilms cultured under static conditions and in a drip-flow apparatus. BMC Genomics 14:364

Villegas E, Gilliland SE. (1998) Hydrogen peroxide production by Lactobacillus delbrueckii subsp. lactis I at 5 ºC. J. Food Sci. 63:1070-1074.

Wessler S, Schneider G, Backert S. (2017) Bacterial serine protease HtrA as a promising new target for antimicrobial therapy? BMC Cell Comm. Sig. 15:4.

Zhao G, Winkler ME. (1995) Kinetic limitation and cellular amount of pyridoxine (pyridoxamine) 5'-phosphate oxidase of *Escherichia coli* K-12. J Bacteriol. 177(4):883-91.

CHAPTER 3: KINETICS OF BULK CELL GROWTH AND QUANTITATIVE PROTEOMICS DESCRIBE AEROBIC METABOLISM IN MICROBUAL FUEL CELL BIOFILMS OF *S. ONEIDENSIS* MR-1

3.1 Introduction

Bioelectrical systems (BESs) represent an emerging technology for a variety of applications including generation of renewable energy [Jadhav et al. 2017; Wang and Ren 2013], electrosynthesis of products [Nevin et al. 2010; Lovley and Nevin 2013], and bioelectrochemical sensing [Kaur et al. 2013]. The defining feature of BES systems is the use of a conductive electrode as electron acceptor (or donor) by certain bacteria with capabilities for extracellular electron transfer (EET). The three primary mechanisms for EET include electron shuttling via soluble mediators such as flavins [Kotloski and Gralnick 2013; Okamoto et al. 2014], transfer through outer membrane proteins such as c-type cytochromes [Shi et al. 2009], and conveyance through conductive "nanowire" pilin proteins [Malvankar and Lovley 2013; Gorby et al. 2006]. Additionally, electrons may travel through a conductive biofilm matrix [Malvankar et al. 2012] or directly between different species in a mixed culture [Lovley 2017].

Utilizing all three primary mechanisms of EET, species in genus *Shewanella* are models for anaerobic respiration in environmental and BES systems [Newton et al. 2009; Hau and Gralnick 2007]. *Shewanella oneidensis* MR-1, the most well-characterized *Shewanella* species, is a gram-negative, facultative anaerobe in class Gammaproteobacteria that was originally isolated from freshwater lake sediment [Myers and Nealson 1988]. Critical features of electricity generation by *Shewanella* in BES

systems have been described thoroughly, including the function of different membrane cytochromes in EET [Shi et al. 2009], the electrochemical kinetics of EET itself [Carmon-Martinez et al. 2013; Pinto et al. 2017], the spatial structure of anode biofilms [McLean et al. 2008], and methods for genetic [West et al. 2017; Voeikova et al. 2013] or BES system engineering [Roy et al. 2012] to improve electricity production. No studies, however, have investigated the holistic physiology of *Shewanella* anode biofilms during electricity generation, compared with aerobic, non-electricity producing biofilms.

Global expression of transcripts, proteins, or metabolites is quantified most effectively by omics methods. Just a few studies, however, have taken an omics approach to studying the physiology of *Shewanella* in BES systems. Recently a targeted proteomics study of strictly anaerobic *S.oneidensis* MR-1 MFCs compared protein expression levels at different set electrode potentials, quantifying differences in abundance of proteins related to the tricarboxylic acid (TCA) cycle [Grobbler et al. 2017; Grobbler et al. 2015]. Another study took an iTRAQ approach to compare electricity-generating cells with planktonic cells to quantify the role of efflux pump TolC [Fowler et al. 2016]. In a transcriptomics study, planktonic *S. oneidensis* MR-1 cells were compared with anode biofilm cells generating electricity [Rosenaum et al. 2012]. That study observed upregulation of transcripts known to be important for EET, including transcripts for the *mtr* pathway. So far, however, no omics work has compared protein expression of *Shewanella* while generating electricity in a biofilm to that in a biofilm that is not generating electricity. Considering the recognized, dramatic differences in the physiology of bacteria living a in biofilm compared with that of planktonic cells [Donne and Dewilder 2015; Stewart and Franklin 2008], a biofilm-to-biofilm proteome

comparison is required to obtain a clear picture of the protein expression that is specific to electricity generation.

Here we applied label-free, shotgun proteomics to compare the physiology of two types of *S. oneidensis* MR-1 biofilms in a single-chamber, air-cathode MFC. In this type of BES, an anode biofilm respires anaerobically, utilizing the anode as electron acceptor. The electrons are conveyed to a cathode with a surface exposed to air, where they reduce oxygen to water [Liu et al. 2005]. In this MFC design the reactor body is a single chamber without a membrane separator; cells that detach from the anode into the bulk solution may attach to the cathode surface and form an aerobic biofilm. This aerobic biofilm consumes nutrients in the bulk solution aerobically, eventually resulting in loss of Coulombic efficiencies and power densities [Kiely et al. 2011]. The air-cathode MFC system therefore supports anaerobic and aerobic biofilms in the same reactor, thereby allowing for a direct comparison of differences in protein expression under identical bulk reactor conditions. With this approach we aimed to distinguish between proteins in the anode biofilm that are unique to electricity generation and proteins merely associated with a biofilm mode of life.

3.2 Experimental Procedures

3.2.1 Bacterial strains and medium

Shewanella oneidensis MR-1 (ATCC 700550) was routinely maintained on Luria-Bertani (LB) medium and agar plates. MR-1 inoculum for MFCs was grown aerobically in LB in 500 mL flasks (30°C, 200 rpm) to late log phase (OD ~3.0). Buffer for MFCs ("running buffer") contained 48.7 mM NaH_2PO4, 57.7 mM $Na_2HPO_4 \cdot 7H_2O$, 28 mM

NH_4Cl, 1.7 mM KCl, 3.4 mM $MgCl_2 \cdot 6H_2O$, 1 µM Na_2SeO_4 [Liu et al. 2005; Pinchuk et al. 2011]. After adjusting pH to 7.2 with NaOH and autoclaving, filter-sterilized $CaCl_2$ solution was added to 6.8 µM, along with 10 mL/L filter-sterilized trace mineral supplement (ATCC, Manassas, VA), 10 mL/L trace vitamin solution, and a filter-sterilized solution of yeast extract and tryptone (Difco, BD, Franklin Lakes, NJ) that resulted in a final concentration of 0.01% of each [von Canstein et al. 2007]. Filter-sterilized D,L-lactate was added to a concentration of 18 mM.

3.2.2 Microbial fuel cell construction and operation

An air-cathode MFC design was used, based on a previous design [Liu et al. 2005], with modifications. Autoclave-safe, polypropylene schedule 40 pipe (IPEX, Pineville, NC), cut into slices with width of 3.81 cm used as the reactor body. Anode material was non wet-proofed carbon cloth, while cathodes were constructed from 30% wet-proofed carbon cloth (Fuel Cell Earth, Woburn, MA). Four diffusion layers of a mixture of PTFE (Sigma-Aldrich, St. Louis, MO) and CV-XC72 carbon powder (Fuel Cell Earth, Woburn, MA) were applied to the exterior side of the cathode and heat-treated at 400°C for 30 minutes. A mixture of 0.75 mg platinum/cm^2 (Sigma-Aldrich, St. Louis, MO) and Nafion binder (Sigma-Aldrich, St. Louis, MO) was spread and dried on the solution side of the cathode as a catalyst for the cathode reaction. Anode and cathode were placed on opposite sides of the slice of polypropylene piping, such that the effective anode and cathode sizes were each 7.0 cm^2. Sheets of Lexan were cut into 10.2 cm x 10.2 cm squares, and aligned holes for screws were drilled into each corner of each Lexan square. A 7.0 cm^2 hole was cut in one Lexan sheet to allow air to diffuse to the interior side of the air-cathode. Plumbing gasket material was placed between the Lexan

square and the anode or cathode, to minimize leakage. Titanium wire (Wytech, Rahway, NJ) was used for the conductive leads. All layers of the MFCs were cinched together with the four screws at the corners of the reactor; due to the partially-flexible nature of Lexan, reactors could be tightened down to stop leakages.

Triplicate autoclaved MFCs were inoculated in a laminar flow hood with three milliliters of late-log MR-1 culture. The remaining volume of the MFCs were filled with running buffer, and leads were attached to a 5.5 kΩ external resistor (Elenco, Wheeling, IL). Voltage was recorded automatically across all replicate MFCs every five minutes with a 16-channel Picolog 1216 multimeter (Pico Technologies, Cambridgeshire, UK) connected to a personal computer. MFCs were inoculated for three successive batches, until a repeatable maximum voltage was observed, after which the cathode was changed to a fresh cathode and experiments were conducted by replacing all medium in batch mode. For experiments in which it was desired to have an initial OD_{600} in the MFC bulk solution greater than zero, solution from the previous batch was diluted with buffer to create the desired starting OD_{600}. Since MR-1 can use tryptone and yeast extract as carbon sources for electricity generation, polarization curves were run with and without the 0.01% medium supplement. Polarization curves were conducted by first allowing the MFC to reach a maximum voltage after medium replacement and then changing the external resistance stepwise (50-10,000 Ω), allowing the MFC to run 15-30 minutes at each external resistance level.

3.2.3 Bulk phase cell growth and analyte testing

Concentration of oxygen in the bulk solution of MFCs was measured by removing a 1 mL sample with a 1 mL syringe and needle and depositing the sample into a cuvette.

The probe from an OM-4 oxygen meter (Microelectrodes, Inc., Bedford, NH) was inserted into the sample after calibration of the sensor to 21% atmospheric oxygen. After subsequent measurement of optical density at 600 nm (OD_{600}), the sample was filtered and stored at -20°C. Organic acids in the samples were measured using a Shimadzu Prominence high performance liquid chromatography (HPLC) system equipped with a RID-10A refractive index detector and controlled by LCSolution 1.25 software. Organic acids were separated on an Aminex HPX-87H (Bio-Rad, Hercules, CA) column (300 mm × 7.8 mm, particle size 9 μm) in a mobile phase of 0.01 N sulfuric acid at a flow rate of 0.6 mL/min. The oven temperature was 65°C, and the analysis time was 20 min.

3.2.4 Protein harvest and digestion

At peak voltage generation, anode and cathode were removed and immediately frozen in liquid N_2, in 50 mL conical tubes, and stored at -80 °C until protein extraction. Anodes and cathodes were thawed on ice for 30 minutes and cut in half lengthwise. The entire biofilm was scraped from each anode and cathode half using a sterile razor blade. The anode or cathode and its scraped material was placed in hot (95°C) lysis buffer (50 mM ammonium bicarbonate, 1% sodium deoxycholate (SDC), pH 8.2) and sonicated (50% duty cycle) for one minute, one second on, two seconds off. The mixture was cooled to room temperature and the sonication cycle was repeated. The samples then were subjected to a freeze-thaw cycle by placing into liquid N_2. After thawing in a hot water bath (95°C), the samples were sonicated again. Samples were centrifuged (5000 x g, 10 minutes) and the supernatant was isolated to a siliconized tube, which was centrifuged (14,000 x g for 20 minutes) to remove remaining cell debris.

Protein concentration of the supernatant was quantified by BCA assay (Pierce Thermo Scientific, Waltham, MA). An appropriate volume for 100 µg of protein was combined with 10% (v/v) 100 mM dithiotreitol and proteins were denatured at 60°C for 20 minutes. Five microliters of 375 mM iodoacetamide were added to each sample for cysteine alkylation at room temperature in the dark for 40 minutes. Then 0.5 µL of 50 mM $CaCl_2$ was added, along with five micrograms of Promega Gold mass spectrometry grade trypsin (Promega, Fitchburg, WI). Acetonitrile was added to result in a final concentration of 9% ACN. Digestion reactions progressed at 38°C for 12 h, after which an addition 1 ug of trypsin was added and the digestion reaction was allowed to continue for 1 h. Digestion reactions were stopped by adding 100% formic acid to decrease pH to ~2. Digestions were centrifuged (13,000 x g, 20 minutes) to collect SDC that precipitated with the drop in pH. A volume containing 20 µg peptides was evaporated and the resulting peptide pellets (transparent for anode samples, yellow for cathode samples) were resuspended in 20 µL equilibration solution and residual detergent and contaminants were removed with a C-18 spin column (Pierce Thermo Fisher, Madison, WI), following the manufacturer's instructions. Eluted peptides were evaporated to dryness and resuspended in 3% acetonitrile, 0.1% formic acid for LC-MS/MS analysis.

3.2.5 ESI-LC-MS/MS sample analysis

Two micrograms of resuspended peptides were loaded onto a C18 trap (200 um ID, 0.5 mm length, 120 A, Eksigent Technologies). A 2%~80% gradient of acetonitrile with 0.1% formic acid was used to elute the peptides from the trap and column (C18, 75 um ID, 150 mm length, 120 A, Eksigent Technologies) at a flow rate of 300 nL/min. Peptides were eluted into the electrospray ionization source of an ABSciex TripleTOF

5600 (Danahar, Washington D.C., USA). Up to 50 MS^2 scans followed each MS^1 scan, according to the order of intensity. Two technical replicate LC-MS/MS shots were run for each biological replicate MFC anode or cathode.

3.2.6 Protein identification, quantification, and statistical analysis

Acquired MS data (.wiff files from Analyst v.1.5 TR) were processed with ProteinPilot (v.4.5 beta), using a .fasta database consisting of the entire *S.oneidensis* MR-1 proteome (www.uniprot.org) without isoforms. The search was conducted in ProteinPilot using rapid search ID and no biological modifications. False discovery rate (FDR) was calculated with a decoy database consisting of reversed sequences from the target database, with FDR protein identification significance threshold ≤ 0.01. All .wiff files (technical replicates and biological replicates) were searched simultaneously. The intensities of precursor ions for the top three peptides associated with each identified protein [Silva et al. 2006] were summed with a quantitation microapp (v. 1.0) in PeakView software (v. 1.1.1, ABSciex). Previous studies have noted linear correlation between the precursor ion intensities of the top three peptides for a protein and the abundance of that protein in the original sample [Silva et al. 2006].

Data normalization and assessment of summary statistics were conducted using R statistical package (v. 3.1.2). The raw, summed precursor ion intensity values were $\log_2$-transformed and the median value of the technical replicate was subtracted from each $\log_2$-transformed value. Data reproducibility was assessed by coefficient of variance (CV) plots of raw and normalized intensity values, across each technical replicate. The mean was calculated for each protein across two technical replicate LC-MS/MS shots to generate a normalized intensity value for that protein in each biological replicate.

Transformed, normalized mean intensity values for each protein were used for paired t-test hypothesis testing between anode and cathode of three replicate MFCs. A q-value multiple hypothesis testing approach was used [Storey 2002]. Q-values were calculated with the qvalue package in R, using the total list of p-values generated by paired t-tests between anode and cathode for each MFC reactor. Proteins with q-value < 10% were considered significant between anode and cathode. All of the proteins identified as significant also met the customary criterion for differential expression: ($\log_2$(co-culture/pure culture) $\leq$ -1 for proteins less abundant in the anode biofilm or $\log_2$(co-culture/pure culture) $\geq$1 for proteins more abundant in the co-culture. Significant proteins more abundant in the anode biofilm were searched, mapped and annotated with Blast2GO software v.2.8 (www.blast2go.org). KEGG maps were obtained and used to identify pathways containing more and less abundant proteins.

3.3 Results and Discussion

3.3.1 MR-1 air-cathode MFC performance characteristics

A polarization curve on current generation with 18 mM lactate and 0.01% of tryptone/yeast extract supplement resulted in a maximum power density of 0.08 ± 0.01 W/m^2 of anode surface area at a current density of 0.18 ± 0.01 A/m^2, using an external resistance (R_{ext}) of 3.3 kΩ (Figure 5). In subsequent experiments an external resistance of 5.5 kΩ was used, in order to increase the batch time to measure dissolved oxygen (DO) and bulk OD_{600}. When the MFC medium was replaced, current increased immediately, peaking after two hours and then declining over the rest of the batch (Figure 6a). Within the first half-hour after medium replacement, DO in the bulk solution decreased by 50% from ~8% O_2 to 4% O_2 (Figure 6b). By 20 h into the batch, lactate in

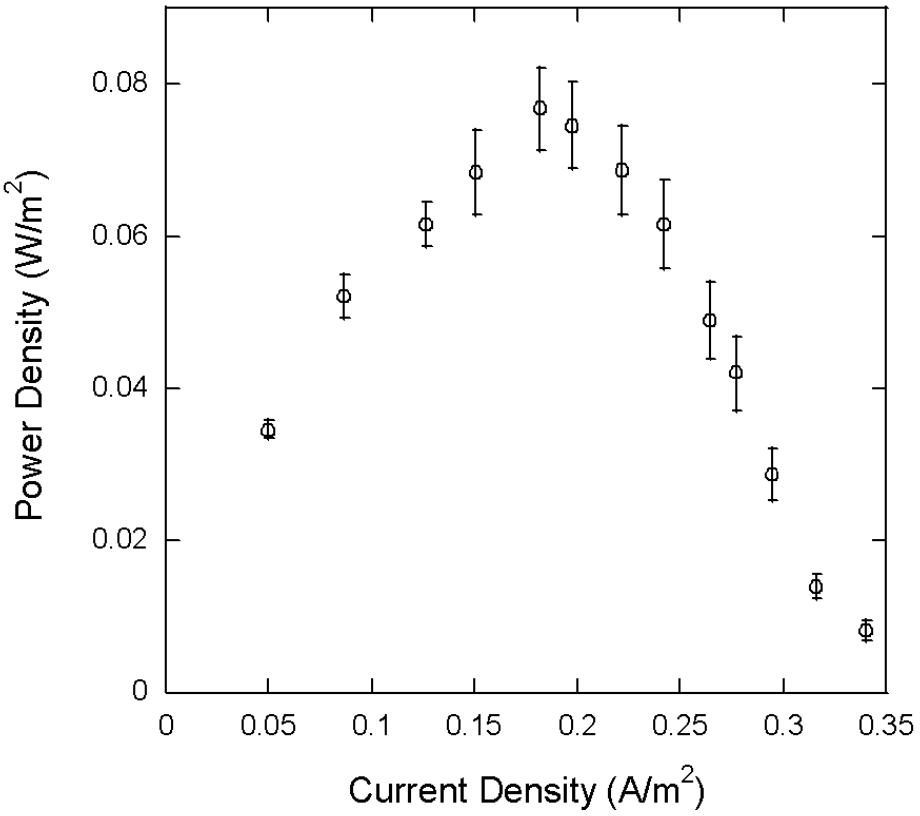

Figure 5: Polarization curve of MR-1 MFCs operating on 18 mM lactate as carbon source, with 0.01% yeast extract and 0.01% tryptone supplement. Maximum power density was achieved at an external resistance of 3.3 kΩ.

the medium was depleted, after which current density decreased precipitously. Acetate was detected in the bulk solution only at 5.5 h, after which no acetate was observed. In contrast to a previous study that observed improvement in MR-1 MFC performance over multiple batches in air-cathode MFCs (Watson and Logan 2009), here a 74.5% decrease in maximum current density was observed over the course of nine successive batches of three replicate MR-1 air-cathode MFCs (Figure 7). Previously, decreases in single-

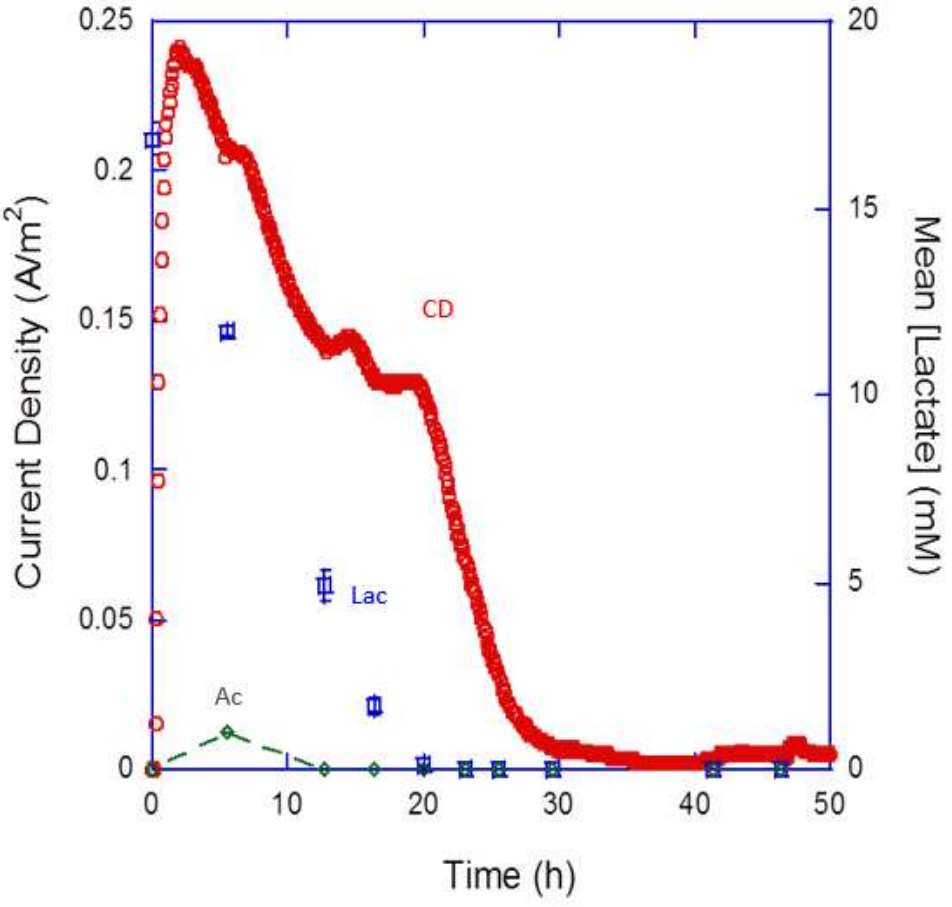

Figure 6a: Change in current density (CD) and concentrations of lactate (Lac) and acetate (Ac) in bulk MFC solution over the course of a batch. Current density from one representative replicate of three replicate MFCs is shown. For organic acids, each data point is the mean of three replicate MFCs and error bars represent the standard deviation across those replicates.

chamber MFC performance over multiple batches have been attributed to competitive use of nutrients by biofilms growing aerobically on the surface of the air-cathode [Kiely et al. 2011]. Here, replacement of the MFC cathode increased maximum current density by

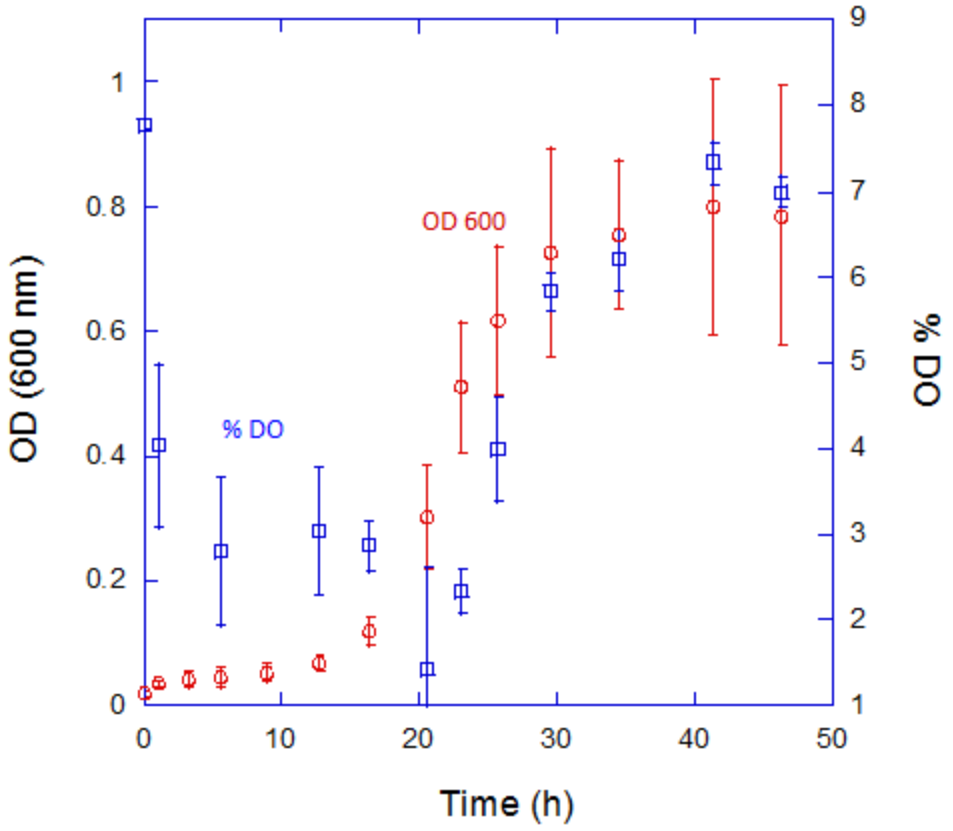

Figure 6b: Change in OD (600 nm) and dissolved oxygen (%DO) over the course of a MFC batch after anode biofilm enrichment and cathode replacement. Each data point is the mean of three replicate MFCs and error bars represent the standard deviation across those replicates.

nearly 560% for one batch, after which the performance immediately decreased again to previous low levels (Figure 8). It is unlikely that any cathode biofilm formed during the first batch after cathode replacement could compete sufficiently with anode current generation to cause the rapid decrease in maximum current density in subsequent batches with the new cathode. Rather, the cathode-replacement experiments suggest that electricity production by the anode biofilm itself had been degraded, perhaps due to intrusion of oxygen or the sustained stress of electricity generation over multiple batches (see section 3.3.7 below).

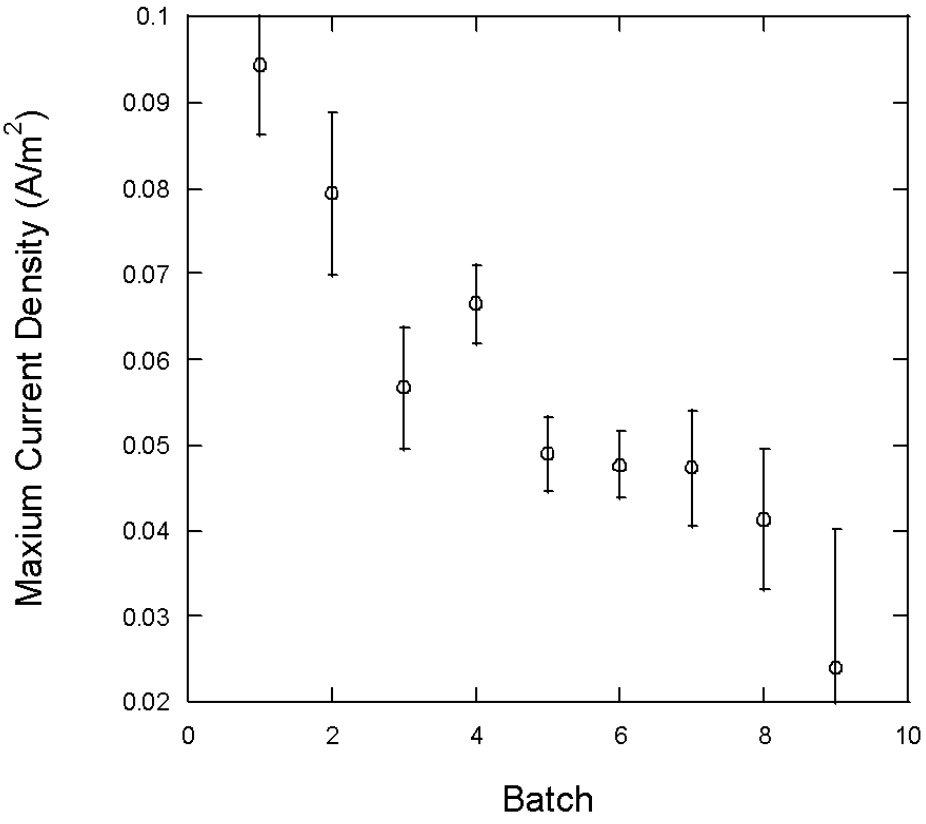

Figure 7: Decrease in maximum current density achieved over the course of multiple batches of *S. oneidensis* MR-1 air-cathode MFCs. Medium consisted of 18 mM lactate with 0.01% tryptone and 0.01% yeast extract. Medium in batch 4 was replaced before allowing the voltage of the previous batch to decrease to a zero-point. Error bars represent standard deviation across three replicate air-cathode MFC reactors.

3.3.2 Growth kinetics of anode and bulk solution cells

During the first 10 hours after replacing the MFC medium, the OD_{600} of the bulk solution increased slowly (Figure 6b). Similarly, an increase in OD_{600} was observed when all carbon sources (lactate, yeast extract, and tryptone) were removed from the medium (Appendix SI 3.1: Figure S9). The lack of carbon source and high variability in

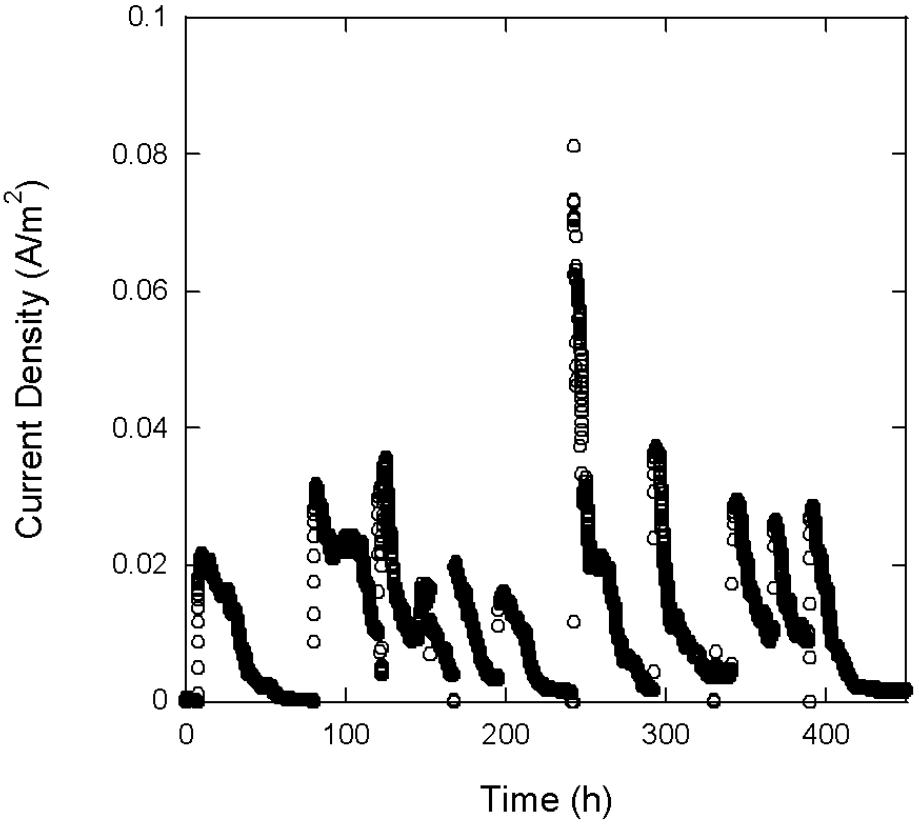

Figure 8: Voltage for *S. oneidensis* MR-1 MFC before and after cathode replacement. Maximum current density increased to >0.08 A/m^2 for the first batch after replacing the cathode with an unused cathode, after which it returned back to the lower levels observed prior to cathode replacement.

OD_{600} readings suggests that the increase in OD_{600} during this initial period was due to detachment of cells from the anode biofilm rather than growth of bulk cells. After approximately 10 hours, however, bulk OD_{600} began increasing exponentially with a specific growth rate of 0.19 ± 0.02 h^{-1}. While DO had dropped directly after medium replacement, it dropped further as bulk OD_{600} entered exponential growth, reaching a low point of < 2% (Figure 6b). Since there were few cells in the bulk solution or attached to the cathode at the beginning of the batch due to rinsing out the MFC and replacing the cathode, the immediate drop in DO after replacing the medium likely was due to DO

consumption by anode biofilm cells. The delay in the onset of exponential growth of planktonic cells that were inoculated into the MFC reactor in the presence of an anode (Appendix SI 3.1: Figure S10) is consistent with competition for DO by anode cells. It is unclear, however, the extent to which the consumption of DO by anode cells enhanced or degraded current generation. Previous work has shown that the presence of oxygen can improve the performance of MR-1 in MFCs, due to increased biomass production and closing of redox balances [TerAvest et al. 2013; Rosenbaum et al. 2010; Biffinger et al. 2008]. The use of oxygen as an electron acceptor by anode biofilm cells, however, also decreases Coulombic efficiency (CE) [Rosenbaum et al. 2010] by diverting electrons to aerobic respiration that otherwise would enter the MFC circuit. Here, the initial spike in current density immediately after medium replacement appeared to align with consumption of DO, suggesting that depletion of DO contributed to the leveling off and decline in current density (Figures 6a and 6b). The decrease in maximum current density over several batches observed in the present study, however, is consistent with an increasing proportion of anode biofilm cells switching to aerobic respiration (section 3.1). It seems unlikely, therefore, that in the present study the current density was limited by low DO due to DO consumption at the beginning of the batch. Rather, current density more likely was limited by independent factors such as diffusion of lactate through the anode biofilm, internal resistance, or cathodic limitations [Lee et al. 2009; Fan et al. 2008; Rismani-Yazki et al. 2008].

An increase in DO beginning at ~20 hours coincided with mid-exponential growth of planktonic cells in the bulk solution as well as with both the depletion of lactate and a final sharp decrease in current density (Figures 6a and 6b). The increase in

DO continued as OD_{600} increased further, eventually returning to approximately the starting DO by the end of the batch. This increase in DO was unexpected: growth of planktonic cells in the bulk solution was assumed to be aerobic, since facultative bacteria like MR-1 generally prefer to utilize oxygen as electron acceptor when it is available [Morris and Schmidt 2013; Dawood et al. 1998]. It is possible that planktonic cells were using soluble redox mediators [von Canstein et al. 2007; Lanthier et al. 2008] for growth in the bulk solution, though in that case a less precipitous drop in current density during that period (20-30 h) might be expected as reduced redox compounds are oxidized at the anode. Regardless, whether aerobic or anaerobic, growth of planktonic cells after 20 hours must have occurred using a stored energy source or degraded organic material from the biofilm, since lactate was depleted by that point. With the depletion of lactate, aerobic respiration of planktonic (and anode) cells would have slowed enough that DO could accumulate in solution as the bulk solution was mixed.

The kinetics of growth of planktonic cells in the bulk solution of air-cathode MFCs are important for overall MFC performance in a number of ways. As described above, the more substrate consumed by bulk cells, the lower the CE. Furthermore, bulk cells attach to the air-cathode surface and eventually foul it with aerobic biofilm. This cathode biofilm consumes nutrients in the medium, further reducing CE and maximum current density [Kiely et al. 2011]. Cells in the bulk solution originate from the anode biofilm, detaching due to agitation or in response to microaerobic conditions of the solution [Thormann et al. 2004]. Quantifying the detachment rates of anode bacteria could be useful for determining operational parameters (e.g., agitation rates) that minimize anode biofilm detachment. Similarly, in a continuous flow MFC, anode

biofilm detachment rates could suggest dilution rates that wash out bulk cells before they can attach to the cathode. Since decreasing MFC retention time eventually also will decrease substrate usage efficiency, future experiments with continuous MFCs should identify the range of retention times at which anode detachment, bulk growth, and cathode biofilm attachment and detachment each occur. The density of bulk cells could be used as an indicator of the dilution rate at which anode cells begin to detach and grow in the bulk solution, thereby initiating cathode fouling and losses in CE. This range will change based on MFC parameters such as biofilm species, influent characteristics, and reactor configuration; operational strategies to minimize bulk growth and cathode fouling ultimately will improve power generation, CE, and consistency of MFC performance.

3.3.3 Summary of MR-1 comparative biofilm proteomics results

A proteomics approach was taken to quantify differences in physiology between MR-1 generating electricity and growing aerobically. In contrast to previous work that compared anode biofilm protein expression with protein expression of cells in a planktonic culture [Fowler et al. 2016; Rosenbaum et al. 2012], here anode biofilm was compared with biofilm growing aerobically on the cathode. Biomass on the cathode was considerably more robust than on the anode; specific protein yield from the cathode was four times greater than that from the anode (Appendix SI 3.1: Figure S11). Of the 308 quantified proteins that were in common between anode and cathode, 44 and 33 proteins were significantly more and less abundant, respectively, in the anode biofilm compared with the cathode biofilm. Many of the proteins previously shown to be associated with electricity generation in MR-1 (e.g., the Mtr system, conductive pili, and outer membrane cytochromes) are membrane- bound or surface proteins [Bouhenni et al. 2010].

Similarly, though many non-membrane proteins were identified, more than 86% (39/44) of the proteins that were significantly more abundant in the anode biofilm were membrane-associated proteins. The use of sodium deoxycholate (SDC) detergent during protein extraction may have contributed to enrichment of membrane proteins [Proc et al. 2010].

Since the purpose of this study was to characterize proteins uniquely related to current generation by MR-1 biofilms, analysis focused on proteins significantly more abundant in the anode biofilm. The significantly more proteins in the anode biofilm were analyzed according to Gene Ontology (GO) level 3 and level 4 categories using Blast2GO software (www.blast2go.com) (Figures 9a and 9b). The level 3 categories with the greatest number of protein associations included: single-organism cellular process, establishment of localization, and response to stimulus. Additional "response" categories included response to stress, response to external stimulus, and response to a chemical. At the level 4 GO domain, categories with abundant protein assignments included transport, taxis, oxidation-reduction process, and cell communication. Categories for carbohydrate derivative metabolic process and polysaccharide localization also were represented, suggesting more active synthesis of biofilm exopolysaccharide (EPS) in a still-developing anode biofilm compared with a more mature, aerobic cathode biofilm.

3.3.4 Significantly more abundant proteins in the anode relevant to current generation

When ProteinPilot database searches were conducted on each biological replicate MFC anode individually, protein Q8ED60 (SO_2907) was the top ranked protein for each

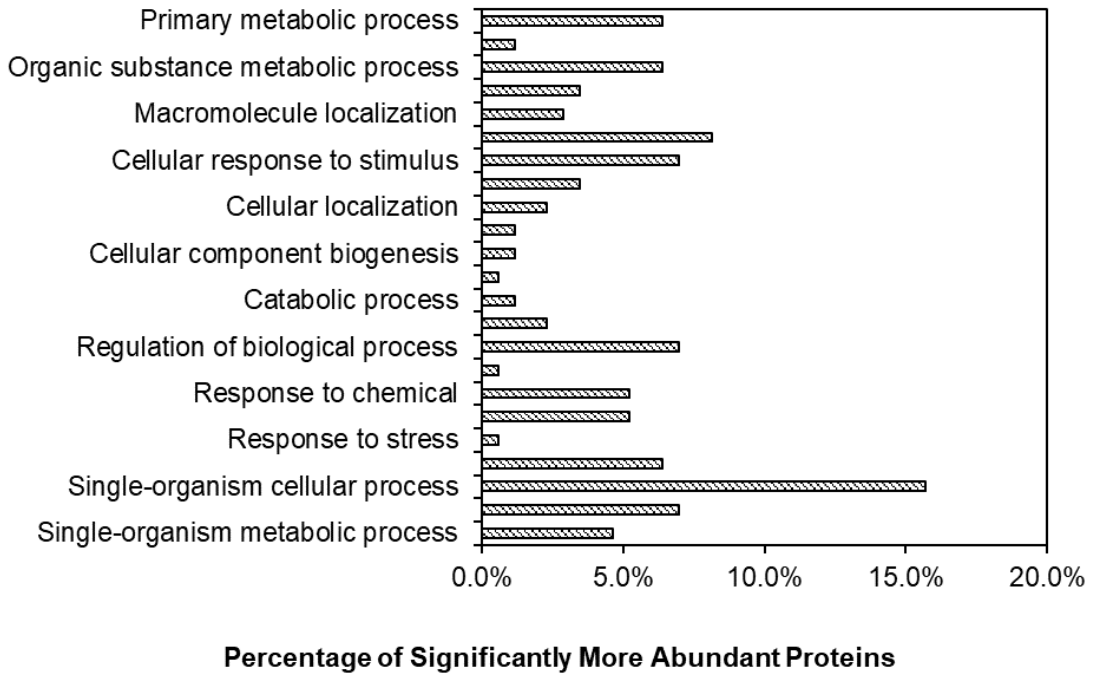

Figure 9a: Blast2GO distribution into GO level 3 categories of proteins significantly more abundant in anode compared with cathode biofilm cells.

replicate anode (highest ProteinPilot "Unused" score and high number of 95% confidence peptides). A previous study suggested that Q8ED60 is essential for dissimilatory iron reduction by MR-1 [Qian et al. 2011], but no investigations of Q8ED60 have been conducted in connection with current generation in MFCs. While this protein, a putative TonB-dependent receptor protein, was identified in two of the three cathode biological replicates, it had a very low "Unused" score and no peptides with >95% confidence in those samples. Therefore, Q8ED60 abundances could not be compared between anode and cathode since it was barely detected in the cathode samples at all. Nevertheless, the strong showing of Q8ED60 among proteins from each anode biofilm and its nearly

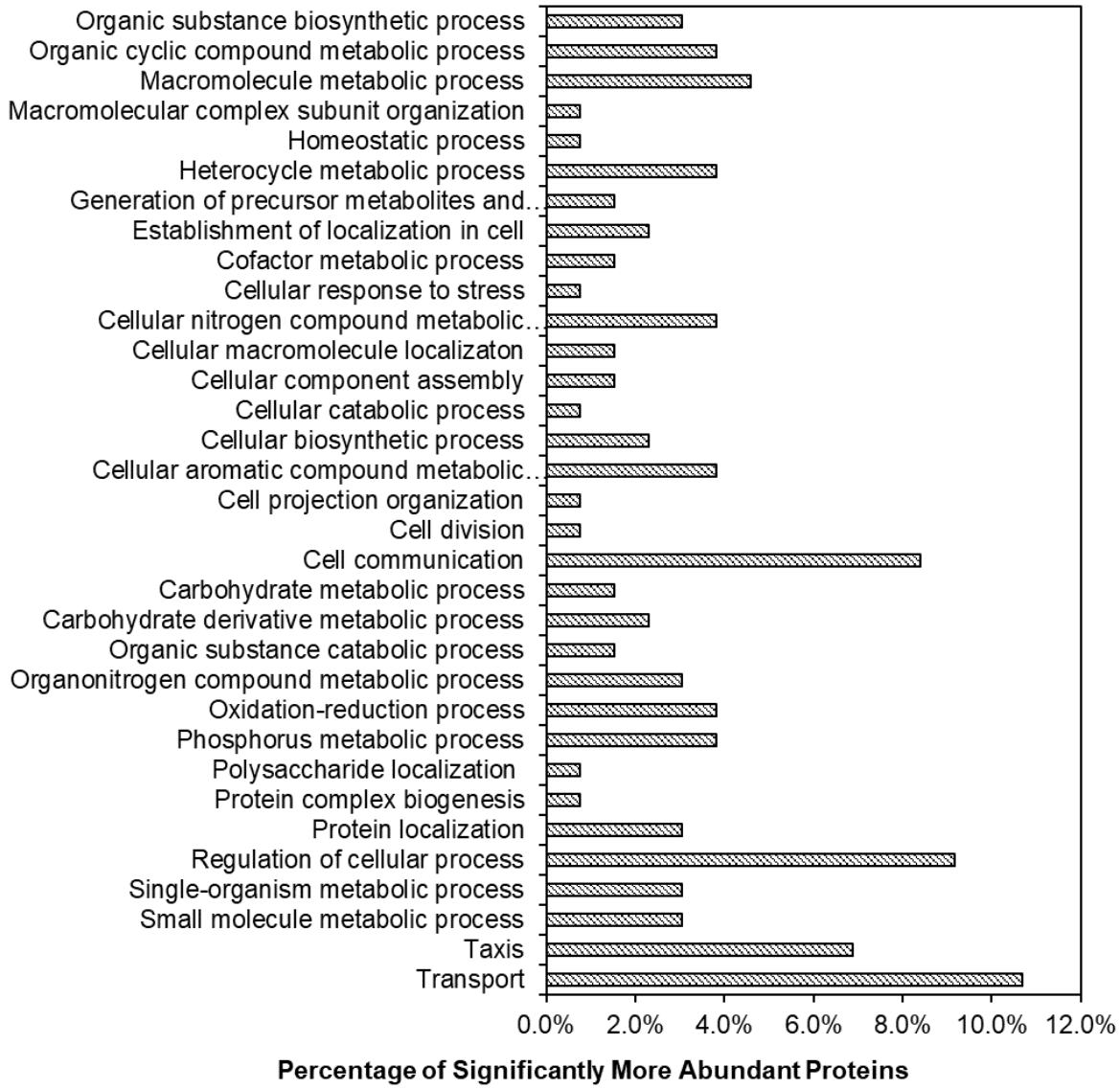

Figure 9b: Blast2GO distribution into GO level 4 categories of proteins significantly more abundant in anode compared with cathode biofilm cells.

complete absence in the aerobic cathode samples strongly suggest that this protein is important for current generation. TonB proteins interact with TonB-dependent receptors to facilitate active transport into the periplasmic space of solutes such as iron-siderophore complexes or vitamin B12 that either are present in very low concentration outside the cell or are poorly-transported across non-specific porins [Postle et al. 2003; Koebnik et

al. 2000]. It is possible that during any sort of anaerobic respiration, including respiration of a MFC anode, MR-1 engages a TonB-dependent receptor system to detect anaerobic electron acceptors. Two other TonB proteins were significantly more abundant in the anode biofilm, including an outer membrane signaling receptor (Q8EEF5) (Table 2).

Several cytochrome or cytochrome-associated proteins related to current generation by MR-1 were identified among anode biofilm proteins. All proteins in the Mtr system for extracellular respiration were detected. Decaheme c cytochromes MtrA and OmcA as well as porin MtrB, each of which are essential for extracellular electron transfer [Coursolle et al. 2010; Bretschger et al. 2007], were significantly more abundant in the anode biofilm (Table 2).

Table 2: Proteins identified in both anode and cathode biofilms that were significantly more abundant (q<0.1) in the anode biofilm

Uniprot ID	Protein Name	Log2(An/Cath)	q-value
	Taxis or Chemotaxis		
Q8E8U9	Methyl-accepting chemotaxis protein with Cache sensory domain	2.5	0.043
Q8E939	Energy taxis-modulating methyl-accepting chemotaxis protein with Cache_1 sensory domain	4.5	0.059
Q8EHE5	Chemotaxis signal transduction system methyl accepting sensory transducer	3.8	0.033

Q8EHZ8	Methyl accepting sensory transducer with Cache_1 small molecule binding domain	3.2	0.061
Q8EEX1	Energy taxis modulating methyl accepting sensory transducer with Cache_2 sensory domain	4.3	0.074
Q8EAQ8	Chemotaxis signal transduction system methyl accepting sensory transducer	3.2	0.062
Q8EI62	Methyl accepting sensory transducer with Cache_2 small molecule binding domain	3.4	0.061
Q8E837	Methyl-accepting chemotaxis protein	2.9	0.078
Q8ECT0	Methyl-accepting chemotaxis protein	4.2	0.033
	Stress or Virulence		
Q8E8H1	Proton-coupled multidrug efflux pump MFP component VmeA	1.4	0.043
Q8EHK6	Nucleoside-specific outer membrane porin OmpK	4.1	0.090
Q8EAX2	Adenylate cyclase YgiF (EC 4.6.1.1)	4.1	0.043
Q8ECG4	Polysaccharide deacetylase	1.8	0.043
Q8EGN2	Outer membrane protein YfaZ	2.3	0.059
Q8EC05	Small conductance mechanosensitive ion channel protein MscS	4.0	0.065
	Respiration		

Q8EJ62	Ubiquinol-cytochrome c reductase cytochrome c1 subunit PetC (EC 1.10.2.2)	4.5	0.061
Q8E8J8	Diheme cytochrome c4 CytcB	3.9	0.078
Q8EFY9	TonB2 energy transduction system inner membrane component TtpC	4.9	0.065
Q8EAZ6	NAD(P) transhydrogenase subunit beta (EC 1.6.1.2) (Nicotinamide nucleotide transhydrogenase subunit beta)	4.0	0.090
Q8EG33	Extracelllular iron oxide respiratory system surface decaheme cytochrome c component OmcA	4.3	0.042
Q8EG35	Extracelllular iron oxide respiratory system periplasmic decaheme cytochrome c component MtrA	2.6	0.078
Q8EK36	Cytochrome c maturation system membrane anchored thioredoxin CcmG	2.7	0.078
Q8EAK6	Outer membrane porin Omp35	6.1	0.083
Q8CVD4	Extracellular iron oxide respiratory system outer membrane component MtrB	1.1	0.085
Q8EC58	Cytochrome d ubiquinol oxidase subunit I CydA (EC 1.10.3.-)	4.4	0.059
Q8CX36	Putative negative regulator of univalent cation permeability	2.1	0.043

	Biofilm Development		
Q8ECG4	Polysaccharide deacetylase	1.8	0.043
Q8ECE9	Outer membrane polysaccharide export channel protein Wza	3.3	0.036
Q8ECN7	Outer membrane long-chain fatty acid receptor FadL family	2.9	0.074
	Other		
Q8CMJ0	Putative surface lipoprotein	2.3	0.085
Q8ECN5	Uncharacterized protein	2.0	0.043
Q8EGP9	Flap endonuclease Xni (FEN) (EC 3.1.-.-)	3.7	0.059
Q8ECM6	Protein-export membrane protein SecF	4.3	0.064
Q8EAX9	Uncharacterized protein	1.6	0.083
Q8EGM9	Bifunctional DNA-binding protein / oxidoreductase	2.2	0.061
Q8E999	von Willebrand factor type A domain protein	3.3	0.074
Q8EA04	MSHA major pilin subunit MshA	5.4	0.090
Q8ECM4	SecDF preprotein translocase-associated protein YajC	3.4	0.078
Q8EKI3	Zn-dependent protease with chaperone function	2.9	0.064
Q8EH82	Signal peptidase I (EC 3.4.21.89)	4.3	0.078
Q8EA03	MSHA minor pilin protein MshB	1.5	0.078
Q8CVD3	Periplasmic [Ni-Fe] hydrogenase small subunit HyaA (EC 1.12.7.2)	1.8	0.088

	ATP-dependent zinc metalloprotease FtsH (EC		
Q8EHM2	3.4.24.-)	1.2	0.043
Q8EEF5	ArgR-regulated TonB-dependent receptor	2.8	0.078

Decaheme c cytochrome MtrC, another component of the Mtr pathway, was identified in all three anode biofilm replicates but not in any cathode biofilm replicates, suggesting that it is uniquely expressed in anode biofilms. CymA was identified but not judged significantly more abundant in the anode biofilm. Other cytochrome-related proteins that were significantly more abundant in the anode biofilm included a cytochrome c maturation (ccm) factor protein CcmG, part of the ccm pathway shown to be essential for anaerobic respiration of dissimilatory electron acceptors such as cobalt [Bouhenni et al. 2010; Hau and Gralnick 2007], as well as a diheme cytochrome c4 CytcB protein involved in anaerobic respiration [Kadziola and Larsen 1997].

Several non-cytochrome proteins associated with current generation by MR-1 also were identified. While not strictly essential for current generation, structural proteins of the Msh pilin nanofilament provide a mechanism of electron transfer across the cell membrane [Pirbadian et al. 2014]. Major and minor Msh pilin subunits (MshA and MshB, respectively) were both significantly more abundant in the anode biofilm; MshA was the protein with the second-greatest upward $\log_2$-fold-change in the anode biofilm (Table 1). MshG, a MshA-biogenesis protein associated with the base structure of the Msh system [Fitzgerald et al. 2012], also was identified in two anode biofilm replicates and one cathode biofilm replicate but not judged to be significant. The flavin mechanism for current generation [Marsili et al. 2008; von Canstein et al. 2007] was not well-

represented among significantly more abundant anode proteins. Just one protein associated with flavins was identified in this study; a NAD(P)H:flavin oxidoreductase (SYE4) responsible for riboflavin reductase activity was identified in one of the MFC anode biofilms, but it was not judged to be significant between anode and cathode. No proteins associated with conductive nanowires in the Pil system were identified among either the anode or cathode biofilm proteins, perhaps due to microaerobic conditions. Omp35 (Q8EAK6) also was identified as significantly more abundant in the anode biofilm, with the greatest increase in abundance in the anode, compared with the cathode (log_2-fold change = 6.1). This outer membrane porin is known to be necessary for high rates of anaerobic respiration with fumarate, nitrate, or Fe(III) as electron acceptor, though the mechanism of its action is not clear [Maier and Myers 2004]. Differentially greater expression of Omp35 during growth on an insoluble anode supports the conclusion that this porin is not responsible for transport of dissimilatory electron acceptors. Finally, a periplasmic hydrogenase subunit HyaA (Q8ECO5) was significantly more abundant in the anode biofilm than in the cathode biofilm. A previous study reported NiFe hydrogenase HyaAB as the dominant hydrogenase in the process of reduction of metals as electron acceptors coupled to oxidation of the electron carrier H_2 [Marshall et al. 2008]. Similarly, HyaAB has been shown to produce H_2 from pyruvate in stationary-phase MR-1 without an electron acceptor present [Meshulam-Simon et al. 2007]. While several reports have investigated the capacity of MR-1 to reduce metals or an electrode with electrons from H_2 (free or derived from organic acids [Biffinger et al. 2008] the present study offers the first suggestion of a role for HyaAB dehydrogenase in H_2 production during electricity generation.

3.3.5 TCA cycle proteins

Several proteins associated with the TCA cycle were observed among anode proteins, including GltA and PrpC, two enzymes with citrate synthase activity. GltA catalyses the first step in the oxidative branch of an incomplete anaerobic TCA cycle that generates α-ketoglutarate for glutamate biosynthesis and succinyl-CoA for lysine biosynthesis [Brutinel and Gralnick 2012]. GltA was also identified in each replicate cathode biofilm, while PrpC was not found in any cathode biofilm. This observation is consistent with previous suggestions that PrpC engages in citrate synthase activity only under anoxic conditions [Brutinel and Gralnick 2012]. It is not clear, however, why both GltA and PrpC should be expressed by anode biofilm cells. In a minimal medium it might be expected that anode biofilm cells would require both enzymes to synthesize sufficient quantities of glutamate. But in the medium used in this study, exogenous glutamate was available in the tryptone/yeast extract supplement in the medium. Another possibility is suggested by the detection of SucB in the anode biofilm proteins. SucB is part of the SucB α-ketoglutarate dehydrogenase complex that catalyzes the conversion of α-ketoglutarate to succinyl-CoA in the TCA cycle. Previous studies have shown a reduction in transcription of the *sucB* gene under anoxic conditions, suggesting that succinyl-CoA is generated only in the reductive branch of the TCA cycle [Beliaev et al. 2002]. Other studies have argued instead that SucB is part of an alternate route to generate succinyl-CoA via the oxidative branch of an incomplete anaerobic TCA cycle in MR-1 [Brutinel and Gralnick 2012]. While not identified in cathode biofilms in the present study, the identification of SucB in the anode biofilm suggests either (i) production of succinyl-CoA by SucAB under anoxic conditions or (ii) engagement of the

complete TCA cycle with oxygen as electron acceptor. In the case of option (i), the extra carbon required to produce both succinyl-CoA (for lysine) and α-ketoglutarate (for glutamate) through the oxidative branch of the TCA cycle may explain why both GltA and PrpC are expressed under anaerobic conditions. On the other hand, option (ii) supports the interpretation of growth results (sections 3.3.1 and 3.3.2 above) that some cells in the anode biofilm have transitioned to aerobic respiration, using DO that has intruded into the MFC bulk solution. Furthermore, succinate dehydrogenase subunits SdhA and SdhB were both identified in the anode biofilm with $\log_2$-fold-change greater than 1, though the q-value for each was not significant. Since Sdh is part of the complete (aerobic) TCA cycle, the identification of these proteins in the anode biofilm supports option (ii). However, Sdh is also part of the microbial electron transport chain and as such it may be expressed even if it is not part of an aerobic TCA cycle. These proteomics results therefore do not allow for a definitive decision between options (i) and (ii) for interpreting the role of these TCA proteins in anode cells. These results do suggest, however, new roles for TCA proteins in electricity-producing MR-1 biofilms. The engagement of TCA proteins by MR-1 anode cells may be part of the explanation for previously-noted improvements in electricity generation by MR-1 in the presence of oxygen [Lanthier et al. 2008; Biffinger et al. 2008]. Future work could address questions of which components of the TCA cycle are engaged during electricity generation and how TCA involvement might improve anode usage from an energetics perspective.

3.3.6 Taxis and biofilm formation proteins

The role of taxis proteins in the process of shifting from a planktonic to biofilm mode of life in bacteria is well-documented [Guttenplan and Kearns 2013; Schweinitzer

and Josenhans 2010]. In the present study taxis proteins were highly enriched among the proteins significantly more abundant in the anode compared to the cathode. Nine (~14%) of the proteins significantly more abundant in the anode biofilm were related to taxis or chemotaxis, including two "energy taxis"-modulating, methyl-accepting chemotaxis proteins with cache sensory domains. One of the latter proteins, Q8EEX1, has been shown to be necessary for full energy taxis response to a range of soluble electron acceptors such as TMAO, DMSO, nitrate, and fumarate, as well as congregation of MR-1 around insoluble electron acceptors such as an electrode [Cuthbertson et al. 2009]. In contrast, just one chemotaxis protein, protein phosphatase CheZ, was significantly more abundant in the cathode biofilm. In general, proteins related to taxis and motility are known play a role in the cycle of cell attachment and detachment during biofilm growth [Guttenplan and Kearns 2013], but few studies have compared taxis protein expression between anaerobic and aerobic biofilms of MR-1. The high proportion of taxis proteins among proteins significantly more abundant in the anode biofilm is consistent with an interpretation that the anode biofilm was in a more dynamic state of development than the cathode biofilm. This interpretation is supported by the clearly more robust biofilm on the cathode compared with the anode (Appendix SI 3.1: Figure S11).

In addition to taxis proteins, several proteins directly related to biofilm formation were significantly more abundant in the anode biofilm than in the cathode biofilm. These included a polysaccharide deacetylase (Q8ECG4) important for anchoring of the peptidoglycan layer to surfaces, a polysaccharide export channel protein Wza (Q8ECE9) responsible for polymer export during EPS formation, and a long-chain fatty acid receptor FadL (Q8ECN9) previously associated with a biofilm form of life [Zimaro et al.

2013]. In addition to the TonB-dependent receptor (Q8ED60) discussed above (Section 3.4), an additional ArgR-regulated TonB-dependent receptor protein (Q8EEF5) was judged significantly more abundant in the anode biofilm than in the cathode biofilm. Several studies have noted the association of TonB-dependent receptors with iron-acquisition during active biofilm development [Ritter et al. 2012; Pham et al. 2010; Cursino et al. 2009; Abbas et al. 2007; Takase et al. 2000]. The only protein related to biofilm development that was more abundant in the cathode than in the anode was a multivalent adhesin (Q8EDY5). Thus, even though the biofilms in these reactors had been established for several weeks before harvest, the proteomics results suggest that the anaerobic anode biofilm was in a more active state of development than the cathode biofilm. This may be due to faster maturation of the cathode biofilm due to greater oxygen availability [Kitayama et al. 2017; Wu et al. 2013; McLean et al. 2008; Biffinger et al. 2008].

3.3.7 Stress and virulence proteins

Stress proteins included a multidrug efflux pump component (VmeA), an outer membrane porin OmpK previously observed in to be expressed by *V. alginolyticus* in response to antibiotics [Xiong et al. 2009], a CyaB-like adenylate cyclase YgiF that in *P. aeruginosa* is a controller of virulence response during biofilm formation [Topal et al. 2012], a polysaccharide deacetylase (Q8ECG4) for resistance to lysozyme and immune response, and a small conductive mechanosensitive ion channel protein (MscS) that is expressed in response to hypo-osmotic shock. YfzA was also more abundant in the anode; this protein contains a transmembrane beta (8,10)-barrel also found in proteins such as OmpX and PagP, a membrane enzyme that helps pathogens evade host immune

responses. Also more abundant in the anode biofilm was FtsH, a metalloprotease with diverse functionality, including degradation of membrane proteins, biosynthesis of lipopolysaccharide, and control of responses to heat shock, superoxide, and osmotic stress [Langklotz et al. 2012]. Finally, two proteins related to protein translocation were more abundant in the anode. These included YajC a preprotein translocase responsible for secretion of proteins across the inner membrane before they are incorporated into the lipid bilayer [du Plessis et al. 2011] and signal peptidase I, responsible for cleavage of N-terminal signals from secreted or periplasmic proteins [Tujeta 2005]. An increase in protein translocation to membranes suggests a high level of membrane activity, consistent with increased processes occurring at the cell surface of anode biofilm cells, such as electricity generation, adhesion and biofilm formation, and perhaps signaling between cells within the biofilm [Grobbler et al. 2015].

Previous omics studies have noted a stress response by MR-1 in response to anaerobic respiration [Qiu et al. 2006; Beliaev et al. 2005]. Stress responses in *S.oneidensis* MR-1 to various environmental conditions have been documented [Yin and Gao 2011], though just one study has noted a stress response to current generation in an MFC [Rosenbaum et al. 2012]. That study, however, did not distinguish between the stress associated with use of an electrode and any stress just from a biofilm lifestyle. In the present work, none of the stress proteins more abundant among anode proteins were part of an oxidative stress response previously described in MR-1 [Jiang et al. 2016; Li et al. 2014]; nevertheless, it is possible that stress of electricity-generation contributed to the observed decrease in maximum current generation over multiple batches [Rosenbaum et al. 2012; Lanthier et al. 2008]. The increase in MR-1 proteins associated with a virulence

response is especially interesting since MR-1 is generally considered a non-virulent organism [Heidelberg et al. 2002]. This response may have been induced by a contaminant; since these MFCs are single-chambered, however, contamination by other bacteria would be expected to induce the same response in both anode and cathode biofilms. Future work could focus on the relationship between stress proteins and current generation at an electrode, in order to discover additional features and metabolic requirements of extracellular electron transfer that would be relevant to increasing current generation capacity during MFC scale-up.

3.4 Conclusions

The purpose of this study was to compare protein expression by anaerobic and aerobic biofilms of *S. oneidensis* MR-1 in the same MFC reactor. Aerobic cathode biofilms were derived from planktonic cells that competed with anode biofilm cells for residual oxygen in the single-chamber MFC. Consumption of this residual oxygen by anode biofilm cells—suggested by expression of proteins associated with aerobic TCA cycle metabolism (e.g., GltA, SucB, and Sdh) in anode biofilm cells—may have contributed to decreases in current generation over multiple batches. These decreases in performance also may have been due to the stress of current generation, as suggested by significantly more abundant proteins related to stress and virulence in anode biofilms, compared to aerobic cathode biofilms. Significantly more abundant anode biofilm proteins associated with active biofilm formation suggest that cells on the anode surface are in more of a dynamic state of development than the more mature, aerobic cathode biofilms. This study contributes insights into MR-1 metabolism in MFCs by comparing anaerobic, current generating biofilms to aerobic biofilms in the same reactor. Future

work should pursue the consequences of aerobic metabolism in MFC anode cells, in order to limit losses of electrons to aerobic respiration.

CHAPTER 3 REFERENCES

Abbas A, Adams C, Scully N, Glennon J, O'Gara F. (2007) A role for TonB1 in biofilm formation and quorum sensing in Pseudomonas aeruginosa. FEMS Microbiol. Lett. 2:269-278

Beliaev AS, Thompson DK, Khare T, Lim H, Brandt CC, Li G, *et al*. (2002) Gene and protein expression profiles of *Shewanella oneidensis* during anaerobic growth with different electron acceptors. OMICS 6: 39–60

Beliaev AS, Klingeman DM, Klappenbach JA, Wu L, Romine MF, Tiedje JM et al. (2005) Global transcriptome analysis of *Shewanella oneidensis* MR-1 exposed to different terminal electron acceptors. J Bacteriol 187:7138-7145

Biffinger JC, Byrd JN, Dudley B, Ringeisen BR. (2008) Oxygen exposure promotes fuel diversity for *Shewanella oneidensis* microbial fuel cells. Biosens. Bioelectron. 23:820-826

Bouhenni RA, Vora GJ, Biffinger JC, Shirodkar S, Brockman K, Ray R et al. (2010) The role of *Shewanella oneidensis* MR-1 outer surface structures in extracellular electron transfer. Electroanal. 22:856-864.

Bretschger O, Obraztsova A, Sturm CA, Chang IS, Gorby YA, Reed SB et al. (2007) Current production and metal oxide reduction by *Shewanella oneidensis* MR-1 wild-type and mutants. Appl. Enivron. Microbiol. 73:7003-7012

Brutinel ED, Gralnick JA. (2012) Anomalies of the anaerobic tricarboxylic acid cycle in *Shewanella oneidensis* revealed by Tn-seq. Molec. Microbiol. 86:273-283.

57

Carmona-Martinez AA, Harnisch F, Kuhlicke U, Neu TR, Schroder U. (2013) Electron transfer and biofilm formation of *Shewanella putrefaciens* as function of anode potential. Bioelectrochemistry 93:23-29.

Coursolle D, Baron DB, Bond DR, Gralnik JA. (2010) The Mtr respiratory pathway is essential for reducing flavins and electrodes in *Shewanella oneidensis*. J. Bacteriol. 192:467-474

Cursino L, Li Y, Zaini PA, De La Fuente L, Hoch HC, Burr TJ. (2009) Twitching motility and biofilm formation are associated with tonB1 in Xylella fastidoiosa. FEMS Microbiol. Lett. 2:193-199

Cuthbertson L, Mainprize IL, Naismith JH, Whitfield C. (2009) Pivotal roles of the outer membrane polysaccharide export and polysaccharide copolymerase protein families in export of extracellular polysaccharides in Gram-negative bacteria. Microbiol. Mol. Biol. Rev. 73:155-177

Dawood Z, Ehrenreich L, Brozel VS. (1998) The effect of molecular oxygen on sulfite reduction by *Shewanella putrefaciens*. FEMS Microbiol. Lett. 164:383-387.

Donné J and Dewilde S. (2015) The challenging world of biofilm physiology. Adv. Microb. Physiol. 67:235-292

du Plessis DJF, Nouwen N, Driessen AJM. (2011) The Sec translocase. Biochim. Biophys. Acta – Biomembranes 1808:851-865

Fan Y, Sharbrough E, Liu H. (2008) Quantification of the internal resistance distribution of microbial fuel cells. Environ. Sci. Technol. 42:8101-8107

Fitzgerald LA, Petersen ER, Ray RI, Little BJ, Cooper CJ, Howard EC et al. (2012) *Shewanella oneidensis* MR-1 Msh pilin proteins are involved in extracellular electron transfer in microbial fuel cells. Process Biochem. 47:170-174

Fowler GJS, Pereira-Medrano AG, Jaffe S, Pasternak G, Pham TK, Ledezma P, Hall STE, Ieropoulos IA, Wright PC. (2016) An iTRAQ characterization of the role of TolC during electron transfer from Shewnella *oneidensis* MR-1. 16:2764-2775.

Gorby YA, Yanina S, McLean JS, Rosso KM, Moyles D, Dohnalkova A, Beveridge TJ, Chang IS, Kim BS, Kim KS, Culley DE, Reed SB, Romine MF, Saffarini DA, Hill EA, Guttenplan SB, Kearns DB. (2013) Regulation of flagellar motility during biofilm formation. FEMS Micrbiol. Rev. 37:849-871

Shi L, Elias DA, Kennedy DW, Pinchuk G, Watanabe K, Ishii S, Logan B, Nealson KH, Fredrickson JK. (2006) Electrically conducive bacterial nanowires produced by *Shewanella oneidensis* strain MR-1 and other microorganisms. Proc Nat Acad Sci 103:11358-11363. doi: 10.1073/pnas.0604517103

Grobbler C, Virdis B, Nouwens A, Harnisch F, Rabaey K, Bond PL. (2015) Use of SWATH mass spectrometry for quantitative proteomic investigation of *Shewanella oneidensis* MR-1 biofilms grown on graphite cloth electrodes. System. App. Microbiol. 38:135-139.

Harris HW, El-Naggar MY, Nealson KH. (2012) *Shewanella oneidensis* MR-1 chemotaxis proteins and electron-transport chain components essential for congregation near insoluble electron acceptors. Biochem. Soc. Trans. 40:1167-1177

Hau HH and Gralnick JA. (2007) Ecology and biotechnology of the genus *Shewanella*. Ann. Rev. Microbiol. 61:237-258

Heidelberg JF, Paulsen IT, Nelson KE, Gaidos EJ, Nelson WC, Read TD et al. (2002) Genome sequence of the dissimilatory metal ion-reducing bacterium *Shewanella oneidensis*. Nature Biotechnology 20:1118-1123

Jadhav DA, Ray SG, Ghangrekar MM (2017) Third generation in bio-electrochemical system research – A systematic review on mechanisms for recovery of valuable by-products from wastewater. Ren Sust Energy Rev 76:1022-1031

Kaur A, Kim JR, Michie I, Dinsdale RM, Guwy AJ, Premier GC. Microbial fuel cell type biosensor for specific volatile fatty acids using acclimated bacterial communities. Biosensors and Bioelectronics 47:50-55

Jiang Y, Dong Y, Luo Q, Li N, Wu G, Gao H. (2016) Protection from oxidative stress relies mainly on derepression of Oxy-R-dependent KatB and Dps in *Shewanella oneidensis*. J Bacteriol. 196:445-458

Kadziola A, Larsen S. (1997) Crystal structure of the dihaem cytochrome c_4 from *Pseudomonas stutzeri* determined at 2.2 Å resolution. Structure 5:203-216

Kiely PD, Rader G, Regan JM, Logan BE. (2011) Long-term cathode performance and the microbial communities that develop in microbial fuel cells fed different fermentation end products. Biores. Technol. 102:361-366.

Kitayama M, Koga R, Kasai T, Kouzuma A, Watanabe K. (2017) Structures, compositions and activities of live *Shewanella* biofilms formed on graphite electrodes in electrochemical flow cells. Appl. Environ. Microbiol. doi:10.1128/AEM.00903-17

Koebnik R, Locher KP, Van Gelder P. (2000) Structure and function of bacterial outer membrane proteins: barrels in a nutshell. Molec. Microbiol. 37:239-253

Kotloski NJ and Gralnick JA. Flavin electron shuttles dominate extracellular electron transfer by *Shewanella oneidensis*. mBio 4:e00553-12. doi:10.1128/mBio.00553-12.

Langklotz S, Baumann U, Narberhaus F. (2012) Structure and function of the bacterial AAA protease FtsH. Biochim. Biophys. Acta – Molec. Cell Res. 1:40-48

Lanthier M, Gregory KB, Lovley DR. (2008) Growth with high planktonic biomass in *Shewanella oneidensis* fuel cells. FEMS Microbiol. Lett. 278:29-35

Lee HS, Torres CI, Rittman BE. (2009) Effects of substrate diffusion and anode potential on kinetic parameters for anode-respiring bacteria. Environ. Sci. Technol. 43:7571-7577

Li N, Luo Q, Jiang Y, Wu G, Gao H. (2014) Managing oxidative stresses in *Shewanella oneidensis*: intertwined roles of the OxyR and OhrR regulons. Environ. Microbiol. 16:1821-1834

Liu H, Cheng S, Logan BE. (2005) Production of electricity from acetate or butyrate using a single-chamber microbial fuel cell. Environ. Sci. Technol. 39:658-662.

Lovley DR and Nevin KP. (2013) Electrobiocommodities: powering microbial production of fuels and commodity chemicals from carbon dioxide with electricity. Curr Opin Biotech 24:385-390

Lovley DR (2017) Syntrophy goes electric: direct interspecies electron transfer (DIET). Ann Rev Microbiol 71: 10.1146/annurev-micro-030117-020420

Maier TM and Myers CR. (2004) The outer membrane protein Omp35 affects the reduction of Fe(III), nitrate, and fumarate by *Shewanella oneidensis* MR-1. BMC Microbiol. 4: doi:10.1186/1471-2180-4-23

Malvankar NS, Lau J, Nevin KP, Franks AE, Tuominen MT, Lovley DR. (2012) Electrical conductivity in a mixed-species biofilm. Appl Environ Microbiol 78:5967-5971.

Malvankar NS and Lovley DR. (2013) Microbial nanowires for bioenergy applications. Curr Opin Biotech 27:88-95. doi: 10.1016/j.copbio.2013.12.003

Marshall MJ, Plymale AE, Kennedy DW, Shi L, Wang Z, Reed SB. (2008) Hydrogenase- and outer membrane c-type cytochrome-faciliatated reduction of technetium(VII) by *Shewanella oneidensis* MR-1. Environ. Microbiol. 10:125-136

Marsili E, Baron DB, Shikhare ID, Coursolle D, Gralnik J, Bond DR. (2008) *Shewanella* secretes flavins that mediate extracellular electron transfer. Proc. Nat. Acad. Sci. 105: 3968-3973

McLean JS, Majors PD, Reardon CL, Bilskis CL, Reed SB, Romine MF, Frederickson JK. (2008) Investigations of structure and metabolism within *Shewanella oneidensis* MR-1 biofilms. 74:47-56

Morris RL and Schmidt TM. (2013) Shallow breathing: bacterial life at low O_2. Nat. Rev. Microbiol. 11:205-212

Myers CR and Nealson KH. (1988) Bacterial manganese reduction and growth with manganese oxide as the sole electron accepter. *Science* 240:1319–1321.

Nevin KP, Woodard TL, Franks AE, Summers AM, Lovley DR. (2010) Microbial electrosynthesis: feeding microbes electricity to convert carbon dioxide and water to multicarbon extracellular organic compounds. mBio :e00103-10. doi:10.1128/mBio.00103-10.

Newton GJ, Mori S, Nakamura R, Hashimoto K, Watanabe K. (2009) Analyses of current-generating mechanisms of *Shewanella loihica* PV-4 and *Shewanella oneidensis* MR-1 in microbial fuel cells. App Environ Microbiol 83:7674-7681

Okamoto A, Nakamura R, Nealson KH, Hashimoto K. (2014) Bound flavin model suggests similar electron-transfer mechanisms in *Shewanella* and *Geobacter*. ChemElectroChem 1:1808-1812.

Pham TK, Roy S, Noirel J, Douglas I, Wright PC, Stafford GP. (2010) A quantitative proteomic analysis of biofilm adaptation by the periodontal pathogen Tannerella forsythia. Proteomics 17:3130-3141

Pinchuk GE, Geydebrekht OV, Hill EA, Reed JL, Konopka AE, Beliaev AS, Frederickson JK. (2011) Pyruvate and lactate metabolism by *Shewanella oneidensis* MR-1 under fermentation, oxygen limitation, and fumarate respiration conditions. Appl. Environ. Microbiol. 77:8234-8240.

Pinto D, Coradin T, Laberty-Robert C. (2017) Effect of anode polarization on biofilm formation and electron transfer in *Shewanella oneidensis*/graphite felt microbial fuel cells. Bioelectrochemistry 120:1-9.

Pirbadian S, Barchinger SE, Leung KM, Byun HS, Jangir Y, Bouhenni RA et al. (2014) Shewnella *oneidensis* MR-1 nanowires are outer membrane and periplasmic extensions of the extracellular electron transport components. Proc. Nat. Acad. Sci. 111: 12883-12888. Doi: 10.1073/pnas.1410551111

Postle K, Kadner RJ. (2003) Touch and go: tying TonB to transport. Molec. Microbiol. 49:869-882

Proc JL, Kuzyk MA, Hardie DB, Yung J, Smith DS, Jackson AM, Parker CE, Borchers CH. (2010) A quantitative study of the effects of chaotropic agents, surfactants, and solvents on the digestion efficiency of human plasma proteins by trypsin. J. Proteome Res. 9:5422-5437

Qian Y, Shi L, Tien M. (2011) SO2907, a putative TonB-dependent receptor, is involved in dissimilatory iron reduction by *Shewanella oneidensis* strain MR-1. J. Biol. Chem. 286:33973-33980

Qiu X, Daly MJ, Vasilenko A, Omelchenko MV, Gaidamakova EK, Wu L et al. (2006) Transcriptome analysis applied to survival of *Shewanella oneidensis* MR-1 exposed to ionizing radiation. J Bacteriol. 188:1199-1204

Rismani-Yazki H, Carver SM, Christy AD, Tuovinen OH. (2008) Cathodic limitations in microbial fuel cells: an overview. J Power Sources 180:683-694

Ritter A, Com E, Bazire A, Goncalves MDS, Delage L, Pennec GL, et al. (2012) Proteomic studies highlight outer-membrane proteins related to biofilm development in the marine bacterium *Pseudoalteromonas* sp. D41. Proteomics 12:3180-3192

Rosenbaum M, Cotta MA, Angenent LT. (2010) Aerated *Shewanella oneidensis* in continuously fed bioelectrochemical systems for power and hydrogen production. Biotech. Bioeng. 105:880-888

Rosenbaum MA, Bar HY, Beg QK, Segrè D, Booth J, Cotta MA, Angenent LT. (2012) Transcriptional Analysis of *Shewanella oneidensis* MR-1 with an Electrode Compared to Fe(III)Citrate or Oxygen as Terminal Electron Acceptor. PLoS ONE7(2): e30827. https://doi.org/10.1371/journal.pone.0030827

Roy JN, Luckarift HR, Lau C, Falase A, Garcia KE, Ista LK, Chellamuthu P, Ramasamy RP, Gadhamshetty V, Wanger G, Gorby YA, Nealson KH, Bretschger O, Johnson GR, Atanassov P. (2012) A study of the flavin response by *Shewanella* cultures in carbon-limited environments. RSC Adv. 2:10020-10027

Schweinitzer T, Josenhans C. (2010) Bacterial energy taxis: a global strategy? Arch. Microbiol. 192:507-520

Shi L, Richardson DJ, Wang Z, Kerisit SN, Rosso KM, Zachara JM, Fredrickson JK. (2009) The roles of outer membrane cytochromes of *Shewanella* and *Geobacter* in extracellular electron transfer. Environ Microb Rep 1:220-227

Silva JC, Gorenstein MV, Li G-Z, Vissers JPC, Geromanos SJ. (2006) Absolute quantification of proteins by LCMSE: A virtue of parallel MS acquisition. Molec. Cell. Proteomics 5:144-156

Stewart PS, Franklin MJ. (2008) Physiological heterogeneity in biofilms. Nat. Rev. Microbiol. 6:199-210

Storey JD. (2002) A direct approach to false discovery rates. RSS Series B Statist. Method. 64:479-498

Takase H, Nitanai H, Hoshino K, Otani T. (2000) Requirement of the *Pseuodomonas* aeruginosa tonB gene for high-affinity iron acquisition and infection. Infect. Immun. 68:4498-4504

TerAvest MA, Rosenbaum MA. (2013) Oxygen allows *Shewanella oneidensis* MR-1 to overcome mediator washout in a continuously fed bioelectrochemical system. Bioeng. Biotechnol. 111:692-699

Thormann KM, Saville RM, Shukla S, Pelletier DA, Spormann AM. (2004) Initial phases of biofilm formation in *Shewanella oneidensis* MR-1. J. Bacteriol. 186:8096-8104

Topal H, Fulcher NB, Bitterman J, Salazar E, Buck J, Levin LR, Cann MJ, Wolfgang MC, Steegborn C. (2012) Crystal structure and regulation mechanisms of the CyaB adenylyl cyclase from the human pathogen Pseudomonas aeruginosa. J Molec. Biol. 416:271-286

Tuteja R. (2005) Type I signal peptidase: an overview. Arch. Biochem. Biophys. 441:107-111

Voeikova TA, Emel'yanova LK, Novikova LM, Shakulov RS, Sidoruk KV, Smirnov IA, Il'in VK, Soldatov PE, Tyruin-Kuz'min AY, Smolenskaya TS, Debabov VG. (2013) Intensification of bioelectricity generation in microbial fuel cells using *Shewanella oneidensis* MR-1 mutants with increased reducing activity. Microbiology 82:410-414

von Canstein H, Ogawa J, Shimizu S, Lloyd JR. (2007) Secretion of flavins by *Shewanella* species and their role in extracellular electron transfer. Appl. Environ. Microbiol. 74:615-623

Wang H, Ren ZJ (2013) A comprehensive review of microbial electrochemical systems as a platform technology. Biotech Adv 31:1796-1807

West EA, Jain A, Gralnick JA. (2017) Engineering a native inducible expression system in *Shewanella oneidensis* to control extracellular electron transfer. ACS Synth. Biol. 6:1627-1634.

Wu C, Cheng Y-Y, Yin H, Song X-N, Li W-W, Zhou X-X, Zhao L-P, Tian L-J, Han J-C, Yu H-Q. (2013) Oxygen promotes biofilm formation of *Shewanella* putrefaciens CN32 through a diguanylate cyclase and an adhesion. 3: doi: 10.1038/srep01945

Xiong X-P, Wang C, Ye M-Z, Yang T-C, Peng X-X, Li H. (2009) Differentially expressed outer membrane proteins of Vibrio alginolyticus in response to six types of antibiotics. Mar. Biotechnol. 12:686-695

Yin J and Gao H. (2011) Stress responses of *Shewanella*. Int. J. Microbiol. 2011: doi: 10.1155/2011/863623

Zimaro T, Thomas L, Marondedze C, Garavaglia BS, Gehring C, Ottado J, Gottig N. (2013) Insights into *Xanthomonas axonopodis* pv. *citri* biofilm through proteomics. BMC Microbiol. 13: https://doi.org/10.1186/1471-2180-13-186

CHAPTER 4: LABEL-FREE PROTEOMICS OF A DEFINED, BINARY CO-CULTURE REVEALS DIVERSITY OF COMPETITIVE RESPONSES BETWEEN MEMBERS OF A MODEL SOIL MICROBIAL SYSTEM[2]

4.1 Introduction

Interactions among microorganisms are responsible for complex processes such as nutrient cycling, degradation of recalcitrant lignocellulosic materials, and remediation of pollutants [Widder et al. 2016; Lopez-Mondejar et al. 2016; Prosser et al. 2007]. Microbial interactions also drive healthy or pathogenic dynamics of the human microbiome [Rooks and Garret 2016; Lloyd-Proce et al. 2016; Jian et al. 2016] and may offer opportunities for synthetic biology that are not available from pure cultures [Lindemann et al. 2016; Dolinsek et al. 2016; Zhang et al. 2016]. Studies of microbial interactions face methodological challenges to quantify *in situ* the metabolism of the many species comprising a microbial community. Often macro-level data are measured and correlated with the metabolic capabilities of the organisms that are present, as determined by the relative abundance of 16S rRNA genes or functional genes [Sinclair et al. 2015; Rundell et al. 2014; Langille et al. 2013]. Focusing only on species identity or a small subset of functional genes, however, limits the information that can be obtained regarding the functional activities and interactions of the organisms in the system.

Recently, "meta-omics" approaches have emerged as alternative methods to obtain functional information about complex microbial systems [Wallace et al 2017;

[2] The text and results presented in this chapter were published previously in Chignell et al. 2018 (Chapter 4 References)

Franzosa et al. 2015; Baldrian et al. 2014]. Meta-genomics identifies the metabolic potential of a consortium, while meta-transcriptomics quantifies transcription levels of expressed genes. In contrast, meta-proteomics offers the advantage of quantifying proteins, the functional products of gene expression. This direct linkage to function suggests that a proteomics approach may be most appropriate for answering ecological questions about the actual activities and interactions of detected species, especially considering the lack of correspondence between the abundance of proteins and transcripts [Wang et al. 2017; Edfors et al. 2016]. Meta-proteomics studies of complex microbial consortia face their own challenges, however. These include the lack of confidence in assignment of peptide sequences to proteins derived from unsequenced, uncultured organisms, and the lack of annotation information for most genomic databases. An alternative approach that avoids these problems is to investigate defined co-cultures of well-characterized species with sequenced, annotated genomes. This approach offers several advantages over using undefined communities, including greater confidence in peptide-protein matches, greater meta-proteome coverage, increased control over experimental variables, more options for validation of proteomics results, and more manageable datasets [Herbst et al. 2016]. For many types of microbial interactions, the confidence gained in conclusions about defined co-cultures is worth the tradeoff of restricting analysis to a limited number of model species.

Proteomics studies of defined co-cultures usually compare protein expression by consortium members in co-culture to that in pure culture. This approach has been used to study ecological interactions between thermophiles [Giannone et al. 2011; Muddiman et al. 2010], gut bacteria [Ruiz et al. 2009; Di Cagno et al. 2009], environmental species

[Sedlacek et al. 2016; Sieber et al. 2015], oral cavity-forming species [Klein et al. 2012] and species involved in infections in cystic fibrosis patients [Kluge et al. 2012]. In an engineering context, this proteomics approach has been used to investigate defined consortia associated with lignocellulose hydrolysis and fermentation [Huang and Lefsrud 2012], biogas production [Enoki et al. 2011], and industrial production of a vitamin precursor [Ma et al. 2011]. No proteomics studies, however, have investigated defined consortia of soil microorganisms, despite the known syntrophic [Ren et al. 2015; Kouzuma et al. 2014; Bakker et al. 2013] and antagonistic interactions [Kuzyakov and Blagodatskaya 2015; Tyc et al. 2014; Kent et al. 2002] between soil species and the importance of soil environments in both basic microbial ecology and engineering (e.g., in bioremediation).

The common soil species *Bacillus atrophaeus* (Gram-positive) and *Pseudomonas putida* (Gram-negative) are each known to be active in remediation of contaminants [Barlow et al. 2017; Liu et al. 2016; Gasc et al. 2016; Rani et al. 2012] and in rhizosphere ecology [Abo-Aba et al. 2015; Chen et al. 2013; Neal et al. 2012]. While a few studies have described growth dynamics or exchange of metabolites in co-cultures of similar species [Mukherjee et al. 2012; Simoes et al. 2008], most functional details of interactions between these organisms are unknown. The purpose of this study was to quantify the proteome response of each of these model soil species during co-culture relative to their pure culture, and thereby to suggest mechanisms for interactions between these and other microbes in this important ecosystem.

Accurate quantification of low-abundance proteins is important for microbial ecology, since many critical ecological questions concern the activities of low-

abundance, “rare” species in a consortium [Jousset et al. 2017; Hausmann et al. 2016]. Previous work has shown that the identification and quantification of low-abundance proteins is a critical challenge for proteomics studies, due to LC-MS/MS phenomena such as ion suppression and false discovery [Domon and Aebersold 2010; Choi and Nesvizhskii 2008; Mallet et al. 2004]. Therefore, a secondary goal of the present study was to identify a limit of detection (LOD) of protein-identifying peptides from each species in a mixture of peptides from both species. Determining beforehand the LOD of peptides and proteins from species of interest is an important consideration for reliable and accurate application of proteomics technologies to questions of microbial ecology.

4.2 Experimental Procedures

4.2.1 Bacterial strains, batch cultivation, and monitoring of cultures

Bacillus atrophaeus 1942 (ATCC 9372) and *Pseudomonas putida* KT2440 (ATCC 47054) were maintained routinely on agar plates with 10 g/L tryptic soy broth (TSB). All pre-cultures and cultures were grown in 500-mL baffled Erlenmeyer flasks at 30 °C on 10 g/L TSB with shaking at 200 rpm. For each species, a 30-mL pre-culture was inoculated with three plate colonies and grown to late log-phase (*B. atrophaeus* OD_{600} = 3.06; *P. putida* OD_{600} = 2.27). For each biological condition (pure *B. atrophaeus*, pure *P. putida*, co-culture), triplicate flasks containing 200 mL of 10 g/L TSB were inoculated with a volume of pre-culture previously determined by Gram staining and plate counts to result in approximately equal concentrations (CFU/mL) of each species in the co-culture after 20 h of growth. The use of equal concentrations of each species in the co-culture at harvest was targeted based on LOD results showing that identification was most accurate when peptides from each species were present at

approximately equal concentration. Inoculation volumes were 200 μL of 1:10 dilution of *B. atrophaeus* pre-culture and 100 μL of 1:1000 dilution of *P. putida* pre-culture, delivering approximately five-fold greater *B. atrophaeus* CFUs than CFUs for *P. putida*. The initial OD_{600} of each flask was ≤ 0.003. Growth curves were generated from OD_{600} measurements of 1-mL samples and specific growth rate (μ) was calculated as described in Figure S2 (Appendix SI 4.3). Dry cell weight (DCW) of each culture at the harvest point was determined as the mean mass of the cell pellets from three technical replicate culture samples (10 mL each). For both μ and DCW, statistical differences between culture types were determined by a two-tailed Student's t-test across biological replicates, assuming equal variances.

4.2.2 Supernatant growth experiments

Since proteomics results suggested antagonism by *P. putida* toward *B. atrophaeus*, it was hypothesized that compounds secreted into the culture medium by *P. putida* would have an inhibitory effect on *B. atrophaeus* growth. A defined minimal medium (MHM) supporting robust growth of *B. atrophaeus* and *P. putida* was developed (modified from [Hageman et al. 1984]). This medium consisted of 40 mM MOPS, 4.0 mM KH_2PO_4, 9.5 mM $(NH_4)_2SO_4$, 5.0 mM D,L-lactate, 11.8 mM L-glutamic acid, 245 μM L-tryptophan, 381 μM L-leucine, 8.02 mM L-asparagine, 280 μM $MgSO_4 \cdot 7H_2O$, 15 μM $MnSO_4 \cdot H_2O$, 36 μM $CaCl_2$, 33 μM $FeSO_4 \cdot 7H_2O$, 10 mL/L of trace minerals (ATCC MD-TMS), 10 mL/L trace vitamins (ATCC MD-VS), and 1 L of deionized water. The pH was adjusted to 7.1 with 10 N NaOH.

Four different cultures were grown in triplicate in 200 mL MHM in 500-mL baffled flasks: *B. atrophaeus*, *P. putida*, co-culture, and co-culture with limited iron (0.9

μM instead of 33 μM $FeSO_4 \cdot 7H_2O$ and iron excluded from the trace mineral solution). At late exponential growth, these cultures were harvested, centrifuged at 4000 x g for 30 min, and the supernatant was recovered and stored at 4 °C. After filtration through a 0.2-μm surfactant-free cellulose acetate filter, 20 mL of each supernatant was added to quadruplicate baffled culture flasks (500 mL) containing 20 mL fresh MHM with 66 μM $FeSO_4 \cdot 7H_2O$, 2x trace minerals and 2x of vitamin solution. Each flask then was inoculated with 0.2 mL (0.05 vol%) of an overnight MHM culture of *B. atrophaeus*. During incubation at 30 °C, 200 RPM for ~14 h, growth was monitored *via* OD_{600} measurements. The same experimental approach was used to test inhibitory effects on *B. atrophaeus* growth of the three supernatants from the 10 g/L TSB cultures harvested for proteomics.

4.2.3 Plate growth experiments

In addition to planktonic growth experiments, the effects of any compounds secreted by *P. putida* on the growth of *B. atrophaeus* were tested by disk diffusion. Autoclaved 6.4-mm disks of filter paper were saturated with 20 μL of centrifuged (10,000 x g, 30 min) supernatant from *B. atrophaeus*, *P. putida*, or co-culture grown on 10 g/L TSB. Disks with 3 μL of 0.5 μg/μL ampicillin (Sigma-Aldrich, St. Louis, MO) served as positive controls for growth inhibition. Late-log *B. atrophaeus* culture was added 1:10 (v/v) to warm 10 g/L TSB + 0.7% agar and the mixture was applied as an overlay to 1.5% agar plates. After placing the disks on the agar surfaces the plates were grown overnight at 30 °C and then observed for zones of inhibition.

The effect of physical proximity on colony growth of each species was observed by depositing 2-μL spots of late log-phase culture of each species directly across from

each other on quadruplicate 10 g/L TSB plates. Plates were allowed to grow at 30 °C for two weeks, with observations every 24 h.

4.2.4 Metal limitation experiments

The effect of metal limitation on the ratio of the species in the co-culture was quantified by co-culturing in MHM under normal and low concentrations of iron, magnesium, or zinc. For each metal of interest, a trace metal solution lacking that metal was used and the metal was added to the MHM medium recipe at a normal or limiting concentration: $FeSO_4$ (33 μM and 0.9 μM); $MgCl_2$ (1 mM or 12 μM); $ZnSO_4$ (10 μM or 0 μM). In each of triplicate 500-mL baffled flasks, 50 mL of metal-limited or non-metal-limited MHM was inoculated with 0.05% (v/v) of late-log culture of each species grown on MHM. After 12 h, quadruplicate 10 g/L TSB plates were spread with 50 μL of each replicate culture (metal-limited and non-limited) at dilutions ranging from 10^4-10^7 and incubated for 24 h at 30 °C. The mean CFU count across replicate plates was used to calculate a species ratio for each biological replicate flask. These species ratios were compared between metal-limited and non-limited conditions with a two-tailed Student's t-test, assuming equal variances.

Relative abundance of each species was monitored qualitatively by Gram staining during growth curves. CFU/mL of each culture was quantified by plating 100 μL of serially-diluted culture on 10 g/L TSB agar plates at least in triplicate at multiple dilution levels. Plates were incubated at 30 °C overnight, and distinguishable small, orange (*B. atrophaeus*) and creamy, white (*P. putida*) colonies were counted.

4.2.5 Protein extraction, digestion, and peptide preparation

Cells from each biological replicate culture were collected for proteomics after 20 h growth by centrifuging 2 mL of culture at 4000 x g for 10 min at 4 °C. The remaining culture was centrifuged in 50 mL tubes (BD, Franklin Lakes, NJ), and the supernatant was retained for iron assays (FerroVer; Hach, Loveland, CO) and supernatant growth experiments described in Section 4.2.2. Details of protein extraction and peptide preparation, including buffer composition, are described in the Appendix (SI 4.1.1). Briefly, washed cell pellets from each culture type were sonicated in each of two different buffers formulated for lysis of Gram-negative or Gram-positive cells. Acetone-precipitated proteins were resuspended and prepared for digestion by heat-treatment, reduction of cysteines with dithiothreitol (DTT), and methylation with iodoacetamide (Pierce Life Technologies, Grand Island, NY). The proteins were digested overnight at 38 °C with mass spectrometry-grade trypsin (Trypsin Gold, Promega, Madison, WI). Contaminants were removed with C-18 spin columns (Pierce, Life Technologies, Grand Island, NY) and eluted peptides were dried and resuspended in 3% acetonitrile, 0.1% formic acid for LC-MS/MS analysis.

4.2.6 Peptide dilution experiments to determine LOD

We hypothesized that determining the LOD of proteins from each species against a background of peptides from the other species would be important for choosing the relative abundance of each species to include in the co-culture. Peptide mixtures from each species were resuspended in LC-MS/MS buffer to a total peptide concentration of ~0.5 μg/μL. Equal volumes (10 μL) of these two peptide solutions were combined to generate a sample containing approximately equal peptide concentrations from each species. Then, for each species, the ~0.5 μg/μL peptide solution was diluted serially

(1:10) into the original 0.5 μg/μL peptide solution of the other species. The final result was two sets of samples containing peptides for one species in decreasing orders of magnitude against a background of 0.5 μg/μL peptides from the other species. Finally, for each species, a sample was prepared containing only peptides from that species by combining 10 μL of ~0.5 μg/μL peptide solution with 10 μL LC-MS/MS buffer. The Appendix (SI 4.3: Figure S1) contains an illustration of this dilution schematic. All samples were analyzed with duplicate technical replicate runs by LC-MS/MS.

4.2.7 ESI-LC-MS/MS analysis

One µg of digest was loaded onto a C18 trap (200 μm ID, 0.5 mm length, 120 A, Eksigent Technologies, Dublin, CA). A 2%-80% gradient of acetonitrile with 0.1% formic acid was used to elute the peptides from the trap and column (C18, 75 μm ID, 150 mm length, 120 A, Eksigent Technologies) for 150 minutes at a flow rate of 300 nL/min. Peptides were eluted into the electrospray ionization source of a TripleTOF 5600 (ABSciex) for MS/MS analysis, with one MS^1 scan followed by up to 50 MS^2 scans according to the order of intensity. Three technical replicate LC-MS/MS shots (two for the peptide dilution experiments described in Section 4.2.6) were run per biological replicate, with a wash step between each shot.

4.2.8 Protein identification, label-free quantification, and Gene Ontology analysis

Database searching and protein quantification were conducted on Analyst (v.1.5 TR, ABSciex) .wiff files using ProteinPilot v. 4.5 TR (ABSciex), as detailed in SI. Briefly, .wiff files were searched against a .fasta database comprising the combined Uniprot (www.uniprot.org) proteomes of *B. atrophaeus* 1942 and *P. putida* KT2440.

The sum of precursor ion intensities from the most abundant five peptides for each protein was $\log_2$-transformed, normalized to species abundance and the median subtracted. The mean of the resulting value was calculated across technical replicates for each biological replicate. The resulting values were loaded into the R statistical package (v.3.1.2) and analyzed with the statistical analysis of microarrays (SAM) workflow [Roxas and Li 2008], comparing between biological replicates of co- and pure cultures. After adjustment for multiple testing [Storey 2002], proteins with q-value < 5% were considered significantly different between co-culture and pure culture. These proteins, hereafter referred to as "significant" proteins, were used for subsequent metabolic pathways analysis.

Bacillus or *Pseudomonas* significant proteins were distinguished as less abundant (co-culture/pure culture) < 1) or more abundant (co-culture/pure culture) > 1) in the co-culture. For each species, .fasta files containing sequences for more or less abundant significant proteins were BLAST-searched, mapped and annotated according to Gene Ontology (GO) categories with Blast2GO software v.2.8 (www.blast2go.org). Furthermore, metabolic maps from the KEGG database (http://www.genome.jp/kegg/) were used to determine pathways up- or down-regulated in response to co-culture. Annotations available from Uniprot (www.uniprot.org), as well as from conserved domain searches at NCBI (http://www.ncbi.nlm.nih.gov/), were used to suggest functions of individual significant proteins of interest. Details for protein identification, quantification, and functional analysis are provided in the Appendix (SI 4.1.2).

4.3 Results

4.3.1 Method development to determine LOD of peptides from each species in a mixture of peptides

Phenomena such as ion suppression by highly abundant peptides can diminish accuracy in the detection and quantification of peptides from low-abundance proteins [Ackermann and Berna 2007]. In a mixture of peptides from more than one species, these distortions may be compounded, depending on the species and instrumentation used. Establishing limits of detection (LOD) for peptides in a mixture provides a method for identifying and accounting for these distortions. For these reasons, we aimed to determine accuracy levels for peptide detection at different relative abundances, as part of an application of proteomics to this microbial community.

In the sample containing equal volumes of peptide solution from each species (referred to as "equal peptide mixture" henceforth), a total of 304 proteins (8977 peptides) from *B. atrophaeus* and 381 proteins (9589 peptides) from *P. putida* were identified (1% FDR). The number of protein identifications scaled accurately ($R^2 >$ 0.999) across dilution by three orders of magnitude. Similarly, correlation across dilutions was nearly as good for identified peptides ($R^2 \sim 0.998 – 0.999$) (Figure 10).

In addition, the consistency of protein identification between the pure and mixed samples was examined. In the equal peptide mixture, 257 of the 304 (84.5%) *B. atrophaeus* proteins identified were also found among the 308 proteins identified in a sample containing only *B. atrophaeus* peptides. Similarly, 340 of the 381 (89%) *P. putida* proteins identified in the equal peptide mixture were found among the 444 proteins identified in a sample containing only *P. putida* peptides (Figure 11).

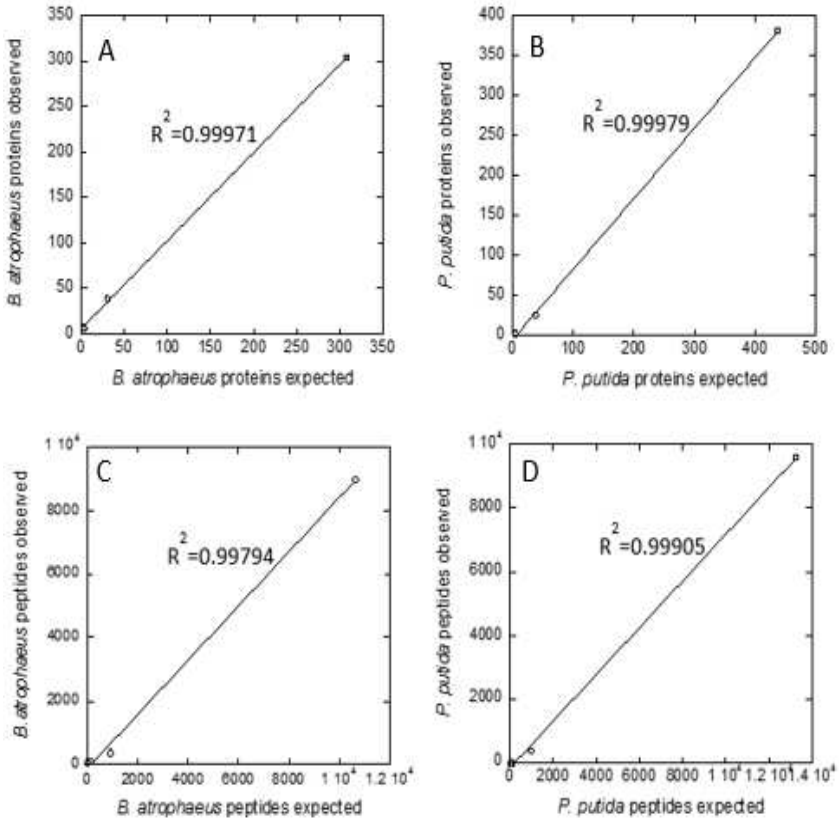

Figure 10**:** Linear correlations between observed identifications of proteins (A-B) or peptides (C-D) for each species compared with values expected if identification scales with total peptide concentration, for pure species peptides diluted into peptides from the other species. Each data point represents the number of proteins or peptides identified by ProteinPilot from two technical replicate LC-MS/MS analyses of the same sample.

Surprisingly, some proteins from each species (47 from *B. atrophaeus*, 41 from *P. putida*) were identified only in the sample containing the constructed mixture of peptides (Figure 11). With serial dilution, the consistency of protein identification decreased (Table 3, Columns 3 and 6).

These proteins consistently were identified across all dilution levels (Table 1, Columns 4 and 7). As *B. atrophaeus* peptides became more diluted in the sample, those

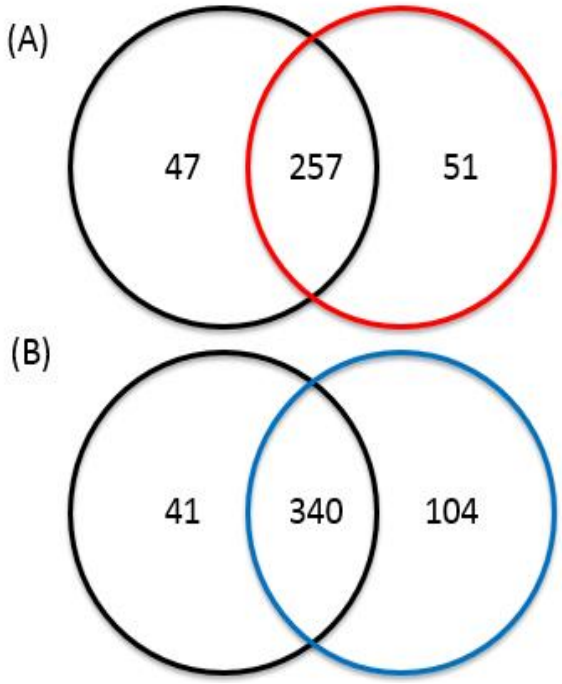

Figure 11: Species-specific protein identifications in common between a sample containing a mixture of ~0.25 µg/µL peptides from *B. atrophaeus* and *P. putida* (black circle) and a sample containing ~0.25 µg/µL peptides from either *B. atrophaeus* alone (red circle in A) or *P. putida* alone (blue circle in B). Protein identifications are from ProteinPilot processing of two combined technical replicate LC-MS/MS runs.

six proteins generally comprised a greater proportion of the total *B. atrophaeus* identified proteins. For example, in the third (10^3) and the sixth dilutions (10^6), all of the identified *B. atrophaeus* proteins were also identified in the sample known to contain only *P. putida* peptides.

Table 3. Number and consistency of protein identifications from each species in constructed peptide mixtures containing decreasing relative abundance of peptides from that species. Identifications were based on combined datasets from two replicate LC-MS/MS runs of each sample. The 10^0 dilution level is an equal peptide mixture

consisting of 50% (v/v) peptides from each species. Increasing dilution levels resulted from diluting that 10^0 sample into 100% peptides from the other species.

Dilution (10^X)	*B. atrophaeus*			*P. putida*		
	IDs	Number (percentage) of IDs shared with 10^0 sample	Number (percentage) of IDs also identified in a pure *P. putida* sample	IDs	Number (percentage) of IDs shared with 10^0 sample	Number (percentage) of IDs also identified in a pure *B. atrophaeus* sample
0	304	257 (100)	3 (1)	381	340 (100)	2 (0.5)
1	39	36 (92)	2 (5)	26	24 (92)	2 (8)
2	7	3 (43)	5 (71)	2	1 (50)	1 (50)
3	4	3 (75)	4 (100)	2	0 (0)	1 (50)
4	2	1 (50)	1 (50)	4	1 (25)	2 (50)
5	6	3 (50)	5 (83)	0	NA (NA)	NA (NA)
6	4	2 (50)	4 (100)	4	3 (75)	1 (25)

4.3.2 Inoculum and culture growth characteristics

The results of the LOD study suggested that the consistency of protein identification decreased considerably after 10-fold dilution. Therefore, we reasoned that a sample containing approximately equal total peptides from each species would be most likely to represent accurately the proteins that were present from each species. Initial co-culture growth studies using an inoculum containing equal CFUs of each species resulted in complete dominance by *P. putida* after 20 h growth, as observed with Gram staining and plate counts (data not shown). When five-fold more *B. atrophaeus* CFUs than *P. putida* CFUs were added as inoculum to the co-culture, there were approximately equal CFUs of each species in the co-culture at the harvest point.

As summarized in Table 4 and shown in the Appendix (SI 4.3: Figure S2), *P. putida* cultures exhibited a significantly greater exponential phase specific growth rate than either *B. atrophaeus* ($p<0.005$) cultures or the co-culture ($p<0.001$).

Table 4. Summary of growth parameters of cultures harvested for proteomics after 20 h growth on 10 g/L tryptic soy broth.

Parameter	*B. atrophaeus*	*P. putida*	Co-culture
Specific growth rate, μ (h^{-1})	0.94 ± 0.02	1.16 ± 0.04	0.9 ± 0.03
Approximate lag phase duration (h)	3.5	6.5	3.5
DCW (10 mL culture) (mg)	12.1 ± 0.4	13.4 ± 0.5	15.7 ± 0.6
Final OD600	3.29 ± 0.16	2.53 ± 0.04	3.24 ± 0.12

The specific growth rate of pure *B. atrophaeus* was not significantly different from that of the co-culture. The duration of the lag phase for both *B. atrophaeus* and the co-culture was 3-4 h, less than the ~6.5 h lag phase for *P. putida*. Inoculating *P. putida* with the same CFU/mL as *B. atrophaeus* decreased the lag phase for *P. putida* pure cultures to ~5.8 h (data not shown), still greater than either *B. atrophaeus* or the co-culture. The dry cell weight (DCW) of the co-culture pellet was significantly greater than that of *B. atrophaeus* ($p<0.002$) or *P. putida* ($p<0.007$). Neither the *P. putida* pure culture nor the co-culture supernatant exhibited a fluorescent green/yellow color that would indicate the presence of the siderophore pyoverdine that *Pseudomonas* species, including *P. putida*, secrete in response to iron limitation [Schalk and Guillon 2013]. Additional growth studies on MHM defined medium indicated a change in total iron concentration during co-culture growth of 30 μg/L (data not shown), well below the estimated total iron concentration in 10 g/L TSB of ~247 μg/L [de Oliveira et al. 2003].

4.3.3 Proteomics results

4.3.3.1 Proteomics results summary

A total of 1146 unique proteins were quantified across all technical and biological replicate samples (1% FDR), of which 1089 proteins (455 from *B. atrophaeus* and 634 from *P. putida*) were identified by two or more peptides. A total of 34914 peptides were identified across all technical replicate runs, of which 5018 peptides were unique and identified with FDR < 1.0%. While the proteome coverage of each species is low (~11% of each species) relative to what can be obtained from pure-culture studies, the total number of protein identifications is comparable to that of proteomics work analyzing co-cultures of microorganisms using similar methodologies [Giannone et al. 2011; Sieber et

al. 2015; Kluge et al. 2012; Enoki et al. 2011]. It is likely that coverage of each species' proteome would have improved by including a fractionation step during sample processing [Ackermann and Berna 2007] or by extracting and processing membrane and cytosolic proteins separately [Domon and Aebersold 2010]. As with any proteomics study, lack of complete proteome identification limits biological interpretation; nevertheless, insights can be obtained that are worth pursuing in additional experimentation, as demonstrated in this study.

For raw intensity data, the mean coefficient of variance (CV) across all technical replicates was 145 ± 23% with a maximum of 188%. After $\log_2$-transformation and normalization, the mean CV decreased to 9.3 ± 1.1%, with a maximum of 10.1%. Of the 1089 quantified proteins with more than one associated peptide, 108 and 173 *B. atrophaeus* proteins were identified as significantly more or less abundant, respectively, in the co-culture compared to the pure culture ($q < 0.05$). Similarly, 137 and 119 *P. putida* proteins were significantly more ("up") or less ("down") abundant ($q < 0.05$), respectively, in the co-culture compared to the pure culture. Selected significantly up and down proteins from each species are listed in Table 5, along with their abundance ratios. Complete lists of significant proteins for each species are provided in the Appendix (SI 4.2: Tables S2-S5).

Table 5. Selected *B. atrophaeus* or *P. putida* significant proteins organized by Gene Ontology category. The "Co/Pure" ratios in the third and fourth columns are the abundance of that protein in co-culture referenced to the abundance in the pure culture, for *B. atrophaeus* and *P. putida*, respectively. Q-Values are multiple test-adjusted error probabilities from SAM testing for significance.

Protein Name	***B. atrophaeus*** **Co/Pure**	***P. putida*** **Co/Pure**	**q-value (%)**
General Metabolism and Gluoconogenesis			
NADP-dependent malic enzyme	3.4		0.0
Alpha-1,4-glucan:maltose-1-phosphate maltosyltransferase	3.0		0.0
Fructose-1,6-bisphosphatase class 1	2.2		0.0
Glyceraldehyde-3-phosphate dehydrogenase	2.0		2.2
2-dehydro-3-deoxyphosphooctonate aldolase 2	1.8		0.0
2-C-methyl-D-erythritol 2,4-cyclodiphosphate synthase	1.7		3.4
Polyhydroxyalkanoate granule-associated protein GA2	1.2		1.4
2-dehydro-3-deoxyphosphooctonate aldolase 1	0.9		3.7
Glucans biosynthesis protein G	0.9		2.7

Sugar ABC transporter, periplasmic sugar-binding protein	0.5		0.7
2-oxoglutarate dehydrogenase complex	0.4		0.0
Porin B	0.4		0.0
Isocitrate dehydrogenase [NADP]	0.3		0.0
Pyruvate kinase	0.3		0.0
Malate dehydrogenase	0.3		0.0
Acetyl-CoA synthetase	0.3		0.0
Succinate dehydrogenase iron-sulfur subunit	0.2		0.0
Succinyl-CoA ligase [ADP-forming] subunit beta	0.2		0.0
Nitrogen Compound Metabolic Process			
2-nitropropane dioxygenase family protein	3.0		0.0
Cryptic glutamate dehydrogenase	0.7		2.2
Glutamine synthetase	0.5	1.0	1.7; 2.7
Nitrogen regulatory protein P-II		0.9	3.7

Cell Division			
UDP-N-acetylmuramoyl-tripeptide--D-alanyl-D-alanine ligase, murF		3.7	0.0
FtsA		3.6	0.0
ZipA homolog		1.4	0.5
OmpA family protein		1.3	0.9
UDP-N-acetylmuramoylalanine--D-glutamate ligase, murD		1.1	2.1
UDP-N-acetylglucosamine 1-carboxyvinyltransferase, murA		0.8	2.1
Cell division protein FtsZ		0.8	2.1
UDP-N-acetylmuramoyl-L-alanyl-D-glutamate--2,6-diaminopimelate ligase, murE	0.6	0.5	1.7; 0.7
D-alanine--D-alanine ligase	0.4		0.8
Regulation of Transcription			
TetR family transcriptional regulator	14.7		0.0

Ribonuclease Y (RNase Y) (EC 3.1.-.-)	12.9		0.0
Putative transcriptional regulator (Lrp/AsnC family) protein	6.3		0.0
Transcription elongation factor NusA	2.8		0.0
GTP-sensing transcriptional pleiotropic repressor CodY	0.3		0.0
Transcription attenuation protein MtrB	0.4		0.5
N utilization substance protein B homolog (Protein NusB)		4.2	0.0
Poly(A) polymerase I (PAP I)		3.1	0.0
Transcriptional regulatory protein RstA, putative		3.0	0.0
N utilization substance protein A (NusA)		2.1	0.0
Response to Stress			
50S ribosomal protein L25 (General stress protein CTC)	3.6		0.0
Lon protease	2.5		0.8
Serine-protein kinase RsbW	2.4		0.8

YceE	0.3		0.0
Putative stress adaptation protein	0.2		0.0
Organic hydroperoxide resistance protein		1.3	0.9
DNA-binding stress protein, putative		0.9	3.7
Universal stress protein family		0.8	2.7
Antibiotic, Toxin, Secondary Metabolite Synthesis or Response			
TetR family transcriptional regulator	14.7		0.0
Putative glycosyltransferase	12.2		0.0
Penicillin-binding lipoprotein 3	6.3		0.0
2,3-dihydroxybenzoate-AMP ligase	5.2		0.0
DNA-directed RNA polymerase subunit beta	0.8		3.4
DNA-directed RNA polymerase subunit beta	0.4		0.5
RND transporter, membrane fusion protein		3.3	0.0
Phenazine biosynthesis protein, PhzF family		2.3	0.0
Phenylacetic acid-specific porin		2.3	0.0

Hydroxyacylglutathione hydrolase (Glyoxalase II)	1.6	0.5
Lactoylglutathione lyase (Glyoxalase I)	1.4	0.5
Toluene-tolerance protein	0.9	2.7

4.3.3.2 General metabolic process

For each species, significant proteins (either more or less abundant in the co-culture) were assigned to Gene Ontology (GO) categories. The GO is a collaborative project to describe gene products in terms of categories of biological processes, cellular components, and molecular function, at up to 15 levels of increasing detail. GO categorization provides an informative initial grouping of proteins to functional categories, in a species-independent manner. For *B. atrophaeus*, 89 of the 108 significantly more abundant proteins (82%) and 150 of the 173 less abundant proteins (87%) in the co-culture were assigned to the broad GO Level 2 category "metabolic process". Most of these metabolic proteins were distributed into more specific GO Level 3 subcategories, including organic substance metabolic processes, nitrogen compound metabolic processes, cellular metabolic processes, and single-organism metabolic processes (Figure 12). GO categorization of *P. putida* proteins assigned 105 of the 137 significantly more abundant *P. putida* proteins (72%) and 88 of the 119 less abundant *P. putida* proteins (74%) to the broad category "metabolic process". The most represented Level 3 GO categories for significant *P. putida* proteins were organic substance

metabolic process, primary metabolic process, cellular metabolic process, and biosynthetic process (Figure 13).

Significant proteins also were analyzed according to pathways in KEGG, a curated database consisting of annotated genes, proteins and metabolites integrated with information about interaction and reaction networks. KEGG is most useful for assigning proteins, especially enzymes, to functional pathways operational in the higher-order biological system. Generally, *B. atrophaeus* significant proteins in KEGG pathways related to central metabolism (TCA cycle, glycolysis, electron transport chain) were less abundant in the co-culture than in the pure culture, while proteins in pathways related to terpenoid and polyketide synthesis were significantly more abundant in the co-culture. Biosynthesis of antibiotics was the most or second-most well-represented KEGG pathway for both more and less abundant *B. atrophaeus* proteins in the co-culture. Pathways for fatty acid biosynthesis (including the acetyl-coA carboxylase enzyme) and glycerolipid metabolism exhibited mixed modulation in response to co-culture (Appendix SI 4.2: Table S12).

Analysis by KEGG categorized *P. putida* proteins more abundant in the co-culture into categories associated with purine metabolism, biosynthesis of antibiotics, amino acid biosynthesis, carbon fixation, and pathways associated with the biosynthesis, elongation, and degradation of fatty acids. Similar to *B. atrophaeus*, biosynthesis of antibiotics was either the first- or second-most well-represented KEGG pathway for both more and less abundant *P. putida* proteins (Appendix SI 4.2: Table S13).

4.3.3.3 Cell division and growth

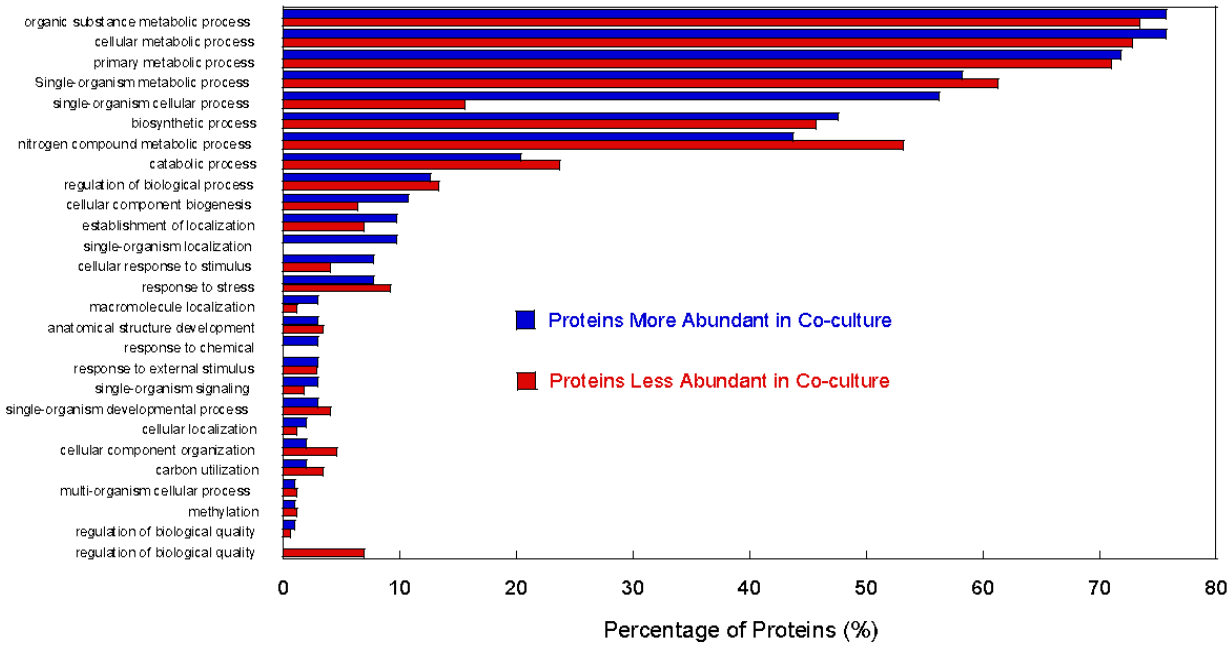

Figure 12: Relative abundance of GO Level 3 categories for significant *B. atrophaeus* proteins.

Modulation in abundance of proteins associated with cell division and growth suggests direct or indirect impacts of co-culture on fundamental growth processes. No *B. atrophaeus* proteins related to growth were more abundant in the co-culture, while two cell growth regulators were less abundant. Two proteins involved in peptidoglycan biosynthesis and three proteins associated with inosine 5'-phosphate (IMP) processing were less abundant, suggesting suppression of transcription and cell division (Table 5). For *P. putida*, in contrast, five cell division proteins were more abundant in the co-culture, including cytokinesis proteins FtsA and a homolog of ZipA. Additionally, the abundance of four of the first six proteins in the *mur* pathway for peptidoglycan

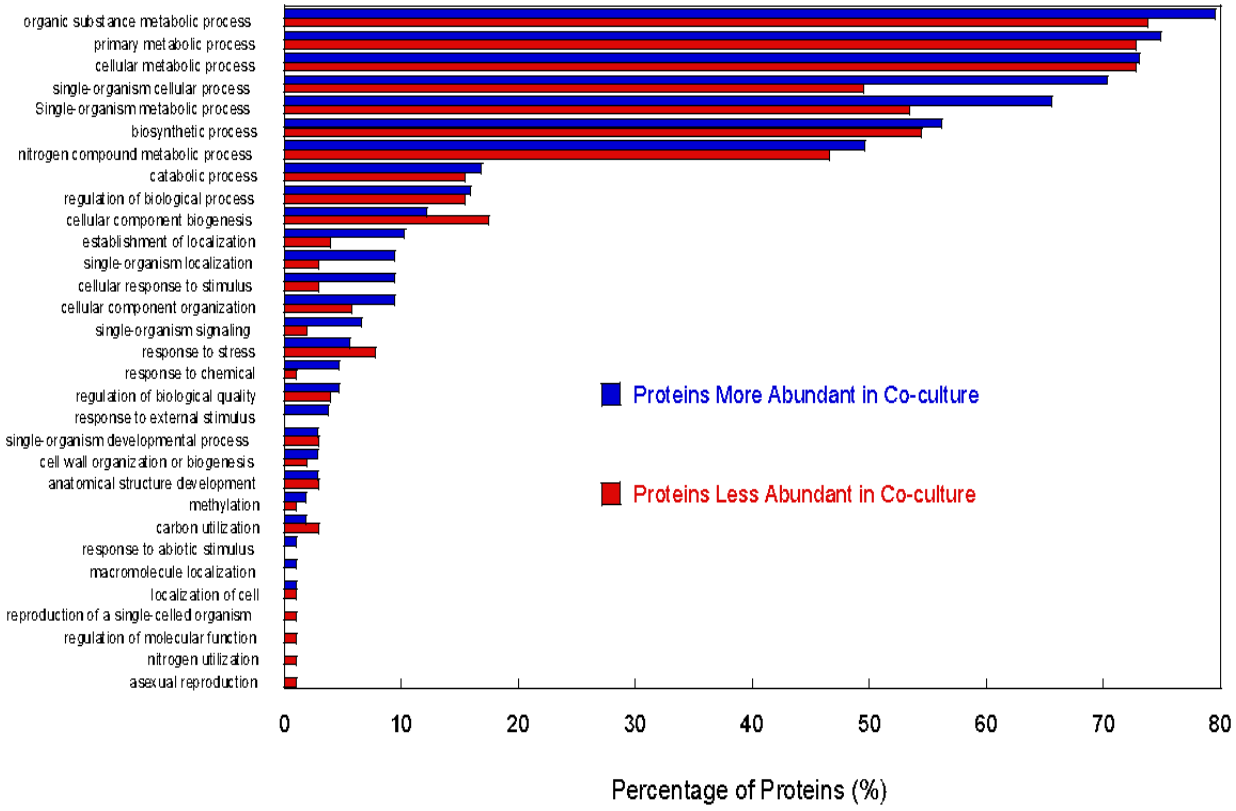

Figure 13: Relative abundance of GO Level 3 categories for significant *P. putida* proteins.

biosynthesis were modulated in response to co-culture. In contrast to *B. atrophaeus*, three *P. putida* proteins related to biosynthesis of IMP were more abundant in the co-culture (Table 5).

4.3.3.4 Regulation of transcription and translation

Proteins associated with GO and KEGG categories of transcription and translation are indicators of overall levels of metabolic activity. Impacts on *B. atrophaeus* proteins associated with the GO transcription category were mixed: 14 more abundant and nine less abundant in the co-culture. KEGG analysis indicated that significant *B. atrophaeus*

proteins in pathways associated with nucleotide metabolism generally were less abundant in the co-culture. On the other hand, 15 *P. putida* proteins associated with transcription were more abundant in the co-culture (including transcriptional regulators NusA and NusB), while just five transcription proteins were less abundant.

Similar to the case of transcription-associated proteins, *B. atrophaeus* translation proteins also showed a mixed response to co-culture. Ribosomal proteins generally increased in abundance: 11 proteins were more abundant and just three were less abundant in the co-culture. In contrast, non-ribosomal translation proteins generally were less abundant in the co-culture. Similarly, KEGG analysis grouped 23 *B. atrophaeus* proteins that were less abundant in the co-culture into the biosynthesis of amino acids pathway, while only four more-abundant proteins were grouped into that pathway. Nine *P. putida* proteins related to translation were more abundant in the co-culture, including a ribosome hibernation promoting factor. Meanwhile, 14 *P. putida* ribosome proteins were less abundant in the co-culture, as well as a ribosome biogenesis protein and three elongation factors (Table 5).

4.3.3.5 Secondary metabolites, antibiotics, and toxins

For each species in the co-culture, significant proteins were assigned to GO categories related to antagonistic compounds. Several *B. atrophaeus* significant proteins indicated a response to antibiotics or toxins. These included a TetR family transcriptional regulator and a glycosyltransferase that had the greatest and third-greatest fold-change, respectively, of any *B. atrophaeus* significant protein (Table 5).

For *P. putida*, biosynthesis of secondary metabolites and of antibiotics were the second- and third-most well represented KEGG pathways, respectively, among significant proteins (Appendix SI 4.2: Table S13). A *P. putida* protein in the PhzF family related to synthesis of the antibiotic and siderophore phenazine, as well as four proteins related to phenylacetic acid transport and degradation were more abundant in the co-culture than in pure culture. A *P. putida* RND transporter involved in antibiotic resistance [Blair et al. 2014] and activated during swarming motility [Overhage et al. 2008], was more abundant in the co-culture (Table 5).

4.3.3.6 Motility, biofilm, and virulence proteins

The *B. atrophaeus* protein with the second-greatest increase in the co-culture was RNAse Y, an enzyme associated with virulence that is responsible for mRNA-degradation during rapid changes in growth conditions [Lehnik-Habrink et al. 2012]. Additionally, four *B. atrophaeus* proteins associated with flagellar processes or chemotaxis were less abundant in the co-culture, while no proteins for these processes were more abundant (Table 5). In contrast, seven *P. putida* proteins associated with flagellar processes or chemotaxis were more abundant in the co-culture, while just two *P. putida* motility proteins, FliC and MreB, were less abundant. The type IV pili twitching motility protein PilT was determined by SAM to be significantly more abundant in the co-culture. There also was a large increase in FtsA, a decrease in FtsZ, and an increase in MinD, changes associated with inhibition of cell division and initiation of filamentous growth [Loose and Mitchison 2014; Shih and Rothfield 2006].

Changes in abundance in proteins related to biofilm production were observed for each species. In addition to the decrease in proteins for flagellar or chemotaxis processes,

B. atrophaeus showed 2.5-fold increased abundance of a master biofilm regulator. *P. putida* showed modulation in proteins associated with alginate production as part of a mucoid phenotype during biofilm production (Table 5). The pleiotropic enzyme SuhB, a regulator of biofilm formation during virulent phenotypes, was more abundant for *P. putida* in the co-culture. Finally, there was increased abundance of *P. putida* proteins (e.g, GlgB) related to intracellular polysaccharide (glycogen) storage, a process that has been associated with carbon storage for biofilm formation [Busuioc et al. 2009].

4.3.3.7 Metal ion binding

Of the 1089 quantified proteins, 213 (~20%) were related to binding of a metal. Nearly all of these metal-binding proteins bound iron, magnesium, or zinc. The set of significant *B. atrophaeus* proteins was more enriched ($p < 0.05$, one-tailed Fisher's exact test) in iron- and zinc-binding proteins than the set of total *B. atrophaeus* proteins (Figure 9A). Likewise, the set of significant *P. putida* proteins was more enriched than the set of total *P. putida* proteins in magnesium-binding proteins (Figure 9B).

Several groups of proteins suggested iron stress in *B. atrophaeus* in co-culture with *P. putida*. Ten (5.8%) of the *B. atrophaeus* proteins less abundant in the co-culture were iron-binding, compared to just three (2.8%) of the more abundant proteins. In contrast, 2.9% and 3.3% of the more and less abundant *P. putida* proteins, respectively, were iron-binding. Furthermore, two significant *B. atrophaeus* proteins were associated with iron acquisition *via* siderophores. 2,3-Dihydroxybenzoate-AMP ligase, more abundant in the co-culture, is necessary for the synthesis of 2,3-dihydroxybenzoyl glycine, a catechol siderophore [Grossman et al. 1993]. The other protein, less abundant in the co-culture (Appendix SI 4.2: Table S9), is an ABC transporter that binds

lipoproteins associated with ferric iron acquistion [Schneider and Hantke 1993]. Additionally, two *B. atrophaeus* proteins associated with ferric iron transport system—both the lipoprotein and the transporter components—were less abundant in the co-culture. Other than the phenazine biosynthesis protein PhzF, no *P. putida* siderophore proteins were identified.

4.3.4 Physiological experiments motivated by proteomics results

Results from preliminary growth experiments and proteomics suggested antagonistic interactions between these two species in co-culture. Co-cultures inoculated with equal CFU of each species were dominated by *P. putida* at the harvest point. Moreover, as described above, there were significant differences in the abundance of proteins from both species that were associated with synthesis and response to antibiotics, siderophore biosynthesis, biofilm formation, swarming motility, and virulence.

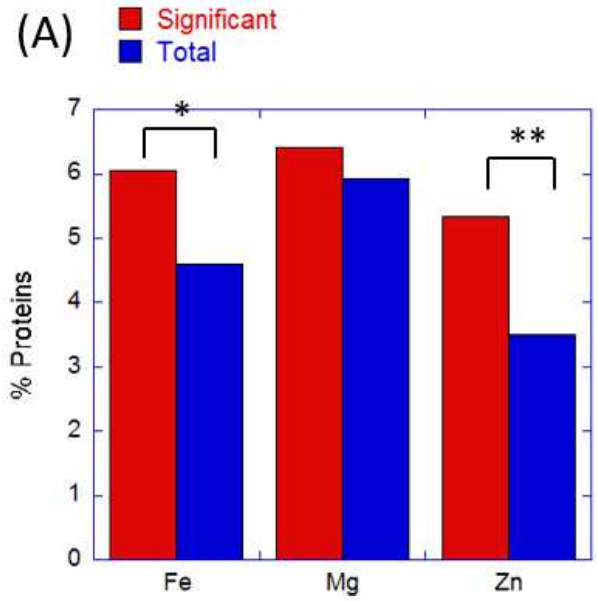

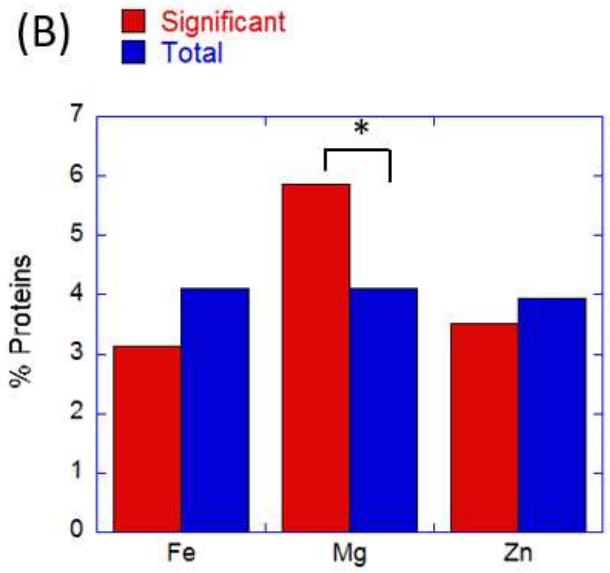

Figure 14: Percentages of significant and total (A) *B. atrophaeus* proteins or (B) *P. putida* proteins identified by LC-MS/MS that were associated with binding iron, magnesium, or zinc. Significance testing was conducted with a Fisher's one-tailed exact test (*p<0.05, **p<0.01).

Follow-up physiological experiments were conducted to obtain additional information on possible antagonistic interactions.

4.3.4.1 B. atrophaeus *growth in the presence of co-culture supernatant*

The upregulation of *P. putida* proteins associated with antibiotic biosynthesis and virulence suggested that there may be soluble factors in the co-culture supernatant that would inhibit *B. atrophaeus* growth. *B. atrophaeus* growing in 50% (v/v) filter-sterilized supernatant from stationary *B. atrophaeus* cultures entered exponential growth phase slightly before cultures of *B. atrophaeus* growing in 50% filter-sterilized supernatant from pure *P. putida* or co-culture (Appendix SI 4.3: Figure S14). No significant

differences in exponential specific growth rate were observed due to the type of supernatant added.

Disk diffusion studies revealed no discernible zones of inhibition on lawns of *B. atrophaeus* around disks saturated with either filter-sterilized or non-filtered supernatant from *P. putida* or the co-culture. Furthermore, no zone of inhibition was observed even after 10X concentration or ethyl acetate extraction of the supernatants. Likewise, use of ethyl acetate extracts of the agar plates from the colony proximity studies (Section 4.3.4.2 below) did not result in observable zones of inhibition on *B. atrophaeus* lawns (data not shown).

4.3.4.2 Colony growth in proximity

Approximately three days after spotting each species in proximity on a 10 g/L TSB plate, *B. atrophaeus* colonies were observed growing away from *P. putida* colonies, while the *P. putida* colonies appeared to advance towards the *B. atrophaeus* colonies (Figure 15A). After approximately one week of growth, filamentous structures were observed radiating from *P. putida* colonies toward *B. atrophaeus* colonies and the plates were suffused with a yellow-colored compound. After two weeks of proximate growth, *P. putida* dominated plate growth, in some cases growing over *B. atrophaeus* colonies (Figure 15B). No filamentous growth structures were observed when *P. putida* was grown alone on a plate (Appendix SI 4.3: Figure S15).

4.3.4.3 Metal-limitation culture experiments

Proteins binding iron and zinc were enriched among significant *B. atrophaeus* proteins compared with non-significant proteins (Section 4.3.3.7). A similar pattern was

observed for *P. putida* proteins binding magnesium. Based on these results, we hypothesized that the relative abundance of each species in co-culture would be affected by limitation of each of these metals. Growth in defined medium under iron or zinc limitation resulted in co-culture dominance by *P. putida*, as indicated by a significant ($p<0.05$, two-tailed t-test, equal variances) decrease in the CFU ratio (CFU *B. atrophaeus*/CFU *P. putida*) (Figure 16). Unlike the cultures used for proteomics grown in 10 g/L TSB medium, the iron-limited co-cultures in defined medium were visibly

(A)

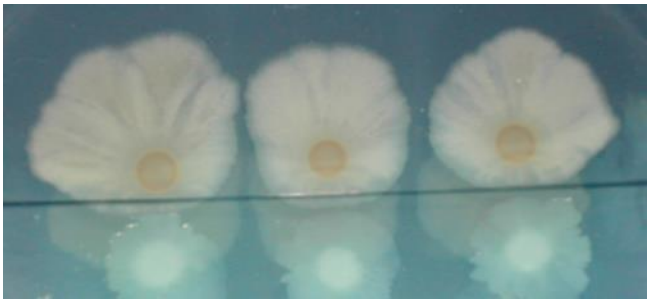

(B)

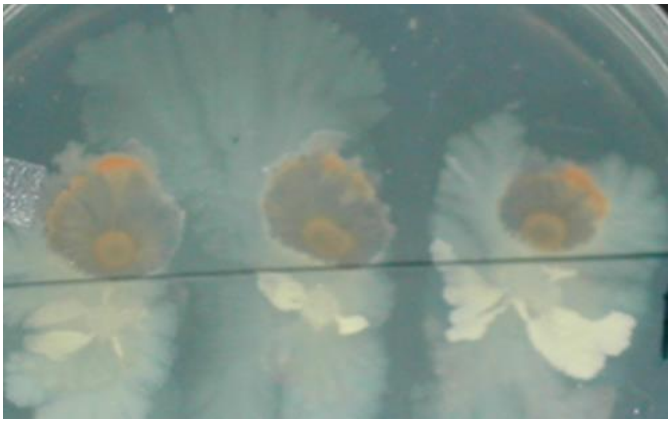

Figure 15: Representative plates (A) three days and (B) two weeks after spotting 2 µL of stationary phase culture of each species across from each other on a 10 g/L TSB plate. *B. atrophaeus* and *P. putida* were colonies are above and below the marked line, respectively. Filamentous structures are visible for *P. putida* after two weeks of growth.

fluorescent green/yellow, consistent with production of pyoverdine siderophore by *P. putida* [Schalk and Guillon 2013]. Conditions of magnesium limitation, on the other hand, resulted in a significant increase in the species CFU ratio, indicating *B. atrophaeus* dominance.

4.4 Discussion

4.4.1 LOD of peptides of a species in a peptide mixture

Proteomic investigations of mixed cultures generally do not first identify LODs for peptides and proteins from the culture members. Not knowing these limits may result in inaccurate identification or quantification of proteins from species present in low relative abundance. Here, the number of protein identifications from either species in the co-culture remained consistent with the number of identifications that would be expected just based on dilution, as the relative abundance of peptides from that species was decreased by 10- or 100-fold (Figure 10). Furthermore, the consistency of identities of those proteins was maintained after 10-fold decrease in relative abundance, but less so with further dilution (Table 3).

For both species, proteins were identified at all dilution levels up to 10^6 (Table 3). However, the proteins that were identified at more diluted levels were often those

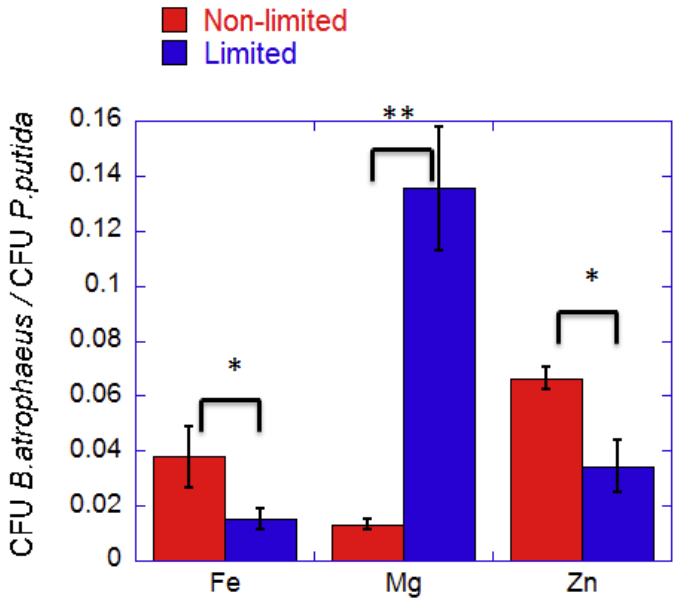

Figure 16**:** CFU ratios for each culture under conditions of non-limited and limited metal concentrations. Non-limiting and limiting concentrations of metals added to the defined minimal medium (MHM): $FeSO_4$ (36 µM and 0.9 µM); $MgCl_2$ (1 mM or 12 µM); $ZnSO_4$ (10 µM or 0 µM). (*p<0.05, **p<0.01, Student's t-test)

identified in samples known not to contain any peptides at all from that species (Appendix SI 4.2: Table S13). This suggests a systematic misidentification of proteins when peptides corresponding to them are at very low concentrations. This misidentification may be due to the use of a database consisting of combined proteomes of both species, as would be the case when using a database derived from a sequenced meta-genome. The use of a combined database also may be responsible for the identification of 47 *B. atrophaeus* proteins and 41 *P. putida* proteins only in the samples containing peptides from both species (Figure 11). Thus, in addition to concerns about non-detection of peptides present in low relative abundance [Keshishian et al. 2007], misidentification of proteins from low-abundance peptides (less than 10X as abundant)

also may be a concern, even after application of a standard 1% FDR filter. This concern may be especially pronounced when using a database of combined proteomes, as is usually the case in meta-proteomics studies.

The goal of this set of experiments was to determine a baseline LOD using a robust peptide separation method (nano- reverse-phase LC). The results suggest that to confidently quantify proteins from any species that is less than 10% as abundant than other species likely would require additional fractionation or depletion steps. The method used here to determine detection and identification limitations would be a beneficial step in other microbial meta-proteomics studies for setting limits on the confidence of protein identification from low-abundance species in a mixed culture.

4.4.2 Physiological and proteomic characteristics of growth and central metabolism

B. atrophaeus exhibited a shorter lag time in batch culture in 10 g/L TSB than *P. putida*, even when both species were inoculated with equivalent CFU/mL (Table 4; Appendix 4.3: Figure S13). However, the specific growth rate of *B. atrophaeus* during exponential phase was less than that of *P. putida* (Table 4). The lag time and specific growth rate of the co-culture more closely mirrored those of *B. atrophaeus*, consistent with an interpretation that *B. atrophaeus* dominated early stages of growth. The increasing dominance of *P. putida* during the course of co-culture growth suggests that, once adapted to medium conditions, *P. putida* was able to outcompete *B. atrophaeus* due to a faster growth rate or other competitive mechanisms. In a previous study, a similar pattern in a co-culture of *B. cereus* and *P. fluorescens* was observed in a continuous chemostat system, showing eventual complete dominance by *P. fluorescens* [Simoes et al. 2008]. Interestingly, in the present study, the dry cell mass concentration of the co-

culture was significantly greater than that of either of the pure cultures (Table 4), suggesting that growth of one or both species was stimulated during co-culture. Alternatively, growth in either pure culture may have been inhibited before complete depletion of nutrients by a mechanism (e.g., quorum sensing) effective in pure cultures that was disrupted in co-culture.

Proteomics results for metabolic proteins generally supported the trends observed in growth kinetics. Previous proteomics studies have reported changes in the abundance of metabolic proteins that were associated with altered growth patterns in response to co-culture [Giannone et al. 2011; Ruiz et al. 2009]. In the present study, a greater percentage of more abundant *P. putida* proteins than less abundant proteins were binned into the GO category “metabolic process." The same was true for the GO categories of cell division (e.g., FtsA), and transcription (e.g., ribonucleases) [Yao et al. 2011]. The converse was true of *B. atrophaeus*. This suggests that co-culturing stimulated *P. putida* metabolism at the expense of *B. atrophaeus* metabolism, an interpretation corroborated by a decrease in abundance of many *B. atrophaeus* proteins associated with glycolysis and the TCA cycle as well as with the phosphotransferase system of sugar uptake (Appendix SI 4.2: Table S9). The suppression of *B. atrophaeus* metabolism is consistent with a scenario in which *P. putida* outcompeted *B. atrophaeus* for nutrients in the co-culture. At the same point in a growth curve, fewer nutrients would have been available for *B. atrophaeus* cells in a co-culture compared with *B. atrophaeus* cells in pure culture. In that case, *B. atrophaeus* cells in the co-culture would have shifted earlier than pure culture *B. atrophaeus* to a physiology more characteristic of early stationary phase. Indeed, several *B. atrophaeus* proteins more abundant in the co-culture suggested a shift

to catabolism of fatty acids (methylisocitrate lyase and NADP-dependent malic enzyme) and nucleotides (deoxyribose-phosphate aldolase).

4.4.3 Biosynthesis of antagonistic compounds

The observed growth patterns in planktonic and plate-based co-cultures suggested antagonism between these two species, both of which are known to synthesize antimicrobial compounds [Weller 2007; Leifert et al. 1995;]. Therefore, we searched the proteomic data for possible mechanisms of antagonism. Evidence for a response to antagonistic compounds was present for both species. The *B. atrophaeus* significant protein with the greatest fold-increase was a TetR regulator, part of the efflux pump response to tetracyline or toxic substances [Blair et al. 2015]. *B. atrophaeus* in co-culture also exhibited increased abundance of a penicillin-binding liproprotein containing a beta-lactamase motif as well as decreased abundance of proteins such as RNA polymerase related to translation and amino acid biosynthesis. Similarly, response of co-cultured *P. putida* to antagonism was reflected in the greater abundance of several proteins in the *paa* pathway for the degradation of phenylacetate. This compound is known to be secreted by *B. licheniformis* as an antimicrobial [Kim et al. 2004], suggesting secretion of a similar compound by *B. atrophaeus*, a *Bacillus* species closely related to *B. licheniformis* [Chun and Bae 2000].

Several *P. putida* proteins more abundant in the co-culture were responsible for phenazine biosynthesis, including PhzF, the critical protein for phenazine production [Parsons et al. 2004]. *Pseudomonas* species, including *P. putida*, are known to secrete more than 80 different types of phenazines, such as phenazine-1-carboxylic acid (PCA), phenazine-1-carboxamide, and pyocyanin [Mavrodi et al. 2006]. These aromatic

compounds fulfill multiple functions for pseudomonads, including iron-scavenging and anti-microbial activity [Price-Whelan et al. 2006; Wood et al. 1996; Piersen and Piersen 1996] as well as signaling for biofilm production [Wang et al. 2011].

Despite the proteomic results suggesting synthesis of antimicrobials by each species in response to co-culture, the growth rate of neither organism was significantly decreased in the presence of supernatant from the co-culture. This suggests that each species may have been able to adapt successfully to antagonistic compounds secreted by the other species. Alternatively, the concentration of antagonistic compounds may have been insufficient to result in the sort of inhibition observed previously for *B. subtilis* in the presence of purified phenazines from *P. aureofaciens* [Toohey et al. 1965]. In any case, the lack of inhibition of *B. atrophaeus* by co-culture supernatant suggests that the initial observations of co-culture dominance by *P. putida* likely was due to the faster growth rate of *P. putida* (Table 4) or some other interaction, rather than inhibitory effects of soluble compounds secreted by *P. putida*. The obvious inhibition of *B. atrophaeus* on a plate (Figure 15) may have been due to greater concentrations of inhibitory compounds secreted by *P. putida* at the interface between colonies on the plate. These compounds may include surfactants associated with changes to a swarming type of motility [Caiazza et al. 2005].

4.4.4 Motility, biofilm, and virulence responses by P. putida

Co-culture with *B. atrophaeus* elicited changes in the *P. putida* proteome that are usually associated with growth on a surface: swarming motility and biofilm formation. The pleiotropic enzyme SuhB, known to be essential for virulence in *P. aeruginosa*, catalyzes the first step in the pathway for streptomycin synthesis; it is implicated in

resistance to antibiotics, biofilm production, motility, and the Type III secretion system [Li et al. 2013]. A biofilm-formation response was suggested by the increase in phenazine-production proteins [Sakhtah et al. 2016; Das et al. 2015; Wang et al. 2011], decrease in FliC [Ghadaksaz et al. 2015; Bardoel et al. 2011] and increase in proteins associated with the production of alginate [Ghadaksaz et al. 2015; Hentzer et al. 2001; Boyd and Chkrabarty 1995] observed in co-culture. The observed decreases in abundance of FliC and GyrA are also consistent with a motility change that is associated with virulence [Osman et al. 2016; Redgrave et al. 2014]. Moreover, a shift to filamentous growth was evidenced clearly by a large increase in the ratio of FtsA to FtsZ, a decrease in RNase E, and an increase in abundance of MinD [Lutkenhaus 2007; Tamura et al. 2006], a phenotype previously associated with swarming motility [Kearns 2010]. Twitching or swarming motility was also suggested by increased abundance of PilT, part of a type IV pilus system known to be essential for virulence in *Pseudomonas* [Kohler et al. 2000; Ghadaksaz et al. 2015; Overhage et al. 2008]. In the present study *P. putida* showed a clear phenotypic change to a swarming-type of motility only in the presence of *B. atrophaeus* (Figure 15; Appendix SI 4.3: Figure S15; Appendix SI 4.2: Table S9). Swarming motility and biofilm production in *P. putida* have been associated previously with production of antibiotics targeting other Pseudomonads [Li et al. 2013], but not in response to a *Bacillus* species. In contrast, little change was observed in the motility of *B. atrophaeus* during growth with *P. putida* on a plate, though *B. atrophaeus* actively grew away from advancing *P. putida*, similar to the recently-reported response of *B. subtilis* in the presence of *Streptomyces* sp. Mg1 [Stubbendieck and Straight 2016]. It is possible that the agar percentage (1.5%) of these plates prevented changes in motility

phenotype in *B. atrophaeus*, while not preventing motility changes in *P. putida* [Kearns 2010]. While the cultures used here for proteomics were planktonic, the increase in biofilm and motility proteins triggered by co-culture suggest that the *P. putida*'s overall virulence response includes proteins associated with surface growth. Future work could identify the particular form of swarming motility induced in *P. putida* by the presence of *B. atrophaeus* during surface-associated growth and investigate how this phenotype could be involved in interactions between the species in planktonic culture.

4.4.5 Metal-binding as competitive strategy

Competitive interactions between species under limiting conditions of certain metals is well-documented [Traxler et al. 2012; Mulcahy and Lewenza 2011; Hibbing et al. 2010]. Numerous studies have described the biosynthesis of siderophores to sequester iron by both *Bacillus* [Hotta et al. 2010] and *Pseudomonas* [Schalk 2008]. In the present study, there was no visual evidence for pyoverdine in any of the co-cultures at the point of harvest for proteomics. Nevertheless, there was proteomic evidence for iron stress in *B. atrophaeus*, as indicated by the synthesis of siderophores and a marked decrease in abundance of iron-binding proteins, including proteins in central metabolic pathways (aconitase, succinate dehydrogenase). Iron stress therefore may have contributed to curtailing *B. atrophaeus* metabolism in the co-culture earlier than in the pure culture, inducing fatty acid or nucleotide metabolism as discussed above (Section 4.4.2). Clearly, there was a modulation in iron-binding protein expression by *B. atrophaeus* in response to co-culture, but the mechanism of this response is not completely clear.

A large proportion (>20%) of all identified proteins in this study were associated with binding metals, particularly iron, zinc, and magnesium (Figure 14). The importance

of these metals for each species was suggested by sensitivities of each species to metal limitation (Figures 14 and 16). Dominance by *P. putida* under iron-limited conditions is not surprising, considering its well-known use of siderophores [Joshi et al 2014]. Competition between bacteria for zinc is less well-understood. While Zur and Zna proteins characteristic of zinc limitation [Prestel et al. 2015; D'Orazio et al. 2015] were not identified in the present study, the increase in *B. atrophaeus* zinc-binding proteins in response to co-culture is consistent with observations for gut microbes when zinc is limited [Gielda and DiRita 2012]. Redundant mechanisms for zinc acquisition [D'Orazio et al. 2015] or superior biosorption capabilities [Joo et al. 2010] in *Pseudomonas* may be responsible for the observed dominance of co-cultures by *P. putida* under zinc limitation. Finally, the sensitivity of *P. putida* to magnesium limitation observed here (Figure 16) is consistent with previous observations for *P. aeruginosa* [Andersen et al. 2010]. Interestingly, changes in magnesium availability have been shown previously to stimulate adhesion and biofilm formation [Mulcahy and Lewenza 2011; Song and Leff 2006] as well as phenazine biosynthesis in *Pseudomonas* species [Guina et al. 2003], consistent with proteome responses observed in the present study in response to competition in co-culture. For each of these metals, significant differences in the abundance of proteins binding the metal may be part of a broad competitive response by each species to the presence of another species. Many previous studies have described competition for metals in soil ecosystems; the contribution of the present work is to describe functional protein expression related to this type of competition between two model soil species. Future work could investigate the significance of changes in abundance of metal-binding

proteins—especially magnesium and zinc—as part of the competition for essential metals within complex soil microbial ecosystems.

CHAPTER 4 REFERENCES

Abo-Aba SEM, Sabir JSM, Baeshen MN, Sabir MJ, Mutwakil MHZ, Baeshen NA, D'Amore R, Hall N. (2015) Draft genome sequence of *Bacillus* species from the rhizosphere of the desert plant *Rhazya stricta*. Genome Announc 3:e00957-15. doi: 10.1128/genomeA.00957-15

Ackermann BL and Berna MJ. (2007) Coupling immunoaffinity techniques with MS for quantitative analysis of low-abundance protein biomarkers. Exp Rev Proteom 4:175-186. doi: 10.1586/14789450.4.2.175

Andersen GG, Yahr TL, Lovewell RR, O'Toole GA. (2010) The *Pseudomonas aeruginosa* magnesium transporter MgtE inhibits transcription of the type III secretion system. Infect Immun 78:1239-1249. doi: 10.1128/IAI.00865-09

Baldrian P, Lopez-Mondejar R (2014) Microbial genomics, transcriptomics and proteomics: new discoveries in decomposition research using complementary methods. App Microbiol Biotechnol 98:1531-1537. doi: 10.1007/s00253-013-5457-x

Bakker MG, Schlatter DC, Otto-Hanson L, Kinkel LL (2013) Diffuse symbioses: roles of plant-plant, plant-microbe and microbe-microbe interactions in structuring the soil microbiome. Molec Ecol 23:1571-1583. doi: 10.1111/mec.12571

Bardoel BW, van der Ent S, Pel MJC, Tommassen J, Pieterse CMJ, van Kessel KPM, et al. (2011) *Pseudomonas* Evades Immune Recognition of Flagellin in Both Mammals and Plants. PLoS Pathog 7:e1002206. doi: 10.1371/journal.ppat.1002206

Barlow J, Gozzi K, Kelley CP, Geilich BM, Webster TJ, Chai Y, Sridhar S, van de Ven AL (2017) High throughput microencapsulation of *Bacillus subtilis* in semi-permeable biodegradable polymersomes for selenium remediation. App Microbiol Biotech 101:455-464. doi: 10.1007/s00253-016-7896-7

Blair JMA, Webber MA, Baylay AJ, Ogbolu DO, Piddock LJV (2015) Molecular mechanisms of antibiotic resistance. Nat Rev Microbiol 13:42-51. doi: 10.1038/nrmicro3380

Blair JMA, Richmond GE, Piddock LJV (2014) Multidrug efflux pumps in Gram-negative bacteria and their role in antibiotic resistance. Fut Microbiol 9:1165-1177. doi: 10.2217/fmb.14.66

Boyd A and Chakrabarty AM (1995) *Pseudomonas aeruginosa* biofilms: role of the alginate exopolysaccharide 15:162-168. doi: 10.1007/BF01569821

Busuioc M, Mackiewicz K, Buttaro BA, Piggot PJ (2009) Role of intracellular polysaccharide in persistence of *Streptococcus mutans*. J Bacteriol 191:7315-7322. doi: 10.1128/JB.00425-09

Caiazza NC, Shanks RMQ, O'Toole GA (2005) Rhamnolipids modulate swarming motility patterns of *Pseudomonas aeruginosa*. J Bacteriol 187:7351-7361. doi: 10.1128/JB.187.21.7351-7361.2005

Chen Y, Yan F, Chai Y, Liu H, Kolter R, Losick R, Guo J-h (2013) Biocontrol of tomato wilt disease by *Bacillus subtilis* isolates from natural environments depends on conserved genes mediating biofilm formation. Environ Microbiol 15:848-864. doi: 10.1111/j.1462-2920.2012.02860.x

Chignell JF, Park S, Lacerda CMR, De Long SK, Reardon KF (2018) Label-free proteomics of a defined, binary co-culture reveals diversity of competitive responses between members of a model soil microbial system. Microb. Ecol. 75:701-719

Choi H and Nesvizhskii AI (2008) False discovery rates and related statistical concepts in mass spectrometry-based proteomics. J Proteome Res 7:47-50. doi: 10.1021/pr700747q

Chun J and Bae KS (2000) Phylogenetic analysis of *Bacillus subtilis* and related taxa based on partial *gyrA* gene sequences. Antonie van Leeuwenhoek 78:123-127. doi: 10.1023/A:1026555830014

Das T, Kutty SK, Tavallaie R, Ibugo AI, Panchompoo J, Sehar S, Aldous L, Yeung AWS, Thomas SR, Kumar N, Gooding JJ, Manefield M (2015) Phenazine virulence factor binding to extracellular DNA is important for *Pseudomonas aeruginosa* biofilm formation. Sci Rep 5: doi: 10.1038/srep08398

de Oliveira Moreira L, Andrade AFB, Vale MD et al (2003) Effects of iron limitation on adherence and cell surface carbohydrates of *Corynebacterium diphtheria* strains. Appl Environ Microbiol 69:5907-5913. doi: 10.1128/AEM.69.10.5907-5913.2003

Di Cagno R, De Angelis M, Coda R, Minervini F, Gobbetti M (2009) Molecular adaptation of sourdough *Lactobacillus plantarum* DC400 under co-cultivation with other lactobacilli. Res Microbiol 160:358-366.

Dolinsek J, Goldschmidt F, Johnson DR (2016) Synthetic microbial ecology and the dynamic interplay between microbial genotypes. FEMS Microbiol Rev 40:961-979. doi: 10.1093/femsre/fuw024

Domon B, Aebersold R (2010) Options and considerations when selecting a quantitative protoemics strategy. Nat Biotech 28:710-721. doi: 10.1038/nbt.1661

D'Orazio M, Mastropasqua MC, Cerasi M, Pacello F, Conosalvo A, Chirullo B, Mortensen B, Skaar EP, Ciavardelli D, Pasquali P, Battistoni A (2015) The capability of *Pseudomonas aeruginosa* to recruit zinc under conditions of limited metal availability is affected by inactivation of the ZnuABC transporter. Metallomics 7:1023-1035. doi: 10.1039/C5MT00017C

Edfors F, Danielsson F, Hallstrom BM, Kall L, Lundberg E, Ponten F, Forsstrom B, Uhlen M (2016) Gene-specific correlation of RNA and protein levels in human cells and tissues. Molec Syst Biol 12:883. doi: 10.15252/msb.20167144

Enoki M, Shinzato N, Sato H, Nakamura K, Kamagata Y (2011) Comparative Proteomic Analysis of *Methanothermobacter themautotrophicus* ΔH in Pure Culture and in Co-Culture with a Butyrate-Oxidizing Bacterium. PLoS ONE 6: e24309. doi: 10.1371/journal.pone.0024309

Franzosa EA, Hsu T, Sirota-Madi A, Shafquat A, Abu-Ali G, Morgan XC, Huttenhower C (2015) Sequencing and beyond: integrating molecular 'omics' for microbial community profiling. Nat Rev Microbiol 13:360-372. doi: 10.1038/nrmicro3451

Ghadaksaz A, Fooladi AAI, Hosseini HM, Amin M (2015) The prevalence of some *Pseudomonas* virulence genes related to biofilm formation and alginate production among clinical isolates. J App Biomed 13:61-68. doi: 10.1016/j.jab.2014.05.002

Gasc C, Richard J-Y, Peyret P (2016) Genome sequence of *Pseudomonas*sp. HUK17, isolated from hexachlorocyclohexane-contaminated soil. Genome Announc 4:e00275-16. doi: 10.1128/genomeA.00275-16

Ghadaksaz A, Fooladi AAI, Hosseini HM, Amin M (2015) The prevalence of some *Pseudomonas* virulence genes related to biofilm formation and alginate production among clinical isolates. J App Biomed 13:61-68. doi: 10.1016/j.jab.2014.05.002

Giannone RJ, Huber H, Karpinets T, Heimerl T, Kuper U, Rachel R, Keller M, Hettich RL, Podar M (2011) Proteomic characterization of cellular and molecular processes that enable the *Nanoarchaeum equitans-Ignicoccus hospitalis* relationship. PLoS ONE 6: e22942. doi: 10.1371/journal.pone.0022942

Gielda LM and DiRita VJ (2012) Zinc competition among the intestinal microbiota. mBio 3:00171-12. doi: 10.1128/mBio.00171-12

Guina T, Wu M, Miller SI, Purvine SO, Yi EC, Eng J, Goodlett DR, Aebersold R, Ernst RK, Lee KA (2003) Proteomic analysis of *Pseudomonas aeruginosa* grown under magnesium limitation. J Amer Soc Mass Spec 14:742-751. doi: 10.1016/S1044-0305(03)00133-8

Grossman TH, Tuckman M, Ellestad S, Osbourne MS (1993) Isolation and characterization of *Bacillus subtilis* genes involved in siderophore biosynthesis: relationship between *B. subtilis* sfpo and *Escherichia coli* entD genes. J Bacteriol 175:6203-6211. doi: 10.1128/jb.175.19.6203-6211.1993

Hageman JH, Shankweiler GW, Wall PR, Franich K, McCowan GW, Cauble SM, Grajeda J, Quinones C (1984) Single, chemically defined sporulation medium for

Bacillus subtilis: growth, sporulation and extracellular protease production. J Bacteriol 160:438-441.

Hausmann B, Knorr K-H, Schreck K, Tringe SG, del Rio TG, Loy A, Pester M (2016) Consortia of low-abundance bacteria drive sulfate reduction-dependent degradation of fermentation products in peat soil microcosms. ISME J 10(10):2365-75. doi: 10.1038/ismej.2016.42

Herbst F-A, Lunsmann V, Kjeldal H, Jehmlich N, Tholey A, von Bergen M, Nielsen JL, Hettich RL, Seifert J, Nielsen PH (2016) Enhancing metaproteomics—The value of models and defined environmental microbial systems. Proteomics 16:783-798. doi: 10.1002/pmic.201500305

Hentzer M, Teitzel GM, Balzer GJ, Heydorn A, Molin S, Givskov M, Parsek MR (2001) Alginate overproduction affects *Pseudomonas aeruginosa* biofilm structure and function. J Bacteriol 183:5395-5401. doi: 10.1128/JB.183.18.5395-5401.2001

Hibbing, ME, Fuqua C, Parsek MR, Peterson SB (2010) Bacterial competition: surviving and thriving in the microbial jungle. Nat Rev Microbiol 8:15-25. doi:10.1038/nrmicro2259

Hotta K, Kim C-Y, Fox DT, Koppisch AT (2010) Siderophore-mediated iron acquisition in *Bacillus anthracis* and related strains. Microbiology 156:1918-1925. doi: 10.1099/mic.0.039404-0

Huang EL, Lefsrud MG (2012) Temporal analysis of xylose fermentation by *Scheffersomyces stipites* using shotgun proteomics. J Ind Microbiol Biotech 39:1507-1514. doi:10.1007/s10295-012-1147-4

Jiang Y, Xiong X, Danska J, Parkinson J (2016) Metatranscriptomic analysis of diverse microbial communities reveals core metabolic pathways and microbiome-specific functionality. Microbiome 4:2. doi: 10.1186/s40168-015-0146-x

Joo J-H, Hassan SHA, Oh S-E (2010) Comparative study of biosorption of Zn^{2+} by *Pseudomonas aeruginosa* and *Bacillus cereus*. Internat Biodeter Biodegrad 64:734-741. doi: 10.1016/j.ibiod.2010.08.007

Joshi H, Dave R, Venugopalan VP (2014) Pumping iron to keep fit: modulation of siderophore secretion helps efficient aromatic utilization in *Pseudomonas putida* KT2440. Microbiology 160: 1393-1400. doi: 10.1099/mic.0.079277-0

Jousset A, Bienhold C, Chatzinotas A et al (2017) Where less may be more: how the rare biosphere pulls ecosystem strings. ISME J 11:853-862. doi: 10.1038/ismej.2016.174

Kearns DB (2010) A field guide to bacterial swarming motility. Nat Rev Microbiol 8:634-644. doi: 10.1038/nrmicro2405

Kent AD and Triplett EW (2002) Microbial communities and their interactions in soil and rhizosphere ecosystems. Ann Rev Microbiol 56:211-236. doi: 10.1146/annurev.micro.56.012302.161120

Keshishian H, Addona T, Burgess M, Kuhn E, Carr SA (2007) Abundance proteins in plasma by targeted mass spectrometry and stabile isotope dilution. Molec Cell Proteomics 6:2212-2229. doi: 10.1074/mcp.M700354-MCP200

Kim Y, Cho J-Y, Kuk J-H, Moon J-H, Cho J-I, Kim Y-C, Park K-H (2004) Identification and antimicrobial activity of phenylacetic acid produced by *Bacillus licheniformis*

isolated from fermented soybean, Chungkook-Jang. Curr Microbiol 48:312-317. doi: 10.1007/s00284-003-4193-3

Klein MI, Xiao J, Lu B, Delahunty CM, Yates JR III, et al. (2012) *Streptococcus mutans* Protein Synthesis during Mixed-Species Biofilm Development by High-Throughput Quantitative Proteomics. PLoS ONE 7: e45795. doi: 10.1371/journal.pone.0045795

Kluge S, Hoffman M, Benndorf D, Rapp E, Reichl U (2012) Proteomic tracking and analysis of a bacterial mixed culture. Proteomics 12:1893-1901. doi: 10.1002/pmic.201100362

Kohler T, Curty LK, Barja F, van Delden C, Pechere J-C (2000) Swarming of *Pseduomonas aeruginosa* is dependent on cell-to-cell signaling and requires flagella and pili. J Bacteriol 182:5990-5996. doi: 10.1128/JB.182.21.5990-5996.2000

Kouzuma A, Kaku N, and Watanabe K (2014) Microbial electricity generation in rice paddy fields: recent advances and perspectives in rhizosphere microbial fuel cells. Appl Microbiol Biotechnol 98: 9521. doi: 10.1007/s00253-014-6138-0

Kuzyakov Y and Blagodatskaya E (2015) Microbial hotspots and hot moments in soil: concept and review. Soil Biol Biochem 83:184-199. doi: 10.1016/j.soilbio.2015.01.025

Langille MGI, Zaneveld J, Caporaso JG et al (2013) Predictive functional profiling of microbial communities using 16S rRNA marker gene sequences. Nat Biotech 31:814-821. doi: 10.1038/nbt.2676

Lehnik-Habrink, M, Lewis RJ, Mader U, Stulke J (2012) RNA degradation in *Bacillus subtilis*: an interplay of essential endo- and exoribonucleases. Molec Microbiol 84:1005-1017. doi: 10.1111/j.1365-2958.2012.08072.x

Leifert C, Li H, Chidburee S, Hampson S, Workman S, Sigee D, Epton HAS, Harbour A (1995) Antibiotic production and biocontrol activity by *Bacillus subtilis* CL27 and *Bacillus pumilis* CL45. J Appl Microbiol 78:97-108. doi: 10.1111/j.1365-2672.1995.tb02829.x

Lindemann SR, Bernstein HC, Song H-S, Fredrickson JK, Fields MW, Shou W, Johnson DR, Beliaev AS (2016) Engineering microbial consortia for controllable outputs. ISME J 10:2077-2084. doi: 10.1038/ismej.2016.26

Li K, Xu C, Jin Y, Sun Z, Liu C, Shi J, Chen G, Chen R, Jin S, Wu W (2013) SuhB is a regulator of multiple virulence genes and essential for pathogenesis of *Pseudomonas aeruginosa*. mBio 4:e00419-13. doi: 10.1128/mBio.00419-13

Liu B, Liu J, Ju M, Li X, Yu Q (2016) Purification and characterization of biosurfactant produced by *Bacillus licheniformis* Y-1 and its application in remediation of petroleum contaminated soil. 107:46-51. doi: 10.1016/j.marpolbul.2016.04.025

Lloyd-Price J and Abu-Ali G, Huttenhower C (2016) The healthy human microbiome. Genome Med 8:51. doi: 10.1186/s13073-016-0307-y

Loose M and Mitchison TJ (2014) The bacterial cell division proteins FtsA and FtsZ self-organize into dynamic cytoskeletal patterns. Nat Cell Biol 16:38-46. doi:10.1038/ncb2885

Lopez-Mondejar R, Zuhlke D, Becher D, Riedel K, Baldrian P (2016) Cellulose and hemicellulose decomposition by forest soil bacteria proceeds by the action of structurally variable enzymatic systems. Sci Rep 6:25279. doi: 10.1038/srep25279

Lutkenhaus J (2007) Assembly dynamics of the bacterial MinCDE system and spatial regulation of the z ring. Ann Rev Biochem 76:539-562. doi: 10.1146/annurev.biochem.75.103004.142652

Ma Q, Zhou J, Zhang W, Meng X, Sun J et al (2011) Integrated Proteomic and Metabolomic Analysis of an Artificial Microbial Community for Two-Step Production of Vitamin C. PLoS ONE 6: e26108. doi: 10.1371/journal.pone.0026108

Mallet CR, Lu Z, Mazzeo JR (2004) A study of ion suppression effects in electrospray ionization from mobile phase additives and solid-phase extracts. Rapid Commun. Mass Spectrom 18: 49–58. doi: 10.1002/rcm.1276

Men Y, Feil H, VerBerkmoes NC, Shah MB, Johnson DR, Lee PKH, West KA, Zinder SH, Anderson GL, Alvarez-Cohen L (2012) Sustainable syntrophic growth of *Dehalococcoides ethenogenes* strain 195 with *Desulfovibrio vulgaris* Hildenborough and *Methanobacterium congolense*: global transcriptomic and proteomics analysis. ISME J 6:410-421. doi: 10.1038/ismej.2011.111

Mavrodi DV, Blankenfeldt W, Thomashow LS (2006) Phenazine compounds in fluorescent *Pseudomonas* spp. biosynthesis and regulation. Ann Rev Phytopath 44:417-445. doi: 10.1146/annurev.phyto.44.013106.145710

Muddiman D, Andrews G, Lewis D, Notey J, Kelly R (2010) Part II: defining and quantifying individual and co-cultured intracellular proteomes of two thermophilic

microorganisms by GeLC-MS^2 and spectral counting. Anal Bioanal Chem 398:391-404. doi: 10.1007/s00216-010-3929-8

Mukherjee AK and Bordoloi NK (2012) Biodegradation of benzene, toluene, and xylene (BTX) in liquid culture and in soil by *Bacillus subtilis* and *Pseudomonas aeruginosa* strains and a formulated bacterial consortium. Environ Sci Pollut Res 19:3380-3388. doi: 10.1007/s11356-012-0862-8

Mulcahy H and Lewenza S (2011) Magnesium Limitation Is an Environmental Trigger of the *Pseudomonas aeruginosa* Biofilm Lifestyle. PLoS ONE 6: e23307. doi: 10.1371/journal.pone.0023307

Neal AL, Ahmad S, Gordon-Weeks R, Ton J (2012) Benzoxazinoids in Root Exudates of Maize Attract *Pseudomonas putida* to the Rhizosphere. PLoS ONE 7: e35498. doi: 10.1371/journal.pone.0035498

Osman KM, Amer AM, Badr JM, Helmy NM, Elhelw RA, Orabi A, Bakry M, Saad ASA (2016) Antimicrobial resistance, biofilm formation and *mecA* characterization of methicillin-susceptible *S. aureus* and non-*S.aureus* of beef meat origin in Egypt. Front Microbiol 7:222. doi: 10.3389/fmicb.2016.00222

Overhage J, Bains M, Brazas MD, Hancock REW (2008) Swarming of *Pseudomonas aeruginosa* is a complex adaptation leading to increased production of virulence factors and antibiotic resistance. J Bacteriol 190:2671-2679. doi: 10.1128/JB.01659-07

Parsons JF, Song F, Parsons L, Calabrese K, Eisenstein E, Ladner JE (2004) Structure and function of the phenazine biosynthesis protein PhzF from *Pseudomonas fluorescens* 2-79. Biochemistry 43:12427-12435. doi: 10.1021/bi049059z

Piersen LS and Piersen EA (1996) Phenazine antibiotic production in *Pseudomonas aureofaciens*: role in rhizosphere ecology and pathogen suppression. FEMS Microbiology Letters 136:101-108. doi: 10.1016/0378-1097(95)00489-0

Prestel E, Noirot P, Auger S (2015) Genome-wide identification of *Bacillus subtilis* Zur-binding sites associated with a Zur box expands its known regulatory network. BMC Microbiol 15:13. doi: 10.1186/s12866-015-0345-4

Price-Whelan A, Dietrich LEP, Newman DK (2006) Rethinking 'secondary' metabolism:physiological roles for phenazine antibiotics. Nat Chem Biol 2:71-78. doi: 10.1038/nchembio764

Prosser JI, Bohannan BJM, Curtis TP et al (2007) The role of ecological theory in microbial ecology. Nat Rev Microbiol 5:384-392

Rani A, Souche Y, Goel R (2012) Comparative in situ remediation potential of *Pseudomonas putida* 710A and *Commamonas aquatica* 710B using plant (*Vigna radiate* (L.) wilczek) assay. Ann Microbiol 63:923-928. doi: 10.1007/s13213-012-0545-1

Redgrave LS, Sutton SB, Webber MA, Piddock LJV (2014) Fluoroquinolone resistance: mechanisms, impact on bacteria, and role in evolutionary success. Trends in Microbiol 22:438-445. doi: 10.1016/j.tim.2014.04.007

Ren D, Madsen JS, Sorensen SJ, Burmolle M (2015) High prevalence of biofilm synergy among bacterial soil isolates in cocultures indicates bacterial interspecific cooperation. ISME J 9:81-89. doi: 10.1038/ismej.2014.96

Rios-Covian D, Sanchez B, Martinez N, Cuesta I, Hernandez-Barranco AM, de los Reyes-Gavilan CG, Gueimonde M (2016) A proteomic approach towards understanding the cross talk between *Bacteroides fragilis* and *Bifidobacterium longum* in coculture. Canad J of Microbiol 62:623-628. doi: 10.1139/cjm-2015-0804

Rooks MG and Garrett, WS (2016) Gut microbiota, metabolites and host immunity. Nat Rev Immun 16: 341-352

Roxas BAP and Li Q (2008) Significance analysis of microarray for relative quantitation of LC/MS data in proteomics. BMC Bioinform 9:187. doi: 10.1186/1471-2105-9-187

Ruiz L, Sanchez B, de los Reyes-Gavilan CG, Gueimonde M, Margolles A (2009) Coculture of *Bifidobacterium longum* and *Bifidobacterium breve* alters their protein expression profiles and enzymatic activities. Int J Food Microbiol 133:148-153. doi: 10.1016/j.ijfoodmicro.2009.05.014

Rundell EA, Banta LM, Ward DV, Watts CD, Birren B, Esteban DJ (2014) 16SrRNA gene survey of microbial communities in Winogradsky columns. PLoS ONE 9: e104134. doi: 10.1371/journal.pone.0104134

Sakhtah H, Koyama L, Zhang Y, Morales DK, Fields BL, Price-Whelan A, Hogan DA, Shepard K, Dietrich LEP (2016) The *Pseduomonas aeruginosa* efflux pump MexGHI-OpmD transports a natural phenazine that controls gene expression and biofilm development. Proc Nat Acad Sci 113:3538-3547. doi: 10.1073/pnas.1600424113

Schalk IJ (2008) Metal trafficking via siderophores in Gram-negative bacteria: specificities and characteristics of the pyoverdine pathway. J Inorg Biochem 102:1159-1169. doi: 10.1016/j.jinorgbio.2007.11.017

Schalk IJ and Guillon L (2013) Pyoverdine biosynthesis and secretion in *Pseudomonas aeruginosa*: implications for metal homeostasis. Environ Microbiol 15:1661-1673. doi: 10.1111/1462-2920.12013

Schneider R and Hantke K (1993) Iron-hydroxamate uptake systems in *Bacillus subtilis*: identification of a lipoprotein as part of a binding protein-dependent transport system. Molec Microbiol 8:111-121. doi: 10.1111/j.1365-2958.1993.tb01208.x

Sedlacek CJ, Nielsen S, Greis KD, Haffey WD, Revsbech NP, Ticak T, Laanbroek HJ, Bollmann A. 2016. Effects of bacterial community members on the proteome of the ammonia-oxidizing bacterium *Nitrosomonas* sp. strain Is79. Appl Environ Microbiol 82:4776–4788. doi: 10.1128/AEM.01171-16

Shih Y-L and Rothfield L (2006) The bacterial cytoskeleton. Microbiol Mol Rev 70:729-754. doi: 10.1128/MMBR.00017-06

Sieber JR, Crable BR, Sheik CS, Hurst GB, Rohlin L, Gunsalus RP, McInerney MJ (2015) Proteomic analysis reveals metabolic and regulatory systems involved in the syntrophic and axenic lifestyle of *Syntrophomonas wolfei*. Front Microbiol 6:115. doi: 10.3389/fmicb.2015.00115

Simoes M, Simoes LC, Pereira MO, Vieira MJ (2008) Antagonism between *Bacillus cereus* and *Pseudomonas fluorescens* in planktonic systems and in biofilms. Biofouling 24:339-349. doi: 10.1080/08927010802239154

Sinclair L, Osman OA, Bertilsson S, Eiler A (2015) Microbial Community Composition and Diversity via 16S rRNA Gene Amplicons: Evaluating the Illumina Platform. PLoS ONE 10: e0116955. doi: 10.1371/journal.pone.0116955

Song B and Leff LG (2006) Influence of magnesium ions on biofilm formation by *Pseudomonas fluorescens*. Microbiol Res 161:355-361. doi: 10.1016/j.micres.2006.01.004

Storey JD (2002) A direct approach to false discovery rates. Statist Methodol 64:479-498. doi: 10.1111/1467-9868.00346

Stubbendieck RM, Straight PD (2016) Escape from Lethal Bacterial Competition through Coupled Activation of Antibiotic Resistance and a Mobilized Subpopulation. PLoS Genet 12: e1005807. doi: 10.1371/journal.pgen.1005722

Tamura M, Lee K, Miller CA, Moore CJ, Shirako Y, Kobayashi M, Cohen SN (2006) RNase E maintenance of proper FtsZ/FtsA ratio required for nonfilamentous growth of *Escherichia coli* cells but not for colony-forming ability. J Bacteriol 188:5145-5152. doi: 10.1128/JB.00367-06

Toohey JI, Nelson CD, Krotkov G (1965) Isolation and identification of two phenazines from a strain of *Pseudomonas aureofaciens*. Canad J Bot 43:1055-1062. doi: 10.1139/b65-122

Traxler MF, Seyedsayamdost MR, Clardy J, Kolter R (2012) Interspecies modulation of bacterial development through iron competition and siderophore piracy. Molec Microbiol 86:628-644. doi: 10.1111/mmi.12008

Tyc O, van den Berg M, Gerards S, van Veen JA, Raaijmakers JM, de Boer W, Garbeva P (2014) Impact of interspecific interactions on antimicrobial activity among soil bacteria. Front Microbiol 5:567. doi: 10.3389/fmicb.2014.00567

Wallace RJ, Snelling TJ, McCartney CA, Tapio I, Strozzi F (2017) Application of meta-omics techniques to understand greenhouse gas emissions originating from ruminal metabolism. Gen Selec Evol 49:9 doi: 10.1186/s12711-017-0285-6

Wang J, Ma Z, Carr SA et al (2017) Proteome profiling outperforms transcriptome profiling for coexpression based gene function prediction. Molec Cell Proteom 16:121-134. doi: 10.1074/mcp.M116.060301

Wang Y, Wilks JC, Danhorn T, Ramos I, Croal L, Newman DK (2011) Phenazine-1-carboxylic acid promotes bacterial biofilm development via ferrous iron acquisition. J Bacteriol 193:3606-3617. doi: 10.1128/JB.00396-11

Weller DM (2007) *Pseudomonas* biocontrol agents of soilborne pathogens: looking back over 30 years. Phytopathology 97:250-256. doi: 10.1094/PHYTO-97-2-0250

Widder S, Allen RJ, Pfeiffer T et al (2016) Challenges in microbial ecology: building predictive understanding of community function and dynamics. ISME J 10:2557-2568. doi: 10.1038/ismej.2016.45

Wood DW, Piersen LS (1996) The *phzI* gene of *Pseudomonas aureofaciens* 30-84 is responsible for the production of a diffusible signal required for phenazine antibiotic production. Gene 168:49-53. doi: 10.1016/0378-1119(95)00754-7

Yao S, Richards J, Belasco JG, Bechhofer DH (2011) Decay of a model mRNA in *Bacillus subtilis* by a combination of RNase J1 5' exonuclease and RNase Y endonuclease activities. J Bacteriol 193:6384-6386. doi: 10.1128/JB.05939-11

Zhang H and Wang X (2016) Modular co-culture engineering, a new approach for metabolic engineering. Metab Eng 37:114-121. doi: 10.1016/j.ymben.2016.05.007

CHAPTER 5: META-PROTEOMIC ANALYSIS OF PROTEIN EXPRESSION DISTINCTIVE TO ELECTRICITY-GENERATING BIOFILM COMMUNITIES IN AIR-CATHODE MICROBIAL FUEL CELLS[3]

5.1 Introduction

In bioelectrochemical systems (BESs), electrochemically-active microbes convey electrons to or from a conductive electrode [Wang et al. 2015]. In some BES systems, such as microbial fuel cells (MFCs), bacteria living in a biofilm use the anode as an electron acceptor for electrons harvested from organic materials such as lignocellulosic biomass or waste byproducts, and the resulting current is harnessed to recover energy during wastewater treatment [Logan et al. 2006]. Other BES applications include removal of nutrients [Kelly et al. 2014] or metals [Nancharaiah et al. 2015], desalination [Cao et al. 2009], and generation of bioproducts such as H_2 [Liu et al. 2005], H_2O_2 [Rozendal et al. 2009], or organic molecules from CO_2 and sunlight [Nevin et al. 2010]. Successful commercial application of BES technologies will require increases in current generation and efficiency [Logan et al. 2010]. More detailed information regarding the fundamental mechanisms that enable bioelectricity generation will inform strategies for scale-up and new applications of BES technology [Rittman et al. 2008].

Descriptions of electricity generation in BESs have relied primarily on model BES genera. Current generation mechanisms described for model BES genera like *Shewanella* and *Geobacter* include indirect electron transfer *via* soluble redox

[3] The text and results presented in this chapter were published previously in Chignell et al. 2018 (Chapter 5 References)

compounds [Marsili et al. 2008], and direct electron transfer *via* outer membrane cytochromes [Estevez-Canales et al. 2015] or pilus-like "nanowires" [Gorby et al. 2006]. These discoveries have informed improvements in BES performance through design of electrode architecture [Logan et al. 2015], identification of limiting factors during electron transfer [Schroder 2007], and attempts at metabolic engineering of microbes or defined community [Yang et al. 2015]. Few studies, however, have attempted to determine which of these current generation mechanisms are most prevalent in mixed culture BES communities or how the interactions between members of BES consortia affect electricity generation. So far, those interactions primarily have been described in terms of community composition, quantified as relative abundance of 16S rRNA genes [Yokoyama et al. 2016; Wrighton et al. 2008]. This kind of ecological approach describes compositional changes of BES community in response to operational changes such as the type of substrate [Zhang et al. 2011]. Metabolic syntrophies among BES community members are thought to explain the generally superior performance of a mixed community compared with pure cultures [Watson and Logan 2010]. However, 16S rRNA profiling is not well suited to provide insights into interactions among community members. Identification of these mechanisms during BES biofilm development may suggest strategies to reduce reactor start-up time or increase community resilience to perturbation, thereby reducing operating costs and supporting commercial scale-up.

Appropriate tools for molecular investigations of microbial community function have emerged only recently [Franzosa et al. 2015]. Proteomics, in particular, has been useful for profiling protein expression of defined or undefined microbial communities

[Lacerda and Reardon 2009]. These "meta-proteomics" studies have identified metabolic mechanisms behind multi-species fermentation [Ma et al. 2011], methanogenesis [Lu et al. 2014], or community response to a toxic perturbation [Lacerda et al. 2007]. A few studies have used proteomics methods to investigate electricity generation by model species or isolates [Fowler et al. 2016; Kavanagh et al. 2016]. Meta-proteomics examinations of BES systems, however, have been limited to a single investigation of protein expression of biocathode biofilm organisms under optimal and sub-optimal conditions [Leary et al. 2015]. That study identified several biocathode proteins associated with an optimal reactor potential for use of an electrode as an electron donor to fix CO_2. The question of the proteins associated with anode mixed-species biofilms that generate electricity has not yet been addressed.

The goal of this study was to characterize protein expression that is distinctive to a MFC anode community when it is generating electricity. Specifically, a label-free meta-proteomics approach was used to compare protein expression in acetate-fed MFC anode biofilms before and after the onset of robust current generation. Since the types and abundances of proteins expressed depend on the types and abundances of microbial genera present in the community, we quantified changes in MFC community structure across developmental stages in terms of relative abundance of operational taxonomical units (OTUs). This information about community structure was integrated with meta-proteomics results in two ways. First, protein expression was normalized to abundance levels of individual genera during significance testing for differential expression of proteins. Second, OTU quantification was used as a method of orthogonal "validation" of meta-proteomics results by comparing relative abundance of genera based on OTUs

with that based on genera associated with protein identifications. Compared with using a single method, this sort of mixed meta-omics approach offers the possibility of obtaining a more complete picture of the activities and interactions of the anode community members during MFC startup and electricity production. Such a picture may prove useful for improving MFC performance through reactor design, operating conditions, or community structure modification.

5.2 Experimental Procedures

5.2.1 MFC setup, operation, and harvest

The single-chamber, membrane-free, air-cathode MFC design used in this study was similar to a previous design [Liu and Logan 2004] and is described in detail in Appendix SI 5.1.1. The liquid volume of each MFC was 30 ml, and the area of the anode and air-cathode was 7.0 cm^2. The MFCs were autoclaved prior to inoculation with a mixed culture inoculum that was derived from anaerobic digester sludge (Drake Water Reclamation Facility, Fort Collins, CO). The MFCs were fed 30 mM acetate by full batch replacement with a minimal medium described previously [Liu and Logan 2004]. The chemical oxygen demand of the carbon source in the medium (30 mM acetate) was calculated as No exogenous redox mediators were used. MFCs were operated at room temperature with a 1 kΩ external resistor completing the anode-cathode circuit. Anodes from three replicate MFCs were harvested for each of four developmental stages: (i) bulk MFC suspension; (ii) early anode biofilm; (iii) intermediate anode biofilm; (iv) mature anode biofilm. Bulk suspension samples were collected 24 h after inoculation for Stage (i). Stage (ii) was characterized by a current density ≤ 0.05 A/m^2, an order of magnitude lower than in Stage (iii) (~0.6 A/m^2). Stage (iv) was characterized by higher current

densities (0.7-0.8 A/m^2) in repeated batches over a two-year period.

5.2.2 16S rRNA gene sequencing and OTU analysis

Total DNA was extracted from biofilm scraped from each MFC anode using a Powersoil DNA Isolation Kit (MoBio Laboratories, Inc., Carlsbad, CA, USA), according to the manufacturer's instructions. The V3-V7 region of 16S rRNA genes was sequenced at Research and Testing Laboratory (Lubbock, TX) using an Illumina MiSeq platform. Statistical comparison of the relative abundance of operational taxonomical units (OTUs) between communities from the four developmental stages was conducted with a non-parametric multivariate analysis of variance (npMANOVA) test, using the *vegan* package in R [Buttigieg and Ramette 2014], as described in the Appendix (5.1.4). For post-hoc analysis, pairwise Pearson's r correlations were conducted between each anode of each developmental condition using the cor() function in R and plotted using the ggplot() function. Pairwise correlations were tested for significant differences between comparison type (e.g., early-intermediate correlations vs. early-mature correlations) by Tukey's HSD test. Additionally, a non-metric multidimensional scaling (NMDS) plot was generated to compare clustering for each sample type (Appendix SI 5.1.4). Based on the results of the npMANOVA, Pearson's correlations, and NMDS results, a similarity percentage (SIMPER) analysis [Clarke 1993] was conducted on the early and mature anode biofilms. This analysis quantifies the average contribution of each taxon to the overall difference between communities in a Bray-Curtis dissimilarity matrix. Simpson's Diversity Index (SDI) values were computed for each anode biofilm and compared for statistically significant differences between developmental stages with a Welch's t-test.

5.2.3 Proteomic analysis

5.2.3.1 Protein extraction from MFC samples

A protein extraction method was developed specifically for anode biofilms. Briefly, biofilm scraped from each harvested anode was sonicated in lysis buffer (50 mM ammonium bicarbonate, 1% sodium deoxycholate, pH 8.2) for 5 min, subjected to a freeze-thaw cycle, and sonicated again. Sodium deoxycholate was chosen as a detergent to maximize unbiased protein recovery, including from membrane proteins [Leon et al. 2013]. Supernatant containing suspended proteins was collected (14 000 x g for 20 min). Proteins were precipitated, quantified, and trypsin-digested according to standard methods, as described in the Appendix (SI 5.1.5).

5.2.3.2 LC-MS/MS analysis

Two micrograms of resuspended peptides were loaded onto a C18 trap (200 µm ID, 0.5 mm length, 120 Å, Eksigent Technologies) on the front end of a NanoLC 400 (Eksigent Technologies, Redwood City, CA, USA). A 2%-80% gradient of acetonitrile (ACN) with 0.1% formic acid was used to elute the peptides (C18, 75 µm ID, 150 mm length, 120 Å, Eksigent Technologies, Redwood City, CA, USA) at a flow rate of 300 nl/min. Peptides were eluted (150 min) into the electrospray ionization chamber of a TripleTOF 5600 Q-TOF mass spectrometer (ABSciex, Redwood City, CA, USA) and ionized at 80 V. Up to 50 MS^2 scans followed each MS^1 scan, according to the order of intensity. Three technical replicate LC-MS/MS injections were performed for each biological replicate MFC anode. The MS proteomics data will be deposited at the open access library of ProteomeXchange Consortium (http://www.proteomexchange.org/) [Deutsch et al. 2017].

5.2.3.3 Label-free quantification, statistical analysis, and metabolic interpretation of protein data

Proteins were identified from LC-MS/MS spectra (ProteinPilot v.4.5 beta) using a fasta database consisting of the entire bacterial metaproteome (proteome filter "taxonomy: Bacteria (2)," downloaded from Uniprot 2-15-15). The false discovery rate (FDR) was computed by ProteinPilot with a reversed-sequence decoy database using a threshold ≤ 0.01. For each protein, a modified version of the distributed normalized spectral abundance factor (NSAF) [Zhang et al. 2010] was computed with custom R scripts, using the ProteinPilot "Unused Score". For proteins identified in both early and intermediate MFC samples, this NSAF value was normalized to OTU abundance of the corresponding genus for that protein, thus accounting for population shifts in the community. Since no proteins were identified as differentially expressed after applying a q-value multiple testing correction [Storey 2002], but the histogram of p-values showed a right skew (Figure 17), we present instead proteins-of-interest (POIs) that had $\log_2$-fold-change greater than 1 or less than -1 and $p<0.05$ in a Student's t-test [Pascovici et al. 2016]. For proteins detected only in one of the anode developmental stages ("uniquely detected proteins," UDPs), Fisher's Exact Tests implemented in Blast2GO (v.3.1.0) identified Gene Ontology (GO) categories significantly enriched (FDR < 0.05) [Benjamini and Hochberg 1995] among either the early or intermediate UDPs. Since this study was concerned with proteins that are distinctive to current generation in MFCs, subsequent analysis focused on POIs with $\log_2$-fold-change > 1 as well as UDPs in intermediate MFCs (UDPIs). Analysis of KEGG pathways enriched among UDPIs was conducted by GhostKOALA, an automatic metagenome annotation server that

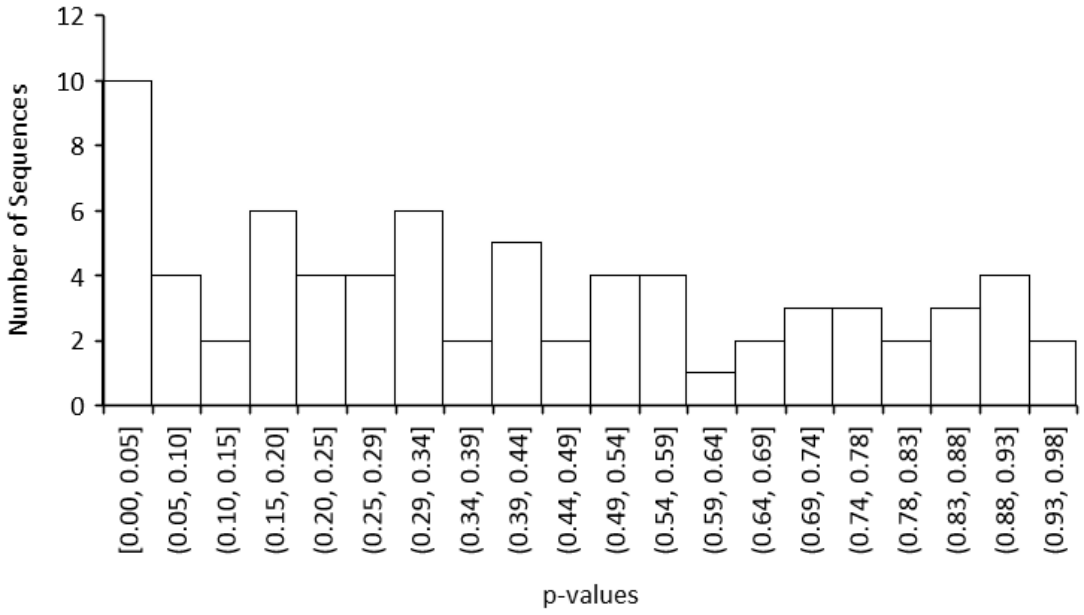

Figure 17: Histogram of all p-values from a Student's t test (assuming equal variances) comparing modified NSAF values for proteins identified in common between early and intermediate replicate anode biofilms. X-axis values [a,b] indicate the range of p-values for each bin

characterizes gene functions and pathways based on KEGG Orthology sequence assignments [Kanehisa et al. 2016]. As for OTUs, the diversity of genera in early and intermediate communities was quantified by SDI on the relative abundance values of proteins identified by GhostKOALA, across replicate anode samples. Diversity in early or intermediate stages was compared by a two-tailed Welch's t-test on SDI values. A detailed description of protein identification, spectral count quantification, and statistical comparison is provided (Appendix SI 5.1.6).

5.2.4 Scanning electron microscopy (SEM)

Sections (3 cm x 3 cm) of harvested anodes were removed with a sterile razor blade. Biofilms were fixed to the anode surface with an aqueous solution of 1.5%

formaldehyde and 2.5% glutaraldehyde for 2 h at room temperature. Samples were washed with phosphate buffer and then sequentially in 60%, 70%, 80%, 90%, and 100% aqueous solutions of ethanol. Residual ethanol was evaporated and samples were visualized on a Hitachi TM3000 SEM (Schaumburg, IL, USA).

5.3 Results

5.3.1 Current generation and MFC anode colonization

The purpose of this study was to identify protein expression that is unique to MFC anode biofilm communities during electricity generation. Therefore, MFC anodes were harvested at different developmental stages before and after robust current generation was detected. The developmental stage of MFC biofilms was identified by current densities at the harvest point: 0.053 ± 0.006 A/m^2, 0.620 ± 0.043 A/m^2, and 0.764 ± 0.035 A/m^2 for early, intermediate, and mature MFC biofilms, respectively. Early MFC biofilms were harvested after 130.3 ± 9.1 h of operation, at very low levels of electricity generation (Figure 18).

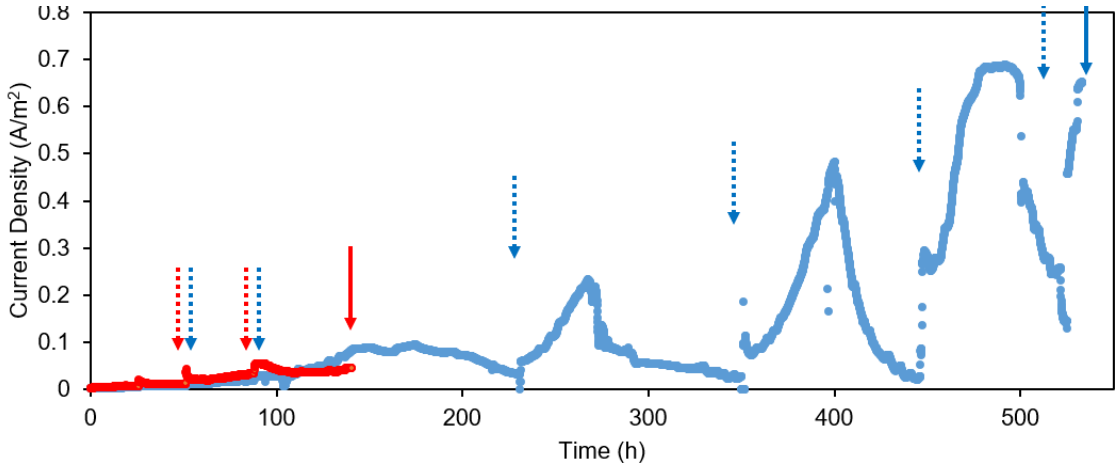

Figure 18: Representative current density of air–cathode MFCs that were compared with proteomics. Current density rose due to partial or complete replacement of medium. Dashed arrows represent full batch replacement of all medium in the MFC. Solid arrows indicate harvest point. Early anodes (red) were harvested 130.3 ± 9.1 h after inoculation, while intermediate anodes (blue) were harvested 523.7 ± 35.0 h after inoculation. Mature MFC performance data are shown in Appendix SI 5.3: Figure S19

Initial adhesion of cells to anode fibers was observable at this stage, compared to unused carbon cloth (Appendix SI 5.3: Figure S16). Intermediate MFCs were harvested after 482.6 ± 56.1 h, when current density increased to 0.6 A/m^2. More extensive cell growth and biofilm structures were observed on intermediate anodes, compared to early anodes (Appendix SI 5.3: Figure S16). Mature anode biofilms were harvested from several batches generating a maximum current density of 0.7-0.8 A/m^2 for more than two years (>17,000 h) (Appendix SI 5.3: Figure S17). Multiple layers of cells surrounded by a thick extracellular matrix were observed on mature anodes (Appendix SI 5.3: Figure S16).

5.3.2 MFC biofilm community structure based on 16S gene amplicons and proteins

Significant differences ($p<0.001$, non-parametric MANOVA) in community composition as measured by OTUs were observed among the four MFC developmental stages (Appendix SI 5.2: Table S14). As a post-hoc test, pairwise Pearson's r correlations were calculated between each biological replicate of each developmental stage (Figure 19; Appendix SI 5.2: Table S14).

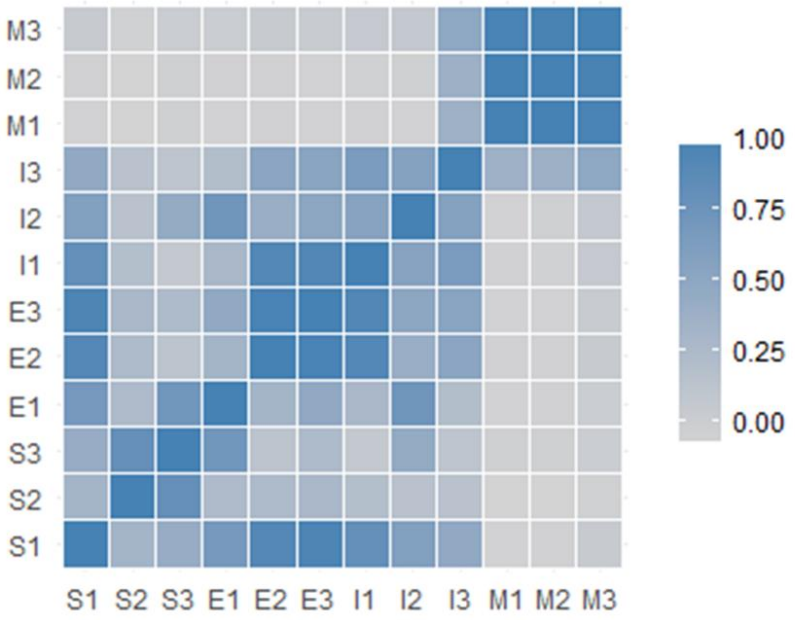

Figure 19: Matrix of Pearson's correlations from pairwise comparisons between consecutive pairs of samples from the bulk solution (S), early anode (E), intermediate anode (I), and mature anode (M), with respect to 392 different OTUs. As specified by the legend, darker colors indicate a higher Pearson's coefficient and thus more similarity between the two samples compared. A one-way ANOVA on Pearson's coefficients confirmed that the MFC developmental stages were significantly different ($p < 2 \times 10^{-9}$)

The correlation was lowest between the mature anode biofilm OTUs and OTUs from either the bulk solution (Pearson's $r = 0.005 \pm 0.004$) or early anode communities (Pearson's $r = 0.011 \pm 0.007$) (Figure 19; Appendix SI 5.2: Table S14). The greatest degree of correlation was found between early and solution communities ($r = 0.52 \pm 0.30$) and early and intermediate communities ($r = 0.53 \pm 0.22$). The latter correlation between early and intermediate communities was significantly ($p<0.05$, Tukey's HSD) better than that between early and mature biofilms ($r = 0.01 \pm 0.01$), consistent with the emergence of the intermediate biofilm community from the early community. Interestingly, the taxonomic diversity of the intermediate biofilm was significantly ($p<0.005$, Welch's t-

test) much greater than that of any of the other stages, exhibiting a SDI value more than twice that of the early biofilm (Table 6). The increase in diversity likely contributed to the lower clustering of intermediate anode biofilm samples in the NMDS plot, compared to the other sample types (Appendix SI 5.3: Figure S18).

Table 6: Comparison of Simpson's Diversity Index values for MFC communities at different developmental stages. The enumeration method refers to sequenced 16S rRNA gene amplicons (OTUs) or LC-MS/MS-identified proteins assigned to taxonomical groups by GhostKOALA. The error term is the standard deviation across microbial consortia for three independent replicate MFC anodes. GhostKOALA protein information for solution and mature biofilm communities is not available (NA) since proteomics analysis was not conducted on those samples.

Enumeration Method	**Solution**	**Early**	**Intermediate**	**Mature**
OTUs	0.28 ± 0.13	0.30 ± 0.12	0.85 ± 0.03	0.50 ± 0.05
GhostKOALA proteins	NA	0.43 ± 0.07	0.80 ± 0.01	NA

Since the early and mature communities were significantly different according to both npMANOVA and Pearson's r correlation, SIMPER analysis was conducted to determine the percent contribution of individual taxa to the dissimilarity between those two communities. This analysis identified OTU 132 (*Acinetobacter*), 333 (*Geobacter*), and 96 (*Pseudomonas*) contributing most to the differences between early and mature biofilm communities, with SIMPER cumulative contribution scores of 0.77, 0.41, and 0.63, respectively. This result from SIMPER analysis was corroborated by the decreasing relative abundance of total *Gammaproteobacteria* (*Acinetobacter*, *Pseudomonas*) and increasing *Deltaproteobacteria* (*Geobacter*) as the biofilms

progressed from early to mature stages (Appendix SI 5.2: Tables S15 and S16). Moreover, the shift in dominance across the developmental stages between those three OTUs can be seen clearly in relative abundances of prominent OTUs (relative abundance greater than or equal to 1.0%) across developmental stages. Nearly all of the relative abundance attributed to each genus was due to the same OTUs (Appendix SI 5.2: Tables S16 and S17). For example, across all developmental stages nearly all of the relative abundance of *Geobacter* was due to OTU333, which had no identified species. Over the four developmental stages sampled, the number of OTUs with relative abundance greater than or equal to 1.0% decreased from seven (solution) to six (early biofilm), then increased to 17 OTUs (intermediate biofilm) before decreasing to just four OTUs in the mature biofilms. Genera that emerged to more than 1.0% in the intermediate biofilm included *Thauera* (OTU198), *Alcaligenes* (OTU288), *Geobacter* (OTU333), and an unknown *Synergistales* (OTU204). Of these, only the latter two OTUs were prominent in the mature biofilm; together with an unknown bacterium and an *Actinomyces*, they comprised over 86% of the mature community.

The relatively high degree of overall correlation between the early and solution communities (Appendix SI 5.2: Table S14) as well as the dominance of both early and solution communities by *Gammproteobacteria*—i.e., *Acinetobacter* (OTU132) and *Pseudomonas* (OTUs 356 and 96) (Appendix SI 5.2: Tables S15, S16, S17)—suggested that those genera were early colonizers of the anode. Interestingly, *Pseudomonas* OTU356 was the most dominant in the solution community but was only present at ~1.0% in the early biofilm community (Appendix SI 5.2: Table S17). In contrast, relative abundance of *Pseudomonas* OTU96 increased in abundance in the early biofilm

compared to the solution community, suggesting that the species of *Pseudomonas* represented by OTU356 did not attach to the anode effectively.

The GhostKOALA and OTU datasets were significantly correlated (adjusted R^2 = 0.914, p-value < $2.2e^{-16}$) with regard to taxonomical relative abundance (Appendix SI 5.3: Figures S20 and S21). The taxonomies of OTUs and proteins both showed dominance of early anode biofilm communities by non-enteric *Gammaproteobacteria*, with increased relative abundance in intermediate biofilms for *Alpha-*, *Beta-*, and *Deltaproteobacteria*, as well as for *Actinobacteria*, *Synergistetes*, and *Firmicutes* (*Clostridia*) (Figure 20).

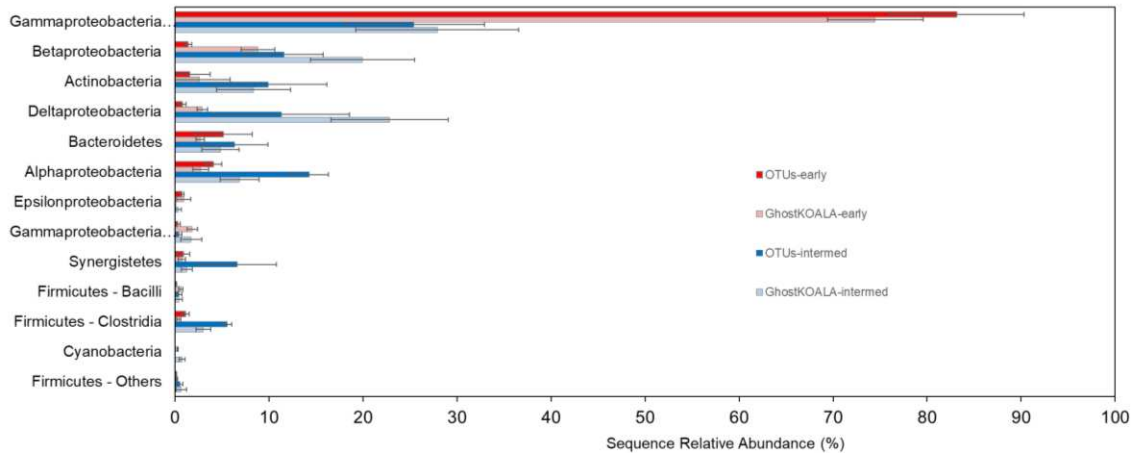

Figure 20: Relative abundances of genera associated with OTUs from 16S rRNA gene sequencing or GhostKOALA protein categorization. Relative abundances are from OTUs of early anode biofilms (dark red), GhostKOALA of early anode biofilms (light red), OTUs of intermediate biofilms (dark blue), and GhostKOALA of intermediate anode biofilms (light blue). Error bars represent standard deviations across samples from three independent biological replicate MFC anode biofilms. Only genera with relative abundance greater than 0.5% for at least one sample type are shown; a table of full relative abundance values is available in Appendix SI 5.2: Table S19

Moreover, OTU and GhostKOALA protein methods agreed that the taxonomic diversity of the intermediate MFCs was significantly ($p<0.005$, Welch's t-test) greater than that of the early MFCs. With respect to diveristy, SDI values based on GhostKOALA protein identifications were 0.43 ± 0.07 and 0.80 ± 0.01 for early and intermediate anode samples, respectively (Table 6). There was no significant difference between the two methods in SDI values for either the early ($p>0.2$, Welch's t-test) or intermediate communities ($p>0.1$, Welch's t-test). The broad phylogenetic agreement between the two methods with respect to genera identifications suggested that a representative extraction of proteins across set of different members of the MFC community had been achieved.

5.3.3 Proteomics Results

5.3.3.1 Summary of proteomics data features

The purpose of this study was to describe distinctive protein expression in MFC anode biofilm communities that are generating electricity compared to those that are not. Ideally, samples for this proteomic comparison would come from MFC biofilms that were identical in community composition and differed only with respect to current generation. In that case, any differences between the two meta-proteomes would be attributable to current generation, rather than to differences in community composition. While not identical in community composition, (see previous section) the early and intermediate biofilms were more similar than the early and mature biofilms (Figure 19; Appendix SI 5.2: Table S14). However, the intermediate anodes generated current densities nearly as high (~81%) as those generated by mature anodes. Therefore, we considered a comparison of the early and intermediate conditions to be the most reasonable approach to compare differences in anode biofilm protein expression with and

without electricity production, while limiting as much as possible the extent to which those differences are just due to different community composition.

Across all LC-MS/MS samples for early and intermediate MFC biofilms, 8557 protein identifications were made at 1% FDR (5932 proteins identified by more than one peptide), resulting in 3866 non-redundant identifications across technical replicates. Across replicate anode biofilm samples, 1430 early and 1194 intermediate non-redundant proteins were identified (Appendix SI 5.3: Figure S22). Of the 853 proteins identified in at least one technical replicate of at least two anodes in a condition, 377 proteins were identified only in early anode biofilms, 182 proteins were identified only in intermediate anodes, and 87 proteins were identified in both early and intermediate anodes (Appendix SI 5.3: Figure S23). With a q-value multiple testing correction, none of these 87 proteins was identified as differentially expressed. Since the histogram of p-values generally was skewed right (Figure 17), however, the seven proteins with $p<0.05$ and $\log_2$-fold-change greater than 1 or less than -1 are presented as POIs between the two conditions (Table 7). Five of those POIs had a $\log_2$-fold-change greater than 1, indicating greater abundance in the intermediate compared with the early biofilms. Therefore a total of 187 proteins were determined to be either a UDPI (UDP detected only in intermediate anode biofilms) or a POI more abundant in the intermediate biofilms. Subsequent metabolic analysis focused on these 187 proteins as representatives of changes in the proteome most distinctively associated with the onset of electricity production.

Table 7: Proteins of interest that were shared in common between early and intermediate MFC biofilms. These proteins met a criterion of $p<0.05$ (Student's t-test, no multiple testing correction) with $\log_2$-fold-change ($\log_2$ FC) of either >1 or <-1 for a ratio of intermediate/early conditions.

Uniprot ID	**Protein Name**	**Genus**	**P-value**	**log_2FC (intermed /early)**
A0A073KKY5	Porin	*Shewanella*	0.016	3.2
A0A077F4W8	Aromatic hydrocarbon degradation protein	*Pseudomonas*	0.007	2.7
A0A077F872	Outer membrane protein H1	*Pseudomonas*	0.007	2.1
A0A067A3Q5	Outer membrane insertion C-terminal signal domain protein	*Pseudomonas*	0.016	2.1
A0A075PCY9	Porin	*Pseudomonas*	0.04	2
A0A077F9B6	Polyribonucleotide nucleotidyltransferase	*Pseudomonas*	0.007	-2.7
A0A066ZUQ4	Aldehyde dehydrogenase family protein	*Pseudomonas*	0.006	-3.4

5.3.3.2 Significant enrichment of membrane and transport proteins

The GO groups gene products into interrelated categories associated with biological processes, cellular components and molecular function. A Fisher's Exact Test identified 18 GO functional categories that were significantly enriched among the set of proteins from intermediate anode biofilms, compared with early anode biofilms (Figure 21).

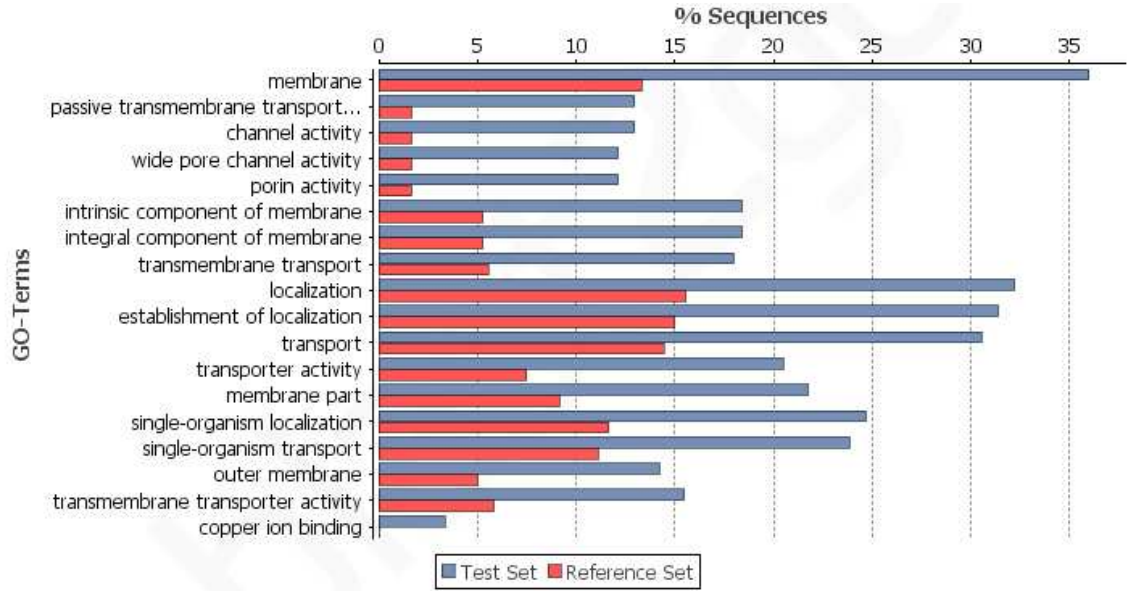

Figure 21: Percentages of intermediate (blue) and early (red) MFC biofilm protein sequences assigned to gene ontology (GO) categories. Significant differences in protein levels between intermediate and early conditions were determined by a Fisher's exact test implemented in Blast2GO v. 3.1.0 with a Benjamini-Hochberg multiple testing correction factor (FDR < 0.05). A total of 733 sequences were assigned to GO categories.

The most enriched GO category was "membrane", which was associated with over 35% of the intermediate proteins but less than 14% of early proteins. Five additional enriched GO categories were explicitly related to membranes (e.g., "integral component of membrane" and "transmembrane transport"), and nearly all of the 12 remaining enriched GO categories among intermediate proteins were related either to transport or

localization. Moreover, four of the five more abundant POIs (and neither of the less abundant POIs) were associated with membrane processes or transport (Table 7). KEGG analysis by GhostKOALA corroborated this enrichment in membrane and transport processes in the intermediate anode biofilms. Of the 134 UDPIs that were identified with KEGG annotations, 35 proteins (26%) fell into the category of "environmental information processing," making it the most abundant KEGG category represented among UDPIs (Figure 22). This category includes subcategories of membrane transport, signal transduction, and signaling molecule interactions (Appendix SI 5.2: Table S18). Additionally, UDPIs involved in fatty acid biosynthesis were an especially abundant type of protein related to membranes—in this case associated with forming the membranes themselves (Appendix SI 5.2: Table S18).

Several of the membrane UDPIs have been explicitly associated with electricity production. The 63 *Geobacter* UDPIs included several cytochromes, including OmcX, a

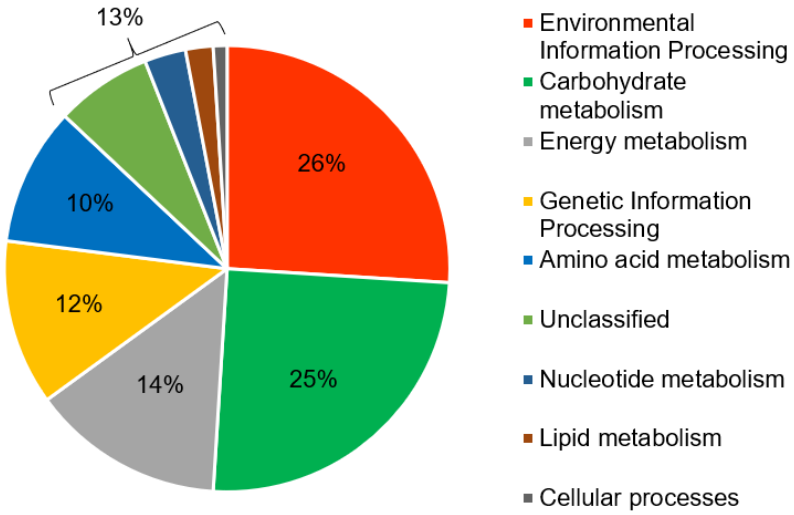

Figure 22: KEGG functional categorization of UDPIs and POIs that were more abundant in intermediate MFC biofilms. Proteins were identified and categorized using the GhostKOALA tool against the entire prokaryotic database.

lipoprotein c-type outer membrane cytochrome (Omc) that has been shown to be necessary for current generation [Butler et al. 2010] (Appendix SI 5.2: Table S17). Additionally, OmcS, a pili-associated cytochrome [Qian et al. 2011] was detected in both conditions and was more abundant in intermediate than early anodes, though not significantly so. No other Omc proteins were identified, which was unexpected considering that membrane proteins generally were significantly enriched among UDPIs, and Omc proteins have been shown to be critical for electron transfer to the anode by some genera, including *Geobacter* [Shi et al. 2009]. The lack of detected *Geobacter* Omc proteins suggests that it used a different mechanism for electron transfer during these initial stages of current generation.

5.3.3.3 Central carbon metabolism

Central metabolic pathways represented among UDPIs included the TCA cycle, fatty acid β-oxidation, fatty acid biosynthesis, and acetate uptake and activation (Appendix SI 5.2: Table S17). Anaerobic central metabolism was represented by Por and Kor enzymes, the anaerobic analogs to pyruvate dehydrogenase and α-ketoglutarate dehydrogenase, respectively [Baughn et al. 2009; Kerscher and Oesterhelt 1981]. Carbohydrate metabolism was the second most abundant KEGG category represented among UDPIs (Figure 22), despite the lack of carbohydrates in the medium. These proteins likely were participating in gluconeogenesis; enzymes were found among UDPIs that covered the gluconeogenesis pathway from oxaloacetate to glyceraldehyde-3-phosphate. Additionally, isocitrate lyase was a UDPI from *Thauera*, a facultative genus that comprised 5.9 ± 1.9% of the intermediate MFC anode community. This enzyme

catalyzes the key step of the glyoxylate shunt, the anabolic cycle that converts a C_2 compound like acetate/acetyl-CoA to C_4 compounds for entry into gluconeogenesis [Ensign 2006].

5.3.3.4 Nitrogen metabolism

Glutamate dehydrogenase (GDH) was the most abundant UDPI in terms of relative abundance of OTUs in the intermediate biofilms. It was also the most well-represented UDPI across taxa, detected in five different genera (Appendix SI 5.2: Table S18). This enzyme stores or releases ammonia during amino acid synthesis; in strict anaerobes, GDH may act as an electron sink in association with aminotransferases, two of which also were identified for *Geobacter* [Kolmeder et al. 2012]. A nitrogen-fixation scaffold protein NifU was one of seven *Geobacter* UDPIs that were associated with iron sulfur cluster binding [Ueki and Lovley 2010].

Evidence for both nitrification and denitrification was found among intermediate MFCs. The combination of ammonium as the supplied nitrogen source and microaerobic conditions provided a suitable environment for nitrification, as suggested by detection of *Nitrosomonas* OTUs. Evidence for denitrification included a UDPI for *Pseudomonas stutzeri*, a well-known denitrifier, as well as two UDPIs from genus *Nitratireductor* [Labbe et al. 2004]. Additional denitrifying UDPIs included nitrite reductase, nitric oxide reductase, a nitrate-induced formate dehydrogenase, and three nitrous oxide reductases (NosZ) (Appendix SI 5.2: Table S17). One of the latter was from *Azoarcus*, a model genus for nitrogen fixation [Hurek and Reinhold-Hurek 2003]. Another NosZ was one of 16 UDPIs from nitrifying-denitrifier *Alcaligenes*, a genus comprising approximately 3% of intermediate OTUs but less than 0.1% of early OTUs.

The activity of NosZ suggests the presence of N_2O, an intermediate formed during both nitrification and denitrification [Stein 2011].

5.3.3.5 Geobacter *interactions within MFC biofilms*

With 63 UDPIs, *Geobacter* was the most abundant genus represented among UDPIs (*Pseudomonas* was second most abundant, with 19 UDPIs). The flagellar UDPI FliC suggested active participation of *Geobacter* in formation of mixed culture biofilm structures [Tran et al. 2008]. Another *Geobacter* UDPI, cysteine synthase A, is known to produce a toxin that inhibits growth and biofilm production of neighboring bacteria [Diner et al. 2012]. Expression of cysteine synthase A suggests that *Geobacter* uses methods of antagonism to suppress the growth of nearby competitors, in addition to outcompeting them with superior capacities for anaerobic respiration of the anode. A *Geobacter* phage tail sheath protein also was a UDPI. Phage proteins recently have been associated with increased growth and Fe(III) respiration by *Geobacter* in uranium-contaminated soils [Holmes et al. 2015]. Finally, superoxide dismutase and rubredoxin:oxygen/nitric oxide oxidoreductase, scavengers of oxygen and nitrogen compounds, were *Geobacter* UPDIs [Khare et al. 2006; Methe et al. 2003].

5.4 Discussion

5.4.1 Community dynamics during MFC biofilm development

The relative abundance of OTUs in the solution and early biofilm samples indicated that early colonizers of the anode included *Acinetobacter* and *Pseudomonas*, two genera generally considered aerobes, though some studies have shown electricity-producing capabilities for members of each [Park et al. 2014; Read et al. 2010]. The

dominance of aerobic or facultative genera in early developmental stages likely was due to the microaerobic conditions of air-cathode MFCs [Liu and Logan 2004]. As the anode biofilm grew in structure and complexity (Appendix SI 5.3: Figure S16), these genera would have declined in relative abundance while anaerobic genera such as *Geobacter* became more prevalent. For example, *Pseudomonas* was a prominent member of both the solution (~58%) and early biofilm samples (~55%) but decreased to ~18% by the intermediate stage and was scarce (<1%) by the mature stage (Appendix SI 5.2: Table S16). Some aerobes persisted in the intermediate MFC community, however, possibly occupying a niche of oxygen consumption to maintain anoxic conditions for anode-reducing genera [Qu et al. 2012]. For example, *Alcaligenes*, an aerobe in Class *Betaproteobacteria*, increased in OTU relative abundance from 0.2 ± 0.2% in the early MFCs to 3.0 ± 2.1% in the intermediate MFCs. Nearly 9% of all UDPIs were from *Alcaligenes*, including proteins involved in the TCA cycle and endogenous peroxide scavenging, suggesting active metabolism by this genus. These results suggest that aerobes in air-cathode MFCs are important both for early colonization of the anode and for successful establishment of an electricity-producing community. Since the importance of oxygen during startup was not known prior to the start of these experiments, oxygen was not measured in these experiments. Future work, however, could modulate dissolved oxygen during MFC startup to determine how the presence of dissolved oxygen affects anode biofilm formation and the development of syntrophic relationships that provide oxygen-tolerance to the mature MFC community. This approach could be especially interesting using different inoculum sources, including those derived from aerobic wastewater that are known to result in more diverse final

anode communities [Khater et al. 2017]. For more complex carbon sources than acetate, the role of aerobes or facultative organisms as oxygen-scavengers would need to be distinguished from their roles as degraders of complex substrates [Jung and Regan 2007; Logan and Regan 2006].

The intermediate MFC achieved a maximum current density 81% of that generated by mature MFCs, despite substantially much lower relative abundance of *Geobacter* (11.0 ± 7.1%) than the mature MFC community (68.7 ± 3.4%) (Appendix SI 5.2: Table S16). One possible explanation is that *Geobacter* need only to reach some threshold abundance level in the biofilm community for the MFC to generate high current densities. In that scenario, current densities continue to increase with additional enrichment of *Geobacter* but not at the same rate as below the threshold *Geobacter* abundance level, perhaps due to other limitations of the MFC reactor system such as internal resistance [Fan et al. 2008]. An alternative explanation is that other genera were responsible for some electricity generation. Indeed, several of the taxa enriched in the intermediate MFCs have been associated previously with electricity production, including *Actinobacteria* [Zhao et al. 2012], *Alphaproteobacteria* [Zhang et al. 2014], *Betaproteobacteria* [Lefebvre et al. 2010], *Epsilonbacteria* [Pereira-Medrano et al. 2013], *Firmicutes* [Wrighton et al. 2008], *Bacteriodetes* [Ha et al. 2012], and *Synergistetes* [Lesnik and Liu 2014]. The presence of these genera in the intermediate anode biofilms, along with the much greater diversity in the intermediate community compared with the mature community (Table 6), suggest the possibility of maintaining a diverse MFC community while still generating high current densities. Previous work has indicated that a diverse anode community with limited *Geobacter* can produce high

current densities, but this occurred when treating complex wastewater with varying characteristics and endogenous organisms [Liu et al. 2011; Patil et al. 2009] or when an aerobic wastewater source was used as inoculum [Khater et al. 2017]. Increased diversity can confer resilience to perturbations with increased community diversity, due to functional redundancy in the community structure [Ishii et al. 2012]. Therefore, the results presented here suggest the possibility that engineering higher MFC community diversity—e.g., through changes in inoculum source [Khater et al. 2017], carbon source [Chae et al. 2009], anode potential [Dennis et al. 2016], or dissolved oxygen concentrations—could improve resilience without sacrificing MFC performance. Future work should investigate the effect of diversity *per se* on MFC current densities, startup time, and resilience to perturbations, perhaps by mixing a base inoculum high in *Geobacter* (e.g., effluent or biofilm material from a mature MFC running on acetate, as suggested previously [Kim et al. 2005]) with more diverse cultures from MFCs or other sources and comparing performance during degradation of influent streams of various complexity.

Comparison of the relative abundance of OTUs across biofilm developmental stages suggested that the intermediate biofilm represented a transitional state between early and mature biofilms. The intermediate community was better correlated to the early community than the mature community was (Appendix SI 5.2: Table S14), consistent with the emergence of the intermediate biofilm community from the early community. Moreover, a lack of correlation (Figure 19) and spatial clustering in a NMDS plot (Appendix SI 5.3: Figure S18) among intermediate biofilm replicate samples with respect to OTUs,), may be explained by high variability in the intermediate biofilms during a

transitional stage. Only a few studies have investigated MFC community dynamics during startup. The increase in *Geobacter* relative abundance observed during transition from early (~6 days' operation) to intermediate (~20 days' operation) was consistent with a previous study using an acetate-fed, air-cathode MFC [Paitier et al. 2017]. In that study, however, there was a clear decrease in *Bacillus* and little change in *Pseudomonas* relative abundance, while in the present study *Bacillus* was nearly non-detectable in any sample and *Pseudomonas* clearly decreased. The difference likely was due to different inoculum sources (primary clarifier vs. anaerobic digester sludge). Interestingly, in both studies *Rhizobiales* increased in relative abundance over the 6-20 day timescale. The biofilm community continued to evolve after current density had achieved a high level, decreasing in diversity, as observed previously [Zhang et al. 2014; Lesnik and Liu 2014; Yates et al. 2012]. In the intermediate biofilm there were 17 prominent OTUs that included a mixture of both aerobic (*Pseudomonas*, *Alcaligenes*, *Acinetobacter*, *Rhodococcus*) and anaerobic (*Geobacter*, *Synergistales*, *Clostridium*, *Rhizobiales*) taxa (Appendix SI 5.2: Table S17). In contrast, the mature biofilms were dominated by fewer than five genera, the most prominent of which by far was *Geobacter*, consistent with many previous examinations of anode communities [Chae et al. 2009; Logan and Regan 2006]. The second most abundant genus in the mature MFCs—an unknown member of *Bacteria*—may have been responsible for consuming residual oxygen to generate anaerobic conditions. The establishment of anoxic conditions is supported by the anode activity of *Geobacter* as well as by the persistence of *Synergistales*, an anaerobic, biogas producer that previously was identified as a member of a MFC "core microbiome" [Lesnik and Liu 2014]. The reduction in number of OTUs suggests that MFC anode

community development is competitive: initially, many electrogenic genera attach to the anode but they are outcompeted (or actively suppressed, as suggested by proteomics results) by organisms with superior electricity generating capabilities, such as *Geobacter*.

The correlation of genera from OTUs with that from protein identifications (Table 6; Appendix SI 5.3: Figures S20, S21) serves to corroborate the taxonomical part of the proteomics results. The proteomics results may be used, however, to gain additional taxonomical information about organisms identified by OTUs that was not provided by the OTU method. For example, in the intermediate biofilm an unknown *Rhizobiales* (OTU380) is a prominent OTU, but sequencing did not provide more detailed taxonomical information. In the proteomics results for the intermediate biofilm, however, UDPIs were identified for *Nitratireductor*, a genus in Order *Rhizobiales*. Similarly, UDPIs were identified for *Mycobacterium* and *Synergistes*, members of Order *Actinomycetales* and Order *Synergistales*, respectively, each of which was a prominent OTU in the intermediate anodes (Appendix SI 5.2: Table S17). This use of taxonomical information suggests an additional way that proteomics results and OTU data from 16S rRNA gene sequencing may be integrated.

Applying the findings reported here to scaled-up MFC systems, it is important to note that at scale the influent wastewater in municipal wastewater treatment would have a much more complex mixture of carbon sources than simply acetate, as in the present study. Moreover, the calculated COD of 1.92 g OD/L in these MFCs (Appendix SI 5.1.1) was an order of magnitude greater than the ~200 mg/L COD typically observed for primary clarifier effluent in municipal wastewater treatment plants [Liu et al. 2004]. The results of the present study were focused, however, on protein expression and

community dynamics during start-up; these results would be relevant to initial stages of scaled-up systems in which a single carbon source such as acetate is fed in order to enrich in electricity-producing genera like *Geobacter* before transferring to a more complex waste stream for treatment [Marassi et al. 2019; Logan et al. 2006]. Moreover, BES systems have been shown to recover energy from "high strength" wastewaters with COD greater than municipal wastewater (i.e., >1 g COD/L), such as wastewaters derived from industrial or biorefinery processes [Hamza et al. 2016]. For example, BES systems have been used to recover energy from high strength wastewater streams derived from brewery fermentation [Wen et al. 2009], paper recycling [Huang and Logan 2008], molasses production [Sevda et al. 2013], dairy wastewater [Marassi et al. 2019], and hydrogen-producing dark fermentation processes [Mohan et al. 2019]. The findings reported here for MFCs operating on high-strength acetate medium may be especially relevant in the latter case, since the effluent from dark fermentation is highly-enriched in acetate [Zhang et al. 2015]. While much previous research has reported on the high Coulombic efficiencies achieved with BES systems for low-strength wastewater such as municipal wastewater, application of BES systems to high strength wastewaters may also be appropriate as part of an initial anaerobic or anoxic treatment that reduces COD (and therefore aeration costs) in downstream aerobic treatment steps [Hamza et al. 2016]. Finally, part of the intention of the present study was to quantify protein expression and community dynamics in MFCs for the first time using proteomics. In order to maximize chances for success, the most simple, model MFC system conditions were used (air-cathode MFC, acetate as carbon source present in non-limiting concentrations). Since this study has demonstrated the efficacy of proteomics to investigate MFCs, future

studies could use this information as a starting point to investigate more complex MFC operating conditions that may be more directly relevant to municipal wastewater treatment.

5.4.2 Membrane proteins in Geobacter *and other species*

Membrane and transport proteins were significantly (Fisher's Exact Test $p<0.05$) more abundant in intermediate MFC biofilms, compared with early MFC biofilms (Figure 21). Likewise, four of the five POIs more abundant in intermediate MFC biofilms were associated with membranes (Table 7). Membrane proteins contributing to structural integrity may be important during biofilm maturation. Moreover, mechanisms of inter-species chemical signaling through membrane channels [Ryan and Dow 2008] may play an important role in the development of effective electricity-generating MFC biofilms, and warrants additional study.

Membrane UDPIs for *Geobacter* included those involved in the steps of electron transfer in anaerobic respiration: NADH dehydrogenase, inner membrane *cb* cytochrome complex, ResB-like cytochromes, and OMC proteins (Appendix SI 5.2: Table S18). OMC proteins—outer membrane, c-type cytochromes containing a CXXCH motif—are responsible for exocellular transfer of electrons out of the cell to acceptors such as Fe(III) or an electrode [Lesnik and Liu 2014]. Only two OMC proteins were detected in early and intermediate anode samples. OmcS, located along conductive type IV pili [Leang et al. 2010], was identified here in both early and intermediate MFCs, but OmcS was not a POI after normalization to *Geobacter* OTUs. Expression of OmcS has been shown to be independent of expression of other OMC proteins [Malvankar et al. 2012]; nevertheless, the lack of detected *Geobacter* OMC proteins was unexpected, since

OMC proteins generally are associated with current generation by this genus [Estevez-Canales et al. 2015]. It is possible that OMC proteins were simply not recovered during protein extraction, though this would be surprising, considering the enrichment of membrane proteins overall among UDPIs. Alternatively, considering that a dearth of OMC protein expression does not preclude completely current generation [Yi et al. 2009], it is possible that alternative methods of electron transfer were being used by *Geobacter* during these initial stages of robust current generation [Smith et al. 2014]. Competition with other species in the MFC biofilm may have altered patterns of OMC expression by *Geobacter*. In fact, the lack of detected OMC proteins may in fact be consistent with the hypothesis that other genera in the community were responsible for electricity generation in these intermediate MFCs (previous section). Additional proteomic studies comparing *Geobacter* protein expression during electricity production as part of a community with that in pure culture would shed light on important interactions that affect initial stages of electricity production.

5.4.3 Gluconeogenesis and fatty acid metabolism by Geobacter *and* Thauera

As biofilms grew in intermediate MFCs, carbohydrate requirements for exopolysaccharide (EPS) production would have increased (Appendix SI 5.3: Figure S16). Since acetate was the sole carbon source available, the sugars used to produce EPS must have been synthesized through gluconeogenesis. In *Geobacter*, the UDPI succinyl:acetate coenzyme A transferase converts acetate to acetyl-CoA, the substrate for the Por enzyme (also a UDPI) to synthesize pyruvate *en route* to phosphoenolpyruvate (PEP) and then to 3-phosphoglycerate. The latter is the substrate for phosphoglycerate kinase, another *Geobacter* UDPI that is associated with gluconeogenesis.

In contrast to *Geobacter*, gluconeogenesis in *Thauera* was fed by the glyoxylate cycle, as indicated by isocitrate lyase and PEP carboxykinase as UDPIs. A previous meta-proteomics study identified the glyoxylate cycle as an up-regulated process during the aerobic phase of enhanced biological phosphate removal by wastewater community [Wilmes et al. 2008]. *Thauera*, a facultative genus found in wastewater, is known for production of abundant EPS [Prombutara and Allen 2016]. The gluconeogenesis activity observed here suggests that *Thauera* was actively involved in building biofilm in intermediate MFC anodes, perhaps as an aerobic syntrophic partner of *Geobacter*. Therefore, operating MFCs under conditions favorable for *Thauera* (i.e., microaerobically, with aromatic compounds as carbon source) could encourage such syntrophy and biofilm building, promoting faster initial biofilm establishment on the anode during MFC startup.

When carbohydrates are limited, β-oxidation of fatty acids provides acetyl-CoA that enters the TCA/glyoxylate cycle [Popov et al. 2005]. The UDPI evidence for β-oxidation was surprising here, since the 30 mM acetate in the MFC medium would have been expected to provide sufficient acetyl-CoA for both energy-generation and anabolic processes. For *Geobacter*, β-oxidation may have been coupled with the activity of Kor [Shi et al. 2009]. The products of β-oxidation also may have been used for biosynthesis of new fatty acids through the FASII system [Zhang and Rock 2012]; *Geobacter* and *Thauera* UDPIs of this system were found. An enhanced rate of fatty acid turnover would be consistent with the overall enrichment of membrane proteins in intermediate stage MFC biofilms as cytochromes or transport proteins are inserted into the lipid bilayer. Thus the proteomics results presented here suggest that adding medium

components that promote fatty acid biosynthesis could assist anode biofilm development during startup [Wen et al. 2011].

5.4.4 Interactions in MFC biofilms

Interactions between organisms in a multispecies biofilm are critical for the emergence of higher-order biofilm properties such as functional stability [Hansen et al. 2007]. Recent advances in omics methods have revealed coordinated interactions between cells in complex biofilms [Roume et al. 2015; Ishii et al. 2015; Burmolle et al. 2014]. Here, antagonism by *Geobacter* toward other biofilm genera was suggested by the UDPI cysteine synthase A. This protein is part of a contact-dependent inhibition system, a direct cell-to-cell interaction mechanism used by some species for broad-spectrum inhibition of biofilm formation by other species [Kaundal et al. 2016]. The intermediate anode biofilm clearly exhibited a rapid rise in diversity compared with the early biofilm (Table 6), possibly including genera that have electrogenic abilities. Increased competition at the intermediate stage may have elicited antagonistic protein expression by *Geobacter* to actively inhibit competitors in the biofilm. Few previous studies have investigated this sort of antagonism by Geobacter in mixed consortia or the extent to which the dominance of *Geobacter* in MFCs or other anaerobic communities may be due to active inhibition of other genera, in addition to the metabolic advantages conferred by its robust capabilities for anaerobic respiration. *Geobacter* may gain additional competitive advantages through flagellar chemotaxis to gain proximity to the anode surface. Flagella such as FliC, a *Geobacter* UDPI in the present study, have been associated with biofilm proliferation [He et al. 2012] as well as with current generation [Yi et al. 2009] or respiration of dissimilatory iron oxides by *Geobacter* [Smith et al.

2013]. Future work could take a strain-resolved proteomics approach [Brooks et al. 2015] to comparing protein expression in BESs by *Geobacter* in pure culture [Kavanagh et al. 2016] or as a dominant member of a constrained community to that as part of a diverse consortium. This study could identify differences in Geobacter's role or mechanisms of action when involved with different types of communities, and perhaps identify mechanisms of antagonism against competitors, especially during MFC startup.

Several UDPIs were associated with the production of, or response to, hydrogen peroxide, a product of aerobic metabolism that plays roles in cell signaling, competitive inhibition, or spatial differentiation in biofilms [Jang et al. 2016]. A superoxide dismutase UDPI suggests that *Geobacter* may be producing hydrogen peroxide, to which UDPIs from other genera (*Rhodococcus* and *Alcaligenes*) may have responded (Appendix SI 5.2: Table S18). In addition to enabling *Geobacter* to withstand microaerobic conditions, peroxide production may be a method of competitive inhibition to kill off cells from other genera, releasing DNA that can stimulate biofilm formation [Okshevsky et al. 2015].

Finally, several UDPIs suggested a response to reactive nitrogenous species, particularly NO and N_2O (Appendix SI 5.2: Table S18) [Schreiber et al. 2012]. In intermediate anodes, both nitrifiers and denitrifiers were found in low relative abundance, in contrast to the high relative abundance of OTUs (~3%) and UDPIs (~8.5%) for *Alcaligenes*. This nitrifying-denitrifying genus has been shown to convert ammonium to molecular N_2 under aerobic conditions, generating N_2O as a byproduct [Shoda and Ishikawa 2014]. The generation of N_2 from denitrification by *Alcaligenes* may have triggered expression of the nitrogen-fixation UDPI NifU in *Geobacter* [Kolmeder et al.

2012]. Nitrification and/or denitrification may have two negative impacts on electricity generation in MFCs: reducing nitrogen availability for electricity-generating genera and providing nitrate as an electron acceptor that competes with the anode. Additional study of nitrogen metabolism during MFC biofilm community development may suggest methods to reduce these negative impacts, or, alternatively, assist recent efforts to apply BES technologies for nitrogen removal or recovery.

5.4.5 Conclusions

This study is the first to investigate global protein expression distinctive to electricity generation by a mixed microbial community. Changes in protein expression and community structure as a MFC begins producing electricity inform fundamental understanding of anode biofilm function and strategies to improve MFC performance. The results presented here suggest that community composition during MFC anode biofilm development is dynamic, shifting from dominance by aerobic taxa in early developmental stages to dominance by *Geobacter*. During that transition, an intermediate stage generates robust current densities, but with considerably greater community diversity than mature MFCs. Initiation of electricity production was associated with enrichment in membrane proteins related to transport and electron transfer, though not in conductive pili. Proteins involved in central carbon metabolism such as the TCA/glyoxylate cycle and gluconeogenesis that were enriched during electricity production suggest EPS biosynthesis by *Geobacter* and *Thauera* genera. Interactions between members of the electricity-producing community were indicated by proteins responsible for the production and response to reactive compounds such as N_2O. Competitive interactions between *Geobacter* and other MFC community members were

suggested by a contact dependent inhibition CysK protein and a phage tail protein in *Geobacter*. The results presented in this study suggest strategies to manipulate anode community interactions—for example, promoting aerobic EPS formation during early biofilm development, or reducing nitrification and denitrification—that may reduce start-up times and improve efficiency of electricity generation in air-cathode MFCs or other BES technologies. This kind of mechanistic information will be critical for scale-up and integration of BES applications into the landscape of new technologies generating bioenergy from renewable biomass.

CHAPTER 5 REFERENCES

Baughn AD, Garforth SJ, Vilcheze C, Jacobs WR. (2009) An anaerobic-type α-ketoglutarate ferredoxin oxidoreductase completes the oxidative tricarboxylic acid cycle of *Mycobacterium tuberculosis*. PLoS Pathog 5; doi: 10.1371/journal.ppat.1000662.

Benjamini Y and Hochberg Y. (1995) Controlling the false discovery rate: a powerful and practical powerful approach to multiple testing. J Royal Stat. Soc, Series B. 57:289-300.

Brooks B, Mueller RS, Young JC, Morowitz MJ, Hettich RL and Banfield JF. (2015) Strain resolved microbial community proteomics reveals simultaneous aerobic and anaerobic function during gastrointestinal tract colonization of a preterm infant. Front. Microbiol. 6:654. doi: 10.3389/fmicb.2015.00654.

Burmolle M, Ren D, Bjarnsholt T, Sorensen SJ. (2014) Interactions in multispecies biofilms: do they actually matter? Trends Microbiol. 22:84-91.

Butler JE, Young ND, Lovley DR. (2010) Evolution of electron transfer out of the cell: comparative genomics of six *Geobacter* genomes. BMC Genom. doi: 10.1186/1471-2164-11-40

Buttigieg PL and Ramette A. (2014) A guide to statistical analysis in microbial ecology: a community-focused, living review of multivariate data analyses. FEMS Microb. Ecol. 90: 534-550.

Cao X, Huang X, Liang P, Xiao K, Zhou Y, Zhang X, et al. (2009) A new method for water desalination using microbial desalination cells. Env. Sci. Technol. 43:7148

7152.

Chae KJ, Choi MJ, Lee JW, Kim KY, Kim IS. (2009) Effect of different substrates on the performance, bacterial diversity, and bacterial viability in microbial fuel cells. Bioresour. Technol. 100:3518-3525.

Chalima A, Hatzidaki A, Karnaouri A, Topakas E. (2019) Integration of a dark fermentation effluent in a microalgal-based biorefinery for the production of high-added value omega-3 fatty acids. App. Energy 241:130-138.

Chignell JF, De Long SK, Reardon KF. (2018) Meta-proteomic analysis of protein expression distinctive to electricity-generating biofilm communities in air-cathode microbial fuel cells. Biotechnol. Biofuels 11:121

Clarke, KR. (1993) Non-parametric multivariate analyses of changes in community structure. Austral. Ecol. 18:117-143.

Dennis PG, Virdis B, Vanwonterghem I, Hassan A, Hugenholtz P, Tyson GW, et al. (2016) Anode potential influences the structure and function of anodic electrode and electrolyte-associated microbiomes. Sci. Rep. doi:10.1038/srep39114

Deutsch EW, Csordas A, Su Z, Jarnuczak A, Perez-Riverol Y, Ternent T, et al. (2017) The ProteomeXchange consortium in 2017: supporting the cultural change in proteomics public data deposition. Nuc. Acids Res. 45(D1): D1100-D1106.

Diner EJ, Beck CM, Webb JS, Low DA, Hayes CS. (2012) Identification of a target cell permissive factor required for contact-dependent growth inhibition (CDI). Genes Dev. 1:515-525.

Ensign SA. (2006) Another microbial pathway for acetate assimilation. Science 331:294-295.

Estevez-Canales M, Kuzume A, Borjas Z, Fueg M, Lovley DR, Wandlowski T, et al. (2015) A severe reduction in the cytochrome C content of *Geobacter sulfurreducens* eliminates its capacity for extracellular electron transfer. Environ. Microbiol. Reports 7:219-226.

Fan Y, Sharbrough E, Liu H. (2008) Quantification of the internal resistance distribution of microbial fuel cells. Environ. Sci. Technol. 42:8101-8107.

Fowler GJ, Pereira-Medrano AG, Jaffe S, Pasternak G, Pham TK, Ledezma P, et al. (2016) An iTRAQ characterization of the role of TolC during electron transfer from *Shewanella oneidensis* MR-1. Proteomics 16:2764-2775.

Franzosa EA, Hsu T, Sirota-Madi A, Shafquat A, Abu-Ali G, Morgan XC, et al. (2015) Sequencing and beyond: integrating molecular 'omics' for microbial community profiling. Nat. Rev. Microbiol. 13:360-372.

Gorby YA, Yanina S, McLean JS, Rosso KM, Moyles D, Dohnalkova A et al. (2006) Electrically conductive bacterial nanowires produced by *Shewanella oneidensis* strain MR-1 and other microorganisms. Proc. Nat. Acad. Sci. 103:11358-11363.

Ha PT, Lee TK, Rittman BE, Park J, Chang IS. (2012) Treatment of alcohol distillery wastewater using a *Bacteroidetes*-dominant thermophilic microbial fuel cell. Environ. Sci. Technol. 46:3022-3030.

Hamza RA, Iorhemen OT, Tay JH. (2016) Advances in biological systems for the treatment of high-strength wastewater. J. Water Proc. Eng. 10:128-142

Hansen SK, Rainey PB, Haagensen JAJ, Molin S. (2007) Evolution of species interactions in a biofilm community. Nature 445:533-536.

He Y, Xu T, Fossheim LE, Zhang X-H. (2012) FliC, a Flagellin Protein, Is Essential for the Growth and Virulence of Fish Pathogen *Edwardsiella tarda*. PLoS ONE doi: 10.1371/journal.pone.0045070.

Holmes DE, Giloteaux L, Chaurasia AK, Williams KH, Luef B, Wilkins MJ, et al. (2015) Evidence of *Geobacter*-associated phage in a uranium-contaminated aquifer. ISME J. 9:333-346.

Huang LP and Logan BE. (2008) Electricity generation and treatment of paper recycling wastewater using a microbial fuel cell. Appl Microbiol Biotechnol 80: 349-355

Hurek T and Reinhold-Hurek B. (2003) *Azoarcus* sp. Strain BH72 as a model for nitrogen-fixing grass endophytes. J Biotechnol. 106(2-3):169-178.

Ishii S, Suzuki S, Norden-Krichmar TM, Nealson KH, Sekiguchi Y, Gorby YA, et al. (2012) Functionally stable and phylogenetically diverse microbial enrichments from microbial fuel cells during wastewater treatment. PLoS ONE doi: 10.1371/journal.pone.0030495.

Ishii S, Suzuki S, Tenney A, Norden-Krichmar TM, Nealson KH, Bretschger O. (2015) Microbial metabolic networks in a complex electrogenic biofilm recovered from a stimulus-induced metatranscriptomics approach. Sci. Rep. doi: 10.1038/srep14840.

Jang IA, Kim J, Park W. (2016) Endogenous hydrogen peroxide increases biofilm formation by inducing exopolysaccharide production in *Acinetobacter oleivorans* DR1. Sci. Rep. doi: 10.1038/srep21121.

Jung S and Regan JM. (2007) Comparison of anode bacterial communities and performance in microbial fuel cells with different electron donors. Appl. Microbiol. Biotechnol. 77:393-402

Kanehisa M, Sato Y, Morishima K. (2016) BlastKOALA and GhostKOALA: KEGG tools for functional characterization of genome and metagenome sequences. J Mol Biol. 428:726-731.

Kaundal S, Uttam M, Thakur KG. (2016) Dual role of a biosynthetic enzyme, CysK, in contact dependent growth inhibition in bacteria. PLoS ONE doi: 10.1371/journal.pone.0159844

Kavanagh P, Botting CH, Jana PS, Leech D, Abram F. (2016) Comparative proteomics implicates a role for multiple secretion systems in electrode-respiring *Geobacter sulfurreducens* biofilms. J. Proteome Res. 15:4135-4145.

Kelly PT and He Z. (2014) Nutrients removal and recovery in bioelectrochemical systems: a review. Biores. Technol. 153:351-360

Kerscher L and Oesterhelt D. (1981) Purification and properties of two 2-oxoacid:ferredoxin oxidoreductases from *Halobacterium halobium*. Eur J Biochem. 116:587-594.

Khare T, Esteve-Nunez A, Nevin KP, Zhu W, Yates JR, Lovley D, et al. (2006) Differential protein expression in the metal-reducing bacterium *Geobacter sulfurreducens* strain PCA grown with fumarate or ferric citrate. Proteomics 6:632-640.

Khater DZ, El-Khatib KM, Hassan HM. (2017) Microbial diversity structure in acetate single chamber microbial fuel cell for electricity generation. J. Gen. Eng. Biotechnol 15:127-137.

Kim JR, Min B, Logan BE. (2005) Evaluation of procedures to acclimate a microbial fuel cell for electricity generation. Biotechnol. Prod. Proc. Eng. 68:23-30.

Kolmeder CA, de Been M, Nikkila J, Ritamo I, Mättö J, Valmu L, et al. (2012) Comparative metaproteomics and diversity analysis of human intestinal microbiota testifies for its temporal stability and expression of core functions. PLoS ONE doi:10.1371/journal.pone.0029913.

Labbe N, Parent S, Villemur R. (2004) *Nitratireductor aquibiodomus* gen. nov., sp. Nov., a novel alpha-proteobacterium from the marine denitrification system of the Montreal Biodome (Canada). Int J Syst. Evol. Microbiol. 54:269-273.

Lacerda, CM, Choe LH, Reardon KF. (2007) Metaproteomic analysis of a bacterial community response to cadmium exposure. J Proteome Res. 6:1145-1152.

Lacerda C, Reardon KF. (2009) Environmental proteomics: applications of proteome profiling in environmental microbiology and biotechnology. Brief Funct. Genomic Proteomic 8:75-87

Leang C, Qian X, Mester T, Lovley DR. (2010) Alignment of the c-type cytochrome OmcS along pili of *Geobacter sulfurreducens*. Appl. Env. Microbiol. 76:4080-4084.

Leary DH, Hervey WJ, Malanoski AP, Wang Z, Eddie BJ, Tender GS, Vora GJ, Tender LM, Lin B, Strycharz-Glaven SM. (2015) Metaproteomic evidence of changes in protein expression following a change in electrode potential in a robust biocathode microbiome. Proteomics. 15:3486-3496.

Lefebvre O, Nguyen TTH, Al-Mamun A, Chang IS, Ng HY. (2010) T-RFLP reveals high β-Proteobacteria diversity in microbial fuel cells enriched with domestic wastewater. J App. Microbiol. 109:839-850.

Leon, IR, Schwammle V, Jensen ON, Sprenger RR. (2013) Quantitative assessment of in-solution digestion efficiency identifies optimal protocols for unbiased protein analysis. Mol Cell Proteomics 12:2992-3005.

Lesnik KL and Liu H. (2014) Establishing a core microbiome in acetate-fed microbial fuel cells. App. Microbiol. Biotechnol. 8:4187-4196.

Liu G, Yates MD, Cheng S, Call DF, Sun D, Logan BE. (2011) Examination of microbial fuel cell start-up times with domestic wastewater and additional amendments. Biores. Technol. 102:7301-7306.

Liu H, Grot S, Logan BE. (2005) Electrochemically assisted microbial production of hydrogen from acetate. Environ. Sci. Technol. 39:4317-4320.

Liu H and Logan BE. (2004) Electricity generation using an air-cathode single chamber microbial fuel cell in the presence and absence of a proton exchange membrane. Environ. Sci. Tech. 38:4040-4046.

Liu H, Ramnarayanan R, Logan BE. (2004) Production of electricity during wastewater treatment using a single chamber microbial fuel cell. Environ. Sci. Technol. 38:2281-2285

Logan BE. (2004) Scaling up microbial fuel cells and other bioelectrochemical systems. Appl. Microbiol. Biotechnol. 85:1665-1671.

Logan BE, Hamelers B, Rozendal R, Schroder U, Keller J, Freguia S, et al. (2006) Microbial fuel cells: Methodology and Technology. Environ. Sci. Technol. 40:5181-5192

Logan BE and Regan JM. (2006) Electricity-producing bacterial communities in microbial fuel cells. Trends Microbiol. 14:512-518.

Logan BE, Wallack MJ, Kim K-Y, He W, Feng Y, Saikaly P. (2015) Assessment of microbial fuel cell configurations and power densities. *Environ. Sci. Technol. Lett*. 2:206-214.

Lu F, Bize A, Guillot A, Monnet V, Madigou C, Chapleur O, et al. (2014) Metaproteomics of cellulose methanisation under thermophilic conditions reveals a surprisingly high proteolytic activity. ISME J. 8:88-102.

Ma Q, Zhou J, Zhang W, Meng X, Sun J, Yuan Y-J. (2011) Integrated proteomic and metabolomics analysis of an artificial microbial community for two-step production of vitamin C. PLoS ONE doi: 10.1371/journal.pone.0026108.

Malvankar NS, Tuominen MT, Lovley DR. (2012) Lack of cytochrome involvement in long-range electron transport through conductive biofilms and nanowires of *Geobacter sulfurreducens*. Energ. Environ. Sci. 5: 8651–8659.

Marassi RJ, Hermanny RS, Silva GC, Silva FT, Paiva TCB. (2019) Electricity production and treatment of high-strength dairy wastewater in a microbial fuel cell using acclimated electronic consortium. Int. J. Environ. Sci. Technol. 16:7339-7348.

Marsili E, Baron DB, Shikhare ID, Coursolle D, Gralnick JA, Bond DR. (2008) *Shewanella* secretes flavins that mediate extracellular electron transfer. Proc. Nat. Acad. Sci. 105:3968-3973.

Methe BA, Nelson KE, Eisen JA, Paulsen IT, Nelson W, Heidelberg JF et al. (2003) Genome of *Geobacter sulfurreducens*: metal reduction in subsurface environments. Science 302:1967-1969.

Mohan SV, Rohit MV, Amulya K, Kumar AN, Modestra JA, Sravan JS, Hemalatha M, Chatterjee S, Ranadheer P, Swathi K. (2019) Acidogenic biohydrogen production integrated with biorefinery approach. In Biomass, Biofuels, Biochemicals: Biohydrogen (2nd Ed.) Ed. Pandey A, Mohan SV, Chang J-S, Hallenbeck PC, Larroche C. ISBN: 978-0-444-64203-5. https://doi.org/10.1016/B978-0-444-64203-5.00014-9

Nancharaiah YV, Mohan SV, Lens PNL. (2015) Metals removal and recovery in bioelectrochemical systems: a review. Biores. Technol. 195:102-114.

Nevin KP, Woodard TL, Franks AE, Summers AM, Lovley DR. (2010). Microbial electrosynthesis: feeding microbes electricity to convert carbon dioxide and water to multicarbon extracellular organic compounds. mBio doi:10.1128/mBio.00103-10.

Okshevsky M, Regina VR, Meyer RL. (2015) Extracellular DNA as a target for biofilm control. Curr. Opin. Biotechnol. 33:73-80.

Paitier A, Godain A, Lyon D, Haddour N, Vogel TM, Monier J-M. (2017) Microbial fuel cell anodic microbial population dynamics during MFC start-up. Biosens. Bioelectron. 92:357-363.

Park T-J, Ding W, Cheng S, Brar MS, Ma APY, Tun HM, et al. (2014) Microbial community in microbial fuel cell (MFC) medium and effluent enriched with purple photosynthetic bacterium (*Rhodopseudomonas* sp.). AMB Express. doi: 10.1186/s13568-014-0022-2.

Pascovici D, Handler DCL, Wu JX, Haynes PA. (2016) Multiple testing corrections in quantitative proteomics: a useful but blunt tool. Proteomics 16:2448-2453.

Patil SA, Surakasi VP, Koul S, Ijmulwar S, Vivek A, Shouche YS, Kapadnis BP. (2009) Electricity generation using chocolate industry wastewater and its treatment in activated sludge based microbial fuel cell and analysis of developed microbial community in the anode chamber. Biores. Technol. 100:5132-5139.

Pereira-Medrano AG, Knighton M, Fowler GJS, Ler ZY, Trong KP, Ow SY, et al. (2013) Quantitative proteomic analysis of the exoelectrogenic bacterium *Arcobacter butzleri*

ED-1 reveals increased abundance of a flagellin protein under anaerobic growth on an insoluble electrode. J. Proteomics 78:197–210.

Popov VN, Moskalev EA, Shevchenko MU, Eprintsev AT. (2005) Comparative analysis of glyoxylate cycle key enzyme isocitrate lyase from organisms of different systematic groups. J Evol. Biochem. Physiol. 41:631-639.

Prombutara P and Allen MS. (2016) Flocculation-related gene identification by whole-genome sequencing of *Thauera aminoaromatica* MZ1T floc-defective mutants. Appl. Environ. Microbiol. 82:1646-1652.

Qian X, Mester T, Morgado L, Arakawa T, Sharma ML, Inoue K, et al. (2011) Biochemical characterization of purified OmcS, a c-type cytochrome required for insoluble Fe(III) reduction in *Geobacter sulfurreducens*. Biochim. Biophys. Acta. 2011;1807:404-412.

Qu Y, Feng Y, Wang X, Logan BE. (2012) Use of a coculture to enable current production by *Geobacter sulfurreducens*. Appl. Env. Microbiol. 78:3484-3487.

Read ST, Dutta P, Bond PL, Keller J, Rabaey K. (2010) Initial development and structure of biofilms on microbial fuel cell anodes. BMC Microbiol. doi**:** 10.1186/1471-2180-10-98

Rittman B, Krajmalnik-Brown R, Halden, RU. (2008) Pre-genomic, genomic and postgenomic study of microbial communities involved in bioenergy. Nat. Rev. Microbiol. 6:604-612

Roume H, Heintz-Buschart A, Muller EEL, May P, Satagopam VP, Laczny CC, et al. (2015) Comparative integrated omics: identification of key functionalities in microbial community-wide metabolic networks. Biofilms and Microbiomes. doi:10.1038/npjbiofilms.2015.7

Rozendal RA, Leone E, Keller J, Rabaey K. (2009) Efficient hydrogen peroxide generation from organic matter in a bioelectrochemical system. Electrochem. Commun. 11:1752-1755.

Ryan RP and Dow JM. (2008) Diffusible signals and interspecies communication in bacteria. Microbiology. 154:1845-1858.

Schreiber F, Wunderlin P, Udert KM, Wells GF. (2012) Nitric oxide and nitrous oxide turnover in natural and engineered microbial communities: biological pathways, chemical reactions, and novel technologies. Front. Microbiol. doi: 10.3389/fmicb.2012.00372.

Schroder U. (2007) Anodic electron transfer mechanisms in microbial fuel cells and their energy efficiency. Phys. Chem. Chem. Phys. 9:2619-2629.

Sevda S, Dominguez-Benetton X, Vanbroekhoven K, De Wever H, Sreekrishnan TR, Pant D. (2013) High strength wastewater treatment accompanied by power generation using air cathode microbial fuel cell. App Energy 105:194-206

Shi L, Richardson DJ, Wang Z, Kerisit SN, Rosso KM, Zachara JM, et al. (2009) The roles of outer membrane cytochromes of *Shewanella* and *Geobacter* in extracellular electron transfer. Environ. Microbiol. Rep. 1:220-227.

Shoda M and Ishikawa Y. (2014) Heterotrophic nitrification and aerobic denitrification of high-strength ammonium in anaerobically digested sludge by *Alcaligenes faecalis* strain No. 4. J. Biosci. Bioeng. 117:737-741.

Smith JA, Lovley DR, Tremblay P-L.(2013) Outer cell surface components essential for Fe(III) oxide reduction by *Geobacter metallireducens*. Appl. Env. Microbiol. 79:901-907

Smith JA, Tremblay P-L, Shrestha PM, Snoeyenbos-West OL, Franks AE, Nevin KP, *et al*. (2014) Going Wireless: Fe(III) oxide reduction without pili by *Geobacter sulfurreducens* strain JS-1. Appl. Environ. Microbiol. 80:4331-4340.

Stein LY. (2011) Surveying N_2O-producting pathways in bacteria. Methods Enzymol. 486:131-152.

Storey JD. (2002) A direct approach to false discovery rates. Stat. Methodol. Ser. B. 64:479-498.

Tran HT, Krushkal J, Antommattei FM, Lovley DR, Weis RM. (2008) Comparative genomics of *Geobacter* chemotaxis genes reveals diverse signaling function. BMC Genom. doi: 10.1186/1471-2164-9-471.

Ueki T. and Lovley DR. (2010) Novel regulatory cascades controlling expression of nitrogen-fixation genes in *Geobactersulfurreducens*. Nuc. Acids Res. 38: 7485-7499.

Wang H, Park J, Ren ZJ. (2015) Practical energy harvesting for microbial fuel cells: a review. Environ. Sci. Technol. 49:3267-3277.

Watson VJ, Logan BE. (2010) Power production in MFCs inoculated with *Shewanella oneidensis* MR-1 or mixed cultures. Biotechnol. Bioeng. 105:489-498.

Wen Q, Wu Y, Cao D, Zhao L, Sun Q. (2009) Electricity generation and modeling of microbial fuel cell from continuous beer brewery wastewater. Biores. Technol. 100:4171-4175

Wen Q, Kong F, Ma F, Ren Y, Pan Z. (2011) Improved performance of air-cathode microbial fuel cell through additional Tween 80. J. Pow. Sour. 2011;196:899-904.

Wilmes P, Andersson AF, Lefsrud MG, Wexler M, Shah M, Zhang B, et al. (2008) Community proteogenomics highlights microbial strain-variant protein expression within activated sludge performing enhanced biological phosphorous removal. ISME J. 22:853-864.

Wrighton KC, Agbo P, Warnecke F, Weber KA, Brodie EL, DeSantis TZ, et al. (2008) A novel ecological role of the *Firmicutes* identified in thermophilic microbial fuel cells. ISME J 2:1146-1156.

Yang Y, Wu Y, Hu Y, Cao Y, Poh CL, Cao B, et al. (2015) Engineering electrode-attached microbial consortia for high-performance xylose-fed microbial fuel cell. ACS Catal. 5:6937-6945

Yates MD, Kiely PD, Call DF, Rismani-Yazdi H, Bibby K, Peccia J, Regan JM, Logan BE. (2012) Convergent development of anodic bacterial communities in microbial fuel cells. J. ISME doi:10.1038/ismej.2012.42.

Yi H, Nevin KP, Kim BC, Franks AE, Klimes A, Tender TM, et al. (2009) Selection of a variant of *Geobacter sulfurreducens* with enhanced capacity for current production in microbial fuel cells. Biosens. Bioelectron. 24:3498-3503.

Yokoyama H, Ishida M, Yamashita T. (2016) Comparison of anodic community in microbial fuel cells with iron oxide-reducing community. J Microbiol Biotechnol. 26:757-762.

Zhang F, Zhang Y, Ding J, Dai K, van Loosdrecht MCM, Zeng RJ. (2015) Stable acetate production in extreme-thermophilic (70 °C) mixed culture fermentation by selective enrichment of hydrogenotrophic methanogens. Sci. Rep. 4:5268. https://doi.org/10.1038/srep05268

Zhao G, Ma F, Wei L, Chua H, Chang CC, Zhang XJ. (2012) Electricity generation from cattle dung using microbial fuel cell technology during anaerobic acidogenesis and the development of microbial populations. Waste Manag. 32:1651-1658.

Zhang H, Chen X, Braithwaite D, He Z. Phylogenetic and Metagenomic Analyses of Substrate-Dependent Bacterial Temporal Dynamics in Microbial Fuel Cells. PLoS ONE 9: e107460. doi:10.1371/journal.pone.0107460.

Zhang Y, Min B, Huang L, Angelidaki I. (2011) Electricity generation and microbial community response to substrate changes in microbial fuel cell. Bioresour. Technol. 102:1166-1173.

Zhang Y, Wen Z, Washburn MP, Florens L. Refinements to label free proteome quantitation: how to deal with peptides shared by multiple proteins. Anal. Chem. 2010;82:2272-2281.

Zhang Y-M and Rock CO. Will the initiator of fatty acid synthesis in *Pseudomonas aeruginosa* please stand up? J. Bacteriol. 2012;194:5159-5161.

CHAPTER 6: CONCLUSIONS AND FUTURE DIRECTIONS

6.1 Significance and contributions of project

Despite their ancient origins, biofilms have only recently become the subject of intensive scientific study. Biotechnologies that take advantage of unique features of biofilms, moreover, are still in a dynamic stage of development. The present work contributes to the characterization of those unique features through the application of quantitative proteomics to four different biofilm biotechnologies. Unlike conventional approaches that reduce observations to pre-determined target proteins, a proteomics approach quantifies protein expression across a system in order to answer questions and generate new hypotheses at various levels of complexity.

Chapter 2 attempted to distinguish distinctive metabolic features of bacteria in biofilms from those in planktonic culture. This simple comparison between cell phenotypes aimed to identify **what** is unique about cells in a biofilm compared with planktonic cells, when both cell types are performing the same function. Using *Lactobacillus delbrueckii* lactis as a model, we discovered a 31% relative increase in the diversity of metabolic categories into which biofilm proteins were categorized, compared to planktonic samples. There was also a relative increase in abundance of proteins related to catalytic activity and a relative decrease in proteins related to cell replication and solute transport. Riboflavin biosynthesis and fatty acid metabolism suggested redox functions, energy storage, and membrane turnover that was distinctive to biofilm cells. Finally, a stress response was detected that may have been due to increased metabolic rates of biofilm cells or due to taxing conditions in the biofilm such as decreased pH or

heterogeneous nutrient concentrations. These insights provide confirmation on a molecular level of increased metabolic rates observed in studies that show higher productivity using biofilms compared with planktonic cells (e.g, in a continuously stirred tank reactor).

Chapter 3 distinguished protein expression between aerobic and electricity-generating biofilms of *Shewanella oneidensis* MR-1. In this case, two biofilms were compared to ask **which** proteins are more abundant for a biofilm performing a useful function. Three proteins not previously associated with electricity generation were more abundant in anode biofilms compared with aerobic, cathode biofilms. Future work would investigate the functions of these proteins, particularly the role of active transport TonB-dependent proteins in current generation, in order to identify strategies to engineer *S. oneidensis* MR-1 for bioproduct generation during bioelectrosynthesis. Relieving conditions that contribute to the stress response observed for *S. oneidensis* MR-1 biofilms on the anode—e.g., through optimization of medium ingredients—could improve BES performance. The possible detection of aerobic TCA cycle protein expression in anode biofilms contributes to current reports on the effects of oxygen on current generation by this facultative strain. To address the implications of a microaerobic environment, the kinetics of oxygen consumption and growth in the bulk solution of an air-cathode MFC were described for the first time. Using this information, the dilution rate of a continuous MFC could be set higher than the specific growth rate of cells in the bulk, to minimize losses of nutrients to bulk cell growth and to wash out bulk cells before they can attach to the cathode and foul it with aerobic biofilm. This approach would be especially relevant to mixed culture BES systems applied to wastewater treatment since (1) an air-cathode

BES is the most likely design for wastewater applications, (2) loss of Coulombic efficiency is critical for any BES in which power generation is the primary goal and (3) cleaning or replacing a cathode fouled by biofilm would consume time and materials at a large scale and risks damage to the anaerobic anode community by exposure to air. Future work would quantify rates of cell detachment from the anode biofilm (the source of bulk cells) and identify dilution rates at which bulk cells begin to accumulate in the bulk solution, under different influent conditions.

In Chapter 4 the complexity of the system under investigation increased due to the inclusion of more than one species. We discovered that, in response to co-culture with *Bacillus atrophaeus*, *Pseudomonas putida* expressed an array of proteins associated with a surface-bound phenotype. This sort of *P. putida* phenotype was observed during co-cultures on an agar plate, triggering avoidance by *B. atrophaeus* colonies. This virulent *P. putida* phenotype, along with patterns of protein expression related to metal sequestration and biosynthesis of antagonistic compounds, suggested mechanisms for **how** biofilms begin to form under conditions of competitive stress. Additionally, differential protein expression in *B. atrophaeus* in the co-culture (particularly nucleotide and fatty acid metabolism) suggested that *B. atrophaeus* had entered stationary phase earlier than *P. putida* in the co-culture, perhaps due to being outcompeted for nutrients or due to active antagonism. This kind of information is not easily obtained by other methods, indicating the power of a proteomics approach to suggest answers and develop new hypotheses about macro-level observations. The defined co-culture approach to microbial ecology has become popular in recent years, especially in omics studies. One criticism of this approach is that the findings are of limited value since it is dubious to

extrapolate from an artificially-constructed community to what occurs in nature. On the contrary, the defined co-culture approach seems analogous to conducting physiological tests in a controlled lab environment with any isolated strain. Describing features of the organism observed under lab conditions does not entail a claim that the organism will necessarily behave that way in nature. Rather, the lab results give clues to the organism's behavioral *capabilities*. In the same way, proteomic investigation of co-cultures provides insights into the capabilities of certain organisms—not discernible using conventional methods—in controlled, interactive situations. The interactions identified through proteomics then serve as topics of investigation for future, *in* studies.

Chapter 5 described an investigation of the most complex type of biofilm system considered here: an undefined mixed culture in dynamic stages of development. Taking a time-course approach, this study asked **when** a function of interest emerges and **who** in the biofilm community is responsible for it. This was the first proteomic investigation of an electricity-generating, mixed culture biofilm in a BES. To quantify protein expression in large meta-proteomics datasets that could not be analyzed by ProteinPilot software, we developed novel, in-house bioinformatics protocols for peptide spectrum matching and quantitation by spectral counting. Several novel features of BES protein expression emerged as the biofilm became electrochemically active, including carbon storage through the glyoxylate pathway by *Thauera* species, competitive inhibition by *Geobacter*, and responses to reactive compounds generated from denitrification. Proteomics results, in conjunction with 16S rRNA gene sequencing of the bacterial community, suggested for the first time that a BES biofilm with high species diversity can generate electricity at a robust level compared with BES biofilms dominated by

Geobacter. Clearly the community members responsible for electricity production in developing BES biofilms are not limited to *Geobacter* species; these results suggest candidates for new electrochemically active species. Moreover, protein expression related to aerobic metabolism as well as to fatty acid biosynthesis suggested hypotheses that maintaining microaerobic conditions and providing polysorbate during initial biofilm formation could improve start-up times. It is not clear that either of these hypotheses would have been considered without these meta-proteomics results. Moreover, it is difficult to see how a defined co-culture approach to a BES system would have been able to provide the same depth of information about interactions within the biofilm consortium as that revealed here by meta-proteomics.

In addition to describing mechanisms of biofilm functionality, the work presented here also made methodological contributions to proteomic analysis of biofilms. The requirement for removal of ECM from biofilm protein samples became very clear during the work described in Chapter 2. We also addressed for the first time the importance of determining limits of detection and quantification of proteins of interest when analyzing a mixture of proteins from different species (Chapter 4). In Chapter 5, we developed a novel strategy to address a fundamental quantitation problem in label-free proteomics: accounting for multiple peptide-spectrum matches. An in-house bioinformatics quantitation strategy was developed based on the Unused Score provided by ProteinPilot software for each peptide-spectrum match. In Chapter 5, moreover, we developed a method for successfully extracting and processing proteins from BES anode biofilms. The anaerobic nature of anode biofilms leads to extreme sample limitation and low protein recovery, similar to that observed in previous proteomics studies of

environmental biofilms [Leary et al. 2012]. The success of the method developed in this work in extracting representative protein samples from the anode biofilm was suggested by the high degree of correlation (adjusted $R^2 = 0.914$, p-value $< 2.2e^{-16}$) between proteins and 16S rRNA gene sequencing with respect to taxonomical relative abundance. In this analysis, however, only those genera with relative abundance greater than 0.5% of the consortium were included. This is an arbitrary threshold. In order to determine rigorously the relative abundance that a species or protein must reach in order to be quantified accurately, a similar enterprise to determine limits of quantitation to that described in Chapter 4 for a binary co-culture should be conducted for multi-species systems like a BES biofilm. The first step in this process would involve spiking proteins extracted from a BES with proteins from a well-annotated species not usually found in the BES, such as *E. coli*—a strategy demonstrated in the first sections of Chapter 4.

6.2 Challenges for biofilm proteomics revealed in this work

As in most proteomics studies, the present work used an experimental design based on comparing samples from biological replicates. As discussed in Chapter 1 (Section 1.2.2), however, each biofilm has a unique, non-reproducible structure; pooling observations across replicates may not be ideal for proteomic (or any omics) analysis of biofilms. Differences in structure can have strong effects on the physiology of cells in the ECM, for example, due to microniches containing different abundances of nutrients. In Chapter 2, the lack of correlation in relative protein abundance among the replicate biofilm samples—in some cases showing more similarity with planktonic samples than with other biofilms—illustrates the difficulty in considering different biofilms to be "replicates". Differences between replicate biofilms likely are a result of small

differences in operational conditions or surface features that result in larger differences once the biofilm is mature. As described in Chapter 3, the microaerobic conditions of a bioreactor like an air-cathode MFC can play an outsized role in the performance of the reactor and the metabolism of the anode biofilm. A parameter like dissolved oxygen concentration, however, can be difficult to control precisely (one example is the large standard deviation for the dissolved oxygen measurements for the first 20 h of operation). Moreover, as shown in Chapter 5, "replicate" mixed culture biofilm reactors can differ considerably in community composition and protein expression, even when they are inoculated with the same mixed culture and are operated under identical conditions. Surely, one contributing factor is lack of reproducibility in protein recovery between biofilms, as demonstrated by the differences in protein identifications for each replicate intermediate MFC biofilm (Appendix SI 5.3: Figure S7B). This variation across replicate samples likely results in loss of information as differences between the experimental and control group are masked during significance testing. Changes in experimental design, as suggested below (section 6.3), may be required when conducting biofilm -omics studies.

A persistent problem in meta-proteomics work is the question whether a matched metagenome (meta-proteome) is necessary to achieve high quality meta-proteomics results. That is, does using a search database built from DNA extracted from the same samples under consideration by proteomics result in more and more confident peptide and protein identifications compared with using publicly-available sequences (e.g., the entire set of bacterial genomes available from NCBI)? A recent study reported mixed results, noting that a matched metagenome was very important for some gut microbiota sample types but not clearly better for others [Tanca et al. 2016]. In Chapter 5 we elected

to use the complete set of bacterial protein sequences publicly available from Uniprot (www.uniprot.org) as our database for searching MS/MS spectra. Part of our reasoning here was that BES communities are expected to contain a lower proportion of unknown or non-sequenced organisms than very complex communities, e.g., gut microbial communities, that might require a matched database. It is not clear that a matched database is necessary or even beneficial for all sample types, or that using a matched database adds enough value to justify the considerable time and expense required to sequence a new metagenome for every meta-proteomics project. This last consideration is especially relevant when there is a lack of annotation available for a newly-sequenced metagenome: will sequencing the metagenome be worth the effort and expense if functional annotation is low-confidence or not available? We suggest that the decision on whether to use a matched metagenome database should be project-specific, depending on the type of consortium under consideration and the research questions of the project. We predict that as the collection of publicly-available sequences (including from diverse environmental consortia) continues to grow, the quality of results from the two types of databases will converge, making sequencing new metagenomes less critical.

Finally, as mentioned briefly above (section 6.1), a considerable challenge for biofilm proteomics is development of methods for extraction and preparation of proteins from biofilms. As observed in Chapter 2, even with appropriate peptide clean-up procedures, if proteins extracted from biofilms are not precipitated prior to downstream processing, the accuracy and quality of spectral IDs decreases due to contamination of the LC-MS/MS with ECM. On the other hand, acetone precipitation—a standard method for removing contaminants from protein samples—is known to result in considerable losses

(40-50%) of proteins in a sample. This high degree of sample loss during precipitation undercuts the quantitative goals of proteomics, especially for low-abundance proteins [Feist and Hummon 2015]. Moreover, losses from acetone precipitation likely do not cut across all protein families equally, calling into question the accuracy and scope of protein quantification. Additional study to determine the amount and types of proteins lost from a sample during clean-up methods such as acetone precipitation will further the development of methods for proteomics of biofilms and other protein-limited sample types. For this task, more effective methods without precipitation will need to be developed than that used in Chapter 2, in order to assess the protein profile before and after precipitation.

6.3 Future Directions and Concluding Remarks

The results presented in this work suggest that each individual biofilm is a dynamic, unique system. This fact is reflected by the variation between "replicate" biofilms discussed above (section 6.2), as well as by the shifts in protein expression across stages of biofilm development that are presented in Chapter 5. Two biofilms harvested at slightly different developmental stages may have considerable differences in protein expression. Moreover, as Chapter 3 suggested, dramatic modulations in protein expression may begin at the very moment that a biofilm phenotype is initiated, while cells are still growing planktonically. Accounting for the unique features of each biofilm in a proteomics workflow may require a change in experimental approach. An actively-emerging field of proteomics in cancer research is "single-cell" proteomics, in which the entire proteomes of individual cells are quantified to distinguish cancer cells from non-cancer cells [Budnik et al. 2017]. A similar approach targeting different cell populations

in the same biofilm might be appropriate, since even biofilms of a single species likely contain populations of cells in different metabolic states or experiencing different micro-niches, due to stochastic differences in ECM structure. In this approach, rather than comparing protein abundance statistically across "replicate" biofilms, the focus instead would be on detailed assessments of distinct populations within a single biofilm [Taniguchi et al. 2010]. For example, populations of *S. oneidensis* MR-1 cells in the MFC biofilm of Chapter 3 that were using the anode as electron acceptor could be distinguished from other populations in the anode biofilm that were using trace oxygen. This approach would treat each individual biofilm as a unique system with features that may or may not be duplicated in other biofilms cultivated under the same conditions. The analysis then would be repeated for additional biofilms and generalization or significance testing would occur at the level of metabolic pathways rather than at the level of protein abundance. Clearly this approach would become much more complex if applied to multi-species biofilms; the defined co-culture approach presented in Chapter 4 might be most appropriate to reduce the complexity of studying individual cell populations and their interactions.

A fairly obvious next step from the present research would be to design co-cultures for BESs. Several recently published studies have already taken that approach, in order to identify functional interactions at work in BES systems. For example, an anode-respiring organism such as *S. oneidensis* MR-1 or *Geobacter* can be co-cultured in a BES with a fermentative organism such as *E. coli* [Wang et al. 2015; Bourdakos et al. 2014]. Future work would apply a proteomics approach to these BES co-cultures in

order to provide additional layers of insight into interactions between these species in a BES biofilm.

Pushing this co-culture proteomics approach further, however, would combine a mixed culture like a BES biofilm with a well-characterized species. The well-characterized species, if integrated into the community, would be hypothesized to perform some function that the community cannot perform—e.g., in the case of BESs, such a function would be production of electricity from formic acid as carbon source [Kiely et al. 2010]. Since *S. oneidensis* MR-1 happens to use formic acid during current generation, that species would be a good candidate for introduction to the mixed culture, either in the inoculation stage or before changing the carbon source to formic acid. Proteomics then could verify that the introduced species is indeed performing the desired function and also obtain additional information about its interactions with other members of the consortium. This approach would require the same sort of limit of detection and quantification work that we demonstrated in Chapter 3. Moreover, the candidate species should be absent from the mixed culture initially (*Shewanella* species generally are not abundant in wastewater mixed cultures). In this way, proteomics could be used to discover information about interactions in a mixed culture, relying on high quality annotation of the well-characterized species, rather than less high quality or absent annotation of the undefined mixed culture.

In summary, the work presented in this dissertation investigated functional protein expression in four different bacterial systems with varying levels of complexity, in order to answer four questions about biofilms: What protein expression makes them distinct from planktonic cultures? Which proteins are expressed when the biofilm performs a

function of interest? How is biofilm protein expression triggered under competitive stress? When during biofilm development does a function of interest emerge and who is responsible for it? We discovered evidence that protein expression is more diverse in biofilms compared with planktonic cultures and that it shifts toward catalytic activity at the expense of cell replication and motility. We showed that two biofilms of the same species with very different functionalities had overlap in protein expression that suggested answers to questions that could not be answered by conventional kinetic growth studies. We discovered protein expression in response to co-culture that was characteristic of a virulent biofilm phenotype, suggesting how the interactions between species may trigger biofilm formation. Finally, at the highest level of complexity, protein expression in an undefined mixed culture biofilm suggested specific interactions between consortium members and strategies to decrease reactor start-up time and resilience. Each of these studies revealed new discoveries about the functioning of cells in biofilms and provided suggestions about how to improve that biofilm biotechnology. Due to its capacity to provide this kind of useful information, proteomics should be considered an important tool for continuous improvement of biofilm biotechnologies, as they become more prevalent in bioenergy and bioproducts engineering.

CHAPTER 6 REFERENCES

Budnik B, Levy E, Slavov N. (2017) Mass-spectrometry of single mammalian cells quantifies proteome heterogeneity during cell differentiation. bioRxiv. doi: https://doi.org/10.1101/102681

Feist P, Hummon AB. (2015) Proteomic challenges: sample preparation techniques for microgram-quantity protein analysis from biological samples. Int J Mol Sci 16:3537-63.

Kiely PD, Rader G, Regan JM, Logan BE. (2011) Long-term cathode performance and the microbial communities that develop in microbial fuel cells fed different fermentation endproducts. Biores. Technol. 102:361-366.

Leary DH, Hervey WJ, Li RW, Deschamps JR, Kusterbeck AW, Vora GJ. (2012) Method Development for Metaproteomic Analyses of Marine Biofilms. Anal. Chem. 84:4006-4013.

Tanca A, Palomba A, Fraumene C, Pagnozzi D, Manghina V, Deligios M, Muth T, Rapp E, Martens L, Addis MF, Uzzau S. (2016) The impact of sequence database choice on metaproteomic results in gut microbiota studies. Microbiome 4:51 doi: 10.1186/s40168-016-0196-8

Taniguchi Y, Choi PJ, Li G-W, Chen H, Babu M, Hearn J, Emili A, Xie XS. (2010) Quantifying *E. coli* Proteome and Transcriptome with Single-Molecule Sensitivity in Single Cells. Science 329:533-538

APPENDICES

Chapter 2 Supplemental Information

SI 2.1 Supplemental Tables

Table S1: Statistical differences between precipitated and non-precipitated samples. *p*-Values from paired t-tests between precipitated and non-precipitated samples with respect to identification of different features by ESI-LC-MS/MS.

Feature Type	*p*-Value
Proteins	1.34E-08
Peptides	3.82E-12
Spectra	7.37E-11

Table S2: Summary of proteomic features for comparison of biofilm and planktonic cells. Feature identifications across precipitated sample types (ME: biofilm from microetched flow cell surface; E: planktonic control cultures).

Sample Type	Unique protein IDs (1% FDR)[1]	Unique peptide IDs (1% FDR)	Unique spectra IDs (1% FDR)
ME 1	837	8069	45257
ME 2	797	6103	35755
ME 3	772	7553	41929
E 1	768	7515	40468
E 2	787	7437	41756
E 3	762	7101	39229

[1]FDR abbreviates false discovery rate, as determined by ProteinPilot's decoy sequence analysis during protein identification.

Table S3: Complete list of proteins with p-value < 0.05 (Student's t-test) and $log_2FC > 1$ or < -1, when comparing ME biofilms and planktonic cultures. Values of "log_2FC" represent the ratio of ME biofilms ("ME") to planktonic (P) cultures with respect to transformed, normalized sum of intensity values for that protein.

Uniprot ID	Protein Name	p-value	log_2FC (ME/P)
F0HT97	Uncharacterized protein	0.002	5.46
F0HVT3	Organophosphate reductase (EC 1.1.1.218)	0.004	4.22
F0HWC0	Glycerol kinase (EC 2.7.1.30)	0.001	3.84
F0HVV4	Uncharacterized protein	0.040	3.78
F0HW47	Glutamine ABC superfamily ATP binding cassette transporter, ABC protein	0.040	3.68
F0HTI6	UPF0145 protein rpoB	0.040	3.43
F0HSW4	Phosphate ABC superfamily ATP binding cassette transporter, membrane protein	0.006	3.14
F0HXA9	CRP/FNR family transcriptional regulator	0.011	3.06
F0HY33	30S ribosomal protein S20	0.026	3.02
F0HU57	Penicillin-binding protein 2B (EC 2.3.2.-)	0.028	2.74
F0HV70	ATP-dependent DNA helicase (EC 3.6.1.-)	0.008	2.70
F0HU84	Transcriptional repressor NrdR	0.026	2.60

F0HTG4	Uncharacterized protein	0.022	2.57
F0HVV9	DNA starvation/stationary phase protection protein Dps	0.009	2.51
F0HWL3	Uncharacterized protein	0.002	2.47
F0HXN5	HPr kinase/phosphorylase (HPrK/P) (EC 2.7.11.-) (EC 2.7.4.-) (HPr(Ser) kinase/phosphorylase)	0.021	2.43
F0HX95	Glutamyl-tRNA(Gln) amidotransferase subunit A (Glu-ADT subunit A) (EC 6.3.5.7)	0.037	2.40
F0HV15	Integral membrane protein	0.011	2.28
F0HVY4	4-oxalocrotonate tautomerase (EC 5.3.2.-)	0.000	2.22
F0HYG8	Acetyl-coA carboxylase carboxyl transferase subunit alpha (EC 6.4.1.2)	0.024	2.21
F0HXK9	NAD kinase (EC 2.7.1.23) (ATP-dependent NAD kinase)	0.050	2.06
F0HYG1	Malonyl CoA-acyl carrier protein transacylase (EC 2.3.1.39)	0.013	2.04
F0HYA4	Pseudouridine synthase (EC 5.4.99.-)	0.007	2.02
F0HTT9	1-acylglycerol-3-phosphate O-acyltransferase (EC 2.3.1.51)	0.032	2.00

F0HTR3	Riboflavin biosynthesis protein RibF (EC 2.7.7.2)	0.010	1.95
F0HWL5	Phosphonate ABC superfamily ATP binding cassette transporter, binding protein	0.006	1.85
F0HXK0	Uncharacterized protein	0.043	1.66
F0HWS2	Bleomycin hydrolase (EC 3.4.22.40)	0.000	1.47
F0HXR9	Protein of hypothetical function DUF147	0.022	1.42
F0HU65	Membrane protein OxaA 2	0.042	1.39
F0HVW7	Group 2 glycosyl transferase (EC 2.4.1.-)	0.049	1.38
F0HUB3	Uncharacterized protein	0.047	1.38
F0HXE4	Glutamyl aminopeptidase (EC 3.4.11.7)	0.030	1.33
F0HV03	PTS family maltose porter EIICB component (EC 2.7.1.69)	0.005	1.28
F0HVL8	LemA family protein	0.000	1.24
F0HU63	TrmH family RNA methyltransferase	0.014	1.22
F0HTR1	Protein GrpE (HSP-70 cofactor)	0.000	1.20
F0HY81	3-oxoacyl-[acyl-carrier-protein] reductase (EC 1.1.1.100)	0.010	1.19

F0HWI6	UDP-N-acetylmuramyl-tripeptide synthetase (EC 6.3.2.-) (UDP-MurNAc-tripeptide synthetase)	0.006	1.18
F0HTQ9	Chaperone protein DnaJ	0.001	1.16
F0HX46	30S ribosomal protein S5	0.001	1.16
F0HXV8	UDP-N-acetylmuramoylalanyl-D-glutamate--2, 6-diaminopimelate ligase (EC 6.3.2.13)	0.010	1.15
F0HYH8	Excisionase family DNA binding domain protein	0.045	1.08
F0HUF2	Preprotein translocase	0.046	1.05
F0HU75	50S ribosomal protein L35	0.032	1.05
F0HT37	Adherence and virulence protein A	0.006	1.04
F0HWZ5	Cold-shock DEAD box protein A (EC 3.6.1.-)	0.042	1.03
F0HUY6	PTS family mannose porter, IID component (EC 2.7.1.69)	0.041	1.03
F0HWP1	Gfo/Idh/MocA family oxidoreductase (EC 1.-.-.-)	0.045	-1.01
F0HYF9	3-oxoacyl-[acyl-carrier-protein] synthase 3 (EC 2.3.1.180) (3-oxoacyl-[acyl-carrier-protein] synthase III) (Beta-ketoacyl-ACP synthase III)	0.017	-1.04

F0HXH9	APC family amino acid-polyamine-organocation transporter	0.026	-1.07
F0HTY5	Serine/threonine protein phosphatase 1 (EC 3.1.3.16)	0.025	-1.07
F0HVV5	Uncharacterized protein	0.046	-1.18
F0HUP2	ABC superfamily ATP binding cassette transporter, ABC protein (EC 3.6.3.-)	0.005	-1.20
F0HVS0	5-methyltetrahydropteroyltriglutamate--homocysteine S-methyltransferase (EC 2.1.1.14)	0.015	-1.20
F0HTB6	4-hydroxy-tetrahydrodipicolinate reductase (HTPA reductase) (EC 1.17.1.8)	0.040	-1.21
F0HW26	6-phosphogluconate dehydrogenase, decarboxylating (EC 1.1.1.44)	0.025	-1.21
F0HXJ0	Regulatory protein RecX	0.008	-1.23
F0HY37	Elongation factor Tu (EF-Tu)	0.028	-1.26
F0HY18	TPR repeat-containing protein	0.006	-1.28
F0HWW4	MutT/nudix family hydrolase	0.007	-1.30
F0HXT7	Zinc/manganese ABC superfamily ATP binding cassette transporter, binding protein	0.028	-1.34

F0HUK4	Deoxyxylulose-5-phosphate synthase (EC 2.2.1.7)	0.008	-1.37
F0HWT5	HicB family toxin-antitoxin system	0.009	-1.39
F0HUD3	Uncharacterized protein	0.017	-1.39
F0HXY0	Uncharacterized protein	0.020	-1.40
F0HUU3	Homoserine kinase (HK) (HSK) (EC 2.7.1.39)	0.024	-1.41
F0HXL7	Putative tRNA (cytidine(34)-2'-O)-methyltransferase (EC 2.1.1.207) (tRNA (cytidine/uridine-2'-O-)-methyltransferase)	0.040	-1.45
F0HWF9	FMN-binding protein	0.049	-1.50
F0HUE6	UPF0297 protein HMPREF5505_0543	0.038	-1.56
F0HX90	N-acetylmuramoyl-L-alanine amidase (EC 3.5.1.28)	0.003	-1.77
F0HXY9	HAD superfamily hydrolase	0.018	-1.93
F0HXD4	Mannitol-1-phosphate 5-dehydrogenase (EC 1.1.1.17)	0.024	-2.11
F0HWM8	MFS family major facilitator transporter	0.037	-2.29
F0HUU6	Uncharacterized protein	0.000	-2.31
F0HUQ4	Uncharacterized protein	0.028	-3.32

F0HTX7	50S ribosomal protein L28	0.001	-3.64

Table S4: Complete list of proteins with p-value < 0.05 (Student's t-test) and $\log_{1.5}$FC > 1 or < -1, when comparing ME biofilms and planktonic cultures. Values of "$\log_{1.5}$FC" represent the ratio of ME biofilms to planktonic cultures with respect to transformed, normalized intensity sums.

Uniprot ID	Protein Name	P-value	$\log_{1.5}$FC (ME/Plank)
F0HVT3	Organophosphate reductase (EC 1.1.1.218)	0.001	7.31
F0HT97	Uncharacterized protein	0.066	6.78
F0HWM6	N-6 adenine-specific DNA methylase YitW (EC 2.1.1.72)	0.043	6.62
F0HVV4	Uncharacterized protein	0.025	6.49
F0HT15	Uncharacterized protein	0.164	6.21
F0HSW6	Phosphate-specific transport system accessory protein PhoU	0.127	6.18
F0HX46	30S ribosomal protein S5	0.027	5.36
F0HW47	Glutamine ABC superfamily ATP binding cassette transporter, ABC protein	0.079	5.29
F0HUQ5	3-hydroxyacyl-[acyl-carrier-protein] dehydratase FabZ (EC 4.2.1.59) ((3R)-hydroxymyristoyl-[acyl-carrier-protein] dehydratase) (Beta-hydroxyacyl-ACP dehydratase)	0.238	5.24

F0HXW8	ATP synthase subunit alpha (EC 3.6.3.14) (ATP synthase F1 sector subunit alpha) (F-ATPase subunit alpha)	0.298	5.18
F0HX95	Glutamyl-tRNA(Gln) amidotransferase subunit A (Glu-ADT subunit A) (EC 6.3.5.7)	0.010	5.17
F0HWC0	Glycerol kinase (EC 2.7.1.30)	0.032	4.95
F0HTZ7	Exodeoxyribonuclease 7 small subunit (EC 3.1.11.6) (Exodeoxyribonuclease VII small subunit)	0.040	4.94
F0HUK3	50S ribosomal protein L33	0.017	4.70
F0HTK2	Endoribonuclease YbeY (EC 3.1.-.-)	0.125	4.67
F0HTI6	UPF0145 protein rpoB	0.042	4.55
F0HV12	Preprotein translocase subunit SecG	0.059	4.40
F0HY45	Oligopeptide ABC superfamily ATP binding cassette transporter, binding protein	0.046	4.24
F0HXN5	HPr kinase/phosphorylase (HPrK/P) (EC 2.7.11.-) (EC 2.7.4.-) (HPr(Ser) kinase/phosphorylase)	0.052	4.20
F0HUQ2	Aminopeptidase C (EC 3.4.22.40)	0.044	4.16
F0HX15	O-acetylhomoserine sulfhydrylase (EC 2.5.1.49)	0.269	4.16

F0HVV9	DNA starvation/stationary phase protection protein Dps	0.012	4.14
F0HVS9	Cob(I)yrinic acid a,c-diamide adenosyltransferase (EC 2.5.1.17)	0.068	4.10
F0HY38	Trigger factor (TF) (EC 5.2.1.8) (PPIase)	0.244	4.05
F0HU84	Transcriptional repressor NrdR	0.066	3.99
F0HVU5	Uncharacterized protein	0.241	3.87
F0HY66	Coenzyme A biosynthesis bifunctional protein CoaBC (EC 4.1.1.36) (EC 6.3.2.5)	0.096	3.85
F0HX92	DNA ligase (EC 6.5.1.2) (Polydeoxyribonucleotide synthase [NAD(+)])	0.186	3.81
F0HW97	Riboflavin synthase subunit alpha (EC 2.5.1.9)	0.154	3.76
F0HV70	ATP-dependent DNA helicase (EC 3.6.1.-)	0.037	3.76
F0HTL1	Diaminopimelate decarboxylase (DAP decarboxylase) (DAPDC) (EC 4.1.1.20)	0.064	3.76
F0HXY8	Tetrahydrofolate synthase (EC 6.3.2.17)	0.109	3.76
F0HY33	30S ribosomal protein S20	0.022	3.74
F0HTW6	UPF0122 protein HMPREF5505_0362	0.240	3.72
F0HX49	Protein translocase subunit SecY	0.046	3.71

F0HTS3	Ribosome-binding factor A	0.166	3.63
F0HWN0	Endopeptidase O (EC 3.4.24.-)	0.154	3.63
F0HYG1	Malonyl CoA-acyl carrier protein transacylase (EC 2.3.1.39)	0.017	3.61
F0HWQ1	Zinc finger domain protein	0.107	3.59
F0HU93	ABC superfamily ATP binding cassette transporter, ABC protein (EC 3.6.3.-)	0.193	3.58
F0HU57	Penicillin-binding protein 2B (EC 2.3.2.-)	0.044	3.58
F0HUC1	MOP superfamily multidrug/oligosaccharidyl-lipid/polysaccharide flippase transporter	0.024	3.57
F0HYG8	Acetyl-coA carboxylase carboxyl transferase subunit alpha (EC 6.4.1.2)	0.012	3.56
F0HXA9	CRP/FNR family transcriptional regulator	0.080	3.53
F0HVY4	4-oxalocrotonate tautomerase (EC 5.3.2.-)	0.001	3.50
F0HSW4	Phosphate ABC superfamily ATP binding cassette transporter, membrane protein	0.009	3.38
F0HUY8	PTS family mannose porter, IIAB component (EC 2.7.1.69)	0.174	3.36

F0HXW3	Uracil phosphoribosyltransferase (EC 2.4.2.9) (UMP pyrophosphorylase) (UPRTase)	0.098	3.36
F0HV37	Glutamine amidotransferase (EC 2.6.-.-)	0.235	3.32
F0HX47	50S ribosomal protein L30	0.164	3.19
F0HYI9	Putative pyruvate oxidase (EC 1.2.3.3) (Fragment)	0.270	3.19
F0HX16	Uncharacterized protein	0.047	3.15
F0HWB9	Glycerol kinase (EC 2.7.1.30)	0.277	3.15
F0HYA4	Pseudouridine synthase (EC 5.4.99.-)	0.038	3.14
F0HTW8	Signal recognition particle receptor FtsY (SRP receptor)	0.073	3.11
F0HVZ5	ABC superfamily ATP binding cassette transporter, permease protein	0.414	3.00
F0HTR3	Riboflavin biosynthesis protein RibF (EC 2.7.7.2)	0.020	2.98
F0HTU0	Aspartate-semialdehyde dehydrogenase (EC 1.2.1.11)	0.066	2.93
F0HXK9	NAD kinase (EC 2.7.1.23) (ATP-dependent NAD kinase)	0.025	2.91
F0HX37	50S ribosomal protein L29	0.204	2.90
F0HTI4	Triacylglycerol lipase (EC 3.1.1.3)	0.120	2.88

F0HYE9	GTP diphosphokinase (EC 2.7.6.5)	0.169	2.84
F0HXM1	Protease	0.222	2.82
F0HVL8	LemA family protein	0.028	2.81
F0HTQ9	Chaperone protein DnaJ	0.000	2.80
F0HWL5	Phosphonate ABC superfamily ATP binding cassette transporter, binding protein	0.020	2.74
F0HY65	Arginine repressor	0.184	2.71
F0HTT7	30S ribosomal protein S2	0.415	2.71
F0HW22	Membrane protein insertase YidC (Foldase YidC) (Membrane integrase YidC) (Membrane protein YidC)	0.358	2.62
F0HXK2	Phosphoenolpyruvate-protein phosphotransferase (EC 2.7.3.9) (Phosphotransferase system, enzyme I)	0.363	2.61
F0HYC0	Uncharacterized protein (Fragment)	0.462	2.58
F0HTT9	1-acylglycerol-3-phosphate O-acyltransferase (EC 2.3.1.51)	0.094	2.58
F0HWL3	Uncharacterized protein	0.038	2.57

F0HU09	Branched-chain amino acid ABC superfamily ATP binding cassette transporter, ABC protein (EC 3.6.3.-) (Fragment)	0.110	2.55
F0HXE4	Glutamyl aminopeptidase (EC 3.4.11.7)	0.036	2.55
F0HWK5	Sugar ABC superfamily ATP binding cassette transporter, ABC protein (EC 3.6.3.-)	0.064	2.55
F0HY50	Dihydrofolate reductase (EC 1.5.1.3)	0.216	2.53
F0HTY7	Methionyl-tRNA formyltransferase (EC 2.1.2.9)	0.162	2.48
F0HUB3	Uncharacterized protein	0.077	2.47
F0HWS2	Bleomycin hydrolase (EC 3.4.22.40)	0.001	2.44
F0HU65	Membrane protein OxaA 2	0.042	2.43
F0HVW7	Group 2 glycosyl transferase (EC 2.4.1.-)	0.071	2.42
F0HV15	Integral membrane protein	0.032	2.41
F0HT80	Phosphoglycerate mutase (EC 5.4.2.-)	0.163	2.36
F0HWZ5	Cold-shock DEAD box protein A (EC 3.6.1.-)	0.091	2.35
F0HTJ6	DNA primase (EC 2.7.7.-)	0.182	2.34
F0HWV6	HAD family hydrolase	0.332	2.28
F0HXR9	Protein of hypothetical function DUF147	0.045	2.27

F0HVJ7	Uncharacterized protein	0.135	2.25
F0HWS6	GMP reductase (EC 1.7.1.7) (Guanosine 5'-monophosphate oxidoreductase)	0.162	2.24
F0HUU4	Threonine synthase (EC 4.2.3.1)	0.027	2.23
F0HXV8	UDP-N-acetylmuramoylalanyl-D-glutamate--2, 6-diaminopimelate ligase (EC 6.3.2.13)	0.028	2.21
F0HUN4	Uncharacterized protein	0.467	2.20
F0HY23	Peptide deformylase (PDF) (EC 3.5.1.88) (Polypeptide deformylase)	0.182	2.20
F0HV03	PTS family maltose porter EIICB component (EC 2.7.1.69)	0.007	2.18
F0HVX7	ISCpe2 transposase	0.138	2.15
F0HTG4	Uncharacterized protein	0.014	2.15
F0HV39	Succinate-semialdehyde dehydrogenase (EC 1.2.1.16)	0.550	2.12
F0HWK6	Maltose ABC superfamily ATP binding cassette transporter, maltose-binding protein	0.027	2.10
F0HWM5	Anaerobic ribonucleoside-triphosphate reductase-activating protein (EC 1.97.1.-)	0.003	2.05

F0HY08	S4 domain protein	0.145	2.05
F0HWH7	Chromosome partitioning protein SpoOJ	0.121	2.05
F0HU63	TrmH family RNA methyltransferase	0.039	2.03
F0HY81	3-oxoacyl-[acyl-carrier-protein] reductase (EC 1.1.1.100)	0.012	2.02
F0HY15	Uncharacterized protein	0.092	2.02
F0HW09	DHH family phosphoesterase	0.371	1.97
F0HYE8	Ribosomal protein L11 methyltransferase (L11 Mtase) (EC 2.1.1.-)	0.134	1.96
F0HXH7	Ornithine decarboxylase (EC 4.1.1.17)	0.047	1.96
F0HTQ0	Permease	0.192	1.94
F0HUH7	tRNA-specific adenosine deaminase (EC 3.5.4.33)	0.320	1.93
F0HTB5	Aspartate transaminase (EC 2.6.1.1)	0.189	1.93
F0HUK1	Transcription termination/antitermination protein NusG	0.048	1.89
F0HUF2	Preprotein translocase	0.041	1.89
F0HX71	Regulatory protein	0.096	1.87
F0HUH3	Uncharacterized protein	0.297	1.87

F0HWZ2	UDP-N-acetylglucosamine 1-carboxyvinyltransferase (EC 2.5.1.7) (Enoylpyruvate transferase) (UDP-N-acetylglucosamine enolpyruvyl transferase)	0.220	1.86
F0HWV7	Large-conductance mechanosensitive channel	0.223	1.83
F0HXT2	Phosphotyrosine protein phosphatase (EC 3.1.3.48)	0.410	1.83
F0HWX8	P-type 2 magnesium transport ATPase (EC 3.6.3.2)	0.052	1.83
F0HY07	Uncharacterized protein	0.537	1.82
F0HY01	UDP-N-acetylmuramoylalanine--D-glutamate ligase (EC 6.3.2.9) (D-glutamic acid-adding enzyme) (UDP-N-acetylmuramoyl-L-alanyl-D-glutamate synthetase)	0.109	1.81
F0HUJ2	DNA-binding protein HU	0.369	1.81
F0HYF3	Aspartate--tRNA ligase (EC 6.1.1.12) (Aspartyl-tRNA synthetase)	0.014	1.81
F0HXK0	Uncharacterized protein	0.130	1.81
F0HXW9	ATP synthase gamma chain (ATP synthase F1 sector gamma subunit) (F-ATPase gamma subunit)	0.144	1.80
F0HW18	Chromosomal replication initiator protein DnaA	0.193	1.79

F0HVA1	Eps operon transcriptional regulator EpsIIA	0.044	1.78
F0HW88	D-alanine transfer protein DltB	0.046	1.78
F0HVN6	Ribosomal RNA large subunit methyltransferase H (EC 2.1.1.177) (23S rRNA (pseudouridine1915-N3)-methyltransferase) (23S rRNA m3Psi1915 methyltransferase) (rRNA (pseudouridine-N3-)-methyltransferase RlmH)	0.364	1.76
F0HTK4	30S ribosomal protein S21	0.101	1.73
F0HWI4	Response regulator	0.192	1.72
F0HX30	50S ribosomal protein L4	0.242	1.72
F0HY49	Thymidylate synthase (TS) (TSase) (EC 2.1.1.45)	0.373	1.69
F0HWR6	Oligopeptide ABC superfamily ATP binding cassette transporter, permease protein	0.104	1.67
F0HTL7	Aldose 1-epimerase (EC 5.1.3.3)	0.394	1.67
F0HWN4	Lipoprotein	0.205	1.67
F0HU05	50S ribosomal protein L21	0.080	1.66
F0HXS2	Hydrolase	0.312	1.65
F0HT37	Adherence and virulence protein A	0.021	1.65

F0HU60	Phenylalanine--tRNA ligase beta subunit (EC 6.1.1.20) (Phenylalanyl-tRNA synthetase beta subunit)	0.101	1.63
F0HVN7	Serine protease HtrA (EC 3.4.21.-)	0.025	1.63
F0HVH2	Uncharacterized protein	0.124	1.60
F0HYH8	Excisionase family DNA binding domain protein	0.053	1.60
F0HUQ0	DUTP diphosphatase (EC 3.6.1.23)	0.338	1.57
F0HVF8	Cell wall-associated hydrolase	0.397	1.56
F0HTP6	Glutamine ABC superfamily ATP binding cassette transporter, membrane protein	0.184	1.56
F0HWL9	Oligopeptide ABC superfamily ATP binding cassette transporter, binding protein	0.387	1.56
F0HWY9	Uncharacterized protein	0.213	1.54
F0HX51	Translation initiation factor IF-1	0.488	1.53
F0HU41	DegV family protein	0.013	1.53
F0HWI6	UDP-N-acetylmuramyl-tripeptide synthetase (EC 6.3.2.-) (UDP-MurNAc-tripeptide synthetase)	0.007	1.51
F0HT20	Uncharacterized protein	0.506	1.50
F0HTW0	50S ribosomal protein L19	0.278	1.50

F0HUF6	DNA mismatch repair protein HexB (Fragment)	0.178	1.48
F0HWH6	Sporulation initiation inhibitor protein Soj	0.337	1.48
F0HXF3	Exopolyphosphatase (EC 3.6.1.11)	0.166	1.48
F0HXT9	Probable transcriptional regulatory protein HMPREF5505_1736	0.550	1.48
F0HV47	Protease synthase and sporulation negative regulatory protein pai 1 (EC 2.3.1.-)	0.177	1.48
F0HWE3	Aminopeptidase N (EC 3.4.11.2)	0.010	1.47
F0HU99	Foldase protein PrsA (EC 5.2.1.8)	0.012	1.46
F0HWG9	NADPH-dependent FMN reductase domain protein (EC 1.1.1.-)	0.066	1.46
F0HXL8	Uncharacterized protein	0.656	1.44
F0HTW5	Signal recognition particle protein (Fifty-four homolog)	0.155	1.44
F0HU32	Xaa-Pro dipeptidyl-peptidase (EC 3.4.14.11) (X-Pro dipeptidyl-peptidase) (X-prolyl-dipeptidyl aminopeptidase)	0.612	1.44
F0HVB6	Trehalose operon transcriptional repressor	0.090	1.43
F0HTR1	Protein GrpE (HSP-70 cofactor)	0.008	1.42

F0HUY6	PTS family mannose porter, IID component (EC 2.7.1.69)	0.110	1.42
F0HX76	GntR family transcriptional regulator	0.545	1.42
F0HUE9	DHH family protein	0.191	1.41
F0HYH5	Aldehyde-alcohol dehydrogenase	0.002	1.40
F0HU98	Orotate phosphoribosyltransferase (OPRT) (OPRTase) (EC 2.4.2.10)	0.203	1.39
F0HWH4	Ribosomal RNA small subunit methyltransferase G (EC 2.1.1.-) (16S rRNA 7-methylguanosine methyltransferase)	0.306	1.39
F0HWV2	Homocysteine S-methyltransferase (EC 2.1.1.10)	0.045	1.39
F0HXJ9	ATP-dependent Clp protease	0.229	1.38
F0HU19	Adenylosuccinate lyase (ASL) (EC 4.3.2.2) (Adenylosuccinase)	0.188	1.38
F0HWK8	Maltose/maltodextrin ABC superfamily ATP binding cassette transporter, permease protein	0.187	1.38
F0HVD7	Uncharacterized protein (Fragment)	0.159	1.37
F0HU07	Cystathionine beta-lyase (EC 4.4.1.8)	0.565	1.36

F0HU97	Orotidine 5'-phosphate decarboxylase (EC 4.1.1.23) (OMP decarboxylase)	0.511	1.35
F0HV11	Ribonuclease R (RNase R) (EC 3.1.13.1)	0.506	1.34
F0HTT3	Isoprenyl transferase (EC 2.5.1.-)	0.301	1.33
F0HVT6	Exodeoxyribonuclease III (EC 3.1.11.2)	0.420	1.32
F0HYG7	Acetyl-coenzyme A carboxylase carboxyl transferase subunit beta (ACCase subunit beta) (Acetyl-CoA carboxylase carboxyltransferase subunit beta) (EC 6.4.1.2)	0.286	1.32
F0HXY4	Probable tRNA sulfurtransferase (EC 2.8.1.4) (Sulfur carrier protein ThiS sulfurtransferase) (Thiamine biosynthesis protein ThiI) (tRNA 4-thiouridine synthase)	0.349	1.31
F0HX57	Energy-coupling factor transporter ATP-binding protein EcfA (ECF transporter A component EcfA) (EC 3.6.3.-)	0.483	1.31
F0HUJ5	50S ribosomal protein L10	0.090	1.30
F0HW07	Replicative DNA helicase DnaB (EC 3.6.1.-)	0.065	1.29
F0HWS4	Transcription elongation factor GreA (Transcript cleavage factor GreA)	0.006	1.27

F0HX04	tRNA(Ile)-lysidine synthase (EC 6.3.4.19) (tRNA(Ile)-2-lysyl-cytidine synthase) (tRNA(Ile)-lysidine synthetase)	0.579	1.26
F0HWY6	Uncharacterized protein	0.415	1.25
F0HXS1	Phosphoglucosamine mutase (EC 5.4.2.10)	0.484	1.25
F0HXQ9	Hydrolase	0.102	1.25
F0HWD5	Fumarate hydratase class II (Fumarase C) (EC 4.2.1.2)	0.104	1.24
F0HY54	Methionine import ATP-binding protein MetN (EC 3.6.3.-)	0.659	1.23
F0HYB3	Transcriptional regulator	0.480	1.23
F0HY92	Glutamate 5-kinase (EC 2.7.2.11) (Gamma-glutamyl kinase)	0.435	1.23
F0HWI3	Multidrug resistance ABC superfamily ATP binding cassette transporter, membrane protein	0.068	1.18
F0HT47	Phosphoserine aminotransferase (EC 2.6.1.52) (Phosphohydroxythreonine aminotransferase)	0.239	1.16
F0HX83	NH(3)-dependent NAD(+) synthetase (EC 6.3.1.5)	0.090	1.15

F0HXQ6	Triosephosphate isomerase (TIM) (EC 5.3.1.1) (Triose-phosphate isomerase)	0.326	1.15
F0HVB4	Uncharacterized protein	0.170	1.14
F0HWM2	Asparagine synthetase (EC 6.3.5.4)	0.303	1.13
F0HUR7	Dipeptidase PepV (EC 3.4.13.-)	0.150	1.13
F0HU52	Rhodanese family protein	0.543	1.11
F0HU76	Translation initiation factor IF-3	0.102	1.10
F0HYG3	3-oxoacyl-[acyl-carrier-protein] synthase 2 (EC 2.3.1.179)	0.282	1.09
F0HXY3	Cysteine desulfurase (EC 4.4.1.-)	0.577	1.08
F0HYD7	Uncharacterized protein	0.234	1.06
F0HTT1	Peptidase (EC 3.4.24.-)	0.332	1.05
F0HX06	33 kDa chaperonin (Heat shock protein 33 homolog)	0.559	1.03
F0HX26	30S ribosomal protein S7	0.002	1.03
F0HVT1	Uncharacterized protein	0.045	1.02
F0HTZ0	Guanylate kinase (EC 2.7.4.8) (GMP kinase)	0.477	1.02
F0HWP9	Tyrosine--tRNA ligase (EC 6.1.1.1) (Tyrosyl-tRNA synthetase)	0.385	1.00

F0HWA7	Hydrolase	0.297	1.00
F0HW81	P-ATPase superfamily P-type ATPase cadmium transporter (EC 3.6.3.4)	0.175	-1.01
F0HY48	D-lactate dehydrogenase (EC 1.1.1.28)	0.301	-1.01
F0HVP2	DNA-binding response regulator	0.125	-1.02
F0HWR0	Oligopeptide ABC superfamily ATP binding cassette transporter, binding protein	0.226	-1.02
F0HY20	Pyridine nucleotide-disulfide oxidoreductase (EC 1.8.1.-)	0.395	-1.02
F0HVG7	SagA protein	0.132	-1.02
F0HW66	ABC superfamily ATP binding cassette transporter, binding protein	0.185	-1.02
F0HTU5	Multidrug ABC superfamily ATP binding cassette transporter, ABC protein (EC 3.6.3.44)	0.009	-1.03
F0HUE2	Thioredoxin	0.011	-1.03
F0HVG9	Uncharacterized protein	0.464	-1.03
F0HWU9	ATP-grasp superfamily protein	0.187	-1.03
F0HWZ9	Peptidyl-tRNA hydrolase (PTH) (EC 3.1.1.29)	0.034	-1.04
F0HV16	Glycosyl transferase CpoA (EC 2.4.1.-)	0.056	-1.05

F0HTD3	LD-carboxypeptidase	0.516	-1.06
F0HT24	Penicillin-binding protein 1A (EC 2.4.1.-) (EC 3.4.-.-)	0.297	-1.07
F0HW08	50S ribosomal protein L9	0.060	-1.08
F0HUC2	Leucine--tRNA ligase (EC 6.1.1.4) (Leucyl-tRNA synthetase)	0.083	-1.08
F0HX64	Oligopeptide ABC superfamily ATP binding cassette transporter, binding protein	0.025	-1.09
F0HUE1	Uncharacterized protein	0.672	-1.09
F0HUG0	Redox-sensing transcriptional repressor Rex	0.198	-1.09
F0HUF7	DNA mismatch repair protein MutS	0.532	-1.11
F0HUH6	DNA polymerase III, gamma/tau subunit DnaX (EC 2.7.7.7)	0.430	-1.12
F0HWI7	Aspartate racemase (EC 5.1.1.13)	0.090	-1.13
F0HW77	ABC superfamily ATP binding cassette transporter, binding protein	0.575	-1.13
F0HTJ8	Glycine--tRNA ligase alpha subunit (EC 6.1.1.14) (Glycyl-tRNA synthetase alpha subunit)	0.160	-1.13
F0HYB1	Tetratricopeptide repeat family protein	0.087	-1.14

F0HWJ0	Tagatose-6-phosphate kinase (EC 2.7.1.144)	0.572	-1.15
F0HTU6	Uncharacterized protein	0.641	-1.16
F0HY24	Glutathione-disulfide reductase (EC 1.8.1.7)	0.139	-1.17
F0HT48	Phosphoglycerate mutase (EC 5.4.2.-)	0.250	-1.17
F0HUC6	S-adenosylmethionine synthase (AdoMet synthase) (EC 2.5.1.6) (MAT) (Methionine adenosyltransferase)	0.458	-1.18
F0HY13	5'-methylthioadenosine/S-adenosylhomocysteine nucleosidase 1 (EC 3.2.2.9) (5'-methylthioadenosine/S-adenosylhomocysteine nucleosidase) (5'-methylthioadenosine/S-adenosylhomocysteine nucleosidase 2)	0.372	-1.19
F0HTS9	DNA polymerase III PolC-type (PolIII) (EC 2.7.7.7)	0.064	-1.19
F0HUH2	Thymidylate kinase (EC 2.7.4.9) (dTMP kinase)	0.419	-1.20
F0HTI3	Uncharacterized protein	0.331	-1.21
F0HX05	ATP-dependent zinc metalloprotease FtsH (EC 3.4.24.-)	0.445	-1.21

F0HW57	Glucosamine-6-phosphate deaminase (EC 3.5.99.6) (GlcN6P deaminase) (Glucosamine-6-phosphate isomerase)	0.215	-1.21
F0HY16	tRNA-specific 2-thiouridylase MnmA (EC 2.8.1.-)	0.133	-1.23
F0HVV0	Uncharacterized protein	0.070	-1.24
F0HWI0	Uncharacterized protein	0.029	-1.24
F0HX11	Lysine--tRNA ligase (EC 6.1.1.6) (Lysyl-tRNA synthetase)	0.119	-1.24
F0HXK4	Adaptor protein	0.339	-1.25
F0HX34	50S ribosomal protein L22	0.122	-1.28
F0HTN8	Transcriptional regulator	0.223	-1.30
F0HX03	RNA-binding protein	0.295	-1.30
F0HWZ8	CBS domain protein	0.269	-1.32
F0HUM6	Uncharacterized protein	0.740	-1.33
F0HXG2	Ribose-5-phosphate isomerase A (EC 5.3.1.6) (Phosphoriboisomerase A)	0.066	-1.33
F0HTF9	GPH family glycoside-pentoside-hexuronide:cation symporter	0.544	-1.34
F0HWM3	ATP-grasp superfamily protein	0.496	-1.34

F0HXH1	ATP-dependent RNA helicase	0.374	-1.35
F0HTU7	UPF0291 protein HMPREF5505_0343	0.314	-1.36
F0HX97	Diacylglycerol kinase catalytic domain protein (EC 2.7.1.107)	0.462	-1.37
F0HUJ8	Glycosyltransferase (EC 2.4.1.-)	0.643	-1.37
F0HVC2	Methionine-R-sulfoxide reductase (EC 1.8.4.-)	0.158	-1.37
F0HU02	Elongation factor P (EF-P)	0.480	-1.37
F0HTP5	Glutamine ABC superfamily ATP binding cassette transporter, ABC protein	0.013	-1.38
F0HUV0	6-phosphofructokinase (EC 2.7.1.11)	0.358	-1.39
F0HY43	Nitroreductase	0.316	-1.39
F0HXI1	UDP-N-acetylglucosamine 2-epimerase (EC 5.1.3.14)	0.160	-1.40
F0HT27	Cell cycle protein GpsB	0.216	-1.41
F0HXQ5	Phosphoglycerate kinase (EC 2.7.2.3)	0.150	-1.43
F0HXK8	GTP diphosphokinase (EC 2.7.6.5)	0.140	-1.44
F0HUG9	Initiation-control protein YabA	0.393	-1.44
F0HUC8	DedA family membrane protein	0.555	-1.45

F0HUY7	PTS family mannose porter, IIC component (EC 2.7.1.69)	0.047	-1.45
F0HX40	50S ribosomal protein L24	0.095	-1.46
F0HWI2	ABC superfamily ATP binding cassette transporter	0.001	-1.50
F0HYA9	GTPase Der (GTP-binding protein EngA)	0.094	-1.50
F0HY51	E1-E2 family cation-transporting ATPase (EC 3.6.3.-)	0.458	-1.50
F0HU81	Threonine--tRNA ligase (EC 6.1.1.3) (Threonyl-tRNA synthetase)	0.024	-1.50
F0HY04	Cell division protein ftsA	0.018	-1.51
F0HTE1	Glyceraldehyde-3-phosphate dehydrogenase (EC 1.2.1.12)	0.313	-1.52
F0HYF9	3-oxoacyl-[acyl-carrier-protein] synthase 3 (EC 2.3.1.180) (3-oxoacyl-[acyl-carrier-protein] synthase III) (Beta-ketoacyl-ACP synthase III)	0.035	-1.52
F0HXW6	ATP synthase subunit b (ATP synthase F(0) sector subunit b) (ATPase subunit I) (F-type ATPase subunit b)	0.088	-1.53
F0HUH8	Methyltransferase domain protein	0.224	-1.53

F0HXL2	Undecaprenyl-diphosphatase (EC 3.6.1.27) (Bacitracin resistance protein) (Undecaprenyl pyrophosphate phosphatase)	0.066	-1.53
F0HT11	Mevalonate kinase (EC 2.7.1.36)	0.023	-1.54
F0HU55	5-formyltetrahydrofolate cyclo-ligase (EC 6.3.3.2)	0.277	-1.55
F0HUD4	Catabolite control protein A	0.122	-1.56
F0HT17	DNA replication protein DnaD	0.047	-1.58
F0HWB8	Adenosylcobyric acid synthase (EC 6.3.5.10)	0.240	-1.59
F0HXD3	PTS system, mannitol-specific IIA component (EC 2.7.1.69)	0.056	-1.59
F0HVV5	Uncharacterized protein	0.135	-1.60
F0HX28	30S ribosomal protein S10	0.018	-1.60
F0HTI9	PTS family protein, cellobiose-specific IIA component (EC 2.7.1.69)	0.042	-1.60
F0HYB9	Uncharacterized protein	0.185	-1.60
F0HXP0	UvrABC system protein A (UvrA protein) (Excinuclease ABC subunit A)	0.239	-1.61
F0HTS8	Ribosome maturation factor RimP	0.227	-1.61
F0HUH9	Bifunctional protein PyrR	0.375	-1.63

F0HV00	PTS family glucose porter, IIA component (EC 2.7.1.69)	0.169	-1.65
F0HUE5	Putative Holliday junction resolvase (EC 3.1.-.-)	0.150	-1.67
F0HU04	50S ribosomal protein L27	0.206	-1.68
F0HV66	Uncharacterized protein	0.020	-1.69
F0HTS6	Cytosolic protein YlxR	0.297	-1.71
F0HUH1	Protein of hypothetical function DUF970	0.181	-1.71
F0HTD4	tRNA/rRNA methyltransferase	0.216	-1.72
F0HSX1	NUDIX family hydrolase	0.082	-1.73
F0HTF6	Asparagine--tRNA ligase (EC 6.1.1.22) (Fragment)	0.102	-1.74
F0HXI9	23S rRNA (Uracil-5-)-methyltransferase (EC 2.1.1.-)	0.105	-1.74
F0HWE9	Secreted protein	0.382	-1.74
F0HV99	Undecaprenyl-phosphate galactose phosphotransferase (EC 2.7.8.6)	0.546	-1.74
F0HX48	50S ribosomal protein L15	0.520	-1.75
F0HWF9	FMN-binding protein	0.129	-1.77
F0HVC4	dTDP-4-dehydrorhamnose reductase (EC 1.1.1.133)	0.039	-1.80

F0HWW1	Uncharacterized protein	0.099	-1.82
F0HXC1	LIVCS family branched chain amino acid:cation symporter	0.126	-1.83
F0HWZ6	Holo-[acyl-carrier-protein] synthase (Holo-ACP synthase) (EC 2.7.8.7) (4'-phosphopantetheinyl transferase AcpS)	0.007	-1.83
F0HWY5	Bifunctional protein GlmU	0.206	-1.84
F0HXJ8	Uncharacterized protein	0.066	-1.84
F0HWE1	LysM domain protein	0.137	-1.85
F0HXW1	Protoporphyrinogen oxidase (EC 1.3.3.4)	0.221	-1.86
F0HX36	50S ribosomal protein L16	0.382	-1.89
F0HVS7	Lactate dehydrogenase (Oxidoreductase)	0.096	-1.89
F0HTZ6	Farnesyltranstransferase (EC 2.5.1.29)	0.084	-1.90
F0HU03	X-Pro dipeptidase PepP (EC 3.4.11.9)	0.509	-1.92
F0HX81	Glycosyltransferase group 1 protein (EC 2.4.1.-)	0.195	-1.92
F0HU71	HD domain protein	0.054	-1.92
F0HW06	Uncharacterized protein	0.005	-1.93
F0HVZ2	GNAT family acetyltransferase	0.038	-1.93

F0HUH4	Recombination protein RecR	0.258	-1.94
F0HUU9	PTS family sucrose porter, EIIBC component ScrA (EC 2.7.1.69)	0.340	-1.94
F0HXM2	3-oxoacyl-[acyl-carrier-protein] reductase (EC 1.1.1.100)	0.072	-1.95
F0HWZ3	50S ribosomal protein L31 type B	0.296	-1.96
F0HTW9	Chromosome partition protein Smc	0.129	-1.96
F0HTY6	Ribosomal RNA small subunit methyltransferase B	0.173	-1.96
F0HXL3	Uncharacterized protein	0.035	-1.97
F0HVP8	YbfG like protein	0.258	-1.97
F0HTY5	Serine/threonine protein phosphatase 1 (EC 3.1.3.16)	0.016	-1.99
F0HXW7	ATP synthase subunit delta (ATP synthase F(1) sector subunit delta) (F-type ATPase subunit delta)	0.200	-2.00
F0HWL4	Universal stress protein UspA	0.244	-2.00
F0HUF9	10 kDa chaperonin (GroES protein) (Protein Cpn10)	0.096	-2.02
F0HY18	TPR repeat-containing protein	0.059	-2.03

F0HW64	ABC superfamily, ATP binding cassette transporter, membrane protein	0.050	-2.04
F0HX33	30S ribosomal protein S19	0.147	-2.04
F0HUG2	ABC superfamily ATP binding cassette transporter, ABC protein (EC 3.6.3.-)	0.049	-2.05
F0HWP1	Gfo/Idh/MocA family oxidoreductase (EC 1.-.-.-)	0.016	-2.05
F0HVA8	Glycerol-3-phosphate dehydrogenase [NAD(P)+] (EC 1.1.1.94) (NAD(P)H-dependent glycerol-3-phosphate dehydrogenase)	0.256	-2.06
F0HXK3	Regulatory protein Spx	0.241	-2.06
F0HTT4	Ribosome-recycling factor (RRF) (Ribosome-releasing factor)	0.269	-2.07
F0HXD2	PTS family mannitol porter, EIICB component (EC 2.7.1.69)	0.144	-2.08
F0HXA8	Uncharacterized protein	0.188	-2.08
F0HWT5	HicB family toxin-antitoxin system	0.043	-2.09
F0HXH9	APC family amino acid-polyamine-organocation transporter	0.080	-2.09

F0HW26	6-phosphogluconate dehydrogenase, decarboxylating (EC 1.1.1.44)	0.017	-2.14
F0HYA3	Segregation and condensation protein B	0.194	-2.15
F0HVF2	Exopolysaccharide biosynthesis protein	0.112	-2.16
F0HUG8	Tetrapyrrole methylase	0.084	-2.20
F0HTJ5	RNA polymerase sigma factor SigA	0.293	-2.22
F0HX45	50S ribosomal protein L18	0.307	-2.22
F0HTB6	4-hydroxy-tetrahydrodipicolinate reductase (HTPA reductase) (EC 1.17.1.8)	0.043	-2.24
F0HUD3	Uncharacterized protein	0.112	-2.25
F0HWV8	Nicotinate phosphoribosyltransferase (EC 6.3.4.21)	0.031	-2.26
F0HW48	Glutamine ABC superfamily ATP binding cassette transporter, membrane protein	0.314	-2.28
F0HTN0	YitT family protein	0.108	-2.29
F0HUP2	ABC superfamily ATP binding cassette transporter, ABC protein (EC 3.6.3.-)	0.015	-2.30
F0HY90	Pyrroline-5-carboxylate reductase (EC 1.5.1.2)	0.084	-2.34
F0HU85	Dephospho-CoA kinase (EC 2.7.1.24) (Dephosphocoenzyme A kinase)	0.104	-2.34

F0HXM4	CDP-diacylglycerol-glycerol-3-phosphate 3-phosphatidyltransferase (EC 2.7.8.5)	0.063	-2.36
F0HX39	50S ribosomal protein L14	0.169	-2.36
F0HVM9	Pyridoxamine 5'-phosphate oxidase (EC 1.4.3.5)	0.061	-2.39
F0HUL8	Glutamate--tRNA ligase (EC 6.1.1.17) (Glutamyl-tRNA synthetase)	0.232	-2.39
F0HVS0	5-methyltetrahydropteroyltriglutamate--homocysteine S-methyltransferase (EC 2.1.1.14)	0.006	-2.41
F0HV45	MIT family metal ion transporter CorA	0.009	-2.43
F0HV64	Lipase	0.053	-2.43
F0HTS5	50S ribosomal protein L7/L12	0.282	-2.46
F0HXA7	MerTP family mercury (Hg2+) permease, binding protein MerP	0.140	-2.53
F0HX98	Uncharacterized protein	0.415	-2.54
F0HUY1	Dipeptidyl-peptidase (EC 3.4.-.-)	0.259	-2.54
F0HW98	Riboflavin biosynthesis protein RibBA	0.234	-2.56
F0HWY2	Ribosomal RNA small subunit methyltransferase A (EC 2.1.1.182) (16S rRNA (adenine(1518)-N(6)/adenine(1519)-N(6))-dimethyltransferase)	0.011	-2.57

	(16S rRNA dimethyladenosine transferase) (16S rRNA dimethylase) (S-adenosylmethionine-6-N', N'-adenosyl(rRNA) dimethyltransferase)		
F0HW92	Uncharacterized protein	0.034	-2.58
F0HXU6	Site-specific DNA-methyltransferase (Adenine-specific)	0.170	-2.58
F0HXD7	ABC superfamily ATP binding cassette transporter, ABC protein (EC 3.6.3.-)	0.197	-2.60
F0HV60	Proline iminopeptidase (PIP) (EC 3.4.11.5) (Prolyl aminopeptidase)	0.073	-2.62
F0HWJ1	PTS system, fructose-specific enzyme IIABC component (EC 2.7.1.69)	0.184	-2.70
F0HTC5	Glutathione-disulfide reductase (EC 1.8.1.7)	0.146	-2.70
F0HU54	S54 family peptidase	0.227	-2.77
F0HXY1	30S ribosomal protein S4	0.117	-2.83
F0HX54	DNA-directed RNA polymerase subunit alpha (RNAP subunit alpha) (EC 2.7.7.6) (RNA polymerase subunit alpha) (Transcriptase subunit alpha)	0.126	-2.89

F0HVP9	Bacitracin transport ATP binding cassette transporter, ABC protein	0.048	-3.00
F0HTV1	Uncharacterized protein	0.172	-3.01
F0HVT4	L-2-hydroxyisocaproate dehydrogenase (EC 1.1.1.-)	0.138	-3.01
F0HTX8	Multidrug ABC superfamily ATP binding cassette transporter, ATPase and permease protein	0.173	-3.02
F0HVL4	Uncharacterized protein	0.031	-3.04
F0HXD4	Mannitol-1-phosphate 5-dehydrogenase (EC 1.1.1.17)	0.051	-3.09
F0HW99	6,7-dimethyl-8-ribityllumazine synthase (DMRL synthase) (LS) (Lumazine synthase) (EC 2.5.1.78)	0.024	-3.12
F0HV21	Arginine deiminase (ADI) (EC 3.5.3.6) (Arginine dihydrolase)	0.233	-3.12
F0HVC9	MIP family glycerol uptake facilitator protein GlpF	0.221	-3.19
F0HWM8	MFS family major facilitator transporter	0.100	-3.21
F0HUK4	Deoxyxylulose-5-phosphate synthase (EC 2.2.1.7)	0.047	-3.22
F0HWE7	Copper-exporting ATPase (EC 3.6.3.4)	0.143	-3.26
F0HV48	Uncharacterized protein	0.028	-3.26

F0HXY0	Uncharacterized protein	0.036	-3.32
F0HT06	DNA topoisomerase 4 subunit A (EC 5.99.1.3) (Topoisomerase IV subunit A)	0.084	-3.33
F0HY87	UPF0340 protein ywlG	0.135	-3.35
F0HXW2	Threonylcarbamoyl-AMP synthase (TC-AMP synthase) (EC 2.7.7.87) (L-threonylcarbamoyladenylate synthase)	0.222	-3.36
F0HTB9	2,3,4,5-tetrahydropyridine-2,6-dicarboxylate N-acetyltransferase (EC 2.3.1.89) (Tetrahydrodipicolinate N-acetyltransferase)	0.097	-3.38
F0HUU2	Aggregation promoting factor	0.048	-3.39
F0HUB5	D-alanyl-D-alanine carboxypeptidase DacA (EC 3.4.16.4)	0.033	-3.40
F0HU06	ArsC family protein (EC 1.20.4.1)	0.103	-3.43
F0HX90	N-acetylmuramoyl-L-alanine amidase (EC 3.5.1.28)	0.007	-3.49
F0HXT7	Zinc/manganese ABC superfamily ATP binding cassette transporter, binding protein	0.035	-3.53
F0HTI7	Permease IIC component	0.104	-3.60

F0HT21	Uncharacterized protein	0.254	-3.69
F0HX52	30S ribosomal protein S13	0.007	-3.74
F0HVJ0	LacI family transcriptional regulator	0.129	-3.74
F0HXY9	HAD superfamily hydrolase	0.012	-3.76
F0HWT2	Inosine-5'-monophosphate dehydrogenase (IMP dehydrogenase) (IMPD) (IMPDH) (EC 1.1.1.205)	0.034	-3.77
F0HWL1	Nucleoside deoxyribosyltransferase (EC 2.4.2.6)	0.079	-3.80
F0HX27	Elongation factor G (EF-G)	0.366	-3.80
F0HVX1	MIP family glycerol uptake facilitator protein GlpF	0.132	-3.87
F0HUU3	Homoserine kinase (HK) (HSK) (EC 2.7.1.39)	0.025	-3.90
F0HU72	Probable nicotinate-nucleotide adenylyltransferase (EC 2.7.7.18) (Deamido-NAD(+) diphosphorylase) (Deamido-NAD(+) pyrophosphorylase) (Nicotinate mononucleotide adenylyltransferase)	0.041	-3.98
F0HXL7	Putative tRNA (cytidine(34)-2'-O)-methyltransferase (EC 2.1.1.207) (tRNA (cytidine/uridine-2'-O-)-methyltransferase)	0.023	-3.98
F0HUM2	Oligopeptide ABC superfamily ATP binding cassette transporter, binding protein	0.157	-4.06

F0HWW4	MutT/nudix family hydrolase	0.034	-4.17
F0HT30	Formate--tetrahydrofolate ligase (EC 6.3.4.3) (Formyltetrahydrofolate synthetase)	0.050	-4.19
F0HXF0	Glutamine ABC superfamily ATP binding cassette transporter, permease protein	0.011	-4.20
F0HX80	UDP-N-acetyl-D-mannosamine transferase (EC 2.4.1.187) (Fragment)	0.355	-4.28
F0HUF3	Holliday junction ATP-dependent DNA helicase RuvB (EC 3.6.4.12)	0.086	-4.28
F0HUB6	Pyruvate oxidase (EC 1.2.3.3) (Fragment)	0.025	-4.28
F0HWD6	DASS family divalent anion:sodium (Na+) symporter	0.055	-4.29
F0HTX7	50S ribosomal protein L28	0.243	-4.38
F0HUM5	Putative biotin carboxylase	0.157	-4.39
F0HUE6	UPF0297 protein HMPREF5505_0543	0.000	-4.40
F0HTV0	Glutamine ABC superfamily ATP binding cassette transporter, binding protein	0.091	-4.50
F0HXJ0	Regulatory protein RecX	0.001	-4.74

F0HUU6	Uncharacterized protein	0.005	-4.75
F0HY37	Elongation factor Tu (EF-Tu)	0.092	-4.85
F0HXV9	Thymidine kinase (EC 2.7.1.21)	0.041	-5.37
F0HUQ4	Uncharacterized protein	0.070	-5.41
F0HXC8	Transcriptional regulator	0.051	-5.71
F0HVF5	Cell wall-associated hydrolase	0.059	-7.42
F0HWN9	Amidase	0.125	-7.58

Table S5: Complete, quantitative Pearson's r coefficient values corresponding to those visualized pictorially in Figure 1 of the main text, for pairwise correlations of protein abundance between each LC-MS/MS sample. As in Figure 1 in the text, "B" refers to samples of biofilms grown on micro-etched surfaces, while "P" refers to planktonic culture samples. Both technical replicates are shown, i.e., "B1" refers to the first technical replicate LC-MS/MS run of the first biological replicate biofilm sample, while "B11" refers to the second technical replicate run of that biofilm, etc.

	B1	B11	B2	B22	B3	B33	P1	P11	P2	P22	E3	E33
B1	1.00	0.55	0.66	0.95	0.54	0.62	0.70	0.77	0.79	0.54	0.64	0.79
B11	0.55	1.00	0.85	0.63	0.94	0.87	0.86	0.78	0.72	0.80	0.82	0.72
B2	0.66	0.85	1.00	0.74	0.80	0.95	0.93	0.92	0.86	0.89	0.95	0.89
B22	0.95	0.63	0.74	1.00	0.58	0.71	0.80	0.82	0.82	0.60	0.74	0.84

B3	0.54	0.94	0.80	0.58	1.00	0.84	0.81	0.75	0.67	0.80	0.80	0.68
B33	0.62	0.87	0.95	0.71	0.84	1.00	0.94	0.92	0.87	0.92	0.96	0.87
P1	0.70	0.86	0.93	0.80	0.81	0.94	1.00	0.95	0.87	0.85	0.94	0.91
P11	0.77	0.78	0.92	0.82	0.75	0.92	0.95	1.00	0.93	0.87	0.95	0.95
P2	0.79	0.72	0.86	0.82	0.67	0.87	0.87	0.93	1.00	0.84	0.88	0.96
P22	0.54	0.80	0.89	0.60	0.80	0.92	0.85	0.87	0.84	1.00	0.92	0.82
P3	0.64	0.82	0.95	0.74	0.80	0.96	0.94	0.95	0.88	0.92	1.00	0.91
P33	0.79	0.72	0.89	0.84	0.68	0.87	0.91	0.95	0.96	0.82	0.91	1.00

Table S6: Complete list of significantly enriched GO categories (Fisher's exact test, $p < 0.05$) among proteins differentially more abundant in ME biofilms compared to the set of remaining proteins. "#Seq" is the number of sequences associated with an enzyme (from Blast2GO).

GO Name	GO ID	GO Category	p-Value	#Seq (ME Biofilm)	#Seq (Remaining)
anion transmembrane transport	GO:0098656	BIOLOGICAL_PROCESS	0.041	2	5

response to temperature stimulus	GO:0009266	BIOLOGICAL_PROCESS	0.049	1	0
response to heat	GO:0009408	BIOLOGICAL_PROCESS	0.049	1	0
response to abiotic stimulus	GO:0009628	BIOLOGICAL_PROCESS	0.049	1	0
regulation of catalytic activity	GO:0050790	BIOLOGICAL_PROCESS	0.049	1	0
regulation of molecular function	GO:0065009	BIOLOGICAL_PROCESS	0.049	1	0
FAD biosynthetic process	GO:0006747	BIOLOGICAL_PROCESS	0.049	1	0
FMN biosynthetic process	GO:0009398	BIOLOGICAL_PROCESS	0.049	1	0

flavin adenine dinucleotide biosynthetic process	GO:0072388	BIOLOGICAL_PROCESS	0.049	1	0
flavin adenine dinucleotide metabolic process	GO:0072387	BIOLOGICAL_PROCESS	0.049	1	0
FAD metabolic process	GO:0046443	BIOLOGICAL_PROCESS	0.049	1	0
FMN metabolic process	GO:0046444	BIOLOGICAL_PROCESS	0.049	1	0
cellular iron ion homeostasis	GO:0006879	BIOLOGICAL_PROCESS	0.049	1	0
cellular metal ion homeostasis	GO:0006875	BIOLOGICAL_PROCESS	0.049	1	0

cellular transition metal ion homeostasis	GO:0046916	BIOLOGICAL_PROCESS	0.049	1	0
cellular cation homeostasis	GO:0030003	BIOLOGICAL_PROCESS	0.049	1	0
metal ion homeostasis	GO:0055065	BIOLOGICAL_PROCESS	0.049	1	0
iron ion homeostasis	GO:0055072	BIOLOGICAL_PROCESS	0.049	1	0
transition metal ion homeostasis	GO:0055076	BIOLOGICAL_PROCESS	0.049	1	0
cation homeostasis	GO:0055080	BIOLOGICAL_PROCESS	0.049	1	0
NADP biosynthetic process	GO:0006741	BIOLOGICAL_PROCESS	0.049	1	0

regulation of carbohydrate metabolic process	GO:0006109	BIOLOGICAL_PROCESS	0.049	1	0
second-messenger-mediated signaling	GO:0019932	BIOLOGICAL_PROCESS	0.049	1	0
glutamyl-tRNA(Gln) amidotransferase complex	GO:0030956	CELLULAR_COMPONENT	0.049	1	0
heat shock protein binding	GO:0031072	MOLECULAR_FUNCTION	0.049	1	0
ATPase regulator activity	GO:0060590	MOLECULAR_FUNCTION	0.049	1	0
nucleoside-triphosphatase regulator activity	GO:0060589	MOLECULAR_FUNCTION	0.049	1	0

molecular function regulator	GO:0098772	MOLECULAR_FUNCTION	0.049	1	0
enzyme regulator activity	GO:0030234	MOLECULAR_FUNCTION	0.049	1	0
identical protein binding	GO:0042802	MOLECULAR_FUNCTION	0.049	1	0
protein homodimerization activity	GO:0042803	MOLECULAR_FUNCTION	0.049	1	0
chaperone binding	GO:0051087	MOLECULAR_FUNCTION	0.049	1	0
adenyl-nucleotide exchange factor activity	GO:0000774	MOLECULAR_FUNCTION	0.049	1	0
FMN adenylyltransferase activity	GO:0003919	MOLECULAR_FUNCTION	0.049	1	0

riboflavin kinase activity	GO:0008531	MOLECULAR_FUNCTION	0.049	1	0
nucleotidyltransferase activity	GO:0016779	MOLECULAR_FUNCTION	0.037	4	23
phosphotransferase activity, alcohol group as acceptor	GO:0016773	MOLECULAR_FUNCTION	7.85E-03	6	32
transferase activity, transferring phosphorus-containing groups	GO:0016772	MOLECULAR_FUNCTION	0.024	9	81
adenyl nucleotide binding	GO:0030554	MOLECULAR_FUNCTION	0.030	13	145
catalytic activity	GO:0003824	MOLECULAR_FUNCTION	0.042	33	529

transferase activity	GO:0016740	MOLECULAR_FUNCTION	7.77E-04	19	177
acylglycerol O-acyltransferase activity	GO:0016411	MOLECULAR_FUNCTION	0.049	1	0
lysophospholipid acyltransferase activity	GO:0071617	MOLECULAR_FUNCTION	0.049	1	0
lysophosphatidic acid acyltransferase activity	GO:0042171	MOLECULAR_FUNCTION	0.049	1	0
1-acylglycerol-3-phosphate O-acyltransferase activity	GO:0003841	MOLECULAR_FUNCTION	0.049	1	0
lysyltransferase activity	GO:0050071	MOLECULAR_FUNCTION	0.049	1	0

transferase activity, transferring amino-acyl groups	GO:0016755	MOLECULAR_FUNCTION	0.049	1	0
morphine 6-dehydrogenase activity	GO:0050109	MOLECULAR_FUNCTION	0.049	1	0
ferric iron binding	GO:0008199	MOLECULAR_FUNCTION	0.049	1	0
oxidoreductase activity, oxidizing metal ions	GO:0016722	MOLECULAR_FUNCTION	0.049	1	0
protein serine/threonine/tyrosine kinase activity	GO:0004712	MOLECULAR_FUNCTION	0.049	1	0
UDP-N-acetylmuramoylalanyl-D-glutamate-2,6-	GO:0008765	MOLECULAR_FUNCTION	0.049	1	0

diaminopimelate ligase activity					
transferase activity, transferring acyl groups	GO:0016746	MOLECULAR_FUNCTION	5.47E-03	5	20
fatty acid synthase activity	GO:0004312	MOLECULAR_FUNCTION	0.041	2	5
S-acyltransferase activity	GO:0016417	MOLECULAR_FUNCTION	0.049	1	0
S-malonyltransferase activity	GO:0016419	MOLECULAR_FUNCTION	0.049	1	0
malonyltransferase activity	GO:0016420	MOLECULAR_FUNCTION	0.049	1	0
[acyl-carrier-protein] S-	GO:0004314	MOLECULAR_FUNCTION	0.049	1	0

malonyltransferase activity					
recombinase activity	GO:0000150	MOLECULAR_FUNCTION	0.049	1	0

SI 2.2 Supplemental Figures

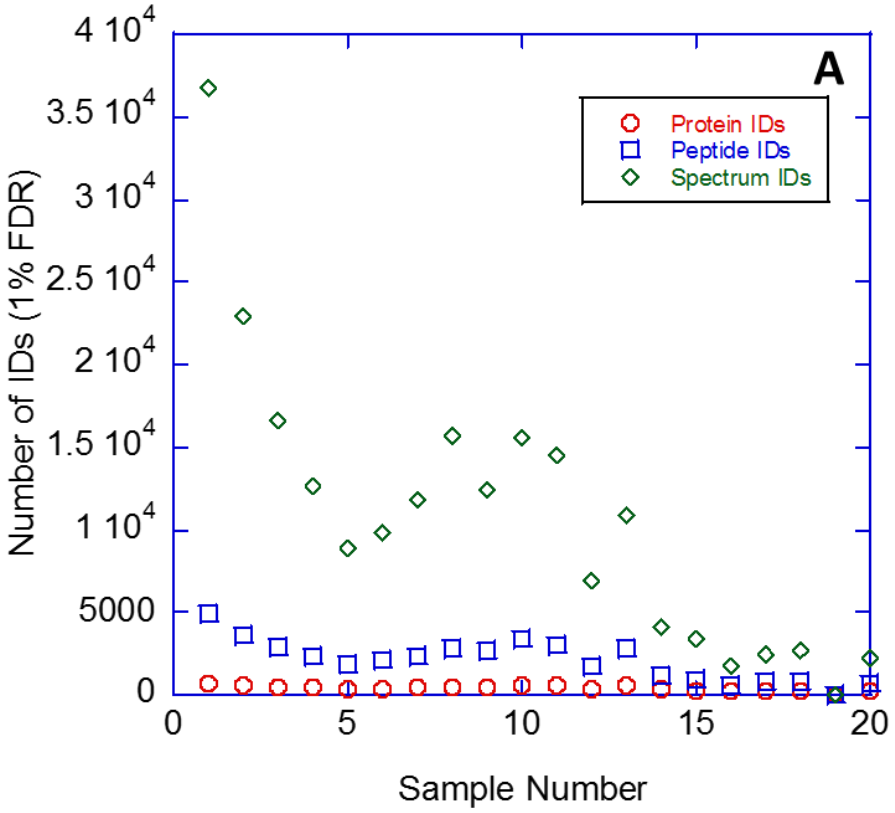

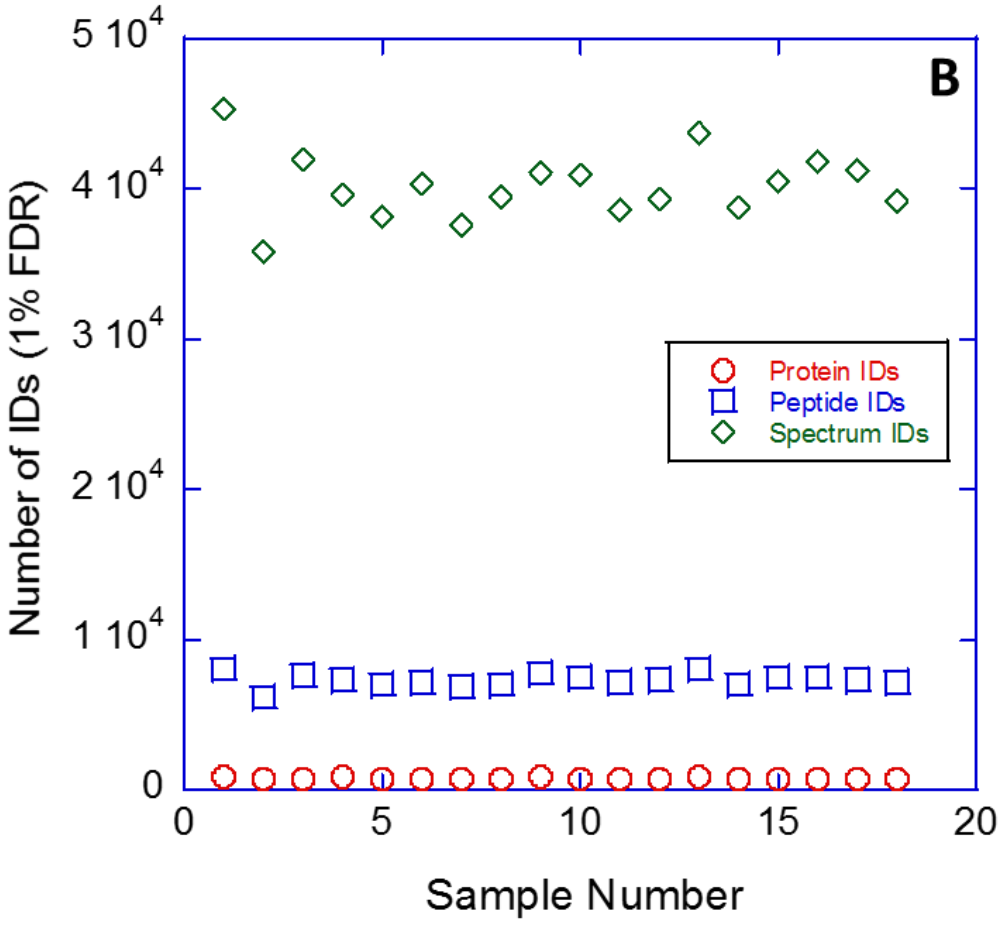

Figure S1: Influence of protein precipitation on proteomic analysis. Number of identifications of proteins, peptides, and spectra across analysis of all 20 different samples of peptides from proteins derived from biofilm or planktonic samples either (A) without a protein precipitation step prior to digestion or (B) with precipitation of proteins by 80% (v/v) acetone prior to digestion. As described in detail in the text, these trends suggest that when biofilm samples were not precipitated prior to processing in the proteomics workflow, the numbers of identifications of each feature type decreased dramatically across the sample set, especially across the first several samples. A similar decrease was not observed when proteins were precipitated with acetone from the biofilm samples prior to processing.

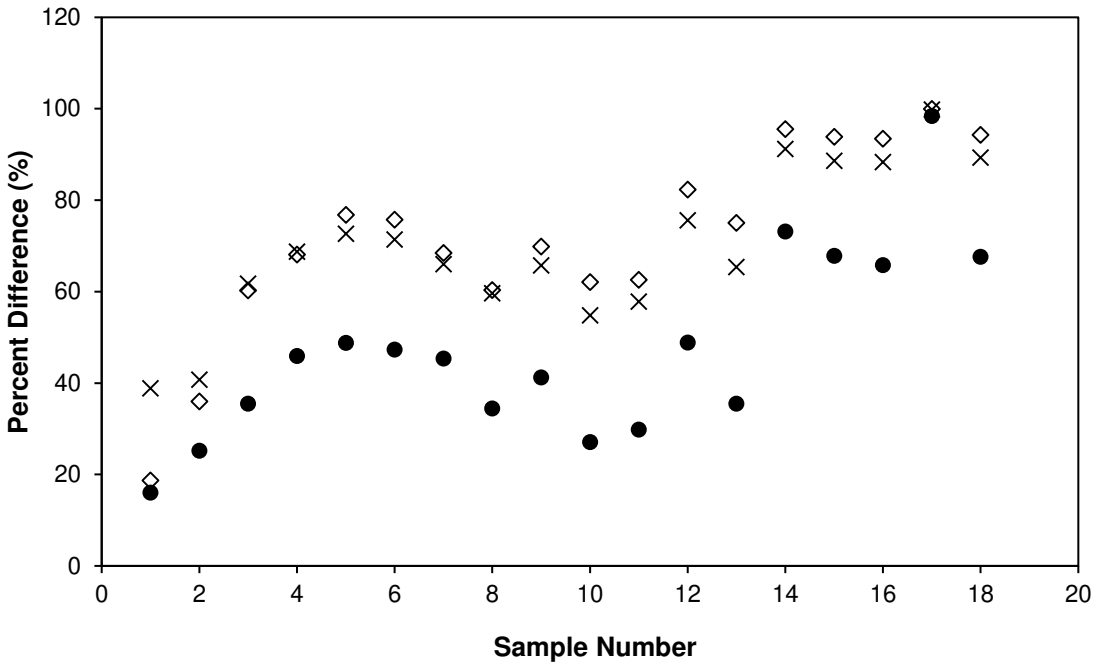

Figure S2: Relative proteomic analysis changes caused by protein precipitation. Percent difference between precipitated and non-precipitated samples with respect to identifications of (●) proteins, (◊) peptides, and (x) spectra, across the sampling order. Percent difference was calculated as: 100%*(precipitated-nonprecipitated)/precipitated. The numbers of identified features for precipitated and nonprecipitated were those reported by ProtenPilot as "Global FDR from Fit" with critical FDR of 1%, after a database search of both technical replicate LC-MS/MS datafiles simultaneously.

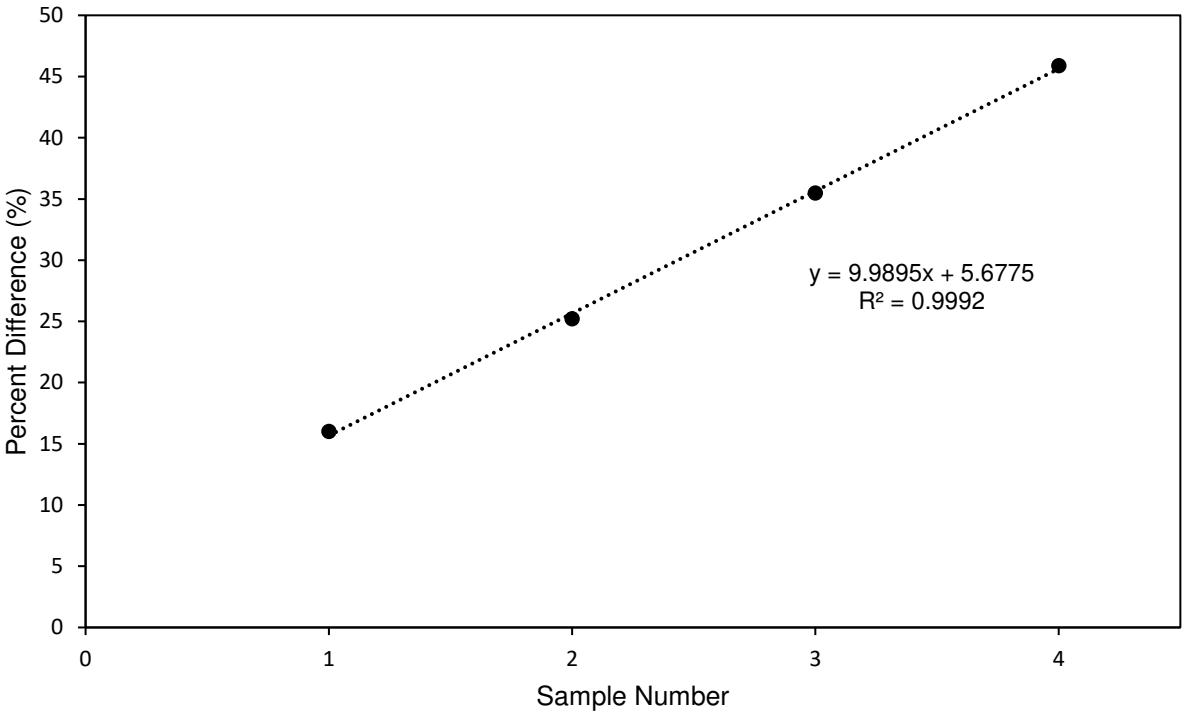

Figure S3: Decrease in protein identifications during ESI-LC-MS/MS analysis of non-precipitated ME biofilm samples. Linear regression of the percent difference between protein identifications from precipitated and non-precipitated forms of the first four samples analyzed by ESI-LC-MS/MS. Each of the four samples were derived from biofilms attached to micro-etched flow cell surfaces.

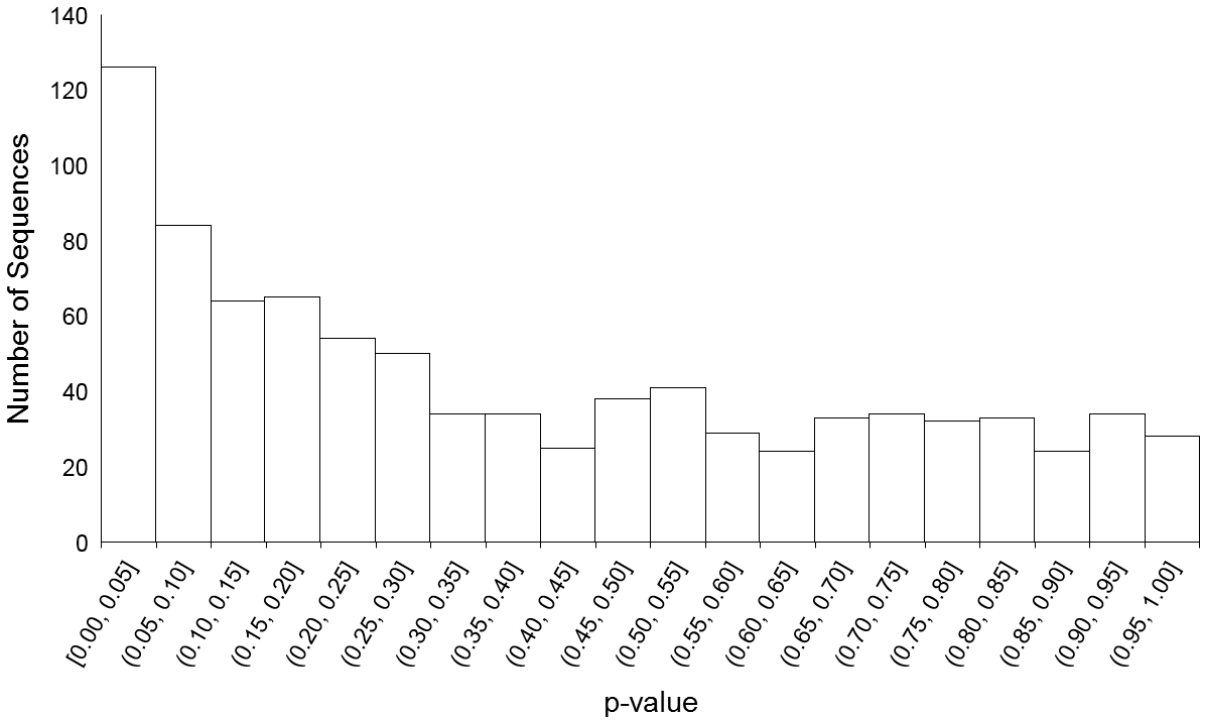

Figure S4: Histogram of Student's *t* test *p* values between proteins from biofilms and planktonic samples. A Student's t test (assuming equal variances) compared $\log_2$-transformed, normalized peptide intensity sums for proteins identified in common between samples from micro-etched biofilms and planktonic cultures.

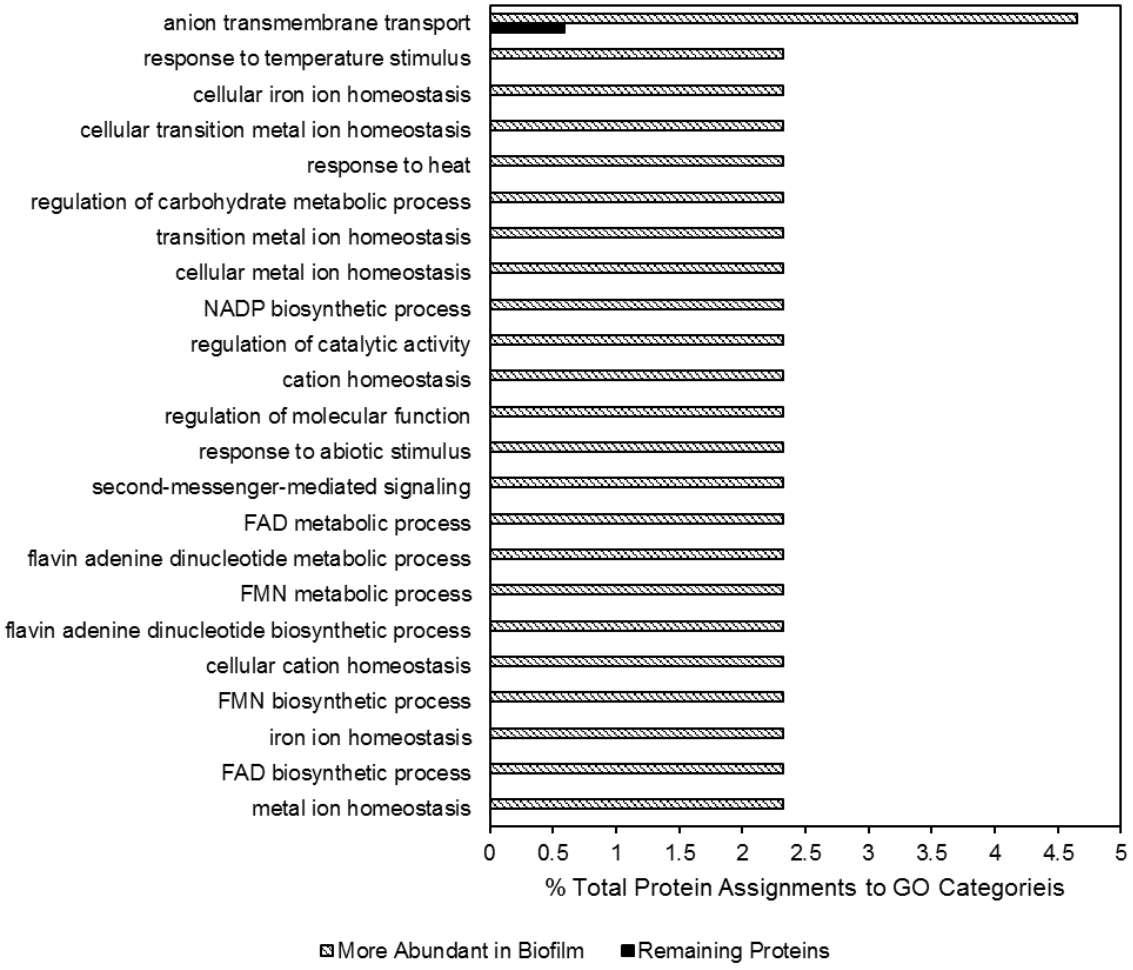

Figure S5: GO Biological Process categories significantly enriched among the 48 DAPs more abundant in ME biofilms. Significance was established using a Fisher's Exact Test ($p<0.05$) comparing DAPs more abundant in ME biofilms with all 838 remaining quantified proteins.

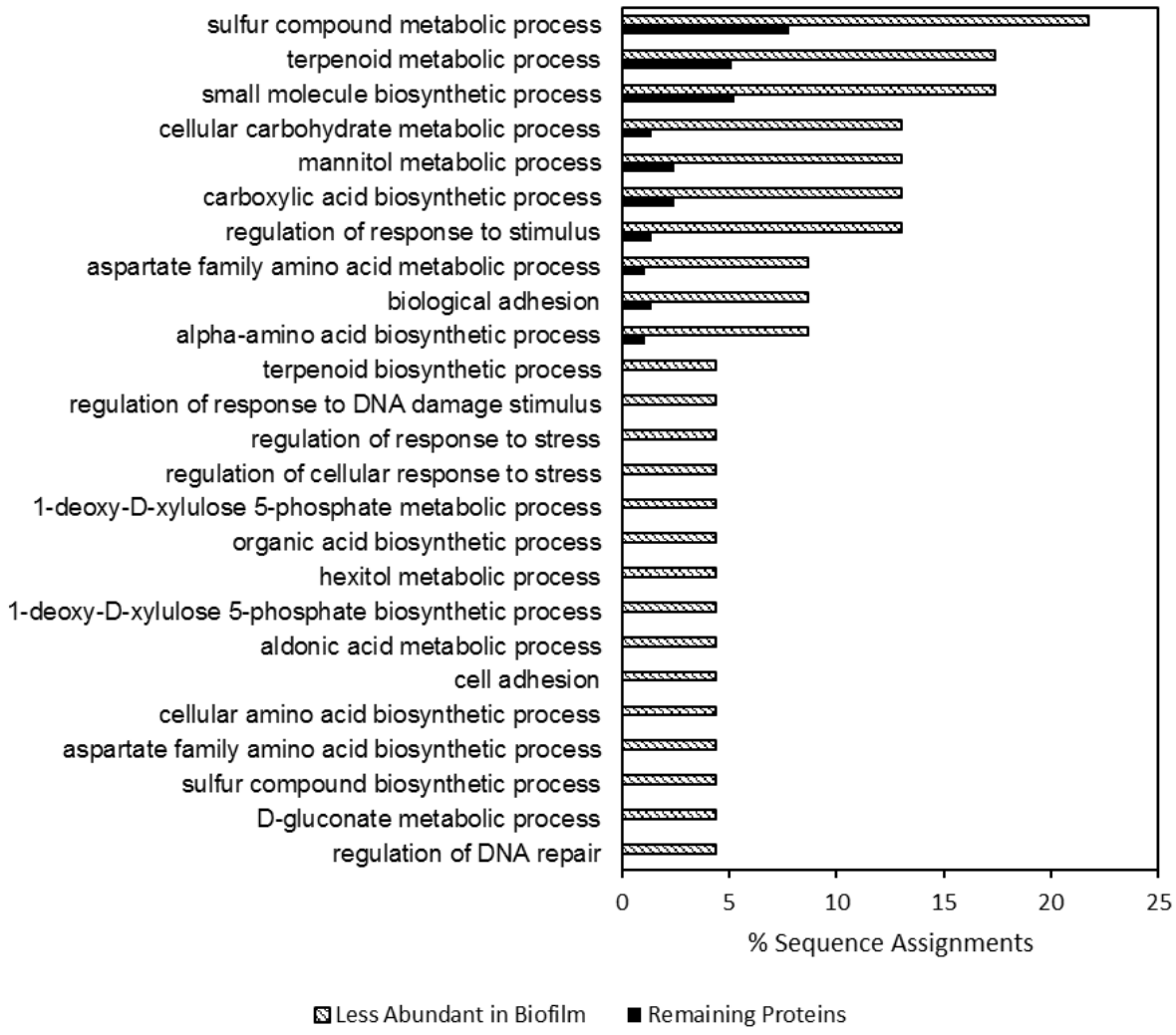

Figure S6: GO Biological Process categories significantly enriched among DAPs more abundant in planktonic cultures, compared with all remaining quantified proteins. Significance established using Fisher's Exact Test, $p < 0.05$.

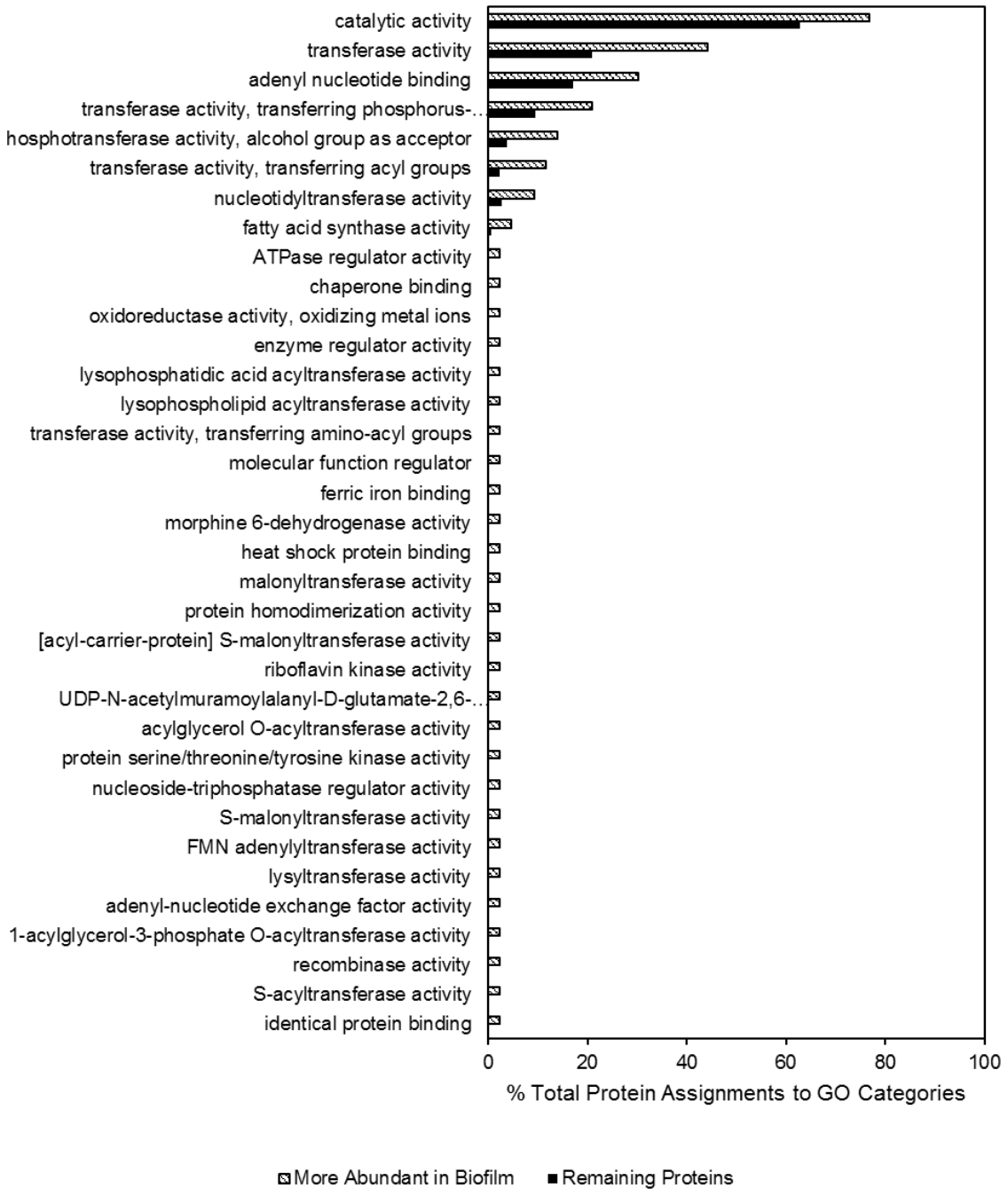

Figure S7: GO Molecular Function categories significantly enriched among the 48 DAPs more abundant in ME biofilms. Significance established using Fisher's Exact Test ($p<0.05$), comparing DAPs more abundant in ME biofilms with all 838 remaining quantified proteins.

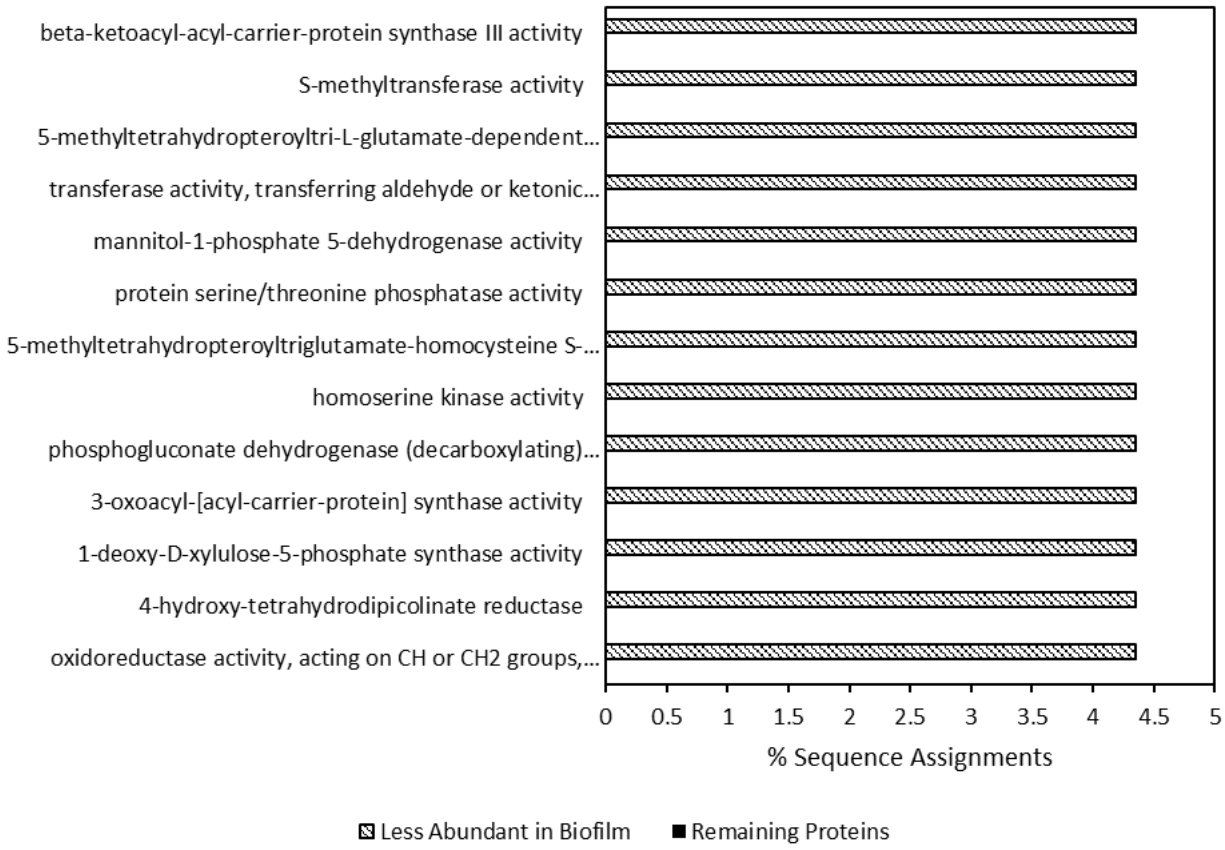

Figure S8: GO Molecular Function categories significantly enriched among DAPs more abundant in planktonic cultures, compared with all remaining quantified proteins. Significance established using Fisher's Exact Test, $p<0.05$. A total of 8 unique less abundant sequences were binned into these categories.

Chapter 3 Supplemental Information

SI 3.1 Supplemental Figures

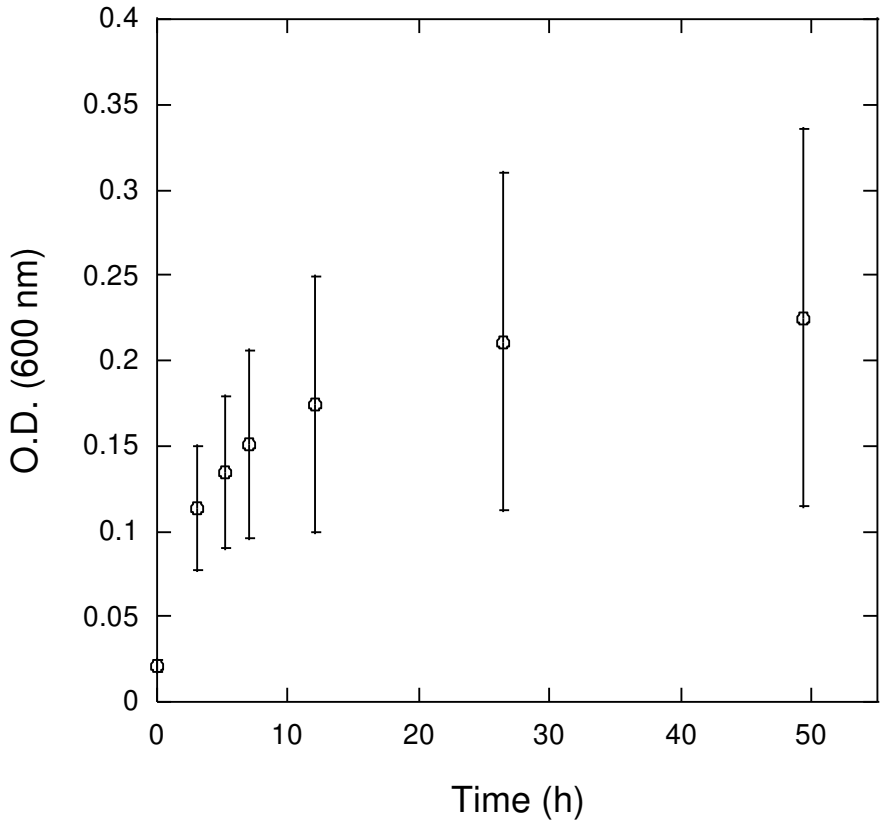

Figure S9: OD (600 nm) of bulk MFC solution with no lactate, yeast extract, or tryptone present in the medium. Each data point is the mean of four replicate MFCs.

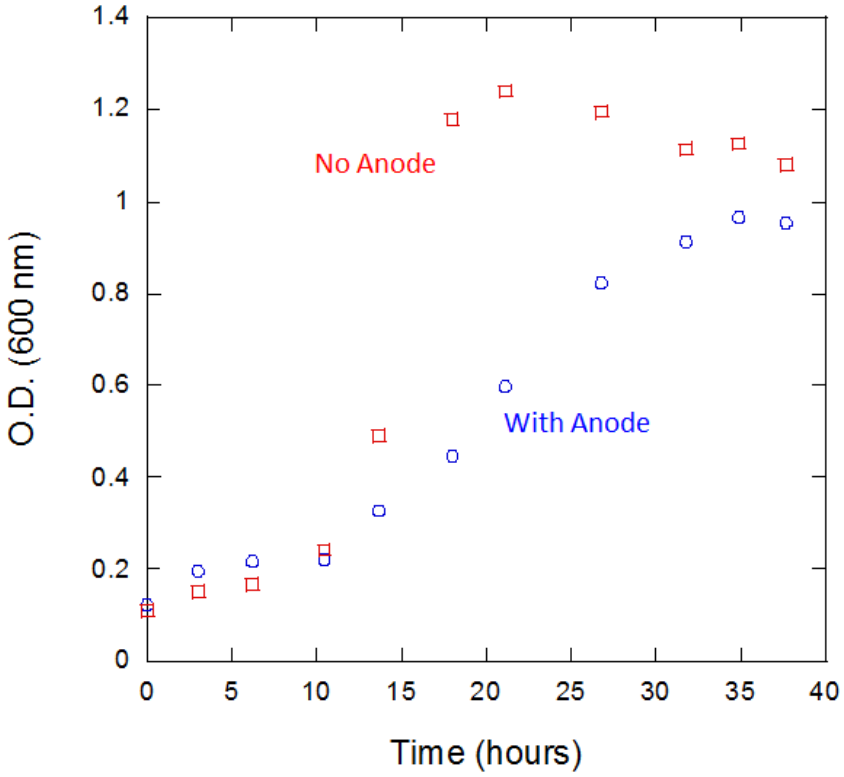

Figure S10: OD (600 nm) of the bulk solution of MFC reactors with and without an electricity-producing anode present. Each data point represents the mean of four replicate MFC reactors with fresh air-cathodes during the first batch after inoculation with *S. oneidensis* MR-1 culture. Error bars are excluded for figure clarity.

(A) (B)

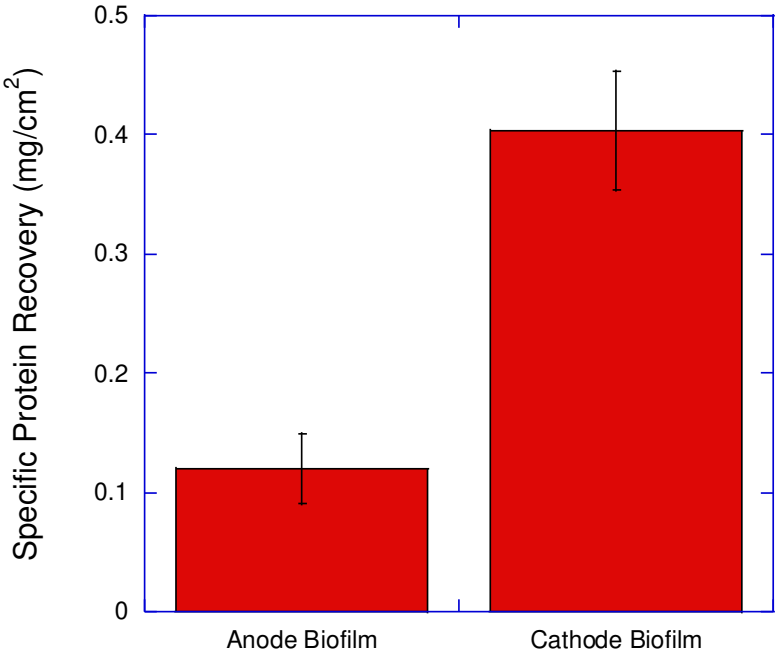

Figure S11: Pictures of anode (A) and cathode (B) MFC biofilms before harvesting for proteomics (top), corresponding to specific protein recovery from biofilm on the anode and cathode (bottom). Bar graphs and error bars represent the means and standard deviations, respectively, from the three MFCs used for proteomics analysis.

Chapter 4 Supplemental Information

SI 4.1 Experimental Procedures

SI 4.1.1 Protein extraction and peptide preparation

The cell pellets collected for proteomics were washed in 2 mL of sterile pH 7 wash buffer composed of 3 mM KCl, 1.5 mM KH_2PO_4, 68 mM NaCl, 14 mM NaH_2PO_4 [Lacerda et al. 2007], in order to remove residual medium. Cells were collected again, the supernatant discarded, and the washed pellet was immediately flash-frozen in liquid nitrogen before storage at -80 °C. Before lysis, pellets were thawed at -20 °C for 1 h then on ice at 4 °C for 2 h. Each pellet was resuspended in 70 µL of a lysis solution consisting of 10 mM Tris-HCl (pH 8), 1.5 mM $MgCl_2$, 10 mM KCl, 0.5 mM dithiothreitol (DTT), 4.3% bacterial protease inhibitor cocktail (Sigma-Aldrich, St. Louis, MO) and 1.0% sodium dodecyl sulfate (SDS). The resuspended pellets were sonicated on ice using a 550 Sonic Dismembrator probe (Fisher Scientific, Hampton, NH) at 20 kHz for 1 min in cycles of 1 second on, 2 seconds off. The lysate was centrifuged 10 min at 10,000 x g, 4 °C, and the supernatant was isolated. The pellets then were subjected to a second round of extraction targeting Gram-positive cells. The pellet was resuspended in 70 µL of a second lysis solution comprised of 10 mM Tris-HCl (pH 8), 1 mM EDTA disodium salt, 0.5 mM DTT, 4.3 % bacterial protease inhibitor, 10% glycerol, and 1 mg/mL lysozyme (Sigma-Aldrich, St. Louis, MO). The pellet was sonicated again as described above. The resulting supernatants were combined to create ~200 µL of raw protein extract. Proteins were precipitated overnight at -20 °C by adding six volumes ice-cold acetone to one volume protein extract. The mixture was centrifuged at 14,000 x g

for 30 min, 4 °C, the acetone supernatant was removed, and residual acetone was removed by evaporation at room temperature for 2 h.

Precipitated protein pellets were resuspended in 150 µL 500 mM triethylammonium bicarbonate (TEAB) + 0.05% SDS, 10 mM DTT, pH 8.0 and sonicated for 10 s as above, in order to disperse and fully dissolve the protein pellet. A volume of protein solution containing 100 µg of protein, as determined by bicinchoninic acid (BCA) assay (Pierce, Life Technologies, Grand Island, NY), was mixed with 10% (v/v) of 100 mM DTT in TEAB and put in a water bath at 60 °C for 30 minutes to denature proteins and reduce cysteine residues. Samples were cooled to room temperature and then were methylated with 5 µL of 475 mM iodoacetamide at room temperature in the dark. To each sample, 9% (v/v) of 100% acetonitrile and 0.5 µL of 50 mM $CaCl_2$ (trypsin co-factor) were added. Mass spectrometry-grade trypsin (Trypsin Gold from Promega, Madison, WI) was added in a 1:20 (w/w) ratio to each sample, and samples were digested overnight (~13 h) at 38°C. Additional trypsin was added to each reaction in a 1:100 (w/w) ratio, and the digestion was allowed to continue for an additional 4 h. The digestion was stopped by adding 2 µL of 100% formic acid to bring the reaction to pH 2. Detergent and contaminants were removed with a C-18 spin column (Pierce, Life Technologies, Grand Island, NY). Eluted peptides were evaporated to dryness and resuspended in 3% acetonitrile, 0.1% formic acid for LC-MS/MS analysis.

SI 4.1.2 Protein identification, label-free quantification, and Gene Ontology analysis

Database searching was conducted on Analyst (v.1.5 TR, ABSciex) .wiff files with ProteinPilot v. 4.5 TR (ABsciex). A .fasta file containing the combined proteomes of *B. atrophaeus* 1942 and *P. putida* KT2440 including isoforms (downloaded from

www.uniprot.org February 2013) along with sequences of common contaminating proteins provided by ProteinPilot was used as the target database. The database search was conducted using rapid search ID with no biological modifications. False discovery rate (FDR) was calculated by ProteinPilot using a decoy database consisting of reversed sequences from the target database, with 1% FDR protein identification significance threshold. For the peptide dilution experiments, both technical replicate .wiff files for a sample level were searched simultaneously; peptides and proteins were identified and quantified from the exported peptide and protein summaries after filtering for the "Unused Score" cutoff reported by the ProteinPilot FDR analysis (1% FDR). For the experiment quantifying intensity of a protein across dilutions, intensity was calculated as the sum of precursor ion intensities for all high-confidence (>95%) peptides across both replicates.

For the co-culture growth proteomics experiments,the.wiff files for all technical replicates corresponding to a biological replicate sample (three each for each species alone and co-culture) were searched simultaneously in ProteinPilot. The resulting .group files were all processed simultaneously with a quantitation microapp (v. 1.0) in PeakView software (v. 1.1.1, ABsciex) to extract the precursor ion intensities for the most abundant five peptides associated with each unique protein, across all nine sample conditions. Previous studies have noted linear correspondence of the combined precursor intensities of the top peptides corresponding to a protein with the abundance of that protein in the original sample [Ning et al. 2012; Silva et al. 2006].

Data normalization and statistical testing were conducted in Excel and R statistical package (v. 3.1.2). For each protein, the intensity values first were normalized

to species abundance, in order to compare protein intensities between co- and pure cultures. For each protein, the intensity value in a technical replicate was multiplied by the ratio of mean CFU/mL of the relevant species across co-culture replicates to CFU/mL in pure culture replicates [Ning et al. 2012]. The resulting values then were $\log_2$-transformed and normalized by subtracting the median value of all proteins in that LC-MS/MS technical replicate. Then for each protein the mean across the three technical replicate LC-MS/MS runs was calculated, for each biological replicate culture.

Data quality was assessed by computing the coefficient of variation (%CV) across all proteins in a technical replicate LC-MS/MS run, both before and after $\log_2$-transformation and normalization. Division by the median was used for %CV assessment instead of median subtraction, to avoid taking square roots of negative numbers in standard deviation calculations. Statistical comparison of transformed, normalized protein intensity values between biological conditions (abundance of a protein in the co-culture vs. in the pure culture) was conducted using the *siggenes* package in R. The Δ values for SAM analysis (Δ= 0.82 for *B. atrophaeus* pure vs. co-culture and Δ=0.38 for *P. putida* pure vs. co-culture) were chosen based on mean FDR of 0.05. The *sam()* command in the *siggenes* package corrects for multiple hypothesis testing with a q-value approach [Storey 2002].

SI 4.2 Supplemental Tables

Table S7: Uniprot ID codes for proteins for each species that were identified in peptide samples known to contain only peptides from the other species, in the LOD delineation portion of this study.

B. atrophaeus	*P. putida*

A0A0H3E5T9	Q88FT2
A0A0H3DYP8	Q88HC7
A0A0H3DXC2	Q88HX0
A0A0H3DWE9	Q877Q1
A0A0H3E3B8	Q88I63
A0A0H3E248	Q88QM8

Table S8: Complete list of *B. atrophaeus* proteins significantly more abundant during co-culture with *P. putida*. The heading "Co/Pure" refers to the ratio of precursor ion intensity for that protein in the co-culture compared with a pure culture. The q-value is the statistical indicator of significance, after adjustment for multiple testing (q < 5% indicates statistical significance)

Uniprot ID	**Protein Name**	**Co/Pure**	**Q-value (%)**
A0A0H3E401	TetR family transcriptional regulator	14.7	0
A0A0H3DYZ0	Ribonuclease Y (RNase Y) (EC 3.1.-.-)	12.9	0
A0A0H3DY18	Putative glycosyltransferase	12.2	0
A0A0H3DX63	DegV family protein	10.6	0
A0A0H3E4M1	Delta-aminolevulinic acid dehydratase (EC 4.2.1.24)	9.1	0
A0A0H3E7F7	Putative heme-dependent peroxidase BATR1942_16800 (EC 1.11.1.-)	8.9	0
A0A0H3E705	Putative phosphatase	8.7	0
A0A0H3E249	3-ketoacyl-(Acyl-carrier-protein) reductase	8	0
A0A0H3E5R0	Single-stranded DNA-binding protein	7.7	0
A0A0H3E399	GMP reductase (EC 1.7.1.7) (Guanosine 5'-monophosphate oxidoreductase)	7.6	0
A0A0H3E1V3	Protein GrpE (HSP-70 cofactor)	7.1	0
A0A0H3E4S8	DNA polymerase (EC 2.7.7.7)	6.9	0
A0A0H3DYE3	Phosphoribosylamine--glycine ligase (EC 6.3.4.13) (GARS) (Glycinamide ribonucleotide synthetase)	6.8	0
A0A0H3E251	Non-canonical purine NTP pyrophosphatase	6.6	0
A0A0H3E0W0	Uncharacterized protein	6.5	0
A0A0H3E361	Putative transcriptional regulator (Lrp/AsnC family)	6.3	0
A0A0H3E9Q7	Penicillin-binding lipoprotein 3	6.3	0
A0A0H3E199	Heme-based dioxygen sensor	6.3	0
A0A0H3DWE9	Heptaprenylglyceryl phosphate synthase (HepGP synthase) (EC 2.5.1.n9)	6.1	0

A0A0H3E6C1	Adenylate kinase (AK) (EC 2.7.4.3)	5.7	0
A0A0H3E2S1	Glutamyl aminopeptidase	5.7	0
A0A0H3E5R7	2,3-dihydroxybenzoate-AMP ligase	5.2	0
A0A0H3E3W4	OpuCA	5.2	0
A0A0H3E5G2	Putative deacylase	5	0
A0A0H3E164	Putative amidohydrolase	4.9	0
A0A0H3DYX2	Aspartate-semialdehyde dehydrogenase (ASA dehydrogenase) (ASADH) (EC 1.2.1.11)	4.9	0
A0A0H3E4R1	Threonine--tRNA ligase (EC 6.1.1.3) (Threonyl-tRNA synthetase)	4.9	0
A0A0H3E732	Cystine ABC transporter (Substrate-binding lipoprotein)	4.8	0
A0A0H3E5T2	Ferredoxin--NADP reductase (FNR) (Fd-NADP(+) reductase) (EC 1.18.1.2)	4.7	0
A0A0H3E5I0	Methylisocitrate lyase (EC 4.1.3.30)	4.6	0
A0A0H3DYI0	Carbamoyl-phosphate synthase (glutamine-hydrolyzing) (EC 6.3.5.5)	4.6	0
A0A0H3E499	Two-component response regulator	4.6	0
A0A0H3DYL0	6-phospho-alpha-glucosidase	4.5	0
A0A0H3E8W6	50S ribosomal protein L29	4.4	0
A0A0H3E9V0	50S ribosomal protein L22	4.3	0
A0A0H3E0F1	Putative ABC efflux transporter ATP-binding protein	4.3	0
A0A0H3DY25	Uncharacterized protein	4.3	0
A0A0H3E3P2	Ribonuclease R (RNase R) (EC 3.1.13.1)	4.2	0
A0A0H3E7B4	Putative iron-sulfur-binding reductase	4.2	0
A0A0H3DX57	UPF0234 protein BATR1942_03145	4.1	0
A0A0H3E456	Uncharacterized protein	4	0
A0A0H3DZY7	Oligopeptide ABC transporter ATP-binding protein	3.9	0
A0A0H3E1W1	Alanine--tRNA ligase (EC 6.1.1.7)	3.8	0
A0A0H3DY64	3-oxoacyl-(Acyl-carrier-protein) reductase	3.8	0
A0A0H3E8W4	30S ribosomal protein S10	3.7	0
A0A0H3E1I7	Geranyltranstransferase	3.7	0
A0A0H3E3U9	Putative NADH-dependent flavin oxidoreductase	3.7	0
A0A0H3E633	50S ribosomal protein L25 (General stress protein CTC)	3.6	0
A0A0H3E3W5	Acetyl-CoA carboxylase biotin carboxylase subunit (EC 6.4.1.2)	3.5	0
A0A0H3E1A5	Putative aminopeptidase	3.5	0
A0A0H3E8H7	Site-specific DNA-binding protein	3.5	0
A0A0H3E795	Uncharacterized protein	3.5	0
A0A0H3E2C2	NADP-dependent malic enzyme	3.4	0
A0A0H3E487	Protein translocase subunit SecA	3.4	0

A0A0H3E8X6	30S ribosomal protein S8	3.2	0
A0A0H3DWK3	Glycerol kinase (EC 2.7.1.30) (ATP:glycerol 3-phosphotransferase) (Glycerokinase)	3.2	0
A0A0H3DZ38	30S ribosomal protein S16	3.2	0
A0A0H3E036	Uncharacterized protein	3.1	0
A0A0H3E733	DNA topoisomerase 3 (EC 5.99.1.2) (DNA topoisomerase III)	3	0
A0A0H3E2Z0	Putative oxidoreductase, 2-nitropropane dioxygenase family protein	3	0
A0A0H3E235	Porphobilinogen deaminase (PBG) (EC 2.5.1.61) (Hydroxymethylbilane synthase) (Pre-uroporphyrinogen synthase)	3	0
A0A0H3E2R3	Bifunctional 3-deoxy-7-phosphoheptulonate synthase/chorismate mutase	2.9	0
A0A0H3E4D9	Aspartate--tRNA(Asp/Asn) ligase (EC 6.1.1.23) (Aspartyl-tRNA synthetase) (Non-discriminating aspartyl-tRNA synthetase)	2.9	0
A0A0H3E4K2	Putative oxidoreductase	2.9	0
A0A0H3E8Z3	50S ribosomal protein L13	2.9	0
A0A0H3DYV8	Transcription elongation factor NusA	2.8	0
A0A0H3E5F4	IolS	2.8	0.47
A0A0H3E6K9	Putative ion channel associated enzyme	2.8	0.47
A0A0H3E9P3	Ribose-phosphate pyrophosphokinase (RPPK) (EC 2.7.6.1) (5-phospho-D-ribosyl alpha-1-diphosphate) (Phosphoribosyl diphosphate synthase) (Phosphoribosyl pyrophosphate synthase)	2.8	0.47
A0A0H3E4X7	YtsP	2.7	0.47
A0A0H3DYR4	GTPase	2.7	0.47
A0A0H3E3V5	Octanoyltransferase LipM (EC 2.3.1.181) (Octanoyl-[acyl-carrier-protein]:[GcvH] N-octanoyltransferase)	2.7	0.47
A0A0H3E1Y7	LexA repressor (EC 3.4.21.88)	2.7	0.47
A0A0H3E8Y9	50S ribosomal protein L17	2.6	0.85
A0A0H3E744	Putative ABC transporter (Binding lipoprotein)	2.5	0.85
A0A0H3E240	Lon protease (EC 3.4.21.53) (ATP-dependent protease La)	2.5	0.85
A0A0H3E188	Master regulator for biofilm formation	2.5	0.85
A0A0H3E0B1	Uncharacterized protein	2.5	0.85
A0A0H3E8F7	30S ribosomal protein S6	2.5	0.85
A0A0H3E160	Branched-chain alpha-keto acid dehydrogenase subunit E2	2.5	0.85
A0A0H3EAR3	Serine-protein kinase RsbW (EC 2.7.11.1) (Anti-sigma-B factor) (Sigma-B negative effector RsbW)	2.4	0.85

A0A0H3DWY5	Uncharacterized protein	2.4	0.85
A0A0H3E9N5	Uncharacterized protein	2.4	0.85
A0A0H3E6K8	Long-chain-fatty-acid--CoA ligase	2.4	0.85
A0A0H3E7B3	Lipoyl synthase (EC 2.8.1.8) (Lip-syn) (Lipoate synthase) (Lipoic acid synthase) (Sulfur insertion protein LipA)	2.4	0.85
A0A0H3E8U8	Peptidase T (EC 3.4.11.4) (Aminotripeptidase) (Tripeptide aminopeptidase)	2.3	0.98
A0A0H3E344	Riboflavin biosynthesis protein RibD	2.2	0.98
A0A0H3E665	50S ribosomal protein L5	2.2	0.98
A0A0H3E198	Succinyl-CoA ligase [ADP-forming] subunit alpha (EC 6.2.1.5)	2.2	0.98
A0A0H3E5Y5	Lipoprotein	2.1	1.68
A0A0H3E178	Signal recognition particle receptor FtsY (SRP receptor)	2.1	1.68
A0A0H3E459	Uncharacterized protein	2.1	1.68
A0A0H3E0I0	PTS system N-acetylglucosamine-specific transporter subunit IICB	2.1	1.68
A0A0H3E901	Pyrimidine-nucleoside phosphorylase (EC 2.4.2.2)	2	1.68
A0A0H3E294	GTPase Obg (GTP-binding protein Obg)	2	1.68
A0A0H3DW54	Putative glycosyltransferase	2	2.19
A0A0H3E2A5	Glyceraldehyde-3-phosphate dehydrogenase (EC 1.2.1.-)	2	2.19
A0A0H3E5C6	Deoxyribose-phosphate aldolase (DERA) (EC 4.1.2.4) (2-deoxy-D-ribose 5-phosphate aldolase) (Phosphodeoxyriboaldolase)	1.8	3.42
A0A0H3DXE0	Uncharacterized protein	1.8	3.42
A0A0H3E7G8	Enoyl-CoA hydratase/3-hydroxyacyl-CoA dehydrogenase	1.8	3.42
A0A0H3DX74	Glycerol-3-phosphate dehydrogenase (EC 1.1.5.3)	1.8	3.42
A0A0H3E110	NAD-dependent malic enzyme (Conversion of malate into pyruvate)	1.7	3.42
A0A0H3DY64	Uncharacterized protein	1.7	3.42
A0A0H3DZM6	Uncharacterized protein	1.7	3.42
A0A0H3DZY1	Tryptophan--tRNA ligase (EC 6.1.1.2) (Tryptophanyl-tRNA synthetase)	1.7	3.42
A0A0H3E9S6	2-C-methyl-D-erythritol 2,4-cyclodiphosphate synthase (MECDP-synthase) (MECPP-synthase) (MECPS) (EC 4.6.1.12)	1.7	3.42
A0A0H3E108	Two-component response regulator	1.6	3.42
A0A0H3E0S2	Ribosomal RNA small subunit methyltransferase B	1.6	3.42

Table S9: Complete list of *B.atrophaeus* proteins significantly less abundant during co-culture with *P. putida*. The heading "Co/Pure" refers to the ratio of precursor ion intensity for that protein in the co-culture compared with a pure culture. The q-value is the statistical indicator of significance, after adjustment for multiple testing (q < 5% indicates statistical significance).

UniprotID	**Protein Name**	**Co/Pure**	**Q-value (%)**
A0A0H3E6N4	YsdC	0.1	0
A0A0H3E9N1	Succinate-semialdehyde dehydrogenase	0.1	0
A0A0H3E2E6	Electron transfer flavoprotein, beta subunit	0.1	0
A0A0H3DWY7	Methylmalonate semialdehyde dehydrogenase [acylating] (MMSA dehydrogenase)	0.2	0
A0A0H3E321	Betaine-aldehyde dehydrogenase (EC 1.2.1.8)	0.2	0
A0A0H3E5Y3	Chaperone protein DnaJ	0.2	0
A0A0H3E557	Dipeptidase PepV	0.2	0
A0A0H3E169	2-methylcitrate dehydratase (EC 4.2.1.79)	0.2	0
A0A0H3DZJ6	Carboxylesterase	0.2	0
A0A0H3E5U1	Putative iron-sulfur scaffold protein	0.2	0
A0A0H3E0W3	Succinyl-CoA ligase [ADP-forming] subunit beta (EC 6.2.1.5) (Succinyl-CoA synthetase subunit beta)	0.2	0
A0A0H3E1I4	AppA	0.2	0
A0A0H3E4P2	Probable transaldolase (EC 2.2.1.2)	0.2	0
A0A0H3E9X9	Anti-sigma factor antagonist	0.2	0
A0A0H3E2H1	LacI family transcriptional regulator	0.2	0
A0A0H3E4J8	Succinate dehydrogenase iron-sulfur subunit (EC 1.3.99.1)	0.2	0
A0A0H3E4Q5	Thioredoxin	0.2	0
A0A0H3E6T7	Putative stress adaptation protein	0.2	0
A0A0H3DXX3	60 kDa chaperonin (GroEL protein) (Protein Cpn60)	0.2	0
A0A0H3E3J5	Oligoendopeptidase F	0.2	0
A0A0H3DXU2	Oligoendopeptidase F	0.2	0
A0A0H3E6Y7	Response regulator aspartate phosphatase	0.2	0
A0A0H3E263	Electron transfer flavoprotein subunit alpha	0.2	0

A0A0H3E2S8	Aspartate aminotransferase (EC 2.6.1.1)	0.2	0
A0A0H3DXH8	Enoyl-CoA hydratase	0.2	0
A0A0H3DWA7	Acetoin reductase/2,3-butanediol dehydrogenase	0.2	0
A0A0H3E4Z5	Thiamine-phosphate synthase (TP synthase) (TPS) (EC 2.5.1.3) (Thiamine-phosphate pyrophosphorylase)	0.2	0
A0A0H3DYU9	Aminotransferase	0.2	0
A0A0H3E049	Putative phosphoesterase BATR1942_03595 (EC 3.1.-.-)	0.2	0
A0A0H3E1Z9	Aconitate hydratase (Aconitase) (EC 4.2.1.3)	0.2	0
A0A0H3E8Q8	Transcription-repair-coupling factor (TRCF) (EC 3.6.4.-)	0.2	0
A0A0H3E167	4-hydroxy-tetrahydrodipicolinate synthase (HTPA synthase) (EC 4.3.3.7)	0.3	0
A0A0H3E5T3	Probable cytosol aminopeptidase (Leucine aminopeptidase) (Leucyl aminopeptidase)	0.3	0
A0A0H3E4P3	Serine hydroxymethyltransferase (SHMT) (Serine methylase) (EC 2.1.2.1)	0.3	0
A0A0H3E334	Polyribonucleotide nucleotidyltransferase (EC 2.7.7.8) (Polynucleotide phosphorylase)	0.3	0
A0A0H3DZ78	Flagellar motor switch protein	0.3	0
A0A0H3E6V1	Acetyl-CoA synthetase (EC 6.2.1.1)	0.3	0
A0A0H3E165	Leucine dehydrogenase	0.3	0
A0A0H3E562	Leucine--tRNA ligase (EC 6.1.1.4) (Leucyl-tRNA synthetase)	0.3	0
A0A0H3E672	Glutamate--tRNA ligase (EC 6.1.1.17) (Glutamyl-tRNA synthetase)	0.3	0
A0A0H3E2Q1	Metal-dependent carboxypeptidase	0.3	0
A0A0H3E4K4	Enoyl-CoA hydratase (EC 4.2.1.17)	0.3	0
A0A0H3E2D8	Uncharacterized protein	0.3	0
A0A0H3E5F2	NADPH dehydrogenase (EC 1.6.99.1)	0.3	0
A0A0H3E6M3	YceE	0.3	0
A0A0H3E2B2	Malate dehydrogenase (EC 1.1.1.37)	0.3	0
A0A0H3E0C7	Aminopeptidase	0.3	0
A0A0H3DXD5	Foldase protein PrsA (EC 5.2.1.8)	0.3	0
A0A0H3E8J1	Inosine-5'-monophosphate dehydrogenase (IMP dehydrogenase) (IMPD) (IMPDH) (EC 1.1.1.205)	0.3	0
A0A0H3DWJ6	Aspartate phosphatase response regulator	0.3	0
A0A0H3E2K8	Pyruvate kinase (EC 2.7.1.40)	0.3	0
A0A0H3DYN9	GTP-sensing transcriptional pleiotropic repressor CodY	0.3	0

A0A0H3E7C3	Fructose-bisphosphate aldolase (EC 4.1.2.13)	0.3	0
A0A0H3E6V5	NH(3)-dependent NAD(+) synthetase (EC 6.3.1.5)	0.3	0
A0A0H3E131	Histidine kinase (EC 2.7.13.3)	0.3	0
A0A0H3E1K9	Chaperone protein DnaK (HSP70) (Heat shock 70 kDa protein) (Heat shock protein 70)	0.3	0
A0A0H3E4W3	Probable thiol peroxidase (EC 1.11.1.-)	0.3	0
A0A0H3DYQ3	Inositol monophosphatase	0.3	0
A0A0H3E688	Putative methyl-accepting transducer	0.3	0
A0A0H3E5F7	6-phosphogluconate dehydrogenase, decarboxylating (EC 1.1.1.44)	0.3	0
A0A0H3E2K4	Isocitrate dehydrogenase [NADP] (EC 1.1.1.42)	0.3	0
A0A0H3DYX4	Uncharacterized protein	0.3	0
A0A0H3E1L7	L-threonine 3-dehydrogenase (EC 1.1.1.103)	0.3	0
A0A0H3E6I5	Uncharacterized protein	0.3	0
A0A0H3DYE6	Putative chemotaxis sensory transducer	0.3	0
A0A0H3E6Z6	Phosphoenolpyruvate carboxykinase [ATP] (PCK) (PEP carboxykinase) (PEPCK) (EC 4.1.1.49)	0.3	0
A0A0H3E524	YtzB	0.4	0
A0A0H3E0U7	Peptide deformylase (PDF) (EC 3.5.1.88) (Polypeptide deformylase)	0.4	0
A0A0H3E2R2	Aldehyde dehydrogenase	0.4	0
A0A0H3E3M2	FeS cluster formation protein	0.4	0
A0A0H3DY45	Putative PTS mannose-specific enzyme IIBCA component	0.4	0
A0A0H3E2U5	Manganese ABC transporter manganese binding lipoprotein	0.4	0
A0A0H3E2R6	Dihydrolipoyllysine-residue succinyltransferase component of 2-oxoglutarate dehydrogenase complex (EC 2.3.1.61)	0.4	0
A0A0H3E8W2	50S ribosomal protein L2	0.4	0
A0A0H3E3J3	Purine nucleoside phosphorylase (EC 2.4.2.1) (Inosine-guanosine phosphorylase)	0.4	0
A0A0H3DZB4	Proline--tRNA ligase (EC 6.1.1.15) (Prolyl-tRNA synthetase)	0.4	0
A0A0H3E3S7	Phosphoglycerate kinase (EC 2.7.2.3)	0.4	0
A0A0H3E1I9	Oligopeptide ABC transporter (Binding lipoprotein)	0.4	0
A0A0H3E1K0	Transketolase (EC 2.2.1.1)	0.4	0.5

A0A0H3E692	DNA-directed RNA polymerase subunit beta (RNAP subunit beta) (EC 2.7.7.6) (RNA polymerase subunit beta)	0.4	0.5
A0A0H3E558	6-phospho-beta-glucosidase	0.4	0.5
A0A0H3DYH7	Nod factor export ATP-binding protein I	0.4	0.5
A0A0H3E3M1	Glyoxal/methylglyoxal reductase	0.4	0.5
A0A0H3E0V2	Branched-chain alpha-keto acid dehydrogenase subunit E2	0.4	0.5
A0A0H3E5Z9	FAD dependent acyl-CoA dehydrogenase	0.4	0.5
A0A0H3E4Y1	Transcription attenuation protein MtrB (Trp RNA-binding attenuation protein)	0.4	0.5
A0A0H3E0B4	Dihydroxy-acid dehydratase (DAD) (EC 4.2.1.9)	0.4	0.5
A0A0H3E1K1	Ribonuclease J (EC 3.1.-.-)	0.4	0.5
A0A0H3E5E4	Putative sugar-phosphate epimerase/isomerase	0.4	0.5
A0A0H3E6A3	2,3-bisphosphoglycerate-independent phosphoglycerate mutase (BPG-independent PGAM) (Phosphoglyceromutase) (iPGM) (EC 5.4.2.12)	0.4	0.5
A0A0H3E675	FMN-dependent NADH-azoreductase (EC 1.7.-.-) (Azo-dye reductase)	0.4	0.5
A0A0H3E181	Putative epimerase	0.4	0.5
A0A0H3DZ55	Methylenetetrahydrofolate--tRNA-(uracil-5-)-methyltransferase TrmFO (EC 2.1.1.74) (Folate-dependent tRNA (uracil-5-)-methyltransferase) (Folate-dependent tRNA(M-5-U54)-methyltransferase)	0.4	0.5
A0A0H3E0J9	Nucleoside diphosphate kinase (NDK) (NDP kinase) (EC 2.7.4.6) (Nucleoside-2-P kinase)	0.4	0.5
A0A0H3DY72	Ribonuclease J (EC 3.1.-.-)	0.4	0.8
A0A0H3E5N8	Probable manganese-dependent inorganic pyrophosphatase (EC 3.6.1.1) (Pyrophosphate phospho-hydrolase)	0.4	0.8
A0A0H3DVP6	Phosphoribosylaminoimidazole-succinocarboxamide synthase (EC 6.3.2.6) (SAICAR synthetase)	0.4	0.8
A0A0H3E0P1	Phosphoenolpyruvate-protein phosphotransferase (EC 2.7.3.9) (Phosphotransferase system, enzyme I)	0.4	0.8
A0A0H3E469	N-acetylglucosamine-6-phosphate deacetylase (EC 3.5.1.25) (GlcNAc 6-P deacetylase)	0.4	0.8
A0A0H3E1U1	UPF0365 protein BATR1942_11000	0.4	0.8

A0A0H3E9V4	D-alanine--D-alanine ligase (EC 6.3.2.4) (D-Ala-D-Ala ligase) (D-alanylalanine synthetase)	0.4	0.8
A0A0H3E4W4	Histidinol-phosphate aminotransferase (EC 2.6.1.9) (Imidazole acetol-phosphate transaminase)	0.4	0.8
A0A0H3DWW0	Acetoin dehydrogenase E1 component TPP-dependent alpha subunit	0.5	0.8
A0A0H3DW88	10 kDa chaperonin (GroES protein) (Protein Cpn10)	0.5	0.8
A0A0H3DZ01	Branched-chain alpha-keto acid dehydrogenase subunit E2	0.5	0.8
A0A0H3E4H8	Histidine--tRNA ligase (EC 6.1.1.21)	0.5	1
A0A0H3DWI6	CspB	0.5	1
A0A0H3E2Z8	Glucose-6-phosphate isomerase (GPI) (EC 5.3.1.9) (Phosphoglucose isomerase) (Phosphohexose isomerase)	0.5	1
A0A0H3E9I6	Pyridoxal 5'-phosphate synthase subunit PdxS (PLP synthase subunit PdxS) (EC 4.3.3.6) (Pdx1)	0.5	1
A0A0H3E5A9	S-adenosylmethionine synthase (AdoMet synthase) (EC 2.5.1.6) (MAT) (Methionine adenosyltransferase)	0.5	1
A0A0H3DYV3	Alpha-phosphoglucomutase	0.5	1
A0A0H3E662	Lysine--tRNA ligase (EC 6.1.1.6) (Lysyl-tRNA synthetase)	0.5	1
A0A0H3E0A3	L-threonine dehydratase (EC 4.3.1.19) (Threonine deaminase)	0.5	1
A0A0H3E5Y1	Cysteine desulfurase (EC 2.8.1.7)	0.5	1
A0A0H3E6C9	Enolase (EC 4.2.1.11) (2-phospho-D-glycerate hydro-lyase) (2-phosphoglycerate dehydratase)	0.5	1.7
A0A0H3E0L2	Dihydrolipoyl dehydrogenase (EC 1.8.1.4)	0.5	1.7
A0A0H3E5M0	Probable glycine dehydrogenase (decarboxylating) subunit 2 (EC 1.4.4.2)	0.5	1.7
A0A0H3E612	Cysteine synthase (EC 2.5.1.47)	0.5	1.7
A0A0H3E0P3	Uncharacterized protein	0.5	1.7
A0A0H3DZ16	Putative ribosome biogenesis GTPase RsgA (EC 3.6.1.-)	0.5	1.7
A0A0H3E1C7	Glutamine synthetase (EC 6.3.1.2)	0.5	1.7
A0A0H3E034	Purine nucleoside phosphorylase DeoD-type (PNP) (EC 2.4.2.1)	0.6	1.7
A0A0H3E355	8-amino-7-oxononanoate synthase (EC 2.3.1.47)	0.6	1.7
A0A0H3E4P8	Succinate dehydrogenase flavoprotein subunit (EC 1.3.99.1)	0.6	1.7

A0A0H3E9S3	ClpC	0.6	1.7
A0A0H3E1I5	Translation initiation factor IF-2	0.6	1.7
A0A0H3E650	Elongation factor Tu (EF-Tu)	0.6	1.7
A0A0H3E6D5	Glyceraldehyde-3-phosphate dehydrogenase (EC 1.2.1.-)	0.6	1.7
A0A0H3DYF7	Iron-dicitrate ABC transporter (Binding lipoprotein)	0.6	1.7
A0A0H3E013	GMP synthase [glutamine-hydrolyzing] (EC 6.3.5.2) (GMP synthetase) (Glutamine amidotransferase)	0.6	1.7
A0A0H3E918	Phosphoglucosamine mutase (EC 5.4.2.10)	0.6	1.7
A0A0H3DZZ3	Putative 6-phosphogluconolactonase	0.6	1.7
A0A0H3E6M2	Flagellin	0.6	1.7
A0A0H3E8R6	ATP-dependent zinc metalloprotease FtsH (EC 3.4.24.-)	0.6	1.7
A0A0H3E4H7	Glutamate-1-semialdehyde 2,1-aminomutase (GSA) (EC 5.4.3.8) (Glutamate-1-semialdehyde aminotransferase)	0.6	1.7
A0A0H3E9M0	Putative iron-siderophore ABC transporter (Binding lipoprotein)	0.6	1.7
A0A0H3E5V0	Homoserine dehydrogenase (EC 1.1.1.3)	0.6	1.7
A0A0H3DYE2	UDP-N-acetylmuramoyl-L-alanyl-D-glutamate--2,6-diaminopimelate ligase (EC 6.3.2.13)	0.6	1.7
A0A0H3E2D5	Acetate kinase (EC 2.7.2.1) (Acetokinase)	0.6	1.7
A0A0H3E699	Elongation factor G (EF-G)	0.6	1.7
A0A0H3E320	Putative phosphotransferase system enzyme IIA component	0.6	1.7
A0A0H3E2H3	Dihydrolipoyl dehydrogenase (EC 1.8.1.4)	0.6	2.2
A0A0H3E6T6	Putative acyl-coenzyme A synthetase	0.6	2.2
A0A0H3E1G4	4-hydroxy-3-methylbut-2-en-1-yl diphosphate synthase (EC 1.17.7.1) (1-hydroxy-2-methyl-2-(E)-butenyl 4-diphosphate synthase)	0.6	2.2
A0A0H3DVR8	Glutamyl-tRNA(Gln) amidotransferase subunit A (Glu-ADT subunit A) (EC 6.3.5.7)	0.6	2.2
A0A0H3E0E1	Pyruvate dehydrogenase (E1 subunit beta)	0.6	2.2
A0A0H3E6R7	Acetyl-coenzyme A carboxylase carboxyl transferase subunit beta (ACCase subunit beta) (Acetyl-CoA carboxylase carboxyltransferase subunit beta) (EC 6.4.1.2)	0.7	2.2

A0A0H3E609	Metalloregulation DNA-binding stress protein	0.7	2.2
A0A0H3E2Y1	3-phosphoshikimate 1-carboxyvinyltransferase (EC 2.5.1.19) (5-enolpyruvylshikimate-3-phosphate synthase)	0.7	2.2
A0A0H3E1Q0	Superoxide dismutase (Fragment)	0.7	2.2
A0A0H3E075	Phosphocarrier protein HPr	0.7	2.2
A0A0H3E2D8	Putative 2-cys peroxiredoxin	0.7	2.2
A0A0H3DZD3	Putative processing protease	0.7	2.2
A0A0H3E0L9	Cryptic glutamate dehydrogenase	0.7	2.2
A0A0H3E668	Glycosyltransferase	0.7	2.2
A0A0H3E6F8	Probable GTP-binding protein EngB	0.7	3.4
A0A0H3DZN4	Acyl-CoA dehydrogenase	0.7	3.4
A0A0H3E8Y2	DNA-directed RNA polymerase subunit alpha (RNAP subunit alpha) (EC 2.7.7.6) (RNA polymerase subunit alpha) (Transcriptase subunit alpha)	0.7	3.4
A0A0H3E8V4	50S ribosomal protein L7/L12	0.7	3.4
A0A0H3E5Y4	Methionine--tRNA ligase (EC 6.1.1.10) (Methionyl-tRNA synthetase)	0.8	3.4
A0A0H3E3H2	YurY	0.8	3.4
A0A0H3E900	Mrp family regulator	0.8	3.4
A0A0H3E642	DNA-directed RNA polymerase subunit beta' (RNAP subunit beta') (EC 2.7.7.6) (RNA polymerase subunit beta') (Transcriptase subunit beta')	0.8	3.4
A0A0H3DWB6	Putative iron(III) dicitrate transporter binding lipoprotein	0.8	3.4
A0A0H3E7F4	FeS assembly protein SufD	0.8	3.4
A0A0H3E6W1	Putative thiol-disulfide oxidoreductase with thioredoxin domain	0.8	3.4
A0A0H3E4H6	Uncharacterized protein	0.8	3.4
A0A0H3E0X6	Non-specific DNA-binding protein HBsu signal recognition particle-like (SRP) component	0.8	3.4
A0A0H3DY27	Bifunctional purine biosynthesis protein PurH	0.8	3.4
A0A0H3DXT3	Gamma-glutamyl phosphate reductase (GPR) (EC 1.2.1.41) (Glutamate-5-semialdehyde dehydrogenase) (Glutamyl-gamma-semialdehyde dehydrogenase)	0.8	3.4
A0A0H3DWG0	Aspartyl/glutamyl-tRNA(Asn/Gln) amidotransferase subunit B (Asp/Glu-ADT subunit B) (EC 6.3.5.-)	0.8	3.4
A0A0H3E4K7	Site-determining protein	0.9	3.4

A0A0H3E932	Methylmalonate semialdehyde dehydrogenase [acylating] (MMSA dehydrogenase) (MMSDH) (MSDH) (EC 1.2.1.27) (Malonate semialdehyde dehydrogenase [acetylating])	0.9	3.4

Table S10: Complete list of *P. putida* proteins significantly more abundant during co-culture with *B. atrophaeus*. The heading "Co/Pure" refers to the ratio of precursor ion intensity for that protein in the co-culture compared with a pure culture. The q-value is the statistical indicator of significance, after adjustment for multiple testing (q < 5% indicates statistical significance).

Uniprot ID	**Protein names**	**Co/Pure**	**q-value(%)**
Q88QH5	N utilization substance protein B homolog (Protein NusB)	4.2	0.0
Q88N80	UDP-N-acetylmuramoyl-tripeptide--D-alanyl-D-alanine ligase (EC 6.3.2.10)	3.7	0.0
Q88N72	Cell division protein ftsA	3.6	0.0
Q88F51	UPF0345 protein PP_4248	3.5	0.0
Q88FN1	1,4-alpha-glucan branching enzyme GlgB (EC 2.4.1.18) (1,4-alpha-D-glucan:1,4-alpha-D-glucan 6-glucosyl-transferase) (Alpha-(1->4)-glucan branching enzyme) (Glycogen branching enzyme) (BE)	3.5	0.0
Q88DG3	Oxidoreductase, short chain dehydrogenase/reductase family	3.4	0.0
Q88RD0	CBS domain protein	3.4	0.0
Q88EI2	Arginine N-succinyltransferase (EC 2.3.1.109)	3.3	0.0
Q88GY1	RND transporter, membrane fusion protein	3.3	0.0
Q88PB9	Glutamyl-tRNA(Gln) amidotransferase subunit A (Glu-ADT subunit A) (EC 6.3.5.7)	3.3	0.0
Q88QA3	Adenine deaminase (ADE) (EC 3.5.4.2) (Adenine aminohydrolase) (AAH)	3.2	0.0
Q88KQ2	Peptidase, M24 family protein	3.2	0.0

Q88DX1	Poly(A) polymerase I (PAP I) (EC 2.7.7.19)	3.1	0.0
Q88FM9	Alpha-1,4-glucan:maltose-1-phosphate maltosyltransferase (GMPMT) (EC 2.4.99.16) ((1->4)-alpha-D-glucan:maltose-1-phosphate alpha-D-maltosyltransferase)	3.0	0.0
Q88HA6	Transcriptional regulatory protein RstA, putative	3.0	0.0
Q88LD5	Amidophosphoribosyltransferase (ATase) (EC 2.4.2.14) (Glutamine phosphoribosylpyrophosphate amidotransferase)	2.9	0.0
Q88FI4	Elongation factor G 2 (EF-G 2)	2.9	0.0
Q88NY2	Amino acid ABC transporter, periplasmic amino acid-binding protein	2.8	0.0
Q88IC0	Peptidyl-prolyl cis-trans isomerase C	2.7	0.0
Q88K22	Phenylalanine--tRNA ligase beta subunit (EC 6.1.1.20) (Phenylalanyl-tRNA synthetase beta subunit) (PheRS)	2.7	0.0
Q88C80	Endoribonuclease	2.6	0.0
Q88LB8	Aminopeptidase N	2.6	0.0
Q88DK8	MaoC domain protein	2.5	0.0
Q88RN3	Oligopeptidase A	2.3	0.0
Q88K24	50S ribosomal protein L20	2.3	0.0
Q88EY5	Phenazine biosynthesis protein, PhzF family	2.3	0.0
Q88MD8	DNA-binding response regulator	2.3	0.0
Q88QM3	50S ribosomal protein L5	2.3	0.0
Q88PT6	Glycerate dehydrogenase	2.3	0.0
Q88HT2	Phenylacetic acid-specific porin	2.3	0.0
Q88DR1	Acyl-CoA thioesterase II	2.3	0.0
Q88CY9	Fructose-1,6-bisphosphatase class 1 (FBPase class 1) (EC 3.1.3.11) (D-fructose-1,6-bisphosphate 1-phosphohydrolase class 1)	2.2	0.0
Q88DB9	Phosphatidylserine decarboxylase proenzyme (EC 4.1.1.65) [Cleaved into: Phosphatidylserine decarboxylase alpha chain; Phosphatidylserine decarboxylase beta chain]	2.2	0.0
Q88FI2	Uncharacterized protein	2.2	0.0

Q88QG7	1-deoxy-D-xylulose-5-phosphate synthase (EC 2.2.1.7) (1-deoxyxylulose-5-phosphate synthase) (DXP synthase) (DXPS)	2.2	0.0
Q88FN6	Glycosyl hydrolase, putative	2.1	0.0
Q88DV6	N utilization substance protein A	2.1	0.0
P59351	UPF0229 protein PP_0396	2.1	0.0
Q88N94	Cytochrome b	2.1	0.0
Q88IA0	Uncharacterized protein	2.0	0.0
Q88R35	Uncharacterized protein	1.9	0.0
Q88I11	Threonine dehydratase family protein	1.9	0.0
Q88HS2	Phenylacetic acid degradation protein PaaI, putative	1.9	0.0
Q88QD6	Acetyl-CoA carboxylase, biotin carboxylase	1.9	0.0
Q88DP5	AMP nucleosidase	1.9	0.0
Q88LX0	2-dehydro-3-deoxyphosphooctonate aldolase 2 (EC 2.5.1.55) (3-deoxy-D-manno-octulosonic acid 8-phosphate synthase 2) (KDO-8-phosphate synthase 2) (KDO 8-P synthase 2) (KDOPS 2) (Phospho-2-dehydro-3-deoxyoctonate aldolase 2)	1.8	0.0
Q88IQ5	Histidine kinase (EC 2.7.13.3)	1.8	0.0
Q88EW4	Histidine kinase (EC 2.7.13.3)	1.8	0.0
Q88M42	Site-determining protein	1.8	0.0
Q88C93	Phosphomannomutase/phosphoglucomutase (PMM / PGM) (EC 5.4.2.2) (EC 5.4.2.8)	1.8	0.0
Q88HT3	Ring-opening enzyme	1.8	0.0
Q88LR1	ATP-dependent RNA helicase DeaD (EC 3.6.4.13) (Cold-shock DEAD box protein A)	1.7	0.0
Q88HS1	3-hydroxyacyl-CoA dehydrogenase PaaC	1.7	0.0
Q88LF6	Glutamate--tRNA ligase (EC 6.1.1.17) (Glutamyl-tRNA synthetase) (GluRS)	1.7	0.0
Q88EI5	N-succinylarginine dihydrolase (EC 3.5.3.23)	1.7	0.0
Q88KI0	Methyl-accepting chemotaxis transducer	1.7	0.0
Q88KZ0	Glyceraldehyde-3-phosphate dehydrogenase (EC 1.2.1.-)	1.7	0.0

Q88FF3	Hydroxyacylglutathione hydrolase (EC 3.1.2.6) (Glyoxalase II) (Glx II)	1.6	0.5
Q88QD9	Acetoin dehydrogenase, alpha subunit	1.6	0.5
Q88DU4	4-hydroxy-tetrahydrodipicolinate reductase (HTPA reductase) (EC 1.17.1.8)	1.6	0.5
Q88C18	Cyclopropane-fatty-acyl-phospholipid synthase, putative	1.6	0.5
Q88P97	Uncharacterized protein	1.6	0.5
Q88E33	Putative reductase PP_4635 (EC 1.3.1.-)	1.6	0.5
Q88EW5	Chemotaxis response regulator protein-glutamate methylesterase of group 1 operon (EC 3.1.1.61)	1.5	0.5
Q88CT5	Pyrroline-5-carboxylate reductase (EC 1.5.1.2)	1.5	0.5
Q88QM2	30S ribosomal protein S14	1.5	0.5
Q88BX1	ATP synthase subunit delta (ATP synthase F(1) sector subunit delta) (F-type ATPase subunit delta) (F-ATPase subunit delta)	1.5	0.5
Q88RK2	Thiol:disulfide interchange protein	1.5	0.5
Q88DF8	Branched-chain amino acid ABC transporter, periplasmic amino acid-binding protein	1.5	0.5
Q88IU0	Protein CsiD	1.5	0.5
Q88EW3	Protein phosphatase CheZ (EC 3.1.3.-) (Chemotaxis protein CheZ)	1.4	0.5
Q88F24	Cell division protein ZipA homolog	1.4	0.5
Q88EX0	Purine-binding chemotaxis protein CheW	1.4	0.5
Q88GE6	Pyrroline-5-carboxylate reductase	1.4	0.5
Q88H69	Acyl-CoA dehydrogenase	1.4	0.5
Q88GF8	Lactoylglutathione lyase (EC 4.4.1.5) (Glyoxalase I)	1.4	0.5
Q88QR3	Uncharacterized protein	1.4	0.5
Q88NN0	Ribonucleoside-diphosphate reductase subunit beta (EC 1.17.4.1)	1.4	0.5
Q88LY9	Uncharacterized protein	1.4	0.5
Q88P65	Glycine dehydrogenase (decarboxylating) 1 (EC 1.4.4.2) (Glycine cleavage system P-protein 1) (Glycine decarboxylase 1) (Glycine dehydrogenase (aminomethyl-transferring) 1)	1.4	0.5

Q88DE9	30S ribosomal protein S18	1.4	0.9
Q88C91	Catabolite repression control protein	1.3	0.9
Q88DD6	Protein HflC	1.3	0.9
Q88QH1	GTP cyclohydrolase-2 (EC 3.5.4.25) (GTP cyclohydrolase II)	1.3	0.9
Q88LR9	Organic hydroperoxide resistance protein	1.3	0.9
Q88Q95	30S ribosomal protein S20	1.3	0.9
Q88L15	Molybdenum cofactor biosynthesis protein B	1.3	0.9
Q88PS5	OmpA family protein	1.3	0.9
Q88MH4	1-deoxy-D-xylulose 5-phosphate reductoisomerase (DXP reductoisomerase) (EC 1.1.1.267) (1-deoxyxylulose-5-phosphate reductoisomerase) (2-C-methyl-D-erythritol 4-phosphate synthase)	1.3	0.9
Q88MF9	Enolase (EC 4.2.1.11) (2-phospho-D-glycerate hydro-lyase) (2-phosphoglycerate dehydratase)	1.3	1.3
Q88LH4	Uncharacterized protein	1.3	1.3
Q88MT2	Polyamine ABC transporter, periplasmic polyamine-binding protein	1.3	1.3
Q88QV1	Tryptophan 2-monooxygenase, putative	1.3	1.3
Q88CS6	Thiazole synthase (EC 2.8.1.10)	1.2	1.3
Q88PL2	Extragenic suppressor protein SuhB	1.2	1.3
Q88KP3	Endoribonuclease, putative	1.2	1.3
Q88PJ7	4-hydroxy-3-methylbut-2-en-1-yl diphosphate synthase (flavodoxin) (EC 1.17.7.3) (1-hydroxy-2-methyl-2-(E)-butenyl 4-diphosphate synthase)	1.2	1.3
Q88GX6	Malate dehydrogenase, putative	1.2	1.3
Q88DY9	Acetolactate synthase, small subunit	1.2	1.3
Q88FH3	NADH dehydrogenase I, F subunit	1.2	1.4
Q88D21	Polyhydroxyalkanoate granule-associated protein GA2	1.2	1.4
Q88QD0	Uncharacterized protein	1.2	1.4
Q88KS6	Acyl-CoA ligase	1.2	1.4
Q88CX4	2,3-bisphosphoglycerate-independent phosphoglycerate mutase (BPG-independent PGAM)	1.2	1.4

	(Phosphoglyceromutase) (iPGM) (EC 5.4.2.12)		
Q88FI0	Isocitrate lyase	1.1	2.1
Q88N78	UDP-N-acetylmuramoylalanine--D-glutamate ligase (EC 6.3.2.9) (D-glutamic acid-adding enzyme) (UDP-N-acetylmuramoyl-L-alanyl-D-glutamate synthetase)	1.1	2.1
Q88CG1	Enhancing lycopene biosynthesis protein 2	1.1	2.1
Q88RA6	Cysteine ABC transporter, periplasmic cysteine-binding protein, putative	1.1	2.1
P0A147	Ribosome hibernation promoting factor	1.1	2.1
P59604	Argininosuccinate synthase (EC 6.3.4.5) (Citrulline--aspartate ligase)	1.1	2.1
Q88N36	3-oxoadipate enol-lactone hydrolase	1.1	2.1
Q88NW6	Outer membrane protein, OmpA family	1.1	2.1
Q88QE0	Acetoin dehydrogenase, beta subunit	1.1	2.1
Q88EI7	Succinylglutamate desuccinylase (EC 3.5.1.96)	1.1	2.1
Q88P99	ABC transporter, ATP-binding protein, putative	1.0	2.7
Q88NG9	Phosphoribosylaminoimidazole-succinocarboxamide synthase (EC 6.3.2.6) (SAICAR synthetase)	1.0	2.7
Q88CW0	ParA family protein	1.0	2.7
Q88D48	ATP-dependent RNA helicase RhlE (EC 3.6.4.13)	1.0	2.7
Q88LX8	GDP-mannose 4,6-dehydratase (EC 4.2.1.47) (GDP-D-mannose dehydratase)	1.0	2.7
Q88CY3	Glutamine synthetase (EC 6.3.1.2)	1.0	2.7
Q88KI3	Uncharacterized protein	1.0	2.7
Q88QB3	3-oxoacyl-(Acyl-carrier-protein) reductase	1.0	2.7
Q88P16	Phosphoribosylformylglycinamidine synthase (FGAM synthase) (FGAMS) (EC 6.3.5.3) (Formylglycinamide ribonucleotide amidotransferase) (FGAR amidotransferase) (FGAR-AT)	1.0	2.7
Q88PT3	Uncharacterized protein	1.0	3.7

Q88EI9	Aspartate kinase (EC 2.7.2.4) (Aspartokinase)	0.9	3.7
Q88MG0	2-dehydro-3-deoxyphosphooctonate aldolase 1 (EC 2.5.1.55) (3-deoxy-D-manno-octulosonic acid 8-phosphate synthase 1) (KDO-8-phosphate synthase 1) (KDO 8-P synthase 1) (KDOPS 1) (Phospho-2-dehydro-3-deoxyoctonate aldolase 1)	0.9	3.7
Q88RM9	Carbonic anhydrase (EC 4.2.1.1)	0.9	3.7
Q88R26	Dipeptidase, putative	0.9	3.7
Q88PY7	Hydrolase, isochorismatase family	0.9	3.7
Q88L37	D-alanyl-D-alanine carboxypeptidase	0.9	3.7
Q88GI8	ABC transporter, permease protein, putative	0.9	3.7
Q88GT0	Acyl-CoA dehydrogenase, putative	0.9	3.7
Q88M00	Mannose-6-phosphate isomerase/mannose-1-phosphate guanylyltransferase	0.9	3.7
Q88DY8	Acetolactate synthase, large subunit, biosynthetic type	0.9	3.7
Q88NJ7	DNA-binding stress protein, putative	0.9	3.7
Q88CT7	Type IV pili twitching motility protein PilT	0.9	3.7
Q88K52	Alkyl hydroperoxide reductase, C subunit	0.9	3.7

Table S11: Complete list of *P. putida* proteins significantly less abundant during co-culture with *B. atrophaeus*. The heading "Co/Pure" refers to the ratio of precursor ion intensity for that protein in the co-culture compared with a pure culture. The q-value is the statistical indicator of significance, after adjustment for multiple testing ($q < 5\%$ indicates statistical significance)

Uniprot ID	**Protein Name**	**Co/Pure**	**Q-value(%)**
Q88P34	Porin B	0.4	0.0
Q88KX8	Uncharacterized protein	0.4	0.0
Q88QZ5	Pyruvate dehydrogenase E1 component (EC 1.2.4.1)	0.4	0.0

Q88GS9	Alkyl hydroperoxide reductase AhpD (EC 1.11.1.15)	0.4	0.0
Q88PJ3	GTPase Der (GTP-binding protein EngA)	0.4	0.7
Q88KV0	Uncharacterized protein	0.4	0.7
Q88QN5	50S ribosomal protein L3	0.5	0.7
Q88QZ6	Acetyltransferase component of pyruvate dehydrogenase complex (EC 2.3.1.12)	0.5	0.7
Q88P38	Sugar ABC transporter, periplasmic sugar-binding protein	0.5	0.7
Q88FB2	Succinyl-CoA ligase [ADP-forming] subunit beta (EC 6.2.1.5) (Succinyl-CoA synthetase subunit beta) (SCS-beta)	0.5	0.7
Q88P52	Arginine deiminase (ADI) (EC 3.5.3.6) (Arginine dihydrolase) (AD)	0.5	0.7
Q88GV6	Uncharacterized protein	0.5	0.7
Q88N81	UDP-N-acetylmuramoyl-L-alanyl-D-glutamate--2,6-diaminopimelate ligase (EC 6.3.2.13) (Meso-A2pm-adding enzyme) (Meso-diaminopimelate-adding enzyme) (UDP-MurNAc-L-Ala-D-Glu:meso-diaminopimelate ligase) (UDP-MurNAc-tripeptide synthetase) (UDP-N-acetylmuramyl-tripeptide synthetase)	0.5	0.7
Q88R06	Formaldehyde dehydrogenase, glutathione-independent	0.5	0.7
Q88ES5	Flagellin FliC	0.5	0.7
Q88LS0	Elongation factor P (EF-P)	0.5	0.7
Q88P67	Aminomethyltransferase (EC 2.1.2.10)	0.5	0.7
Q88MU0	Xenobiotic reductase, putative	0.5	0.7
Q88LC9	Uncharacterized protein	0.6	0.7
Q88I79	CoA-transferase, subunit A, putative	0.6	0.7
Q88FB3	Succinyl-CoA ligase [ADP-forming] subunit alpha (EC 6.2.1.5)	0.6	0.7
Q88IX4	Uncharacterized protein	0.6	0.7
Q88PP2	Surface adhesion protein, putative	0.6	0.9
Q88QP4	50S ribosomal protein L1	0.6	0.9
Q88DU2	Chaperone protein DnaK (HSP70) (Heat shock 70 kDa protein) (Heat shock protein 70)	0.6	0.9
Q88DF1	50S ribosomal protein L9	0.6	1.3
Q88HB7	Glyceraldehyde-3-phosphate dehydrogenase, putative	0.6	1.3
Q88MI0	30S ribosomal protein S2	0.6	1.3
Q88G86	Alcohol dehydrogenase, zinc-containing	0.6	1.3
Q88PT2	Uncharacterized protein	0.6	1.3

Q88QM1	30S ribosomal protein S8	0.7	1.3
Q88NR0	RNA polymerase-associated protein RapA (EC 3.6.4.-) (ATP-dependent helicase HepA)	0.7	1.3
Q88LE7	3-isopropylmalate dehydratase small subunit (EC 4.2.1.33) (Alpha-IPM isomerase) (IPMI) (Isopropylmalate isomerase)	0.7	1.4
Q88PN2	Aminotransferase, class I	0.7	1.4
Q88RD8	Alginate regulatory protein AlgP	0.7	1.4
Q88CI8	Glycine cleavage system H protein 2	0.7	1.4
Q88HW9	Heat shock protein, HSP20 family	0.7	1.4
Q88FS2	Isocitrate dehydrogenase [NADP] (EC 1.1.1.42)	0.7	1.4
Q88IM2	Tn4652, transposase subunit B	0.7	1.4
Q88QM0	50S ribosomal protein L6	0.7	1.4
Q88M20	Fumarate hydratase class II (Fumarase C) (EC 4.2.1.2)	0.7	1.4
Q88MY8	Alginate biosynthesis negative regulator, serine protease AlgY	0.7	1.4
Q88CG4	Polyphosphate kinase (EC 2.7.4.1) (ATP-polyphosphate phosphotransferase) (Polyphosphoric acid kinase)	0.7	1.4
Q88FB1	Dihydrolipoyl dehydrogenase (EC 1.8.1.4)	0.7	1.4
Q88PB7	Rod shape-determining protein MreB	0.7	1.4
Q88P78	DNA-binding protein HU, form N	0.7	1.4
Q88FF8	Chromate reductase (CHRR) (EC 1.6.5.2) (NAD(P)H dehydrogenase (quinone))	0.7	2.1
Q88BX4	ATP synthase subunit beta (EC 3.6.3.14) (ATP synthase F1 sector subunit beta) (F-ATPase subunit beta)	0.7	2.1
P0A171	RNA polymerase sigma-54 factor	0.7	2.1
Q88HS4	Phenylacetate-coenzyme A ligase (EC 6.2.1.30) (Phenylacetyl-CoA ligase)	0.7	2.1
Q88DU1	Protein GrpE (HSP-70 cofactor)	0.7	2.1
Q59692	Cell division protein FtsZ	0.8	2.1
Q88P88	UDP-N-acetylglucosamine 1-carboxyvinyltransferase (EC 2.5.1.7) (Enoylpyruvate transferase) (UDP-N-acetylglucosamine enolpyruvyl transferase) (EPT)	0.8	2.1
Q88N54	Pyruvate kinase (EC 2.7.1.40)	0.8	2.1
Q88QN7	Elongation factor Tu-B (EF-Tu-B)	0.8	2.1
Q88EE8	Uncharacterized protein	0.8	2.1
Q88QP8	Elongation factor Tu-A (EF-Tu-A)	0.8	2.1

Q88N55	60 kDa chaperonin (GroEL protein) (Protein Cpn60)	0.8	2.1
Q88RB8	Response regulator	0.8	2.1
Q88QP3	50S ribosomal protein L10	0.8	2.1
Q88QN9	30S ribosomal protein S7	0.8	2.1
Q877U6	Acetolactate synthase, catabolic, putative	0.8	2.1
Q88F95	Electron transfer flavoprotein-ubiquinone oxidoreductase, putative	0.8	2.1
Q88QR6	Indole-3-glycerol phosphate synthase (IGPS) (EC 4.1.1.48)	0.8	2.1
Q88HS3	Beta-ketoadipyl CoA thiolase PhaD	0.8	2.1
Q88PX7	50S ribosomal protein L25 (General stress protein CTC)	0.8	2.1
Q88PJ6	Histidine--tRNA ligase (EC 6.1.1.21) (Histidyl-tRNA synthetase) (HisRS)	0.8	2.1
Q88P31	Glucose-6-phosphate 1-dehydrogenase (G6PD) (EC 1.1.1.49)	0.8	2.1
Q88FQ0	Dihydroorotate dehydrogenase family protein	0.8	2.7
Q88CV2	3-dehydroquinate synthase (EC 4.2.3.4)	0.8	2.7
Q88RR9	Glycine--tRNA ligase beta subunit (EC 6.1.1.14) (Glycyl-tRNA synthetase beta subunit) (GlyRS)	0.8	2.7
Q88JK1	Universal stress protein family	0.8	2.7
Q88QN2	50S ribosomal protein L2	0.8	2.7
Q88IQ2	Transcriptional regulator MvaT, P16 subunit, putative	0.8	2.7
Q88PG8	Dipeptide ABC transporter, periplasmic dipeptide-binding protein	0.8	2.7
Q88LG1	Aromatic-amino-acid aminotransferase	0.8	2.7
Q88EH6	Acetyl-coenzyme A synthetase 1 (AcCoA synthetase 1) (Acs 1) (EC 6.2.1.1) (Acetate--CoA ligase 1) (Acyl-activating enzyme 1)	0.8	2.7
Q88P44	Glyceraldehyde-3-phosphate dehydrogenase (EC 1.2.1.-)	0.8	2.7
Q88QN3	50S ribosomal protein L23	0.9	2.7
Q88D47	UPF0312 protein PP_4981	0.9	2.7
Q88GK1	NAD(P)H quinone oxidoreductase, putative	0.9	2.7
Q88P95	Arabinose 5-phosphate isomerase (API) (EC 5.3.1.13)	0.9	2.7
Q88GF9	Transcriptional regulator MvaT, P16 subunit, putative	0.9	2.7

Q88KV5	Formate dehydrogenase, beta subunit, putative	0.9	2.7
Q88P53	Ornithine carbamoyltransferase, catabolic (OTCase) (EC 2.1.3.3)	0.9	2.7
P59400	Histidinol dehydrogenase (HDH) (EC 1.1.1.23)	0.9	2.7
Q88PD6	GGDEF domain protein	0.9	2.7
Q88MH8	Uridylate kinase (UK) (EC 2.7.4.22) (Uridine monophosphate kinase) (UMP kinase) (UMPK)	0.9	2.7
Q88C30	Uncharacterized protein	0.9	2.7
Q88NT3	OmpA family protein	0.9	2.7
Q88MH9	Elongation factor Ts (EF-Ts)	0.9	2.7
Q88GQ0	Catalase-peroxidase (CP) (EC 1.11.1.21) (Peroxidase/catalase)	0.9	2.7
Q88KJ8	Uncharacterized protein	0.9	2.7
Q88D03	Glucans biosynthesis protein G	0.9	2.7
Q88M08	DNA gyrase subunit A (EC 5.99.1.3)	0.9	2.7
Q88QW6	Acyl-CoA dehydrogenase, putative	0.9	2.7
Q88GX7	Aromatic-amino-acid aminotransferase	0.9	2.7
Q88HC9	ThiJ/PfpI family protein	0.9	2.7
Q88Q10	50S ribosomal protein L21	0.9	2.7
Q88CU5	Malic enzyme	0.9	2.7
P0A120	DNA polymerase III subunit beta (EC 2.7.7.7)	0.9	2.7
Q88P54	Carbamate kinase	0.9	2.7
Q88P91	Toluene-tolerance protein	0.9	2.7
Q88MU8	Homoserine dehydrogenase (EC 1.1.1.3)	0.9	2.7
Q88CE7	Nitrogen regulatory protein P-II	0.9	3.7
P0A157	50S ribosomal protein L7/L12	1.0	3.7
Q88QZ4	Glutamate-ammonia-ligase adenylyltransferase (EC 2.7.7.42) (Glutamine-synthetase adenylyltransferase) (ATase) ([Glutamate--ammonia-ligase] adenylyltransferase)	1.0	3.7
Q88MB5	Uncharacterized protein	1.0	3.7
Q88N93	Ubiquinol--cytochrome c reductase, cytochrome c1	1.0	3.7
Q88MD5	Ferredoxin--NADP reductase	1.0	3.7
Q88CZ0	Uncharacterized protein	1.0	3.7
P59560	UPF0234 protein PP_1352	1.0	3.7
Q88E32	Beta-ketothiolase	1.0	3.7

Q88QF6	Inorganic pyrophosphatase (EC 3.6.1.1) (Pyrophosphate phospho-hydrolase) (PPase)	1.0	3.7
Q88RW2	Transcriptional regulator MvaT, P16 subunit, putative	1.0	3.7
Q88NW9	Antioxidant, AhpC/Tsa family	1.0	3.7
Q88QM8	50S ribosomal protein L16	1.0	3.7
Q88PD5	Superoxide dismutase [Fe] (EC 1.15.1.1)	1.0	3.7
P0A0Z9	Amino-acid acetyltransferase (EC 2.3.1.1) (N-acetylglutamate synthase) (AGS) (NAGS)	1.1	3.7

Table S12: KEGG categorization of *B. atrophaeus* significantly more or less abundant during co-culture with *P. putida*. Gene Ontology categories are also included for reference.

Uniprot ID	**Protein Name**	**Co/ Pure**	**Q-value (%)**	**Gene Ontology**	**KEGG**
Nucleotide Metabolism					
A0A0H3E705	Putative phosphatase	8.7	0	Integral component of membrane [GO:0016021]; magnesium ion binding [GO:0000287]; phosphatase activity [GO:0016791]	Purine metabolism
A0A0H3E399	GMP reductase (EC 1.7.1.7) (Guanosine 5'-monophosphate oxidoreductase)	7.6	0	GMP reductase activity [GO:0003920]; GMP reductase complex [GO:1902560]; purine nucleotide metabolic process [GO:0006163]	Purine metabolism
A0A0H3E4S8	DNA polymerase (EC 2.7.7.7)	6.9	0	3'-5' exonuclease activity [GO:0008408]; DNA binding [GO:0003677]; DNA-dependent DNA replication [GO:0006261]; DNA-directed DNA polymerase activity	Purine metabolism

				[GO:0003887]; DNA repair [GO:0006281]	
A0A0H3E4S8	DNA polymerase (EC 2.7.7.7)	6.9	0	3'-5' exonuclease activity [GO:0008408]; DNA binding [GO:0003677]; DNA-dependent DNA replication [GO:0006261]; DNA-directed DNA polymerase activity [GO:0003887]; DNA repair [GO:0006281]	Pyrimidine metabolism
A0A0H3DYE3	Phosphoribosylamine--glycine ligase (EC 6.3.4.13) (GARS) (Glycinamide ribonucleotide synthetase) (Phosphoribosylglycinamide synthetase)	6.8	0	'de novo' IMP biosynthetic process [GO:0006189]; ATP binding [GO:0005524]; magnesium ion binding [GO:0000287]; manganese ion binding [GO:0030145]; phosphoribosylamine-glycine ligase activity [GO:0004637]; purine nucleobase biosynthetic process [GO:0009113]	Purine metabolism
A0A0H3E251	Non-canonical purine NTP pyrophosphatase (EC 3.6.1.19) (Non-standard purine NTP pyrophosphatase) (Nucleoside-triphosphate diphosphatase) (Nucleoside-triphosphate pyrophosphatase)	6.6	0	metal ion binding [GO:0046872]; nucleoside-triphosphatase activity [GO:0017111]; nucleoside triphosphate catabolic process [GO:0009143]; nucleoside-triphosphate diphosphatase activity [GO:0047429]; nucleotide binding [GO:0000166]; purine nucleotide metabolic process [GO:0006163]	Purine metabolism
A0A0H3E251	Non-canonical purine NTP pyrophosphatase (EC 3.6.1.19) (Non-standard purine NTP pyrophosphatase) (Nucleoside-triphosphate diphosphatase) (Nucleoside-	6.6	0	metal ion binding [GO:0046872]; nucleoside-triphosphatase activity [GO:0017111]; nucleoside triphosphate catabolic process [GO:0009143]; nucleoside-triphosphate diphosphatase activity [GO:0047429]; nucleotide binding [GO:0000166];	Pyrimidine metabolism

	triphosphate pyrophosphatase)			purine nucleotide metabolic process [GO:0006163]	
A0A0H3E6C1	Adenylate kinase (AK) (EC 2.7.4.3) (ATP-AMP transphosphorylase) (ATP:AMP phosphotransferase) (Adenylate monophosphate kinase)	5.7	0	adenylate kinase activity [GO:0004017]; ATP binding [GO:0005524]; cytoplasm [GO:0005737]; nucleotide biosynthetic process [GO:0009165]	Purine metabolism
A0A0H3DYI0	Carbamoyl-phosphate synthase (glutamine-hydrolyzing) (EC 6.3.5.5)	4.6	0	'de novo' UMP biosynthetic process [GO:0044205]; arginine biosynthetic process [GO:0006526]; ATP binding [GO:0005524]; carbamoyl-phosphate synthase (glutamine-hydrolyzing) activity [GO:0004088]; metal ion binding [GO:0046872]	Pyrimidine metabolism
A0A0H3E9P3	Ribose-phosphate pyrophosphokinase (RPPK) (EC 2.7.6.1) (5-phospho-D-ribosyl alpha-1-diphosphate) (Phosphoribosyl diphosphate synthase) (Phosphoribosyl pyrophosphate synthase)	2.8	0.5	ATP binding [GO:0005524]; cytoplasm [GO:0005737]; kinase activity [GO:0016301]; magnesium ion binding [GO:0000287]; nucleotide biosynthetic process [GO:0009165]; ribonucleoside monophosphate biosynthetic process [GO:0009156]; ribose phosphate diphosphokinase activity [GO:0004749]	Purine metabolism
A0A0H3E901	Pyrimidine-nucleoside phosphorylase (EC 2.4.2.2)	2	1.7	phosphorylase activity [GO:0004645]; pyrimidine nucleobase metabolic process [GO:0006206]; pyrimidine nucleoside metabolic process [GO:0006213]; pyrimidine-nucleoside phosphorylase activity [GO:0016154]	Pyrimidine metabolism

A0A0H3DY27	Bifunctional purine biosynthesis protein PurH	0.8	3.4	'de novo' IMP biosynthetic process [GO:0006189]; IMP cyclohydrolase activity [GO:0003937]; phosphoribosylaminoimidazolecarboxamide formyltransferase activity [GO:0004643]	Purine metabolism
A0A0H3E8R6	ATP-dependent zinc metalloprotease FtsH (EC 3.4.24.-)	0.6	1.7	ATPase activity [GO:0016887]; ATP binding [GO:0005524]; integral component of membrane [GO:0016021]; metalloendopeptidase activity [GO:0004222]; plasma membrane [GO:0005886]; protein catabolic process [GO:0030163]; zinc ion binding [GO:0008270]	Purine metabolism
A0A0H3E013	GMP synthase [glutamine-hydrolyzing] (EC 6.3.5.2) (GMP synthetase) (Glutamine amidotransferase)	0.6	1.7	asparagine biosynthetic process [GO:0006529]; asparagine synthase (glutamine-hydrolyzing) activity [GO:0004066]; ATP binding [GO:0005524]; glutamine metabolic process [GO:0006541]; GMP biosynthetic process [GO:0006177]; GMP synthase (glutamine-hydrolyzing) activity [GO:0003922]; pyrophosphatase activity [GO:0016462]	Purine metabolism
A0A0H3DVP6	Phosphoribosylaminoimidazole-succinocarboxamide synthase (EC 6.3.2.6) (SAICAR synthetase)	0.4	0.8	'de novo' IMP biosynthetic process [GO:0006189]; ATP binding [GO:0005524]; phosphoribosylaminoimidazolesuccinocarboxamide synthase activity [GO:0004639]	Purine metabolism
A0A0H3E0J9	Nucleoside diphosphate kinase (NDK) (NDP kinase)	0.4	0.5	ATP binding [GO:0005524]; CTP biosynthetic process [GO:0006241]; cytoplasm [GO:0005737]; GTP	Purine metabolism

	(EC 2.7.4.6) (Nucleoside-2-P kinase)			biosynthetic process [GO:0006183]; metal ion binding [GO:0046872]; nucleoside diphosphate kinase activity [GO:0004550]; UTP biosynthetic process [GO:0006228]	
A0A0H3E0J9	Nucleoside diphosphate kinase (NDK) (NDP kinase) (EC 2.7.4.6) (Nucleoside-2-P kinase)	0.4	0.5	ATP binding [GO:0005524]; CTP biosynthetic process [GO:0006241]; cytoplasm [GO:0005737]; GTP biosynthetic process [GO:0006183]; metal ion binding [GO:0046872]; nucleoside diphosphate kinase activity [GO:0004550]; UTP biosynthetic process [GO:0006228]	Pyrimidine metabolism
A0A0H3E692	DNA-directed RNA polymerase subunit beta (RNAP subunit beta) (EC 2.7.7.6) (RNA polymerase subunit beta) (Transcriptase subunit beta)	0.4	0.5	DNA binding [GO:0003677]; DNA-directed RNA polymerase activity [GO:0003899]; ribonucleoside binding [GO:0032549]; transcription, DNA-templated [GO:0006351]	Purine metabolism
A0A0H3E692	DNA-directed RNA polymerase subunit beta (RNAP subunit beta) (EC 2.7.7.6) (RNA polymerase subunit beta) (Transcriptase subunit beta)	0.4	0.5	DNA binding [GO:0003677]; DNA-directed RNA polymerase activity [GO:0003899]; ribonucleoside binding [GO:0032549]; transcription, DNA-templated [GO:0006351]	Pyrimidine metabolism
A0A0H3E3J3	Purine nucleoside phosphorylase (EC 2.4.2.1) (Inosine-guanosine phosphorylase)	0.4	0	nucleoside metabolic process [GO:0009116]; purine-nucleoside phosphorylase activity [GO:0004731]	Purine metabolism

A0A0H3E3J3	Purine nucleoside phosphorylase (EC 2.4.2.1) (Inosine-guanosine phosphorylase)	0.4	0	nucleoside metabolic process [GO:0009116]; purine-nucleoside phosphorylase activity [GO:0004731]	Pyrimidine metabolism
A0A0H3E2K8	Pyruvate kinase (EC 2.7.1.40)	0.3	0	glycolytic process [GO:0006096]; magnesium ion binding [GO:0000287]; potassium ion binding [GO:0030955]; pyruvate kinase activity [GO:0004743]	Purine metabolism
A0A0H3E8J1	Inosine-5'-monophosphate dehydrogenase (IMP dehydrogenase) (IMPD) (IMPDH) (EC 1.1.1.205)	0.3	0	GMP biosynthetic process [GO:0006177]; IMP dehydrogenase activity [GO:0003938]; metal ion binding [GO:0046872]; nucleotide binding [GO:0000166]	Purine metabolism
A0A0H3E334	Polyribonucleotide nucleotidyltransferase (EC 2.7.7.8) (Polynucleotide phosphorylase)	0.3	0	3'-5'-exoribonuclease activity [GO:0000175]; cytoplasm [GO:0005737]; magnesium ion binding [GO:0000287]; mRNA catabolic process [GO:0006402]; polyribonucleotide nucleotidyltransferase activity [GO:0004654]; RNA binding [GO:0003723]; RNA processing [GO:0006396]	Purine metabolism
A0A0H3E334	Polyribonucleotide nucleotidyltransferase (EC 2.7.7.8) (Polynucleotide phosphorylase)	0.3	0	3'-5'-exoribonuclease activity [GO:0000175]; cytoplasm [GO:0005737]; magnesium ion binding [GO:0000287]; mRNA catabolic process [GO:0006402]; polyribonucleotide nucleotidyltransferase activity [GO:0004654]; RNA binding	Pyrimidine metabolism

				[GO:0003723]; RNA processing [GO:0006396]	
TCA Cycle					
A0A0H3E160	Branched-chain alpha-keto acid dehydrogenase subunit E2	2.5	0.8	transferase activity, transferring acyl groups [GO:0016746]	Citrate cycle (TCA cycle)
A0A0H3E198	Succinyl-CoA ligase [ADP-forming] subunit alpha (EC 6.2.1.5)	2.2	1	ATP binding [GO:0005524]; ATP citrate synthase activity [GO:0003878]; cofactor binding [GO:0048037]; succinate-CoA ligase (ADP-forming) activity [GO:0004775]	Citrate cycle (TCA cycle)
A0A0H3E4P8	Succinate dehydrogenase flavoprotein subunit (EC 1.3.99.1)	0.6	1.7	succinate dehydrogenase activity [GO:0000104]	Citrate cycle (TCA cycle)
A0A0H3E0L2	Dihydrolipoyl dehydrogenase (EC 1.8.1.4)	0.5	1.7	cell redox homeostasis [GO:0045454]; detoxification of mercury ion [GO:0050787]; dihydrolipoyl dehydrogenase activity [GO:0004148]; flavin adenine dinucleotide binding [GO:0050660]; mercury (II) reductase activity [GO:0016152]; mercury ion binding [GO:0045340]; NADP binding [GO:0050661]	Citrate cycle (TCA cycle)
A0A0H3DZ01	Branched-chain alpha-keto acid dehydrogenase subunit E2	0.5	0.8	transferase activity, transferring acyl groups [GO:0016746]	Citrate cycle (TCA cycle)
A0A0H3DWW0	Acetoin dehydrogenase E1 component TPP-dependent alpha subunit	0.5	0.8	oxidoreductase activity, acting on the aldehyde or oxo group of donors, disulfide as acceptor [GO:0016624]	Citrate cycle (TCA cycle)
A0A0H3E2R6	Dihydrolipoyllysine-residue succinyltransferas	0.4	0	dihydrolipoyllysine-residue succinyltransferase activity [GO:0004149]; L-lysine	Citrate cycle

	e component of 2-oxoglutarate dehydrogenase complex (EC 2.3.1.61) (2-oxoglutarate dehydrogenase complex component E2)			catabolic process to acetyl-CoA via saccharopine [GO:0033512]; oxoglutarate dehydrogenase complex [GO:0045252]; tricarboxylic acid cycle [GO:0006099]	(TCA cycle)
A0A0H3E6Z6	Phosphoenolpyruvate carboxykinase [ATP] (PCK) (PEP carboxykinase) (PEPCK) (EC 4.1.1.49)	0.3	0	ATP binding [GO:0005524]; cytoplasm [GO:0005737]; gluconeogenesis [GO:0006094]; kinase activity [GO:0016301]; metal ion binding [GO:0046872]; phosphoenolpyruvate carboxykinase (ATP) activity [GO:0004612]	Citrate cycle (TCA cycle)
A0A0H3E2K4	Isocitrate dehydrogenase [NADP] (EC 1.1.1.42)	0.3	0	glyoxylate cycle [GO:0006097]; isocitrate dehydrogenase (NADP+) activity [GO:0004450]; magnesium ion binding [GO:0000287]; NAD binding [GO:0051287]; tricarboxylic acid cycle [GO:0006099]	Citrate cycle (TCA cycle)
A0A0H3E2B2	Malate dehydrogenase (EC 1.1.1.37)	0.3	0	cellular carbohydrate metabolic process [GO:0044262]; L-malate dehydrogenase activity [GO:0030060]; malate metabolic process [GO:0006108]; tricarboxylic acid cycle [GO:0006099]	Citrate cycle (TCA cycle)
A0A0H3E1Z9	Aconitate hydratase (Aconitase) (EC 4.2.1.3)	0.2	0	4 iron, 4 sulfur cluster binding [GO:0051539]; aconitate hydratase activity [GO:0003994]	Citrate cycle (TCA cycle)
A0A0H3E0W3	Succinyl-CoA ligase [ADP-forming] subunit beta (EC 6.2.1.5) (Succinyl-CoA	0.2	0	ATP binding [GO:0005524]; magnesium ion binding [GO:0000287]; manganese ion binding [GO:0030145]; succinate-CoA ligase (ADP-forming) activity	Citrate cycle (TCA cycle)

	synthetase subunit beta)			[GO:0004775]; tricarboxylic acid cycle [GO:0006099]	
Glycolysis/Gluconeogenesis					
A0A0H3E160	Branched-chain alpha-keto acid dehydrogenase subunit E2	2.5	0.8	transferase activity, transferring acyl groups [GO:0016746]	Glycolysis / Gluconeogenesis
A0A0H3E0I0	PTS system N-acetylglucosamine-specific transporter subunit IICB	2.1	1.7	integral component of membrane [GO:0016021]; kinase activity [GO:0016301]; N-acetylglucosamine transmembrane transporter activity [GO:0015572]; organelle inner membrane [GO:0019866]; phosphoenolpyruvate-dependent sugar phosphotransferase system [GO:0009401]; plasma membrane [GO:0005886]; protein-N(PI)-phosphohistidine-sugar phosphotransferase activity [GO:0008982]	Glycolysis / Gluconeogenesis
A0A0H3E2A5	Glyceraldehyde-3-phosphate dehydrogenase (EC 1.2.1.-)	2	2.2	glucose metabolic process [GO:0006006]; NAD binding [GO:0051287]; NADP binding [GO:0050661]; oxidoreductase activity, acting on the aldehyde or oxo group of donors, NAD or NADP as acceptor [GO:0016620]	Glycolysis / Gluconeogenesis
A0A0H3E075	Phosphocarrier protein HPr	0.7	2.2	cytoplasm [GO:0005737]; phosphoenolpyruvate-dependent sugar phosphotransferase system [GO:0009401]; protein serine/threonine kinase activity [GO:0004674]	Glycolysis / Gluconeogenesis
A0A0H3E6T6	Putative acyl-coenzyme A synthetase	0.6	2.2	catalytic activity [GO:0003824]	Glycolysis /

					Glucone ogenesis
A0A0H3 E6D5	Glyceraldehyde-3-phosphate dehydrogenase (EC 1.2.1.-)	0.6	1.7	glucose metabolic process [GO:0006006]; NAD binding [GO:0051287]; NADP binding [GO:0050661]; oxidoreductase activity, acting on the aldehyde or oxo group of donors, NAD or NADP as acceptor [GO:0016620]	Glycolys is / Glucone ogenesis
A0A0H3 E0L2	Dihydrolipoyl dehydrogenase (EC 1.8.1.4)	0.5	1.7	cell redox homeostasis [GO:0045454]; detoxification of mercury ion [GO:0050787]; dihydrolipoyl dehydrogenase activity [GO:0004148]; flavin adenine dinucleotide binding [GO:0050660]; mercury (II) reductase activity [GO:0016152]; mercury ion binding [GO:0045340]; NADP binding [GO:0050661]	Glycolys is / Glucone ogenesis
A0A0H3 E6C9	Enolase (EC 4.2.1.11) (2-phospho-D-glycerate hydro-lyase) (2-phosphoglycerate dehydratase)	0.5	1.7	cell surface [GO:0009986]; extracellular region [GO:0005576]; glycolytic process [GO:0006096]; magnesium ion binding [GO:0000287]; phosphopyruvate hydratase activity [GO:0004634]; phosphopyruvate hydratase complex [GO:0000015]	Glycolys is / Glucone ogenesis
A0A0H3 E2Z8	Glucose-6-phosphate isomerase (GPI) (EC 5.3.1.9) (Phosphoglucose isomerase) (Phosphohexose isomerase)	0.5	1	cytoplasm [GO:0005737]; gluconeogenesis [GO:0006094]; glucose-6-phosphate isomerase activity [GO:0004347]; glycolytic process [GO:0006096]	Glycolys is / Glucone ogenesis

A0A0H3DZ01	Branched-chain alpha-keto acid dehydrogenase subunit E2	0.5	0.8	transferase activity, transferring acyl groups [GO:0016746]	Glycolysis / Gluconeogenesis
A0A0H3DWW0	Acetoin dehydrogenase E1 component TPP-dependent alpha subunit	0.5	0.8	oxidoreductase activity, acting on the aldehyde or oxo group of donors, disulfide as acceptor [GO:0016624]	Glycolysis / Gluconeogenesis
A0A0H3E558	6-phospho-beta-glucosidase	0.4	0.5	carbohydrate metabolic process [GO:0005975]; hydrolase activity, hydrolyzing O-glycosyl compounds [GO:0004553]; oxidoreductase activity, acting on the CH-OH group of donors, NAD or NADP as acceptor [GO:0016616]	Glycolysis / Gluconeogenesis
A0A0H3E3S7	Phosphoglycerate kinase (EC 2.7.2.3)	0.4	0	ATP binding [GO:0005524]; cytoplasm [GO:0005737]; glycolytic process [GO:0006096]; phosphoglycerate kinase activity [GO:0004618]	Glycolysis / Gluconeogenesis
A0A0H3E6Z6	Phosphoenolpyruvate carboxykinase [ATP] (PCK) (PEP carboxykinase) (PEPCK) (EC 4.1.1.49)	0.3	0	ATP binding [GO:0005524]; cytoplasm [GO:0005737]; gluconeogenesis [GO:0006094]; kinase activity [GO:0016301]; metal ion binding [GO:0046872]; phosphoenolpyruvate carboxykinase (ATP) activity [GO:0004612]	Glycolysis / Gluconeogenesis
A0A0H3E7C3	Fructose-bisphosphate aldolase (EC 4.1.2.13)	0.3	0	fructose 1,6-bisphosphate metabolic process [GO:0030388]; fructose-bisphosphate aldolase activity [GO:0004332]; glycolytic process [GO:0006096]; zinc ion binding [GO:0008270]	Glycolysis / Gluconeogenesis
A0A0H3E2K8	Pyruvate kinase (EC 2.7.1.40)	0.3	0	glycolytic process [GO:0006096]; magnesium ion binding [GO:0000287]; potassium ion binding	Glycolysis / Gluconeogenesis

				[GO:0030955]; pyruvate kinase activity [GO:0004743]	
A0A0H3E321	Betaine-aldehyde dehydrogenase (EC 1.2.1.8)	0.2	0	betaine-aldehyde dehydrogenase activity [GO:0008802]; glycine betaine biosynthetic process from choline [GO:0019285]; metal ion binding [GO:0046872]	Glycolysis / Gluconeogenesis
A0A0H3E9N1	Succinate-semialdehyde dehydrogenase	0.1	0	aldehyde dehydrogenase [NAD(P)+] activity [GO:0004030]; cellular aldehyde metabolic process [GO:0006081]; gamma-aminobutyric acid catabolic process [GO:0009450]; succinate-semialdehyde dehydrogenase [NAD(P)+] activity [GO:0009013]	Glycolysis / Gluconeogenesis
Carbon Fixation					
A0A0H3E6R7	Acetyl-coenzyme A carboxylase carboxyl transferase subunit beta (ACCase subunit beta) (Acetyl-CoA carboxylase carboxyltransferase subunit beta) (EC 6.4.1.2)	0.7	2.2	acetyl-CoA carboxylase activity [GO:0003989]; acetyl-CoA carboxylase complex [GO:0009317]; ATP binding [GO:0005524]; fatty acid biosynthetic process [GO:0006633]; malonyl-CoA biosynthetic process [GO:2001295]; zinc ion binding [GO:0008270]	Carbon fixation pathways in prokaryotes
A0A0H3E6T6	Putative acyl-coenzyme A synthetase	0.6	2.2	catalytic activity [GO:0003824]	Carbon fixation pathways in prokaryotes
A0A0H3E6D5	Glyceraldehyde-3-phosphate dehydrogenase (EC 1.2.1.-)	0.6	1.7	glucose metabolic process [GO:0006006]; NAD binding [GO:0051287]; NADP binding [GO:0050661]; oxidoreductase activity, acting on the aldehyde or	Carbon fixation in photosynthetic organisms

				oxo group of donors, NAD or NADP as acceptor [GO:0016620]	
A0A0H3E4P8	Succinate dehydrogenase flavoprotein subunit (EC 1.3.99.1)	0.6	1.7	succinate dehydrogenase activity [GO:0000104]	Carbon fixation pathways in prokaryotes
A0A0H3E1K0	Transketolase (EC 2.2.1.1)	0.4	0.5	metal ion binding [GO:0046872]; transketolase activity [GO:0004802]	Carbon fixation in photosynthetic organisms
A0A0H3E3S7	Phosphoglycerate kinase (EC 2.7.2.3)	0.4	0	ATP binding [GO:0005524]; cytoplasm [GO:0005737]; glycolytic process [GO:0006096]; phosphoglycerate kinase activity [GO:0004618]	Carbon fixation in photosynthetic organisms
A0A0H3E6Z6	Phosphoenolpyruvate carboxykinase [ATP] (PCK) (PEP carboxykinase) (PEPCK) (EC 4.1.1.49)	0.3	0	ATP binding [GO:0005524]; cytoplasm [GO:0005737]; gluconeogenesis [GO:0006094]; kinase activity [GO:0016301]; metal ion binding [GO:0046872]; phosphoenolpyruvate carboxykinase (ATP) activity [GO:0004612]	Carbon fixation in photosynthetic organisms
A0A0H3E2K4	Isocitrate dehydrogenase [NADP] (EC 1.1.1.42)	0.3	0	glyoxylate cycle [GO:0006097]; isocitrate dehydrogenase (NADP+) activity [GO:0004450]; magnesium ion binding [GO:0000287]; NAD binding [GO:0051287]; tricarboxylic acid cycle [GO:0006099]	Carbon fixation pathways in prokaryotes
A0A0H3E7C3	Fructose-bisphosphate aldolase (EC 4.1.2.13)	0.3	0	fructose 1,6-bisphosphate metabolic process [GO:0030388]; fructose-bisphosphate aldolase	Carbon fixation in photosyn

				activity [GO:0004332]; glycolytic process [GO:0006096]; zinc ion binding [GO:0008270]	thetic organisms
A0A0H3E2B2	Malate dehydrogenase (EC 1.1.1.37)	0.3	0	cellular carbohydrate metabolic process [GO:0044262]; L-malate dehydrogenase activity [GO:0030060]; malate metabolic process [GO:0006108]; tricarboxylic acid cycle [GO:0006099]	Carbon fixation in photosynthetic organisms
A0A0H3E2B2	Malate dehydrogenase (EC 1.1.1.37)	0.3	0	cellular carbohydrate metabolic process [GO:0044262]; L-malate dehydrogenase activity [GO:0030060]; malate metabolic process [GO:0006108]; tricarboxylic acid cycle [GO:0006099]	Carbon fixation pathways in prokaryotes
A0A0H3E4K4	Enoyl-CoA hydratase (EC 4.2.1.17)	0.3	0	enoyl-CoA hydratase activity [GO:0004300]	Carbon fixation pathways in prokaryotes
A0A0H3E1Z9	Aconitate hydratase (Aconitase) (EC 4.2.1.3)	0.2	0	4 iron, 4 sulfur cluster binding [GO:0051539]; aconitate hydratase activity [GO:0003994]	Carbon fixation pathways in prokaryotes
A0A0H3E2S8	Aspartate aminotransferase (EC 2.6.1.1)	0.2	0	biosynthetic process [GO:0009058]; L-aspartate:2-oxoglutarate aminotransferase activity [GO:0004069]; L-phenylalanine:2-oxoglutarate aminotransferase activity [GO:0080130]; pyridoxal phosphate binding [GO:0030170]	Carbon fixation in photosynthetic organisms
A0A0H3E0W3	Succinyl-CoA ligase [ADP-forming] subunit	0.2	0	ATP binding [GO:0005524]; magnesium ion binding [GO:0000287]; manganese	Carbon fixation pathways

	beta (EC 6.2.1.5) (Succinyl-CoA synthetase subunit beta)			ion binding [GO:0030145]; succinate-CoA ligase (ADP-forming) activity [GO:0004775]; tricarboxylic acid cycle [GO:0006099]	in prokaryotes
Terpenoid Backbone Biosynthesis					
A0A0H3E1I7	Geranyltranstransferase	3.7	0	isoprenoid biosynthetic process [GO:0008299]; transferase activity [GO:0016740]	Terpenoid backbone biosynthesis
A0A0H3E9S6	2-C-methyl-D-erythritol 2,4-cyclodiphosphate synthase (MECDP-synthase) (MECPP-synthase) (MECPS) (EC 4.6.1.12)	1.7	3.4	2-C-methyl-D-erythritol 2,4-cyclodiphosphate synthase activity [GO:0008685]; metal ion binding [GO:0046872]; terpenoid biosynthetic process [GO:0016114]	Terpenoid backbone biosynthesis
A0A0H3E1G4	4-hydroxy-3-methylbut-2-en-1-yl diphosphate synthase (EC 1.17.7.1) (1-hydroxy-2-methyl-2-(E)-butenyl 4-diphosphate synthase)	0.6	2.2	4-hydroxy-3-methylbut-2-en-1-yl diphosphate synthase activity [GO:0046429]; 4 iron, 4 sulfur cluster binding [GO:0051539]; iron ion binding [GO:0005506]; isopentenyl diphosphate biosynthetic process, methylerythritol 4-phosphate pathway [GO:0019288]; terpenoid biosynthetic process [GO:0016114]	Terpenoid backbone biosynthesis
Fatty Acid Metabolism					
A0A0H3E249	3-ketoacyl-(Acyl-carrier-protein) reductase (EC 1.1.1.100)	8	0	3-oxoacyl-[acyl-carrier-protein] reductase (NADPH) activity [GO:0004316]	
A0A0H3E3W5	Acetyl-CoA carboxylase biotin carboxylase subunit (EC 6.4.1.2)	3.5	0	acetyl-CoA carboxylase activity [GO:0003989]; ATP binding [GO:0005524]; biotin carboxylase activity [GO:0004075]; metal ion binding [GO:0046872]	Fatty acid biosynthesis

A0A0H3E2Z0	Putative oxidoreductase, 2-nitropropane dioxygenase family protein	3	0	dioxygenase activity [GO:0051213]; nitronate monooxygenase activity [GO:0018580]	Fatty acid biosynthesis
A0A0H3E6K8	Long-chain-fatty-acid--CoA ligase	2.4	0.8	ligase activity [GO:0016874]	Fatty acid biosynthesis
A0A0H3E6K8	Long-chain-fatty-acid--CoA ligase	2.4	0.8	ligase activity [GO:0016874]	Fatty acid degradation
A0A0H3E7G8	Enoyl-CoA hydratase/3-hydroxyacyl-CoA dehydrogenase	1.8	3.4	3-hydroxyacyl-CoA dehydrogenase activity [GO:0003857]; coenzyme binding [GO:0050662]; fatty acid metabolic process [GO:0006631]	Fatty acid degradation
A0A0H3DY64	Uncharacterized protein	1.7	3.4	3-oxoacyl-[acyl-carrier-protein] reductase (NADPH) activity [GO:0004316]; fatty acid biosynthetic process [GO:0006633]; NAD binding [GO:0051287]	Fatty acid biosynthesis
A0A0H3E6R7	Acetyl-coenzyme A carboxylase carboxyl transferase subunit beta (ACCase subunit beta) (Acetyl-CoA carboxylase carboxyltransferase subunit beta) (EC 6.4.1.2)	0.7	2.2	acetyl-CoA carboxylase activity [GO:0003989]; acetyl-CoA carboxylase complex [GO:0009317]; ATP binding [GO:0005524]; fatty acid biosynthetic process [GO:0006633]; malonyl-CoA biosynthetic process [GO:2001295]; zinc ion binding [GO:0008270]	Fatty acid biosynthesis
A0A0H3E4K4	Enoyl-CoA hydratase (EC 4.2.1.17)	0.3	0	enoyl-CoA hydratase activity [GO:0004300]	Fatty acid degradation
A0A0H3E4K4	Enoyl-CoA hydratase (EC 4.2.1.17)	0.3	0	enoyl-CoA hydratase activity [GO:0004300]	Fatty acid elongation

A0A0H3E4K4	Enoyl-CoA hydratase (EC 4.2.1.17)	0.3	0	enoyl-CoA hydratase activity [GO:0004300]	Biosynthesis of unsat'd fatty acids
A0A0H3E321	Betaine-aldehyde dehydrogenase (EC 1.2.1.8)	0.2	0	betaine-aldehyde dehydrogenase activity [GO:0008802]; glycine betaine biosynthetic process from choline [GO:0019285]; metal ion binding [GO:0046872]	Fatty acid degradation
Drug Metabolism					
A0A0H3E251	Non-canonical purine NTP pyrophosphatase (EC 3.6.1.19) (Non-standard purine NTP pyrophosphatase) (Nucleoside-triphosphate diphosphatase) (Nucleoside-triphosphate pyrophosphatase)	6.6	0	metal ion binding [GO:0046872]; nucleoside-triphosphatase activity [GO:0017111]; nucleoside triphosphate catabolic process [GO:0009143]; nucleoside-triphosphate diphosphatase activity [GO:0047429]; nucleotide binding [GO:0000166]; purine nucleotide metabolic process [GO:0006163]	Drug metabolism - other enzymes
A0A0H3E7B3	Lipoyl synthase (EC 2.8.1.8) (Lip-syn) (Lipoate synthase) (Lipoic acid synthase) (Sulfur insertion protein LipA)	2.4	0.8	4 iron, 4 sulfur cluster binding [GO:0051539]; cytoplasm [GO:0005737]; lipoate synthase activity [GO:0016992]; metal ion binding [GO:0046872]; protein lipoylation [GO:0009249]	Drug metabolism - other enzymes
A0A0H3E013	GMP synthase [glutamine-hydrolyzing] (EC 6.3.5.2) (GMP synthetase) (Glutamine amidotransferase)	0.6	1.7	asparagine biosynthetic process [GO:0006529]; asparagine synthase (glutamine-hydrolyzing) activity [GO:0004066]; ATP binding [GO:0005524]; glutamine metabolic process [GO:0006541]; GMP biosynthetic process [GO:0006177]; GMP synthase (glutamine-	Drug metabolism - other enzymes

				hydrolyzing) activity [GO:0003922]; pyrophosphatase activity [GO:0016462]	
A0A0H3E8J1	Inosine-5'-monophosphate dehydrogenase (IMP dehydrogenase) (IMPD) (IMPDH) (EC 1.1.1.205)	0.3	0	GMP biosynthetic process [GO:0006177]; IMP dehydrogenase activity [GO:0003938]; metal ion binding [GO:0046872]; nucleotide binding [GO:0000166]	Drug metabolism - other enzymes
Biosynthesis of Antibiotics					
A0A0H3E705	Putative phosphatase	8.7	0	integral component of membrane [GO:0016021]; magnesium ion binding [GO:0000287]; phosphatase activity [GO:0016791]	Biosynthesis of antibiotics
A0A0H3DYE3	Phosphoribosylamine--glycine ligase (EC 6.3.4.13) (GARS) (Glycinamide ribonucleotide synthetase) (Phosphoribosylglycinamide synthetase)	6.8	0	'de novo' IMP biosynthetic process [GO:0006189]; ATP binding [GO:0005524]; magnesium ion binding [GO:0000287]; manganese ion binding [GO:0030145]; phosphoribosylamine-glycine ligase activity [GO:0004637]; purine nucleobase biosynthetic process [GO:0009113]	Biosynthesis of antibiotics
A0A0H3E6C1	Adenylate kinase (AK) (EC 2.7.4.3) (ATP-AMP transphosphorylase) (ATP:AMP phosphotransferase) (Adenylate monophosphate kinase)	5.7	0	adenylate kinase activity [GO:0004017]; ATP binding [GO:0005524]; cytoplasm [GO:0005737]; nucleotide biosynthetic process [GO:0009165]	Biosynthesis of antibiotics
A0A0H3E164	Putative amidohydrolase	4.9	0	hydrolase activity [GO:0016787]	Biosynthesis of antibiotics
A0A0H3DYX2	Aspartate-semialdehyde	4.9	0	de novo' L-methionine biosynthetic process	Biosynthesis of

	dehydrogenase (ASA dehydrogenase) (ASADH) (EC 1.2.1.11) (Aspartate-beta-semialdehyde dehydrogenase)			[GO:0071266]; aspartate-semialdehyde dehydrogenase activity [GO:0004073]; cytoplasm [GO:0005737]; diaminopimelate biosynthetic process [GO:0019877]; isoleucine biosynthetic process [GO:0009097]; lysine biosynthetic process via diaminopimelate [GO:0009089]; N-acetyl-gamma-glutamyl-phosphate reductase activity [GO:0003942]; NAD binding [GO:0051287]; NADP binding [GO:0050661]; threonine biosynthetic process [GO:0009088]	antibiotics
A0A0H3E5I0	Methylisocitrate lyase (EC 4.1.3.30)	4.6	0	methylisocitrate lyase activity [GO:0046421]; propionate catabolic process, 2-methylcitrate cycle [GO:0019629]	Biosynthesis of antibiotics
A0A0H3E1I7	Geranyltranstransferase	3.7	0	isoprenoid biosynthetic process [GO:0008299]; transferase activity [GO:0016740]	Biosynthesis of antibiotics
A0A0H3E3W5	Acetyl-CoA carboxylase biotin carboxylase subunit (EC 6.4.1.2)	3.5	0	acetyl-CoA carboxylase activity [GO:0003989]; ATP binding [GO:0005524]; biotin carboxylase activity [GO:0004075]; metal ion binding [GO:0046872]	Biosynthesis of antibiotics
A0A0H3E2R3	Bifunctional 3-deoxy-7-phosphoheptulonate synthase/chorismate mutase	2.9	0	aldehyde-lyase activity [GO:0016832]; aromatic amino acid family biosynthetic process [GO:0009073]; chorismate metabolic process [GO:0046417]; transferase activity [GO:0016740]	Biosynthesis of antibiotics
A0A0H3E9P3	Ribose-phosphate pyrophosphokina	2.8	0.5	ATP binding [GO:0005524]; cytoplasm [GO:0005737];	Biosynthesis of

	se (RPPK) (EC 2.7.6.1) (5-phospho-D-ribosyl alpha-1-diphosphate) (Phosphoribosyl diphosphate synthase) (Phosphoribosyl pyrophosphate synthase)			kinase activity [GO:0016301]; magnesium ion binding [GO:0000287]; nucleotide biosynthetic process [GO:0009165]; ribonucleoside monophosphate biosynthetic process [GO:0009156]; ribose phosphate diphosphokinase activity [GO:0004749]	antibiotics
A0A0H3E160	Branched-chain alpha-keto acid dehydrogenase subunit E2	2.5	0.8	transferase activity, transferring acyl groups [GO:0016746]	Biosynthesis of antibiotics
A0A0H3E198	Succinyl-CoA ligase [ADP-forming] subunit alpha (EC 6.2.1.5)	2.2	1	ATP binding [GO:0005524]; ATP citrate synthase activity [GO:0003878]; cofactor binding [GO:0048037]; succinate-CoA ligase (ADP-forming) activity [GO:0004775]	Biosynthesis of antibiotics
A0A0H3E2A5	Glyceraldehyde-3-phosphate dehydrogenase (EC 1.2.1.-)	2	2.2	glucose metabolic process [GO:0006006]; NAD binding [GO:0051287]; NADP binding [GO:0050661]; oxidoreductase activity, acting on the aldehyde or oxo group of donors, NAD or NADP as acceptor [GO:0016620]	Biosynthesis of antibiotics
A0A0H3E7G8	Enoyl-CoA hydratase/3-hydroxyacyl-CoA dehydrogenase	1.8	3.4	3-hydroxyacyl-CoA dehydrogenase activity [GO:0003857]; coenzyme binding [GO:0050662]; fatty acid metabolic process [GO:0006631]	Biosynthesis of antibiotics
A0A0H3E9S6	2-C-methyl-D-erythritol 2,4-cyclodiphosphate synthase (MECDP-synthase) (MECPP-synthase)	1.7	3.4	2-C-methyl-D-erythritol 2,4-cyclodiphosphate synthase activity [GO:0008685]; metal ion binding [GO:0046872]; terpenoid biosynthetic process [GO:0016114]	Biosynthesis of antibiotics

	(MECPS) (EC 4.6.1.12)				
A0A0H3DXT3	Gamma-glutamyl phosphate reductase (GPR) (EC 1.2.1.41) (Glutamate-5-semialdehyde dehydrogenase) (Glutamyl-gamma-semialdehyde dehydrogenase)	0.8	3.4	cytoplasm [GO:0005737]; glutamate-5-semialdehyde dehydrogenase activity [GO:0004350]; L-proline biosynthetic process [GO:0055129]; NADP binding [GO:0050661]	Biosynthesis of antibiotics
A0A0H3DY27	Bifunctional purine biosynthesis protein PurH	0.8	3.4	'de novo' IMP biosynthetic process [GO:0006189]; IMP cyclohydrolase activity [GO:0003937]; phosphoribosylaminoimidazolecarboxamide formyltransferase activity [GO:0004643]	Biosynthesis of antibiotics
A0A0H3E2Y1	3-phosphoshikimate 1-carboxyvinyltransferase (EC 2.5.1.19) (5-enolpyruvylshikimate-3-phosphate synthase)	0.7	2.2	3-phosphoshikimate 1-carboxyvinyltransferase activity [GO:0003866]; aromatic amino acid family biosynthetic process [GO:0009073]; chorismate biosynthetic process [GO:0009423]; cytoplasm [GO:0005737]	Biosynthesis of antibiotics
A0A0H3E6R7	Acetyl-coenzyme A carboxylase carboxyl transferase subunit beta (ACCase subunit beta) (Acetyl-CoA carboxylase carboxyltransferase subunit beta) (EC 6.4.1.2)	0.7	2.2	acetyl-CoA carboxylase activity [GO:0003989]; acetyl-CoA carboxylase complex [GO:0009317]; ATP binding [GO:0005524]; fatty acid biosynthetic process [GO:0006633]; malonyl-CoA biosynthetic process [GO:2001295]; zinc ion binding [GO:0008270]	Biosynthesis of antibiotics
A0A0H3E1G4	4-hydroxy-3-methylbut-2-en-1-yl diphosphate synthase (EC 1.17.7.1) (1-	0.6	2.2	4-hydroxy-3-methylbut-2-en-1-yl diphosphate synthase activity [GO:0046429]; 4 iron, 4 sulfur cluster binding [GO:0051539]; iron ion	Biosynthesis of antibiotics

	hydroxy-2-methyl-2-(E)-butenyl 4-diphosphate synthase)			binding [GO:0005506]; isopentenyl diphosphate biosynthetic process, methylerythritol 4-phosphate pathway [GO:0019288]; terpenoid biosynthetic process [GO:0016114]	
A0A0H3E6T6	Putative acyl-coenzyme A synthetase	0.6	2.2	catalytic activity [GO:0003824]	Biosynthesis of antibiotics
A0A0H3E5V0	Homoserine dehydrogenase (EC 1.1.1.3)	0.6	1.7	amino acid binding [GO:0016597]; homoserine dehydrogenase activity [GO:0004412]; isoleucine biosynthetic process [GO:0009097]; methionine biosynthetic process [GO:0009086]; NADP binding [GO:0050661]; threonine biosynthetic process [GO:0009088]	Biosynthesis of antibiotics
A0A0H3E918	Phosphoglucosamine mutase (EC 5.4.2.10)	0.6	1.7	carbohydrate metabolic process [GO:0005975]; magnesium ion binding [GO:0000287]; phosphoglucosamine mutase activity [GO:0008966]	Biosynthesis of antibiotics
A0A0H3E6D5	Glyceraldehyde-3-phosphate dehydrogenase (EC 1.2.1.-)	0.6	1.7	glucose metabolic process [GO:0006006]; NAD binding [GO:0051287]; NADP binding [GO:0050661]; oxidoreductase activity, acting on the aldehyde or oxo group of donors, NAD or NADP as acceptor [GO:0016620]	Biosynthesis of antibiotics
A0A0H3E4P8	Succinate dehydrogenase flavoprotein subunit (EC 1.3.99.1)	0.6	1.7	succinate dehydrogenase activity [GO:0000104]	Biosynthesis of antibiotics
A0A0H3E612	Cysteine synthase (EC 2.5.1.47)	0.5	1.7	cysteine biosynthetic process from serine [GO:0006535]; cysteine synthase activity	Biosynthesis of

				[GO:0004124]; transferase activity [GO:0016740]	antibiotics
A0A0H3E0L2	Dihydrolipoyl dehydrogenase (EC 1.8.1.4)	0.5	1.7	cell redox homeostasis [GO:0045454]; detoxification of mercury ion [GO:0050787]; dihydrolipoyl dehydrogenase activity [GO:0004148]; flavin adenine dinucleotide binding [GO:0050660]; mercury (II) reductase activity [GO:0016152]; mercury ion binding [GO:0045340]; NADP binding [GO:0050661]	Biosynthesis of antibiotics
A0A0H3E6C9	Enolase (EC 4.2.1.11) (2-phospho-D-glycerate hydro-lyase) (2-phosphoglycerate dehydratase)	0.5	1.7	cell surface [GO:0009986]; extracellular region [GO:0005576]; glycolytic process [GO:0006096]; magnesium ion binding [GO:0000287]; phosphopyruvate hydratase activity [GO:0004634]; phosphopyruvate hydratase complex [GO:0000015]	Biosynthesis of antibiotics
A0A0H3E0A3	L-threonine dehydratase (EC 4.3.1.19) (Threonine deaminase)	0.5	1	cellular amino acid metabolic process [GO:0006520]; L-threonine ammonia-lyase activity [GO:0004794]; pyridoxal phosphate binding [GO:0030170]	Biosynthesis of antibiotics
A0A0H3E2Z8	Glucose-6-phosphate isomerase (GPI) (EC 5.3.1.9) (Phosphoglucose isomerase) (Phosphohexose isomerase)	0.5	1	cytoplasm [GO:0005737]; gluconeogenesis [GO:0006094]; glucose-6-phosphate isomerase activity [GO:0004347]; glycolytic process [GO:0006096]	Biosynthesis of antibiotics
A0A0H3DZ01	Branched-chain alpha-keto acid dehydrogenase subunit E2	0.5	0.8	transferase activity, transferring acyl groups [GO:0016746]	Biosynthesis of antibiotics

A0A0H3DWW0	Acetoin dehydrogenase E1 component TPP-dependent alpha subunit	0.5	0.8	oxidoreductase activity, acting on the aldehyde or oxo group of donors, disulfide as acceptor [GO:0016624]	Biosynthesis of antibiotics
A0A0H3E469	N-acetylglucosamine-6-phosphate deacetylase (EC 3.5.1.25) (GlcNAc 6-P deacetylase)	0.4	0.8	carbohydrate metabolic process [GO:0005975]; N-acetylglucosamine-6-phosphate deacetylase activity [GO:0008448]; N-acetylglucosamine metabolic process [GO:0006044]	Biosynthesis of antibiotics
A0A0H3DVP6	Phosphoribosylaminoimidazole-succinocarboxamide synthase (EC 6.3.2.6) (SAICAR synthetase)	0.4	0.8	'de novo' IMP biosynthetic process [GO:0006189]; ATP binding [GO:0005524]; phosphoribosylaminoimidazolesuccinocarboxamide synthase activity [GO:0004639]	Biosynthesis of antibiotics
A0A0H3E0J9	Nucleoside diphosphate kinase (NDK) (NDP kinase) (EC 2.7.4.6) (Nucleoside-2-P kinase)	0.4	0.5	ATP binding [GO:0005524]; CTP biosynthetic process [GO:0006241]; cytoplasm [GO:0005737]; GTP biosynthetic process [GO:0006183]; metal ion binding [GO:0046872]; nucleoside diphosphate kinase activity [GO:0004550]; UTP biosynthetic process [GO:0006228]	Biosynthesis of antibiotics
A0A0H3E0B4	Dihydroxy-acid dehydratase (DAD) (EC 4.2.1.9)	0.4	0.5	4 iron, 4 sulfur cluster binding [GO:0051539]; dihydroxy-acid dehydratase activity [GO:0004160]; isoleucine biosynthetic process [GO:0009097]; metal ion binding [GO:0046872]; valine biosynthetic process [GO:0009099]	Biosynthesis of antibiotics
A0A0H3E1K0	Transketolase (EC 2.2.1.1)	0.4	0.5	metal ion binding [GO:0046872]; transketolase activity [GO:0004802]	Biosynthesis of antibiotics

A0A0H3E3S7	Phosphoglycerate kinase (EC 2.7.2.3)	0.4	0	ATP binding [GO:0005524]; cytoplasm [GO:0005737]; glycolytic process [GO:0006096]; phosphoglycerate kinase activity [GO:0004618]	Biosynthesis of antibiotics
A0A0H3E2R6	Dihydrolipoyllysine-residue succinyltransferase component of 2-oxoglutarate dehydrogenase complex (EC 2.3.1.61) (2-oxoglutarate dehydrogenase complex component E2)	0.4	0	dihydrolipoyllysine-residue succinyltransferase activity [GO:0004149]; L-lysine catabolic process to acetyl-CoA via saccharopine [GO:0033512]; oxoglutarate dehydrogenase complex [GO:0045252]; tricarboxylic acid cycle [GO:0006099]	Biosynthesis of antibiotics
A0A0H3E6Z6	Phosphoenolpyruvate carboxykinase [ATP] (PCK) (PEP carboxykinase) (PEPCK) (EC 4.1.1.49)	0.3	0	ATP binding [GO:0005524]; cytoplasm [GO:0005737]; gluconeogenesis [GO:0006094]; kinase activity [GO:0016301]; metal ion binding [GO:0046872]; phosphoenolpyruvate carboxykinase (ATP) activity [GO:0004612]	Biosynthesis of antibiotics
A0A0H3E2K4	Isocitrate dehydrogenase [NADP] (EC 1.1.1.42)	0.3	0	glyoxylate cycle [GO:0006097]; isocitrate dehydrogenase (NADP+) activity [GO:0004450]; magnesium ion binding [GO:0000287]; NAD binding [GO:0051287]; tricarboxylic acid cycle [GO:0006099]	Biosynthesis of antibiotics
A0A0H3E5F7	6-phosphogluconate dehydrogenase, decarboxylating (EC 1.1.1.44)	0.3	0	D-gluconate metabolic process [GO:0019521]; NADP binding [GO:0050661]; pentose-phosphate shunt [GO:0006098]; phosphogluconate dehydrogenase	Biosynthesis of antibiotics

				(decarboxylating) activity [GO:0004616]	
A0A0H3E7C3	Fructose-bisphosphate aldolase (EC 4.1.2.13)	0.3	0	fructose 1,6-bisphosphate metabolic process [GO:0030388]; fructose-bisphosphate aldolase activity [GO:0004332]; glycolytic process [GO:0006096]; zinc ion binding [GO:0008270]	Biosynthesis of antibiotics
A0A0H3E2K8	Pyruvate kinase (EC 2.7.1.40)	0.3	0	glycolytic process [GO:0006096]; magnesium ion binding [GO:0000287]; potassium ion binding [GO:0030955]; pyruvate kinase activity [GO:0004743]	Biosynthesis of antibiotics
A0A0H3E2B2	Malate dehydrogenase (EC 1.1.1.37)	0.3	0	cellular carbohydrate metabolic process [GO:0044262]; L-malate dehydrogenase activity [GO:0030060]; malate metabolic process [GO:0006108]; tricarboxylic acid cycle [GO:0006099]	Biosynthesis of antibiotics
A0A0H3E4K4	Enoyl-CoA hydratase (EC 4.2.1.17)	0.3	0	enoyl-CoA hydratase activity [GO:0004300]	Biosynthesis of antibiotics
A0A0H3E165	Leucine dehydrogenase	0.3	0	cellular amino acid metabolic process [GO:0006520]; oxidoreductase activity, acting on the CH-NH2 group of donors, NAD or NADP as acceptor [GO:0016639]	Biosynthesis of antibiotics
A0A0H3E4P3	Serine hydroxymethyltransferase (SHMT) (Serine methylase) (EC 2.1.2.1)	0.3	0	cytoplasm [GO:0005737]; glycine biosynthetic process from serine [GO:0019264]; glycine hydroxymethyltransferase activity [GO:0004372]; methyltransferase activity [GO:0008168]; pyridoxal phosphate binding [GO:0030170];	Biosynthesis of antibiotics

				tetrahydrofolate interconversion [GO:0035999]	
A0A0H3E167	4-hydroxy-tetrahydrodipicolinate synthase (HTPA synthase) (EC 4.3.3.7)	0.3	0	4-hydroxy-tetrahydrodipicolinate synthase [GO:0008840]; cytoplasm [GO:0005737]; diaminopimelate biosynthetic process [GO:0019877]; lysine biosynthetic process via diaminopimelate [GO:0009089]	Biosynthesis of antibiotics
A0A0H3E1Z9	Aconitate hydratase (Aconitase) (EC 4.2.1.3)	0.2	0	4 iron, 4 sulfur cluster binding [GO:0051539]; aconitate hydratase activity [GO:0003994]	Biosynthesis of antibiotics
A0A0H3E2S8	Aspartate aminotransferase (EC 2.6.1.1)	0.2	0	biosynthetic process [GO:0009058]; L-aspartate:2-oxoglutarate aminotransferase activity [GO:0004069]; L-phenylalanine:2-oxoglutarate aminotransferase activity [GO:0080130]; pyridoxal phosphate binding [GO:0030170]	Biosynthesis of antibiotics
A0A0H3E4P2	Probable transaldolase (EC 2.2.1.2)	0.2	0	carbohydrate metabolic process [GO:0005975]; cytoplasm [GO:0005737]; pentose-phosphate shunt [GO:0006098]; sedoheptulose-7-phosphate:D-glyceraldehyde-3-phosphate glyceronetransferase activity [GO:0004801]	Biosynthesis of antibiotics
A0A0H3E0W3	Succinyl-CoA ligase [ADP-forming] subunit beta (EC 6.2.1.5) (Succinyl-CoA synthetase subunit beta)	0.2	0	ATP binding [GO:0005524]; magnesium ion binding [GO:0000287]; manganese ion binding [GO:0030145]; succinate-CoA ligase (ADP-forming) activity [GO:0004775]; tricarboxylic acid cycle [GO:0006099]	Biosynthesis of antibiotics

A0A0H3E321	Betaine-aldehyde dehydrogenase (EC 1.2.1.8)	0.2	0	betaine-aldehyde dehydrogenase activity [GO:0008802]; glycine betaine biosynthetic process from choline [GO:0019285]; metal ion binding [GO:0046872]	Biosynthesis of antibiotics

Table S13: KEGG categorization of *P. putida* proteins significantly more or less abundant during co-culture with *B. atrophaeus*. Gene Ontology categories are also included for cross-reference.

Uniprot ID	**Protein Name**	**Co/ Pure**	**q-value (%)**	**Gene Ontology**	**KEGG**
Nucleotide Metabolism					
Q88QA3	Adenine deaminase (ADE) (EC 3.5.4.2) (Adenine aminohydrolase) (AAH)	3.18	0.00	adenine catabolic process [GO:0006146]; adenine deaminase activity [GO:0000034]; hypoxanthine salvage [GO:0043103]; nucleotide metabolic process [GO:0009117]; zinc ion binding [GO:0008270]	Purine metabolism
Q88LD5	Amidophosphoribosyltransferase (ATase) (EC 2.4.2.14) (Glutamine phosphoribosylpyrophosphate amidotransferase)	2.94	0.00	'de novo' IMP biosynthetic process [GO:0006189]; amidophosphoribosyltransferase activity [GO:0004044]; metal ion binding [GO:0046872]; nucleoside metabolic process [GO:0009116]; purine nucleobase biosynthetic process [GO:0009113]	Purine metabolism

Q88 DP5	AMP nucleosidase	1.88	0.0 0	AMP nucleosidase activity [GO:0008714]; AMP salvage [GO:0044209]	Purine metabol ism
Q88 C93	Phosphomannomutase/ phosphoglucomutase (PMM / PGM) (EC 5.4.2.2) (EC 5.4.2.8)	1.78	0.0 0	alginic acid biosynthetic process [GO:0042121]; GDP-mannose biosynthetic process [GO:0009298]; lipopolysaccharide biosynthetic process [GO:0009103]; magnesium ion binding [GO:0000287]; phosphoglucomutase activity [GO:0004614]; phosphomannomutase activity [GO:0004615]	Purine metabol ism
Q88 BX1	ATP synthase subunit delta (ATP synthase F(1) sector subunit delta) (F-type ATPase subunit delta) (F-ATPase subunit delta)	1.46	0.5 2	plasma membrane [GO:0005886]; plasma membrane ATP synthesis coupled proton transport [GO:0042777]; proton-transporting ATP synthase activity, rotational mechanism [GO:0046933]; proton-transporting ATP synthase complex, catalytic core F(1) [GO:0045261]	Purine metabol ism
Q88 NN0	Ribonucleoside-diphosphate reductase subunit beta (EC 1.17.4.1)	1.40	0.5 2	deoxyribonucleoside diphosphate metabolic process [GO:0009186]; deoxyribonucleotide biosynthetic process [GO:0009263]; DNA replication [GO:0006260]; metal ion binding [GO:0046872]; ribonucleoside-diphosphate reductase activity, thioredoxin disulfide as acceptor [GO:0004748]; ribonucleoside-diphosphate reductase complex [GO:0005971]	Purine metabol ism
Q88 NG9	Phosphoribosylaminoi midazole-succinocarboxamide	1.04	2.7 4	'de novo' IMP biosynthetic process [GO:0006189]; ATP binding [GO:0005524];	Purine metabol ism

	synthase (EC 6.3.2.6) (SAICAR synthetase)			phosphoribosylaminoimidazolesuccinocarboxamide synthase activity [GO:0004639]	
Q88P16	Phosphoribosylformylglycinamidine synthase (FGAM synthase) (FGAMS) (EC 6.3.5.3) (Formylglycinamide ribonucleotide amidotransferase) (FGAR amidotransferase) (FGAR-AT)	0.98	2.7.4	'de novo' IMP biosynthetic process [GO:0006189]; ATP binding [GO:0005524]; cytoplasm [GO:0005737]; glutamine metabolic process [GO:0006541]; metal ion binding [GO:0046872]; phosphoribosylformylglycinamidine synthase activity [GO:0004642]	Purine metabolism
Q88P54	Carbamate kinase	0.94	2.7.4	arginine metabolic process [GO:0006525]; carbamate kinase activity [GO:0008804]	Purine metabolism
P0A120	DNA polymerase III subunit beta (EC 2.7.7.7)	0.94	2.7.4	3'-5' exonuclease activity [GO:0008408]; cytoplasm [GO:0005737]; DNA binding [GO:0003677]; DNA-directed DNA polymerase activity [GO:0003887]; DNA polymerase III complex [GO:0009360]; DNA replication [GO:0006260]	Purine metabolism
Q88MH8	Uridylate kinase (UK) (EC 2.7.4.22) (Uridine monophosphate kinase) (UMP kinase) (UMPK)	0.91	2.7.4	'de novo' CTP biosynthetic process [GO:0044210]; ATP binding [GO:0005524]; cytoplasm [GO:0005737]; UMP kinase activity [GO:0033862]	Pyrimidine metabolism
Q88FQ0	Dihydroorotate dehydrogenase family protein	0.82	2.7.4	cytoplasm [GO:0005737]; dihydroorotate dehydrogenase activity [GO:0004152]; iron-sulfur cluster binding [GO:0051536]; UMP biosynthetic process [GO:0006222]	Pyrimidine metabolism
Q88QN7	Elongation factor Tu-B (EF-Tu-B)	0.77	2.1.3	cytoplasm [GO:0005737]; GTPase activity [GO:0003924]; GTP	Purine metabolism

				binding [GO:0005525]; translation elongation factor activity [GO:0003746]	
Q88N54	Pyruvate kinase (EC 2.7.1.40)	0.76	2.13	glycolytic process [GO:0006096]; magnesium ion binding [GO:0000287]; potassium ion binding [GO:0030955]; pyruvate kinase activity [GO:0004743]	Purine metabolism
P0A171	RNA polymerase sigma-54 factor	0.74	2.13	DNA binding [GO:0003677]; DNA-directed RNA polymerase activity [GO:0003899]; DNA-templated transcription, initiation [GO:0006352]; identical protein binding [GO:0042802]; sequence-specific DNA binding transcription factor activity [GO:0003700]; sigma factor activity [GO:0016987]	Purine metabolism
P0A171	RNA polymerase sigma-54 factor	0.74	2.13	DNA binding [GO:0003677]; DNA-directed RNA polymerase activity [GO:0003899]; DNA-templated transcription, initiation [GO:0006352]; identical protein binding [GO:0042802]; sequence-specific DNA binding transcription factor activity [GO:0003700]; sigma factor activity [GO:0016987]	Pyrimidine metabolism
Q88BX4	ATP synthase subunit beta (EC 3.6.3.14) (ATP synthase F1 sector subunit beta) (F-ATPase subunit beta)	0.74	2.13	ATP binding [GO:0005524]; ATP hydrolysis coupled proton transport [GO:0015991]; plasma membrane [GO:0005886]; plasma membrane ATP synthesis coupled proton transport [GO:0042777]; proton-transporting ATP synthase	Purine metabolism

				activity, rotational mechanism [GO:0046933]; proton-transporting ATP synthase complex, catalytic core F(1) [GO:0045261]	
TCA Cycle					
Q88QD9	Acetoin dehydrogenase, alpha subunit	1.61	0.52	oxidoreductase activity, acting on the aldehyde or oxo group of donors, disulfide as acceptor [GO:0016624]	Citrate cycle (TCA cycle)
Q88FB1	Dihydrolipoyl dehydrogenase (EC 1.8.1.4)	0.71	1.38	cell redox homeostasis [GO:0045454]; detoxification of mercury ion [GO:0050787]; dihydrolipoyl dehydrogenase activity [GO:0004148]; flavin adenine dinucleotide binding [GO:0050660]; mercury (II) reductase activity [GO:0016152]; mercury ion binding [GO:0045340]; NADP binding [GO:0050661]	Citrate cycle (TCA cycle)
Q88M20	Fumarate hydratase class II (Fumarase C) (EC 4.2.1.2)	0.69	1.38	fumarate hydratase activity [GO:0004333]; fumarate metabolic process [GO:0006106]; tricarboxylic acid cycle [GO:0006099]; tricarboxylic acid cycle enzyme complex [GO:0045239]	Citrate cycle (TCA cycle)
Q88FS2	Isocitrate dehydrogenase [NADP] (EC 1.1.1.42)	0.68	1.38	glyoxylate cycle [GO:0006097]; isocitrate dehydrogenase (NADP+) activity [GO:0004450]; magnesium ion binding [GO:0000287]; NAD binding [GO:0051287];	Citrate cycle (TCA cycle)

				tricarboxylic acid cycle [GO:0006099]	
Q88FB3	Succinyl-CoA ligase [ADP-forming] subunit alpha (EC 6.2.1.5)	0.56	0.74	ATP binding [GO:0005524]; ATP citrate synthase activity [GO:0003878]; cofactor binding [GO:0048037]; succinate-CoA ligase (ADP-forming) activity [GO:0004775]	Citrate cycle (TCA cycle)
Q88QZ6	Acetyltransferase component of pyruvate dehydrogenase complex (EC 2.3.1.12)	0.48	0.74	dihydrolipoyllysine-residue acetyltransferase activity [GO:0004742]; glycolytic process [GO:0006096]; pyruvate dehydrogenase complex [GO:0045254]	Citrate cycle (TCA cycle)
Q88QZ5	Pyruvate dehydrogenase E1 component (EC 1.2.4.1)	0.41	0.00	pyruvate dehydrogenase (acetyl-transferring) activity [GO:0004739]	Citrate cycle (TCA cycle)
Carbon Fixation					
Q88CY9	Fructose-1,6-bisphosphatase class 1 (FBPase class 1) (EC 3.1.3.11) (D-fructose-1,6-bisphosphate 1-phosphohydrolase class 1)	2.25	0.00	cytoplasm [GO:0005737]; fructose 1,6-bisphosphate 1-phosphatase activity [GO:0042132]; gluconeogenesis [GO:0006094]; magnesium ion binding [GO:0000287]	Carbon fixation in photosynthetic organisms
Q88QD6	Acetyl-CoA carboxylase, biotin carboxylase	1.89	0.00	ATP binding [GO:0005524]; biotin carboxylase activity [GO:0004075]; metal ion binding [GO:0046872]	Carbon fixation pathways in prokaryotes
Q88HS1	3-hydroxyacyl-CoA dehydrogenase PaaC	1.73	0.00	3-hydroxyacyl-CoA dehydrogenase activity [GO:0003857]; 3-hydroxybutyryl-CoA dehydrogenase activity [GO:0008691]; coenzyme binding [GO:0050662]; fatty acid metabolic process [GO:0006631]; phenylacetate catabolic process [GO:0010124]	Carbon fixation pathways in prokaryotes

Q88KS6	Acyl-CoA ligase	1.17	1.38	ligase activity [GO:0016874]	Carbon fixation pathways in prokaryotes
Q88E32	Beta-ketothiolase	1.01	3.69	transferase activity, transferring acyl groups other than amino-acyl groups [GO:0016747]	Carbon fixation pathways in prokaryotes
Q88CU5	Malic enzyme	0.94	2.74	malate dehydrogenase (decarboxylating) (NAD+) activity [GO:0004471]; malate metabolic process [GO:0006108]; metal ion binding [GO:0046872]; NAD binding [GO:0051287]	Carbon fixation in photosynthetic organisms
Q88P44	Glyceraldehyde-3-phosphate dehydrogenase (EC 1.2.1.-)	0.85	2.74	glucose metabolic process [GO:0006006]; NAD binding [GO:0051287]; NADP binding [GO:0050661]; oxidoreductase activity, acting on the aldehyde or oxo group of donors, NAD or NADP as acceptor [GO:0016620]	Carbon fixation in photosynthetic organisms
Q88EH6	Acetyl-coenzyme A synthetase 1 (AcCoA synthetase 1) (Acs 1) (EC 6.2.1.1) (Acetate--CoA ligase 1) (Acyl-activating enzyme 1)	0.85	2.74	acetate-CoA ligase activity [GO:0003987]; acetyl-CoA biosynthetic process from acetate [GO:0019427]; AMP binding [GO:0016208]; ATP binding [GO:0005524]; metal ion binding [GO:0046872]	Carbon fixation pathways in prokaryotes
Q88LG1	Aromatic-amino-acid aminotransferase	0.84	2.74	biosynthetic process [GO:0009058]; cellular amino acid metabolic process [GO:0006520]; pyridoxal phosphate binding [GO:0030170];	Carbon fixation in photosynthetic organisms

				transaminase activity [GO:0008483]	
Q88M20	Fumarate hydratase class II (Fumarase C) (EC 4.2.1.2)	0.69	1.38	fumarate hydratase activity [GO:0004333]; fumarate metabolic process [GO:0006106]; tricarboxylic acid cycle [GO:0006099]; tricarboxylic acid cycle enzyme complex [GO:0045239]	Carbon fixation pathways in prokaryotes
Q88FS2	Isocitrate dehydrogenase [NADP] (EC 1.1.1.42)	0.68	1.38	glyoxylate cycle [GO:0006097]; isocitrate dehydrogenase (NADP+) activity [GO:0004450]; magnesium ion binding [GO:0000287]; NAD binding [GO:0051287]; tricarboxylic acid cycle [GO:0006099]	Carbon fixation pathways in prokaryotes
Q88FB3	Succinyl-CoA ligase [ADP-forming] subunit alpha (EC 6.2.1.5)	0.56	0.74	ATP binding [GO:0005524]; ATP citrate synthase activity [GO:0003878]; cofactor binding [GO:0048037]; succinate-CoA ligase (ADP-forming) activity [GO:0004775]	Carbon fixation pathways in prokaryotes
Terpenoid Backbone Biosynthesis					
Q88QG7	1-deoxy-D-xylulose-5-phosphate synthase (EC 2.2.1.7) (1-deoxyxylulose-5-phosphate synthase) (DXP synthase) (DXPS)	2.17	0.00	1-deoxy-D-xylulose 5-phosphate biosynthetic process [GO:0052865]; 1-deoxy-D-xylulose-5-phosphate synthase activity [GO:0008661]; magnesium ion binding [GO:0000287]; terpenoid biosynthetic process [GO:0016114]; thiamine biosynthetic process [GO:0009228]; thiamine pyrophosphate binding [GO:0030976]	Terpenoid backbone biosynthesis
Q88MH4	1-deoxy-D-xylulose 5-phosphate reductoisomerase (DXP	1.29	0.92	1-deoxy-D-xylulose-5-phosphate reductoisomerase activity [GO:0030604];	Terpenoid backbo

	reductoisomerase) (EC 1.1.1.267) (1-deoxyxylulose-5-phosphate reductoisomerase) (2-C-methyl-D-erythritol 4-phosphate synthase)			isopentenyl diphosphate biosynthetic process, methylerythritol 4-phosphate pathway [GO:0019288]; metal ion binding [GO:0046872]; NADPH binding [GO:0070402]; terpenoid biosynthetic process [GO:0016114]	ne biosynthesis
Q88PJ7	4-hydroxy-3-methylbut-2-en-1-yl diphosphate synthase (flavodoxin) (EC 1.17.7.3) (1-hydroxy-2-methyl-2-(E)-butenyl 4-diphosphate synthase)	1.22	1.25	4-hydroxy-3-methylbut-2-en-1-yl diphosphate synthase activity [GO:0046429]; 4 iron, 4 sulfur cluster binding [GO:0051539]; iron ion binding [GO:0005506]; isopentenyl diphosphate biosynthetic process, methylerythritol 4-phosphate pathway [GO:0019288]; terpenoid biosynthetic process [GO:0016114]	Terpenoid backbone biosynthesis
Q88E32	Beta-ketothiolase	1.01	3.69	transferase activity, transferring acyl groups other than amino-acyl groups [GO:0016747]	Terpenoid backbone biosynthesis
Drug Metabolism					
Q88EW5	Chemotaxis response regulator protein-glutamate methylesterase of group 1 operon (EC 3.1.1.61)	1.55	0.52	chemotaxis [GO:0006935]; cytoplasm [GO:0005737]; phosphorelay response regulator activity [GO:0000156]; protein-glutamate methylesterase activity [GO:0008984]	Drug metabolism - other enzymes
Q88FQ0	Dihydroorotate dehydrogenase family protein	0.82	2.74	cytoplasm [GO:0005737]; dihydroorotate dehydrogenase activity [GO:0004152]; iron-sulfur cluster binding [GO:0051536]; UMP	Drug metabolism - other enzymes

				biosynthetic process [GO:0006222]	
Q88G86	Alcohol dehydrogenase, zinc-containing	0.64	1.25	oxidoreductase activity [GO:0016491]; zinc ion binding [GO:0008270]	Drug metabolism - cytochrome P450
Fatty Acid Metabolism					
Q88DR1	Acyl-CoA thioesterase II	2.25	0.00	acyl-CoA hydrolase activity [GO:0047617]; acyl-CoA metabolic process [GO:0006637]	Fatty acid elongation
Q88QD6	Acetyl-CoA carboxylase, biotin carboxylase	1.89	0.00	ATP binding [GO:0005524]; biotin carboxylase activity [GO:0004075]; metal ion binding [GO:0046872]	Fatty acid biosynthesis
Q88HS1	3-hydroxyacyl-CoA dehydrogenase PaaC	1.73	0.00	3-hydroxyacyl-CoA dehydrogenase activity [GO:0003857]; 3-hydroxybutyryl-CoA dehydrogenase activity [GO:0008691]; coenzyme binding [GO:0050662]; fatty acid metabolic process [GO:0006631]; phenylacetate catabolic process [GO:0010124]	Fatty acid degradation
Q88E32	Beta-ketothiolase	1.01	3.69	transferase activity, transferring acyl groups other than amino-acyl groups [GO:0016747]	Fatty acid degradation
Q88QB3	3-oxoacyl-(Acyl-carrier-protein) reductase	0.99	2.74	oxidoreductase activity [GO:0016491]	Fatty acid biosynthesis
Q88HS3	Beta-ketoadipyl CoA thiolase PhaD	0.81	2.13	protocatechuate catabolic process [GO:0019619]; transferase activity, transferring acyl groups other than amino-acyl groups [GO:0016747]	Fatty acid degradation
Q88HS3	Beta-ketoadipyl CoA thiolase PhaD	0.81	2.13	protocatechuate catabolic process [GO:0019619];	Fatty acid

				transferase activity, transferring acyl groups other than amino-acyl groups [GO:0016747]	elongation
Q88G86	Alcohol dehydrogenase, zinc-containing	0.64	1.25	oxidoreductase activity [GO:0016491]; zinc ion binding [GO:0008270]	Fatty acid degradation
Q88R06	Formaldehyde dehydrogenase, glutathione-independent	0.51	0.74	oxidoreductase activity [GO:0016491]; zinc ion binding [GO:0008270]	Fatty acid degradation
Biosynthesis of Antibiotics					
Q88LD5	Amidophosphoribosyltransferase (ATase) (EC 2.4.2.14) (Glutamine phosphoribosylpyrophosphate amidotransferase)	2.94	0.00	'de novo' IMP biosynthetic process [GO:0006189]; amidophosphoribosyltransferase activity [GO:0004044]; metal ion binding [GO:0046872]; nucleoside metabolic process [GO:0009116]; purine nucleobase biosynthetic process [GO:0009113]	Biosynthesis of antibiotics
Q88PT6	Glycerate dehydrogenase	2.29	0.00	NAD binding [GO:0051287]; oxidoreductase activity, acting on the CH-OH group of donors, NAD or NADP as acceptor [GO:0016616]	Biosynthesis of antibiotics
Q88CY9	Fructose-1,6-bisphosphatase class 1 (FBPase class 1) (EC 3.1.3.11) (D-fructose-1,6-bisphosphate 1-phosphohydrolase class 1)	2.25	0.00	cytoplasm [GO:0005737]; fructose 1,6-bisphosphate 1-phosphatase activity [GO:0042132]; gluconeogenesis [GO:0006094]; magnesium ion binding [GO:0000287]	Biosynthesis of antibiotics
Q88QG7	1-deoxy-D-xylulose-5-phosphate synthase (EC 2.2.1.7) (1-deoxyxylulose-5-phosphate synthase) (DXP synthase) (DXPS)	2.17	0.00	1-deoxy-D-xylulose 5-phosphate biosynthetic process [GO:0052865]; 1-deoxy-D-xylulose-5-phosphate synthase activity [GO:0008661]; magnesium ion binding [GO:0000287]; terpenoid biosynthetic process [GO:0016114];	Biosynthesis of antibiotics

				thiamine biosynthetic process [GO:0009228]; thiamine pyrophosphate binding [GO:0030976]	
Q88I11	Threonine dehydratase family protein	1.92	0.00	cellular amino acid metabolic process [GO:0006520]; pyridoxal phosphate binding [GO:0030170]	Biosynthesis of antibiotics
Q88QD6	Acetyl-CoA carboxylase, biotin carboxylase	1.89	0.00	ATP binding [GO:0005524]; biotin carboxylase activity [GO:0004075]; metal ion binding [GO:0046872]	Biosynthesis of antibiotics
Q88C93	Phosphomannomutase/ phosphoglucomutase (PMM / PGM) (EC 5.4.2.2) (EC 5.4.2.8)	1.78	0.00	alginic acid biosynthetic process [GO:0042121]; GDP-mannose biosynthetic process [GO:0009298]; lipopolysaccharide biosynthetic process [GO:0009103]; magnesium ion binding [GO:0000287]; phosphoglucomutase activity [GO:0004614]; phosphomannomutase activity [GO:0004615]	Biosynthesis of antibiotics
Q88HS1	3-hydroxyacyl-CoA dehydrogenase PaaC	1.73	0.00	3-hydroxyacyl-CoA dehydrogenase activity [GO:0003857]; 3-hydroxybutyryl-CoA dehydrogenase activity [GO:0008691]; coenzyme binding [GO:0050662]; fatty acid metabolic process [GO:0006631]; phenylacetate catabolic process [GO:0010124]	Biosynthesis of antibiotics
Q88QD9	Acetoin dehydrogenase, alpha subunit	1.61	0.52	oxidoreductase activity, acting on the aldehyde or oxo group of donors, disulfide as acceptor [GO:0016624]	Biosynthesis of antibiotics
Q88DU4	4-hydroxy-tetrahydrodipicolinate reductase (HTPA	1.59	0.52	4-hydroxy-tetrahydrodipicolinate reductase [GO:0008839]; cytoplasm [GO:0005737];	Biosynthesis of antibiotics

	reductase) (EC 1.17.1.8)			diaminopimelate biosynthetic process [GO:0019877]; lysine biosynthetic process via diaminopimelate [GO:0009089]; NAD binding [GO:0051287]; NADPH binding [GO:0070402]; oxidoreductase activity, acting on CH or CH2 groups, NAD or NADP as acceptor [GO:0016726]	
Q88CT5	Pyrroline-5-carboxylate reductase (EC 1.5.1.2)	1.53	0.52	L-proline biosynthetic process [GO:0055129]; pyrroline-5-carboxylate reductase activity [GO:0004735]	Biosynthesis of antibiotics
Q88MH4	1-deoxy-D-xylulose 5-phosphate reductoisomerase (DXP reductoisomerase) (EC 1.1.1.267) (1-deoxyxylulose-5-phosphate reductoisomerase) (2-C-methyl-D-erythritol 4-phosphate synthase)	1.29	0.92	1-deoxy-D-xylulose-5-phosphate reductoisomerase activity [GO:0030604]; isopentenyl diphosphate biosynthetic process, methylerythritol 4-phosphate pathway [GO:0019288]; metal ion binding [GO:0046872]; NADPH binding [GO:0070402]; terpenoid biosynthetic process [GO:0016114]	Biosynthesis of antibiotics
Q88MF9	Enolase (EC 4.2.1.11) (2-phospho-D-glycerate hydro-lyase) (2-phosphoglycerate dehydratase)	1.27	1.25	cell surface [GO:0009986]; extracellular region [GO:0005576]; glycolytic process [GO:0006096]; magnesium ion binding [GO:0000287]; phosphopyruvate hydratase activity [GO:0004634]; phosphopyruvate hydratase complex [GO:0000015]	Biosynthesis of antibiotics
Q88PL2	Extragenic suppressor protein SuhB	1.23	1.25	inositol monophosphate 1-phosphatase activity [GO:0008934]; inositol phosphate dephosphorylation	Biosynthesis of antibiotics

				[GO:0046855]; phosphatidylinositol phosphorylation [GO:0046854]	
Q88PJ7	4-hydroxy-3-methylbut-2-en-1-yl diphosphate synthase (flavodoxin) (EC 1.17.7.3) (1-hydroxy-2-methyl-2-(E)-butenyl 4-diphosphate synthase)	1.22	1.25	4-hydroxy-3-methylbut-2-en-1-yl diphosphate synthase activity [GO:0046429]; 4 iron, 4 sulfur cluster binding [GO:0051539]; iron ion binding [GO:0005506]; isopentenyl diphosphate biosynthetic process, methylerythritol 4-phosphate pathway [GO:0019288]; terpenoid biosynthetic process [GO:0016114]	Biosynthesis of antibiotics
Q88DY9	Acetolactate synthase, small subunit	1.20	1.25	acetolactate synthase activity [GO:0003984]; amino acid binding [GO:0016597]; branched-chain amino acid biosynthetic process [GO:0009082]	Biosynthesis of antibiotics
Q88KS6	Acyl-CoA ligase	1.17	1.38	ligase activity [GO:0016874]	Biosynthesis of antibiotics
P59604	Argininosuccinate synthase (EC 6.3.4.5) (Citrulline--aspartate ligase)	1.09	2.13	arginine biosynthetic process [GO:0006526]; argininosuccinate synthase activity [GO:0004055]; ATP binding [GO:0005524]; cytoplasm [GO:0005737]	Biosynthesis of antibiotics
P0A0Z9	Amino-acid acetyltransferase (EC 2.3.1.1) (N-acetylglutamate synthase) (AGS) (NAGS)	1.05	3.69	acetyl-CoA:L-glutamate N-acetyltransferase activity [GO:0004042]; arginine biosynthetic process [GO:0006526]; cytoplasm [GO:0005737]	Biosynthesis of antibiotics
Q88NG9	Phosphoribosylaminoimidazole-succinocarboxamide	1.04	2.74	'de novo' IMP biosynthetic process [GO:0006189]; ATP binding [GO:0005524];	Biosynthesis of antibiotics

	synthase (EC 6.3.2.6) (SAICAR synthetase)			phosphoribosylaminoimidazolesuccinocarboxamide synthase activity [GO:0004639]	
Q88E32	Beta-ketothiolase	1.01	3.69	transferase activity, transferring acyl groups other than amino-acyl groups [GO:0016747]	Biosynthesis of antibiotics
Q88P16	Phosphoribosylformylglycinamidine synthase (FGAM synthase) (FGAMS) (EC 6.3.5.3) (Formylglycinamide ribonucleotide amidotransferase) (FGAR amidotransferase) (FGAR-AT)	0.98	2.74	'de novo' IMP biosynthetic process [GO:0006189]; ATP binding [GO:0005524]; cytoplasm [GO:0005737]; glutamine metabolic process [GO:0006541]; metal ion binding [GO:0046872]; phosphoribosylformylglycinamidine synthase activity [GO:0004642]	Biosynthesis of antibiotics
Q88EI9	Aspartate kinase (EC 2.7.2.4) (Aspartokinase)	0.95	3.69	amino acid binding [GO:0016597]; aspartate kinase activity [GO:0004072]; ATP binding [GO:0005524]; cytoplasm [GO:0005737]; lysine biosynthetic process via diaminopimelate [GO:0009089]; methionine biosynthetic process [GO:0009086]; threonine biosynthetic process [GO:0009088]	Biosynthesis of antibiotics
Q88MU8	Homoserine dehydrogenase (EC 1.1.1.3)	0.94	2.74	amino acid binding [GO:0016597]; homoserine dehydrogenase activity [GO:0004412]; isoleucine biosynthetic process [GO:0009097]; methionine biosynthetic process [GO:0009086]; NADP binding [GO:0050661]; threonine biosynthetic process [GO:0009088]	Biosynthesis of antibiotics
Q88GQ0	Catalase-peroxidase (CP) (EC 1.11.1.21) (Peroxidase/catalase)	0.93	2.74	catalase activity [GO:0004096]; heme binding [GO:0020037];	Biosynthesis of

				hydrogen peroxide catabolic process [GO:0042744]; metal ion binding [GO:0046872]; response to oxidative stress [GO:0006979]	antibiotics
Q88P53	Ornithine carbamoyltransferase, catabolic (OTCase) (EC 2.1.3.3)	0.90	2.74	amino acid binding [GO:0016597]; arginine biosynthetic process [GO:0006526]; arginine catabolic process to ornithine [GO:0019547]; cytoplasm [GO:0005737]; ornithine carbamoyltransferase activity [GO:0004585]	Biosynthesis of antibiotics
Q88P44	Glyceraldehyde-3-phosphate dehydrogenase (EC 1.2.1.-)	0.85	2.74	glucose metabolic process [GO:0006006]; NAD binding [GO:0051287]; NADP binding [GO:0050661]; oxidoreductase activity, acting on the aldehyde or oxo group of donors, NAD or NADP as acceptor [GO:0016620]	Biosynthesis of antibiotics
Q88EH6	Acetyl-coenzyme A synthetase 1 (AcCoA synthetase 1) (Acs 1) (EC 6.2.1.1) (Acetate--CoA ligase 1) (Acyl-activating enzyme 1)	0.85	2.74	acetate-CoA ligase activity [GO:0003987]; acetyl-CoA biosynthetic process from acetate [GO:0019427]; AMP binding [GO:0016208]; ATP binding [GO:0005524]; metal ion binding [GO:0046872]	Biosynthesis of antibiotics
Q88LG1	Aromatic-amino-acid aminotransferase	0.84	2.74	biosynthetic process [GO:0009058]; cellular amino acid metabolic process [GO:0006520]; pyridoxal phosphate binding [GO:0030170]; transaminase activity [GO:0008483]	Biosynthesis of antibiotics
Q88CV2	3-dehydroquinate synthase (EC 4.2.3.4)	0.83	2.74	3-dehydroquinate synthase activity [GO:0003856]; aromatic amino acid family	Biosynthesis of

				biosynthetic process [GO:0009073]; chorismate biosynthetic process [GO:0009423]; cytoplasm [GO:0005737]	antibiotics
Q88P31	Glucose-6-phosphate 1-dehydrogenase (G6PD) (EC 1.1.1.49)	0.82	2.13	glucose-6-phosphate dehydrogenase activity [GO:0004345]; glucose metabolic process [GO:0006006]; NADP binding [GO:0050661]; pentose-phosphate shunt [GO:0006098]	Biosynthesis of antibiotics
Q88HS3	Beta-ketoadipyl CoA thiolase PhaD	0.81	2.13	protocatechuate catabolic process [GO:0019619]; transferase activity, transferring acyl groups other than amino-acyl groups [GO:0016747]	Biosynthesis of antibiotics
Q88N54	Pyruvate kinase (EC 2.7.1.40)	0.76	2.13	glycolytic process [GO:0006096]; magnesium ion binding [GO:0000287]; potassium ion binding [GO:0030955]; pyruvate kinase activity [GO:0004743]	Biosynthesis of antibiotics
Q88FB1	Dihydrolipoyl dehydrogenase (EC 1.8.1.4)	0.71	1.38	cell redox homeostasis [GO:0045454]; detoxification of mercury ion [GO:0050787]; dihydrolipoyl dehydrogenase activity [GO:0004148]; flavin adenine dinucleotide binding [GO:0050660]; mercury (II) reductase activity [GO:0016152]; mercury ion binding [GO:0045340]; NADP binding [GO:0050661]	Biosynthesis of antibiotics
Q88M20	Fumarate hydratase class II (Fumarase C) (EC 4.2.1.2)	0.69	1.38	fumarate hydratase activity [GO:0004333]; fumarate metabolic process [GO:0006106]; tricarboxylic acid cycle [GO:0006099];	Biosynthesis of antibiotics

				tricarboxylic acid cycle enzyme complex [GO:0045239]	
Q88FS2	Isocitrate dehydrogenase [NADP] (EC 1.1.1.42)	0.68	1.38	glyoxylate cycle [GO:0006097]; isocitrate dehydrogenase (NADP+) activity [GO:0004450]; magnesium ion binding [GO:0000287]; NAD binding [GO:0051287]; tricarboxylic acid cycle [GO:0006099]	Biosynthesis of antibiotics
Q88G86	Alcohol dehydrogenase, zinc-containing	0.64	1.25	oxidoreductase activity [GO:0016491]; zinc ion binding [GO:0008270]	Biosynthesis of antibiotics
Q88FB3	Succinyl-CoA ligase [ADP-forming] subunit alpha (EC 6.2.1.5)	0.56	0.74	ATP binding [GO:0005524]; ATP citrate synthase activity [GO:0003878]; cofactor binding [GO:0048037]; succinate-CoA ligase (ADP-forming) activity [GO:0004775]	Biosynthesis of antibiotics
Q88R06	Formaldehyde dehydrogenase, glutathione-independent	0.51	0.74	oxidoreductase activity [GO:0016491]; zinc ion binding [GO:0008270]	Biosynthesis of antibiotics
Q88P52	Arginine deiminase (ADI) (EC 3.5.3.6) (Arginine dihydrolase) (AD)	0.49	0.74	arginine catabolic process to ornithine [GO:0019547]; arginine deiminase activity [GO:0016990]; cytoplasm [GO:0005737]	Biosynthesis of antibiotics
Q88QZ6	Acetyltransferase component of pyruvate dehydrogenase complex (EC 2.3.1.12)	0.48	0.74	dihydrolipoyllysine-residue acetyltransferase activity [GO:0004742]; glycolytic process [GO:0006096]; pyruvate dehydrogenase complex [GO:0045254]	Biosynthesis of antibiotics
Q88QZ5	Pyruvate dehydrogenase E1 component (EC 1.2.4.1)	0.41	0.00	pyruvate dehydrogenase (acetyl-transferring) activity [GO:0004739]	Biosynthesis of antibiotics

SI 4.3 Supplemental Figures

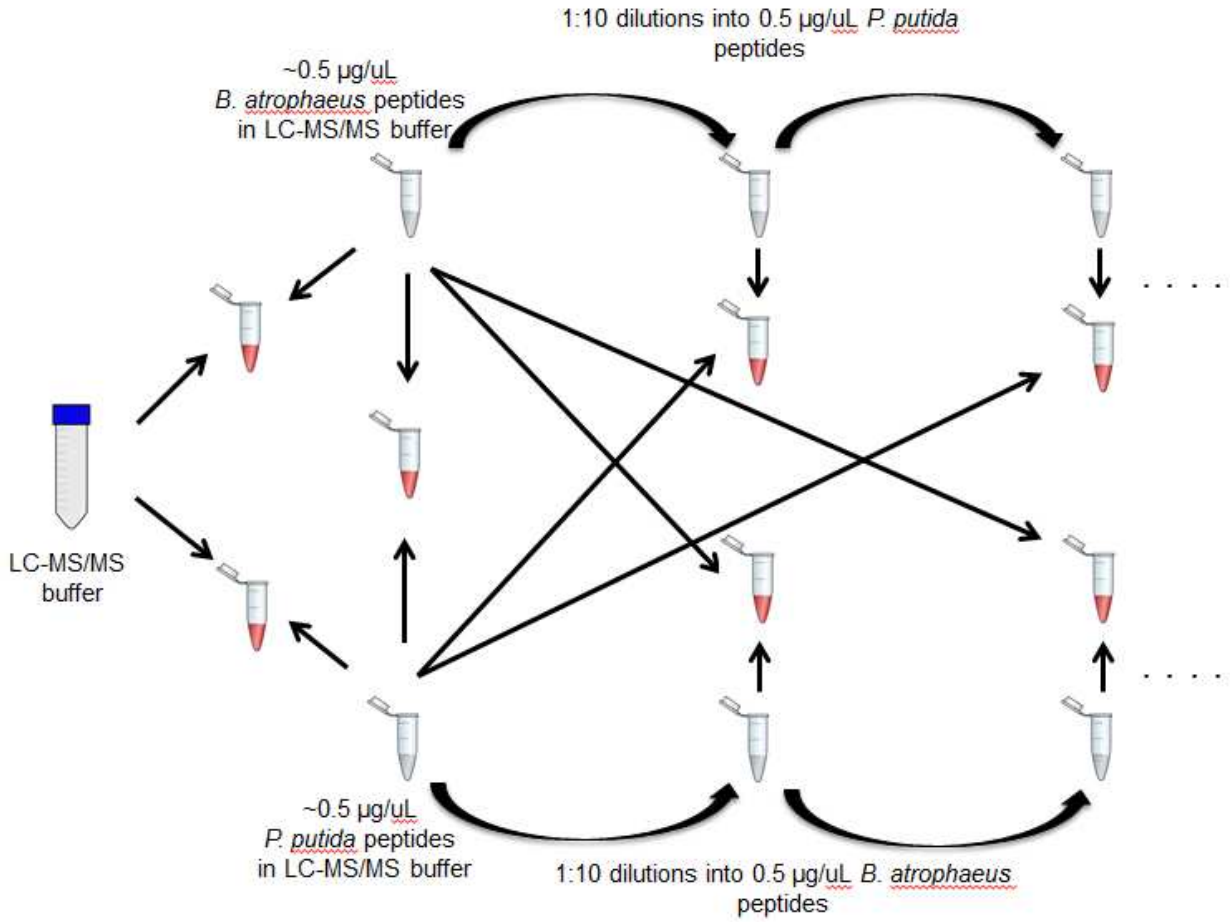

Figure S12: Peptide dilution schematic for experiments to determine limit of quantification for peptides of each species against a background of peptides from the other species. Each straight, black arrow represents a transfer of 10 µL. Each tube icon containing red sample was analyzed in duplicate by nanoLC-MS/MS. Only the first two dilution levels are shown, though samples through seven-fold dilutions were prepared and analyzed.

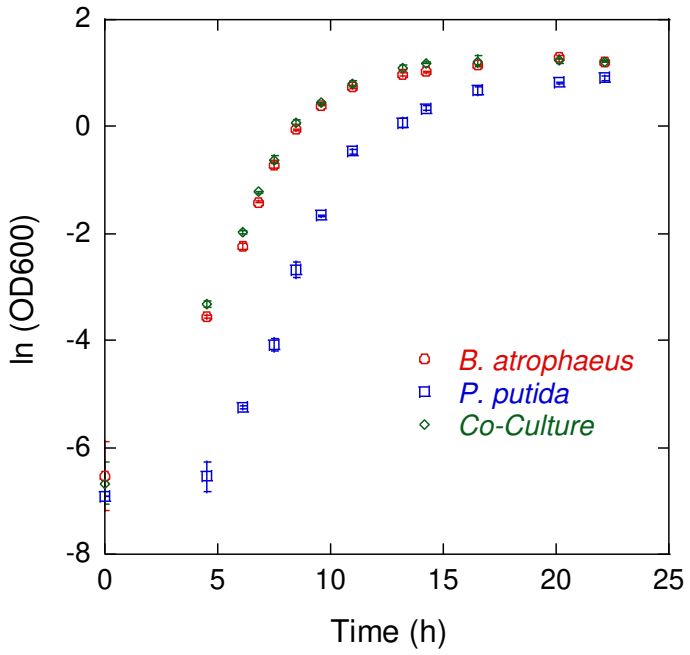

Figure S13: Growth curves for each culture growing in 200 mL 10 g/L tryptic soy broth for proteomics. Specific growth rate (μ) for each biological replicate flask was calculated as the slope of the line connecting three points in the linear part of the curve.

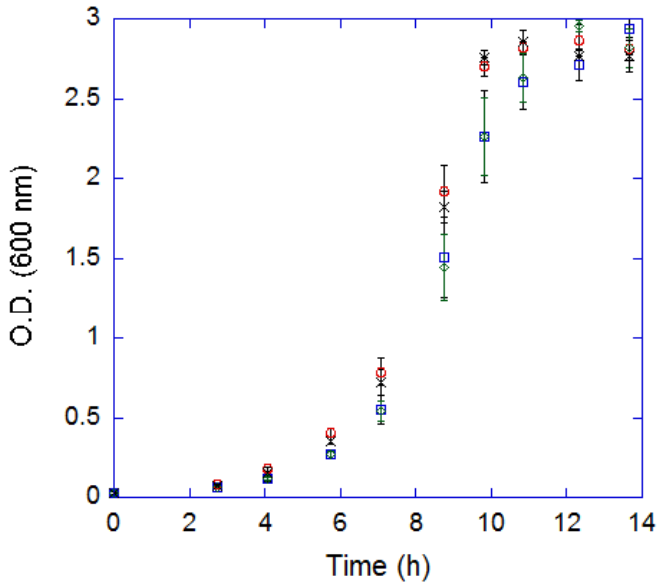

Figure S14: *B.atrophaeus* growth in a medium consisting of 50% fresh MHM defined medium and 50% (v/v) of 0.2 µM-filtered supernatant from 20 h cultures of *B.atrophaeus* (circles), *P.putida* (squares), co-culture with excess (36 µM) iron (diamonds), and co-culture with limited (0.9 µM) iron (cross-hatch). All final medium combinations were supplemented with 36 µM $FeSO_4$, in order to account for any reduced iron in the added supernatant.

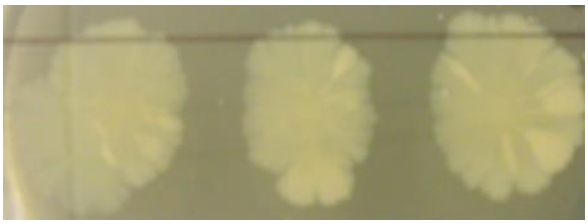

Figure S15: *P.putida* colonies after two weeks' growth on a 10g/L TSB agar plate without *B.atrophaeus*. *P. putida* colonies were spotted below a marked line on the plate, similar to those pictured in Figure 6 in the main text.

SI 4.4 Supplemental Information References

Ning K, Fermin D, Nesvizhskii AI (2012) Comparative analysis of different label-free mass spectrometry based protein abundance estimates and their correlation with RNA-Seq gene expression data. J Proteome Res 11:2261-2271. doi: 10.1021/pr201052x

Silva JC, Gorenstein MV, Li G-Z, Vissers JPC, Geromanos SJ (2006) Absolute quantification of proteins by LCME^{E}. Molec Cell Prot 5:144-156. doi:10.1074/mcp.M500230-MCP200

Storey JD (2002) A direct approach to false discovery rates. Statist Methodol 64:479-498. doi: 10.1111/1467-9868.00346

Chapter 5 Supplemental Information

SI 5.1 Experimental Procedures

5.1.1 Construction and operation of air-cathode MFCs

In a single-chamber, air-cathode MFC, electrogenic microbes living in a biofilm on the surface of a conductive anode utilize that anode as an electron acceptor during anaerobic respiration. Electrons deposited to the anode flow through a circuit to the surface of a cathode, the catalytic surface of which faces the interior of the single MFC chamber. At the cathode surface, oxygen from air diffusing passively through the cathode to the interior, liquid-facing cathode surface is reduced to water. The electrochemical potential of this reduction reaction drives the flow of electrons through the MFC circuit, generating a current [Liu and Logan 2004]. Single-chamber, air-cathode MFCs were constructed based on a previous design from Liu and Logan (2004), with some modifications. Polypropylene schedule 40 pipe (IPEX, Pineville, NC), cut into 3.8 cm slices, was used for the MFC body. The liquid volume of each MFC was ~30 ml, and the circular openings were 7.0 cm^2. Non-wet-proofed carbon cloth and 30% wet-proofed carbon cloth (Fuel Cell Earth, Woburn, MA) were used for the anodes and cathodes, respectively. A mixture of polytetrafluoroethylene (PTFE) (Sigma-Aldrich, St. Louis, MO) and Vulcan XC72 carbon black powder (Cabot, Boston, MA) comprising 15 µl of 30 wt% PTFE per mg carbon powder was applied to the cathode prior to drying at 375 °C for 1 h. Diffusion layers of 60 wt% PTFE solution were applied by coating the outer, air-exposed cathode surface and then drying at 375 °C for 30 min. This process was repeated four times. Platinum catalyst applied to the interior, solution-facing side of the cathode sheet by mixing 7 µl Nafion binder and 3 µl isopropanol per gram of 10 wt% platinum on carbon (all materials from Sigma-Aldrich, St. Louis, MO) to result in 0.5 mg Pt/cm^2 cathode surface. Cathodes were allowed to dry overnight before use. Sheets of

Lexan plastic 1 mm thick were cut into 10.2 cm x 10.2 cm squares, into one of which was cut a 7.0 cm^2 hole to allow for diffusion of air to the solution side of the cathode. Plumbing gasket material (Plumbcraft, Bedford Heights, OH) was placed between the Lexan squares and the anode or cathode. Titanium wire (0.012", Wytech, Rahway, NJ) pressed between the anode and MFC body as a conductive lead. All layers of the MFCs were cinched together with four screws and washers at the corners of the reactor. MFC leads were attached to a 1 kΩ external resistor (Elenco, Wheeling, IL). Voltage was recorded automatically across all MFCs every 5 min with a 16-channel Picolog 1216 multimeter (Pico Technologies, Cambridgeshire, UK) connected to a personal computer. Nine MFCs were constructed using cathodes from the same batch.

All MFC medium components were obtained from Fisher (Pittsburgh, PA). MFC medium consisted of 5.84 g/l NaH_2PO4, 15.47 g/l $Na_2HPO_4 \cdot 7H_2O$, 0.31 g/l NH_4Cl, 0.13 g/l KCl, 10 ml/l ATCC trace mineral supplement solution, 10 ml/l ATCC trace vitamin solution, and 4.08 g/l (30 mM) sodium acetate trihydrate. MFC medium was adjusted to pH 7.0 with 10 N NaOH. The chemical oxygen demand (COD) of the carbon source in the medium was calculated according to a balanced equation for the complete oxidation of acetate (Rittman and McCarty 2001):

$$\frac{1}{8}CO_2 + \frac{1}{8}HCO_3^- + H^+ + e^- \rightarrow \frac{1}{8}CH_3COO^- + \frac{3}{8}H_2O \qquad (1)$$

According to equation (1), there are 8 electron equivalents (e^- eq) per mol acetate. Since acetate has a molecular weight of 59.05 g/mol, for acetate, (59.05 g acetate/mol acetate)/(8 e^- eq/mol acetate) = 7.38 g acetate/e^- eq. The medium for these MFCs contained (59.05 g/mol)*(0.03 mol/L) = 1.77 g acetate/L. Therefore, the oxygen

demand (OD) for the acetate in the minimal medium used in MFCs may be calculated as: (8 g OD/e^- eq)*(1.77 g acetate/L)/(7.38 g acetate/e^- eq) = 1.92 g OD/L.

Inoculum for new MFCs consisted of effluent from a mature MFC originally inoculated with anaerobic digester sludge from Drake Water Reclamation Facility (Fort Collins, CO). This effluent was collected over the course of two years' operation of MFCs on 30 mM sodium acetate. Approximately once per week, 1 g/l each of ferric citrate and sodium acetate was added to this stored inoculum to enrich for metal-respiring anaerobic species. To inoculate new MFCs, 10 ml each of this stored inoculum, fresh MFC effluent, and fresh MFC medium were added to a MFC reactor. During the biofilm enrichment process, no new inoculum was added, but 10 ml of MFC medium was replaced weekly with fresh medium.

5.1.2 Harvest of MFC anodes

Bulk solution samples (i) were harvested 24 h after initial inoculation by transferring all bulk solution into two 15-ml conical tubes, centrifuging (3 000 x g, 20 min), discarding the supernatant, immediately freezing the pellets in liquid nitrogen, and storing the frozen pellets at -80 °C. Early anodes (ii) were harvested once appreciable but low current density (~0.05 A/m^2) was observed (~130 h). Intermediate anodes (iii) were harvested at the point of maximum current density (~0.6 A/m^2) during the batch following the first full replacement of medium (~450-500 h). That medium replacement occurred after current densities had increased appreciably above those observed for early anodes. For mature anodes (iv), anodes were harvested at the point of maximum current density (~0.8 A/m^2) after replacement of medium. Mature MFCs were operated for over

two years in batch mode, replacing medium completely after current density dropped below 0.01 A/m^2.

At the harvest point, anodes were removed from MFCs and immersed briefly in sterile phosphate buffer. A small section was cut out from the center of the anode using a sterile razor blade and prepared for scanning electron microscopy. Anodes then were cut in half from top to bottom, placed in DNAse-free 50-ml conical tubes (Corning, NY), immediately flash-frozen in liquid N_2, and stored at -80 °C until extraction of proteins and DNA.

5.1.3 DNA extraction, amplification, and sequencing

One anode half was thawed gradually by transferring tubes to -20 °C for 4 h and then to 4 °C for 2 h. The entire biofilm was scraped from the anode surface with a sterile razor blade into an extraction tube from the Powersoil DNA Isolation Kit (MoBio Laboratories, Inc., Carlsbad, CA, USA). The scraped anode cloth was added to the tube as well, and the tube was subjected to one freeze-thaw cycle at -80 °C to crack the biofilm. DNA extraction proceeded according to the Powersoil manufacturer's instructions.

DNA samples were amplified for sequencing by Research and Testing Laboratories (Lubbock, TX) according to their standard protocols, using a forward and reverse fusion primer. The forward primer was constructed with (5'-3') the Illumina i5 adapter (AATGATACGGCGACCACCGAGATCTACAC), an 8-10 bp barcode, a primer pad, and the 28F primer (GAGTTTGATCNTGGCTCAG). The reverse fusion primer was constructed with (5'-3') the Illumina i7 adapter (CAAGCAGAAGACGGCATACGAGAT), an 8-10 bp barcode, a primer pad, and the

388R primer (TGCTGCCTCCCGTAGGAGT). Primer pads were designed to ensure the primer pad/primer combination had a melting temperature of 63 °C-66 °C according to methods developed by the lab of Patrick Schloss (http://www.mothur.org/w/images/0/0c/Wet-lab_MiSeq_SOP.pdf). Amplifications were performed in 25 µl reactions with Qiagen HotStar Taq master mix (Qiagen Inc, Valencia, California), 1 ul of each 5uM primer, and 1 ul of template. Reactions were performed on ABI Veriti thermocyclers (Applied Biosytems, Carlsbad, California) under the following thermal profile: 95 °C for 5 min, then 35 cycles of 94 °C for 30 s, 54 °C for 40 s, 72 °C for 1 min, followed by one cycle of 72 °C for 10 min and 4 °C hold. Amplification products were visualized with eGels (Life Technologies, Grand Island, New York). Products were then pooled equimolar and each pool was size selected in two rounds using Agencourt AMPure XP (BeckmanCoulter, Indianapolis, Indiana) in a 0.7 ratio for both rounds. Size selected pools were quantified using the Qubit 2.0 fluorometer (Life Technologies) and loaded on an Illumina MiSeq (Illumina, Inc. San Diego, California) 2x300 flow cell at 10pM.

5.1.4 Quantitation and analysis of 16S rRNA gene amplicons

Results files from 16S rRNA gene sequencing by MiSeq containing counts of operational taxonomical units (OTUs) in each biological replicate sample were used to calculate the proportion of counts (i.e., relative abundance) of each taxon in each anode biofilm. Diversity of early and intermediate MFC communities was compared with two-tailed Welch's t-tests between Simpson's index values.

Multivariate analysis of MFC OTUs was conducted in R using the *vegan* package. Tests for significant differences in OTU relative abundance between communities at all

developmental stages was conducted with a non-parametric multivariate analysis of variance (npMANOVA) test between all biological replicates of all developmental stages, using the *adonis* function [Buttigieg and Ramette 2014]. Pairwise Pearson's r correlations were conducted as a post-hoc analysis between each binary set of MFC developmental stages, in order to determine the developmental stage comparisons that were the driving sources of variation detected in the npMANOVA test. Additionally, a non-metric multidimensioinal scaling (NMDS) plot was constructed by generating a dissimilarity matrix with the Gower distance measure [Kuczynski et al. 2011] from a sample-by-species matrix of OTU counts by the metaMDS function in the R *vegan* package. The NMDS plot then was constructed using the ordiplot, orditorp, and ordihull functions. Since for both of these post-hoc analyses the early and mature communities showed the greatest degree of difference, a similarity percentage (SIMPER) analysis was conducted between the early and mature sample sets using the *simper* function in the *vegan* package. This analysis identifies the OTUs that contributed most to the overall differences between the communities as a whole [Clarke 1993]. Post-hoc comparisons of pairwise Pearsons correlations between each biofilm sample were conducted in R using the cor() function and plotted with ggplot(). Pearson's r coefficients were compared between sample types with a Tukey's HSD test.

5.1.5 Extraction and digestion of proteins from MFC anode biofilms

The remaining anode half was thawed gradually by transferring tubes to -20 °C for 4 h and then to 4 °C for 2 h. The entire biofilm was scraped from each anode half using a sterile razor blade. The anode half and its scraped material was placed into sterile tubes (Corning, NY), to which was added hot (95 °C) lysis buffer (50 mM ammonium

bicarbonate, 1% sodium deoxycholate (SDC), pH 8.2). The samples were subjected to a round of biofilm cracking by freezing in liquid nitrogen and then thawing on ice. Samples then were sonicated on ice (50% duty cycle) for 5 min, 1 s on, 2 s off. Samples were centrifuged (5 000 x g, 10 min) and the supernatant was isolated to a low-bind, siliconized tube, which was centrifuged (14 000 x g for 20 min) to remove remaining cell debris and isolate protein extract in the supernatant.

Proteins were precipitated from the raw extract by adding an ice-cold mixture of trichloroacetic acid (TCA) in acetone (final volumetric ratio of 1:1:8 extract:TCA:acetone) and precipitating overnight in 50 ml conical tubes at -20 °C. The mixtures were centrifuged (10 000 x g, 60 min) and the supernatant was removed. Protein pellets were washed with 2 ml ice-cold acetone, centrifuged again, acetone was removed by evaporation. Protein pellets then were resuspended in 50 mM ammonium bicarbonate, 1% sodium deoxycholate (SDC), 5% acetonitrile (ACN), pH 8.2 and sonicated for 20 s on ice (1 s on, 2 s off) to resuspend the pellet. Concentration of resuspended proteins was quantified by bicinchoninic acid (BCA) assay (Pierce Life Technologies, Carlsbad, CA). Then 50 µg of protein were combined with a volume of 100 mM dithiothreitol (DTT) to result in a final concentration of 20 mM DTT. The mixture was incubated first at 95 °C for 2 min, then at 65 °C for 30 min, to denature and reduce protein sulfide bonds. Five microliters of 375 mM iodoacetamide were added to each sample for cysteine alkylation at room temperature in the dark for 30 min. Then, a sufficient volume of 50 mM ammonium bicarbonate (pH 8.2) was added to result in a final reaction volume of 150 µl, such that the concentration of SDC was below 0.1% during the trypsin digestion. To that mixture 0.5 µl of 50 mM $CaCl_2$ was added, along

with 2.5 μg (1:20 trypsin: protein) of Promega Gold mass spectrometry grade trypsin (Promega, Madison, WI). ACN was added to a final concentration of 8% (v/v) ACN. The digestion was conducted at 38 °C for 9 h, after which double digestion with one μg trypsin was conducted for 4 h. Digestion reactions were stopped by adding 5 μl 100% formic acid to decrease pH to ~2. Digestions were centrifuged (13 000 x g, 20 min) to collect any acid-precipitated SDC. A volume containing 50 μg peptides was evaporated in a speed-vap and the resulting peptide pellets were resuspended in 45 μl of 5% ACN, 0.1% formic acid. Residual detergent and contaminants were removed from 30 ul of the resuspended peptides with a C-18 spin column (Pierce Life Technologies, Carlsbad, CA), following the manufacturer's instructions. Eluted peptides were evaporated and resuspended in 2.5% acetonitrile, 0.1% formic acid for LC-MS/MS analysis (described in main text).

5.1.6 Protein identification, label-free quantification, and statistical analysis

Results files from LC-MS/MS analysis (.wiff files from Analyst v.1.5 TR) were processed with ProteinPilot (v.4.5 beta), using a .fasta database consisting of the entire bacterial proteome (proteome filter "taxonomy: Bacteria [2]," downloaded from Uniprot 2-15-15) along with common contaminants. All three .wiff files corresponding to each technical replicate LC-MS/MS shot that was run for each biological replicate MFC anode were processed simultaneously in the database search. The search was conducted in ProteinPilot using rapid search ID and no biological modifications. False discovery rate (FDR) analysis was conducted using a decoy database consisting of reversed sequences from the bacterial database, with FDR protein identification significance threshold ≤ 0.01. An attempt was made to extract precursor ion intensities using a quantitation

microapp (v. 1.0) in PeakView software (v. 1.1.1, ABsciex). Due to the large file size, however, this quantitation procedure failed, indicating the requirement for an alternative quantitation method. Peptide summaries were exported as .txt files from the .group files produced by ProteinPilot during the database search. These .txt files were imported into R statistical software (v. 3.1.2) for quantitation by spectral counting, using in-house R-scripts, as described below. First, for each biological replicate, technical replicates were separated out based on spectrum ID numbers. Since in the .txt file a given LC-MS/MS spectrum is assigned to more than one peptide, it was necessary to devise a method to handle multiple peptide-spectrum matches (PSMs) to prevent multiple counting of the same spectral evidence. ProteinPilot assigns spectra to peptides with an "Unused Score" defined as the amount of spectral evidence explained by that PSM that is not explained by a higher-ranking peptide. Only the PSM with the highest Unused Score was kept for the purpose of spectral count quantitation. This approach is similar to a "distributed" NSAF approach [Zhang et al. 2010], except that a PSM is retained based on ProteinPilot Unused Score, rather than based on the number of total PSMs assigned to that peptide. The result was a list of unique PSMs, each with the highest observed Unused Score. Peptides then were filtered to retain only those peptides corresponding to proteins with an "N" value equal to or greater than the number of proteins reported by the ProteinPilot FDR analysis that met the 1.0% FDR cutoff. Applying this FDR cutoff, nearly all of the peptide-protein multiple assignments were to proteins from organisms of the same genus. Since downstream analysis focused on higher taxonomical categories (Genus and higher), only the top identification (also used by ProteinPilot for the protein Unused Score assignment) was retained. For cases in which a peptide was matched to homologous

proteins from different genera, the identification corresponding to a genus already represented in the dataset by unique protein identifications was retained. Finally, in the few cases in which a peptide was matched to homologous proteins from different genera that were not otherwise represented in the dataset, only the first assignment provided by ProteinPilot (i.e., with the highest Unused Score) was retained.

Only proteins identified in at least one technical replicate of at least two biological replicate anodes for a condition (early or intermediate) were retained for statistical analysis. Thus, in addition to the qualifications of having a high Unused Score and meeting the 1.0% FDR cutoff as described above, proteins also had to be found across at least two biological replicate anodes to be considered for further analysis. Spectral count (SpC) was calculated for the 853 remaining proteins using the "table" function in R. Then the normalized spectral abundance factor (NSAF) was calculated for each protein in each technical replicate as previously described [Zhang et al. 2010]. The resulting value for each protein was called the "unNSAF" to reflect the fact that PSMs had been filtered according to Unused Score. For each protein, the mean unNSAF value across technical replicates for a biological replicate anode was then normalized to the count of operational taxonomical units (OTUs) of the genus corresponding to the protein, for that biological replicate anode. This normalization step was included to account for changes in the relative abundance of that genus in the consortium when comparing protein expression between developmental stages. Then $\log_2$(unNSAF) was calculated for each protein in each biological replicate MFC. For those proteins found in both early and intermediate anode biofilms, the resulting value was used to compute fold-change ratios between early and intermediate developmental stages as well as to conduct a two-

tailed, homoscedastic Student's t-test between the two developmental stages. Since a multiple testing correction [Storey et al. 2002] resulted in no proteins with $q<0.05$ despite the clear left peak in the p-value histogram (SI Figure S8), only fold-change and p-value cutoffs were used as criteria for proteins of interest (POIs) , as suggested recently [Pascovici et al. 2016]. Those cutoffs were $\log_2$(intermediate/early) >1 or -1 and $p<0.05$. For proteins identified in only one of the two MFC conditions, significance testing was conducted at the pathway level, as described below.

5.1.7 Metabolic pathway analysis with Gene Ontology and KEGG

The set of intermediate MFC proteins was compared with the set of early MFC proteins, using a Fisher's Exact Test based on the FatiGO algorithm [Al-Shahrour et al. 2004] implemented in Blast2GO (v.3.1.0, www.blast2go.com). A Benjamini-Hochberg FDR multiple testing correction (FDR < 0.05) [Benjamini and Hochberg 1995] was applied in the test to identify Gene Ontology pathways that were significantly enriched among the proteins from each developmental stage. This type of significance testing seems especially appropriate for samples containing different genera, since comparable proteins from different genera contribute to the determination of significance of entire pathways, rather than individual proteins.

For analysis with the KEGG database (http://www.genome.jp/kegg/) the combined set of proteins that were either a UDPI or a POI more abundant in the intermediate anode biofilm were assigned to KEGG pathways using the KEGG GhostKOALA tool (http://www.kegg.jp/ghostkoala/). This tool, appropriate for use with metaproteomics datasets, bins submitted proteins into KEGG functional modules and summarizes protein pathway and taxonomic distributions.

5.1.8 Comparison of phylogenies from DNA sequencing and metaproteomics

For each MFC biofilm, species composition was quantitated both in terms of relative abundance of MiSeq OTUs and in terms of relative abundance of proteins associated with genera by the KEGG GhostKOALA tool. These two methods generally agreed on broad phylogenetic trends. As reported in the main text, both MiSeq and GhostKOALA methods showed greater diversity in the intermediate biofilms than in the early biofilms. The linear regression model of all relative abundance values showed a strong overall correlation ($R^2 = 0.914$, p-value $< 2.2e^{-16}$) between the GhostKOALA and MiSeq datasets. Eight of the 10 greatest residuals in the linear model were observed for non-*Enterobacter Gammaproteobacteria*, *Betaproteobacteria* or *Deltaproteobacteria* in the intermediate MFCs. For seven of those residuals, the relative abundance of OTUs was less than the relative abundance of proteins assigned to that taxon (i.e., residuals were greater than 0), perhaps due to the greater number of total taxa identified by the MiSeq method (SI 5.3 Figure S7).

The two methods for determining phylogeny—OTUs and proteins—generally agreed on the identities of the most abundant taxa. For both methods, non-*Enterobacter Gammaproteobacteria* had by far the greatest relative abundance in the early MFCs (83.2 ± 4.1% of OTUs and 74.5 ± 2.9% of GhostKOALA protein identifications). Further, the top five most abundant taxa were the same for MiSeq and GhostKOALA methods, except for *Deltaproteobacteria*, the taxon containing *Geobacter*. That taxon had the third-highest relative abundance in early MFCs based on GhostKOALA categorization of proteins, while it was the eighth most abundant class based on OTUs. For intermediate biofilms, the top five most abundant taxa were the same for both classification methods,

though with some differences in rank (SI 5.2 Table S5). As with the early biofilms, the differences in rank of taxa between the two methods was most pronounced for *Deltaproteobacteria*. This class was the second most abundant in intermediate MFCs according to GhostKOALA classification of proteins (22.8 ± 3.6% of identified proteins) but fourth most abundant according to OTUs (11.3 ± 4.2% of OTUs). Both methods indicated that *Gammaproteobacteria* remained the most abundant taxon in intermediate MFCs (27.9 ± 5.0% of proteins and 25.4 ± 4.3% of OTUs). Several previous metaproteomics studies compared phylogenies gleaned from 16S rRNA gene sequences with those reflected in protein identifications [Qu et al. 2012]. This type of comparison serves as a useful validation of a portion of the proteomics dataset, as well as an indication of the community coverage achieved by protein extraction and identification.

SI 5.2 Supplemental Tables

Table S14: Comparison of OTU relative abundance between four MFC developmental conditions: early (E), intermediate (I), mature (M) and solution (S), as identified by MiSeq sequencing of 16S rRNA genes. Each developmental stage was represented by three independent biological replicate samples. A nonparametric MANOVA p-value was generated by a comparison between all conditions. As a post-hoc test between conditions, each replicate sample was compared against each replicate sample in the other condition by Pearson's pairwise correlation, thereby generating mean and standard deviation Pearsons' r coefficients for each pairwise comparison. Coefficients with different subscript letters indicate Pearson's r coefficients that differ significantly (Tukey's HSD test, $p<0.05$).

Comparison	npMANOVA p-value or Pearson's r coefficient
EIMS	0.00099
EI	0.53 ± 0.22^{a}

EM	0.01 ± 0.01^{b}
ES	0.52 ± 0.30^{a}
IM	0.40 ± 0.23^{a}
IS	0.38 ± 0.20^{a}
MS	0.005 ± 0.004^{b}

Table S15: Relative abundance across developmental stages of OTUs contained within different bacterial classes. Error terms represent standard deviation across three separate MFC anode (or solution) samples.

Class	Solution (%)	Early (%)	Intermediate (%)	Mature (%)
Gammaproteobacteria	90.9 ± 3.3	83.4 ± 7.1	25.6 ± 7.2	1.1 ± 0.6
Deltaproteobacteria	0.1 ± 0.1	0.5 ± 0.5	11.3 ± 7.2	70.1 ± 3.7
Alphaproteobacteria	0.3 ± 0.1	4.1 ± 0.9	14.3 ± 2.0	1.5 ± 0.9
Betaproteobacteria	3.4 ± 1.3	1.4 ± 0.4	11.6 ± 4.1	1.5 ± 0.3
Epsilonproteobacteria	1.7 ± 1.6	0.7 ± 0.2	0.0 ± 0.0	0.0 ± 0.0

Table S16**:** Relative abundance across developmental stages of the three genera responsible for the majority of significant differences between early and mature MFC anode communities. Error terms represent standard deviation across three separate MFC anode (or solution) samples.

Genus	Class	Solution (%)	Early (%)	Intermediate (%)	Mature (%)
Acinetobacter	*Gammaproteobacteria*	25.8 ± 11.3	27.3 ± 28.5	6.7 ± 6.2	0.4 ± 0.2
Pseudomonas	*Gammaproteobacteria*	58.1 ± 18.9	55.1 ± 33.1	17.7 ± 9.9	0.6 ± 0.3
Geobacter	*Deltaproteobacteria*	0.1 ± 0.0	0.5 ± 0.5	11.0 ± 7.1	68.7 ± 3.6

Table S17: Prominent OTUs (relative abundance greater than or equal to 1.0%) in MFC communities at each stage of development. Solution samples were from the bulk solution of the MFCs 24 h after inoculation. The column for OTU shows the identifier for specific OTUs. The column for %OTUs signifies the percentage of total OTUs in that sample that were identified as the specified OTU. The error term represents standard deviation (±SD) across three biological replicate samples.

OTU	Genus	% OTUs (± SD)
Solution		
356	*Pseudomonas*	30.6 ± 27.6
96	*Pseudomonas*	26.1 ± 25.4
132	*Acinetobacter*	25.8 ± 11.3
274	Unknown *Enterobacteriaceae*	6.5 ± 5.2
68	*Comamonas*	2.5 ± 1.3
189	*Arcobacter*	1.7 ± 1.6
154	Unknown *Bacteria*	1.2 ± 1.2
Early		
96	*Pseudomonas*	53.3 ± 32.8
132	*Acinetobacter*	27.1 ± 28.3
78	*Flavobacterium*	4.4 ± 2.8
380	Unknown *Rhizobiales*	3.4 ± 0.8
236	*Rhodococcus*	1.0 ± 1.7
356	*Pseudomonas*	1.0 ± 0.4
Intermediate		
96	*Pseudomonas*	15.6 ± 10.0
333	*Geobacter*	11.0 ± 7.1
380	Unknown *Rhizobiales*	9.2 ± 0.8
132	*Acinetobacter*	6.5 ± 6.1
204	Unknown *Synergistales*	6.3 ± 4.1
198	*Thauera*	5.9 ± 1.9
78	*Flavobacterium*	4.4 ± 3.7
236	*Rhodococcus*	4.0 ± 3.2
391	*Clostridium*	3.3 ± 3.1
154	Unknown *Bacteria*	3.2 ± 3.6
288	*Alcaligenes*	2.1 ± 1.7
152	Unknown *Actinomycetales*	1.9 ± 2.0
356	*Pseudomonas*	1.7 ± 0.8
59	Unknown *Bacteria*	1.2 ± 0.6
165	*Gordonia*	1.2 ± 1.1

314	*Myroides*	1.2 ± 1.6
296	*Brevundimonas*	1.1 ± 0.5
Mature		
333	*Geobacter*	68.7 ± 3.6
154	Unknown *Bacteria*	13.2 ± 7.2
204	Unknown *Synergistales*	2.3 ± 0.5
30	*Actinomyces*	2.0 ± 2.7

Table S18: Selected UDPIs categorized by broad metabolic process, as determined by KEGG, GO, Uniprot, and literature review.

Uniprot ID	Protein Name	Function or Pathway	Genus
	Central Carbon Metabolism		
A5GEB7	Citrate synthase	TCA cycle	*Alcaligenes*
U7U728	Aconitate hydratase B	TCA cycle	*Alcaligenes*
Q1JW62	Aconitate hydratase B	TCA cycle	*Desulfuromonas*
I4N0T6	Aconitate hydratase B	TCA cycle	*Pseudomonas*
U7U739	Citrate synthase	TCA cycle	*Alcaligenes*
U7U7F2	Citrate synthase	TCA cycle	*Alcaligenes*
U7U7F8	Malate dehydrogenase	TCA cycle	*Alcaligenes*
Q74D54	Isocitrate dehydrogenase	TCA cycle	*Geobacter*
Q74EG8	Fumarate hydratase, class I	TCA cycle	*Geobacter*
I7FK92	Phosphoglycerate kinase	Glycolysis/gluconeogenesis	*Geobacter*
V9WRF6	Glyceraldehyde-3-phosphate dehydrogenase	Glycolysis/gluconeogenesis	*Pseudomonas*
A0A081GJT4	Glycogen debranching protein	Glycolysis/gluconeogenesis	*Cyanobium*
W7YDT5	Enolase	Glycolysis/gluconeogenesis	*Saccharicrinis*
N6YGD2	Phosphoenolpyruvate carboxykinase	Gluconeogenesis	*Thauera*
N6XEP4	Isocitrate lyase	Glyoxylate cycle	*Thauera*
	Anaerobic Metabolism		
Q74D51	2-oxoglutarate:ferredoxin oxidoreductase, alpha subunit (KorA)	Anaerobic TCA cycle	*Geobacter*
Q74D50	2-oxoglutarate:ferredoxin oxidoreductase, thiamin diphosphate-binding subunit (KorB)	Anaerobic TCA cycle	*Geobacter*

Q74D49	2-oxoglutarate:ferredoxin oxidoreductase, gamma subunit (KorC)	Anaerobic TCA cycle	*Geobacter*
Q74GZ6	Pyruvate-flavodoxin oxidoreductase (Por)	Anaerobic TCA cycle	*Geobacter*
E3PT29	Pyruvate-flavodoxin oxidoreductase (Por)	Anaerobic TCA cycle	*Clostridium*
B8J4R0	Sulfite reductase, dissimilatory-type alpha subunit	Anaerobic respiration	*Desulfovibrio*
B2YHF8	Dissimilatory sulphite reductase beta subunit (Fragment)	Anaerobic respiration	*Uncultured*
Q8EKJ1	Nitrate-inducible formate dehydrogenase molybdopterin-binding subunit FdnG	Anaerobic respiration	*Shewanella*
	Acetate Metabolism		
Q74FU6	NADPH-Fe(3+) oxidoreductase subunit alpha (SfrA)	Acetate metabolism.	*Geobacter*
Q74FU5	NADPH-Fe(3+) oxidoreductase subunit beta (SfrB)	Acetate metabolism.	*Geobacter*
Q74GS1	Succinyl:acetate coenzyme A transferase	Acetyl-CoA synthesis	*Geobacter*
	Fatty Acid Metabolism		
J0JLY0	Acetyl-CoA acetyltransferase	Fatty acid biosynthesis	*Alcaligenes*
Q74BM2	Acetyl-CoA carboxylase, biotin carboxylase component (Acc-ase)	Fatty acid biosynthesis	*Geobacter*
Q74CR7	3-oxoacyl-[acyl-carrier-protein] synthase 2 (EC 2.3.1.179)	Fatty acid biosynthesis	*Geobacter*
T0AZR6	Acyl carrier protein (ACP)	Fatty acid biosynthesis	*Thauera*
S9ZEL5	3-ketoacyl-ACP reductase (EC 1.1.1.36)	Fatty acid biosynthesis	*Thauera*

A0A022LGX0	Long-chain fatty acid--CoA ligase	Fatty acid β-oxidation	*Dietzia*
S9ZIA5	Acyl-CoA dehydrogenase	Fatty acid β-oxidation	*Thauera*
Q747G7	Biotin-dependent acyl-CoA carboxylase, carboxyltransferase subunit	Fatty acid β-oxidation	*Geobacter*
Q39UX8	Short-chain acyl-CoA dehydrogenase	Fatty acid β-oxidation	*Geobacter*
	Membrane Proteins		
U1XWB5	Membrane protein	Unknown	*Alcaligenes*
U7U8X8	Membrane protein	Unknown	*Alcaligenes*
X5HVW6	Membrane protein	Unknown	*Aeromonas*
H1RM45	Gram-negative type outer membrane porin protein	Transport	*Comamonas*
B9MDB0	Porin Gram-negative type	Transport	*Acidovorax*
X5HGU5	Porin	Transport	*Aeromonas*
A0A022LPU2	ABC transporter substrate-binding protein	Transport	*Dietzia*
A0A073ISB0	Branched-chain amino acid ABC transporter substrate-binding protein	Transport	*Synergistes*
L7X6F0	Membrane protein (Outer membrane protein A)	Receptor; transport	*Aeromonas*
Q74AK2	Sodium/solute symporter family protein	Transport	*Geobacter*
Q39Y99	Outer membrane channel, putative	Transport	*Geobacter*
Q74E95	Sodium/solute symporter family protein	Transport	*Geobacter*
K2N8B7	Basic membrane lipoprotein	Transport	*Nitratireductor*
K2PP47	Cationic amino acid ABC transporter	Transport	*Nitratireductor*

	periplasmic binding protein		
W6XM61	ABC-type transporter, periplasmic subunit	Transport	*Burkholderia*
A0A075PCY9	Porin	Transport	*Pseudomonas*
Q74FD9	Lipoprotein cytochrome c (OmcX)	Electron transfer	*Geobacter*
Q74GH2	Cytochrome c,, and cytochrome b	Electron transfer	*Geobacter*
Q39RK5	ResB-like family cytochrome c	Electron transfer	*Geobacter*
Q74FJ5	ResB-like family cytochrome c biogenesis protein	Electron transfer	*Geobacter*
Q74GA2	NADH dehydrogenase I, G subunit	Electron transport chain	*Geobacter*
A0A067A3Q5	Outer membrane insertion C-terminal signal domain protein	Protein insertion	*Pseudomonas*
W8Q8M8	Outer membrane protein assembly factor BamA	Protein insertion	*Pseudomonas*
A0A077F872	Outer membrane protein H1	Antibiotic resistance	*Pseudomonas*
A0A081UU63	Maltoporin (Maltose-inducible porin)	Transport	*Aeromonas*
A0A085ETL9	Various polyols ABC transporter, periplasmic substrate-binding protein	Transport	*Devosia*
	Stress Response or Interactions		
Q74EI7	Phage tail sheath protein, putative	Phage	*Geobacter*
N6XZL4	Tail sheath protein	Phage	*Thauera*
Q74FS1	Cysteine synthase A	Contact-dependent inhibition	*Geobacter*
Q74E06	Superoxide dismutase	Oxidative stress	*Geobacter*
N6ZL72	Superoxide dismutase	Oxidative stress	*Thauera*
N6Y581	Phenylacetic acid degradation protein PaaD	Response to toxic aromatic	*Thauera*

U7UB80	Alkyl hydroperoxide reductase subunit C	Oxidative stress	*Alcaligenes*
Q74E46	Universal stress protein	Stress	*Geobacter*
	Nitrogen Metabolism		
E3PUH2	Glutamate dehydrogenase	Amino acid biosynthesis	*Clostridium*
G9PT06	Glutamate dehydrogenase	Amino acid biosynthesis	*Synergistes*
R5PD20	Glutamate dehydrogenase	Amino acid biosynthesis	*Odoribacter*
Q74DL1	Glutamate dehydrogenase	Amino acid biosynthesis	*Geobacter*
U7UGI7	Glutamate dehydrogenase	Amino acid biosynthesis	*Prevotella*
A0A022LGN0	Glutamate-binding protein	Amino acid biosynthesis	*Dietzia*
Q760A4	Nitrite reductase (Fragment)	Denitrification or nitrification	*uncultured*
U1YC31	Nitrous-oxide reductase	Denitrification	*Alcaligenes*
A1KA74	NosZ protein	Denitrification	*Azoarcus*
A7UMG8	Nitrous oxide reductase	Denitrification	*uncultured*
Q747H2	Rubredoxin:oxygen/nitric oxide oxidoreductase	Nitric oxide detoxification	*Geobacter*
Q74BM9	Nitrogen fixation protein NifU	Nitrogen fixation	*Geobacter*
E3PUA0	Hydroxylamine reductase/nitrate reductase (EC 1.7.99.1)	Nitrogen assimilation; nitric oxide production	*Clostridium*

Table S19: Complete relative abundance values (mean %OTUs in a sample) for taxa in common between GhostKOALA annotation of proteins and OTUs from MiSeq sequencing of 16S rRNA gene amplicons from early and intermediate MFC anode biofilm samples. Relative abundances of OTUs are also shown for the solution and mature biofilm samples.

Taxon	OTUs - solution	GhostKOALA-early	OTUs-early	GhostKOALA-intermediate	OTUs-intermediate	OTUs - mature

Gammaproteobacteria - Others	84.31	74.49	83.17	27.90	25.41	1.02
Betaproteobacteria	3.36	8.83	1.40	19.95	11.62	1.48
Actinobacteria	0.12	2.63	1.55	8.38	9.95	2.91
Deltaproteobacteria	0.08	2.90	0.77	22.83	11.33	70.13
Bacteroidetes	0.54	2.66	5.17	4.84	6.34	0.73
Alphaproteobacteria	0.27	2.73	4.11	6.86	14.25	1.49
Epsilonproteobacteria	1.67	0.91	0.73	0.37	0.02	0.01
Gammaproteobacteria - Enterobacteria	6.57	1.83	0.26	1.73	0.43	0.08
Synergistetes	0.93	0.73	0.89	1.27	6.65	2.39
Firmicutes - Bacilli	0.02	0.63	0.11	0.41	0.44	0.14
Firmicutes - Clostridia	0.32	0.41	1.13	3.02	5.54	1.38
Cyanobacteria	0.00	0.26	0.00	0.74	0.00	0.00
Firmicutes - Others	0.04	0.21	0.13	0.67	0.51	0.28
Chrysiogenetes	0.00	0.16	0.00	0.00	0.00	0.00
Thermotogae	0.00	0.16	0.00	0.10	0.00	0.00
Fusobacteria	0.00	0.05	0.00	0.00	0.00	0.00
Spirochaetes	0.05	0.22	0.34	0.25	0.18	0.27
Chlamydiae	0.00	0.05	0.00	0.00	0.00	0.00
Planctomycetes	0.00	0.05	0.00	0.00	0.00	0.00
Chlorobi	0.00	0.05	0.00	0.05	0.00	0.00

Euryarchaeota	0.00	0.06	0.00	0.00	0.00	0.00
Caldisericia	0.00	0.06	0.00	0.00	0.00	0.00
Deferribacteres	0.00	0.00	0.00	0.17	0.00	0.00
Chloroflexi	0.00	0.00	0.00	0.10	0.00	0.00
Acidobacteria	0.00	0.00	0.00	0.12	0.00	8.74E-03
Gemmatimonadetes	0.00	0.00	0.00	0.12	0.01	7.03E-03
Verrucomicrobia	0.00	0.00	0.00	0.12	0.00	0.00

SI 5.3 Supplemental Figures

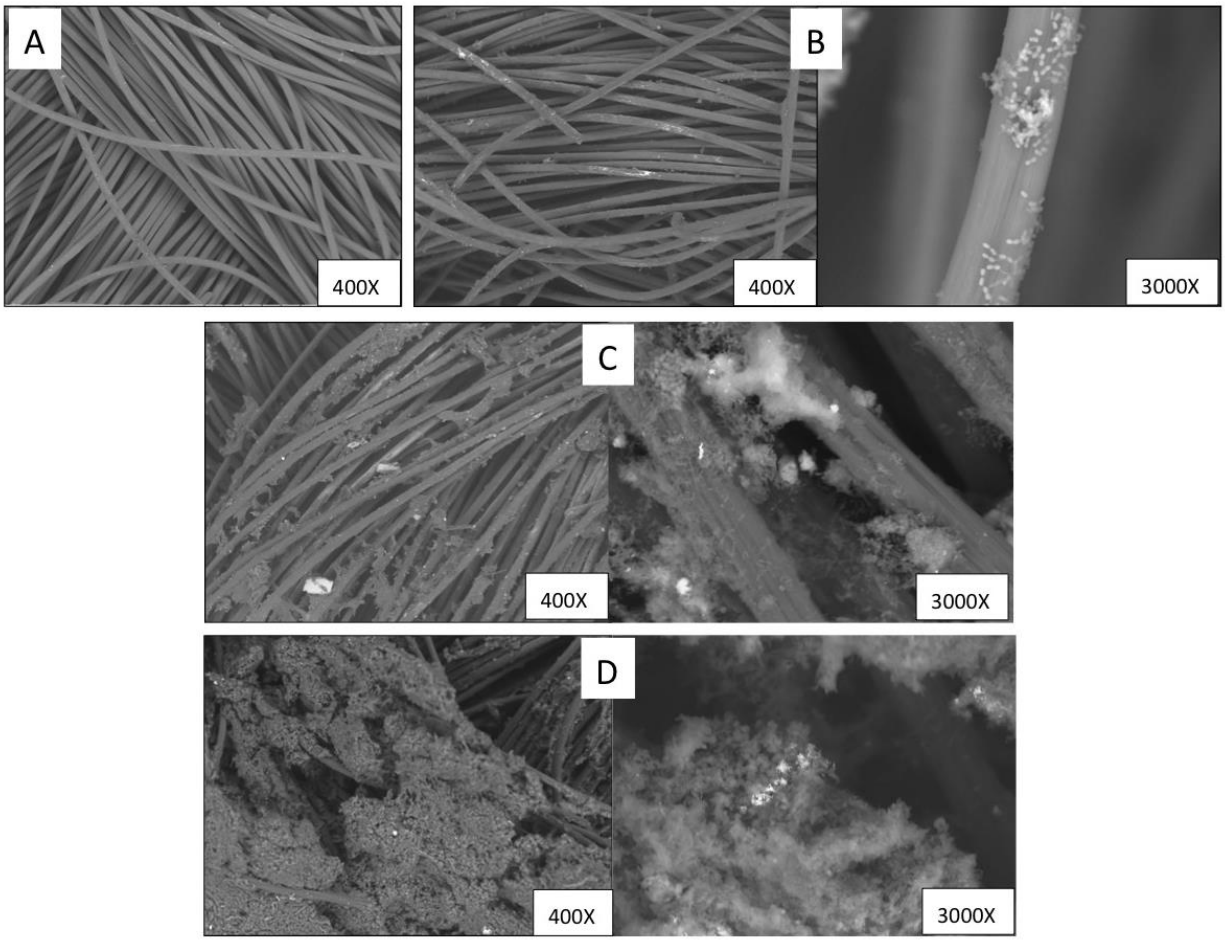

Figure S16: Scanning electron microscope images (400X or 3 000X magnification) of MFC anode carbon cloth fibers at (A) non-inoculated, (B) early, (C) intermediate, and (C) mature stages of biofilm development.

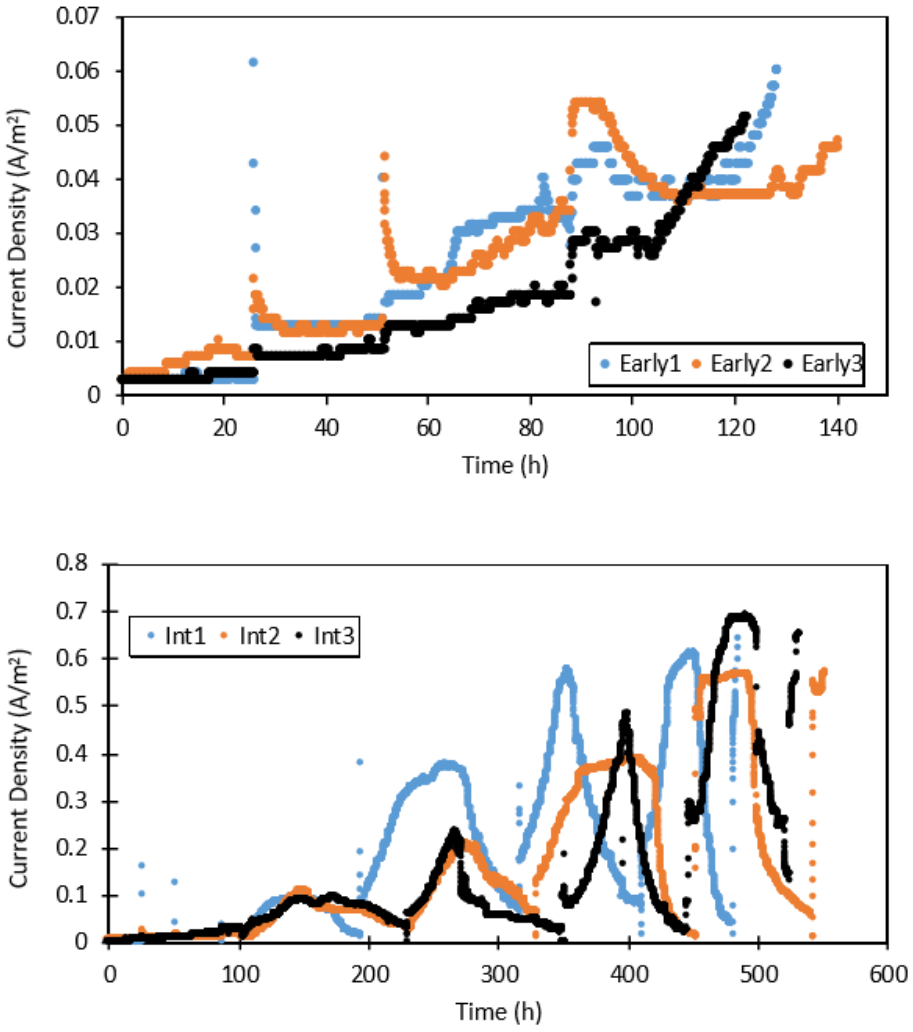

Figure S17: Current density for replicates of early (top) and intermediate (bottom) MFCs (inoculum originally derived from anaerobic digester sludge) after enrichment on batches of 30 mM acetate.

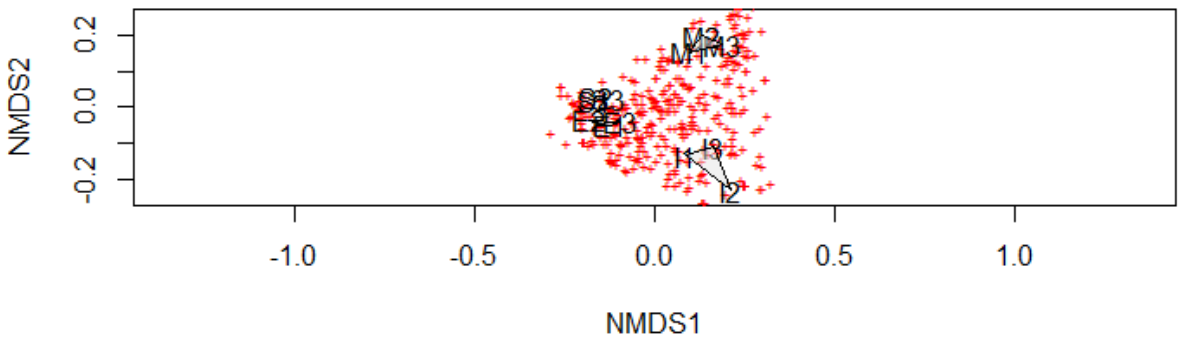

Figure S18: Non-metric multidimensional scaling (NMDS) plot of MFC anode OTUs along two principal coordinates. OTUs were identified by MiSeq sequencing of MFC anode 16S rRNA gene amplicons from three biological replicates of four different developmental conditions: S (solution), E (early biofilm), I (intermediate biofilm), M (mature biofilm). In the R *vegan* package, a Gower dissimilarity matrix was constructed with the metaMDS function from a sample-by-species matrix of OTU counts. The ordiplot, orditorp, and ordihull functions then were used to generate the NMDS plot. Similarity in relative abundance of genera is represented as spatial proximity within the two principal coordinates. Samples for S and E were clustered close enough together to obscure distinction of sample replicates.

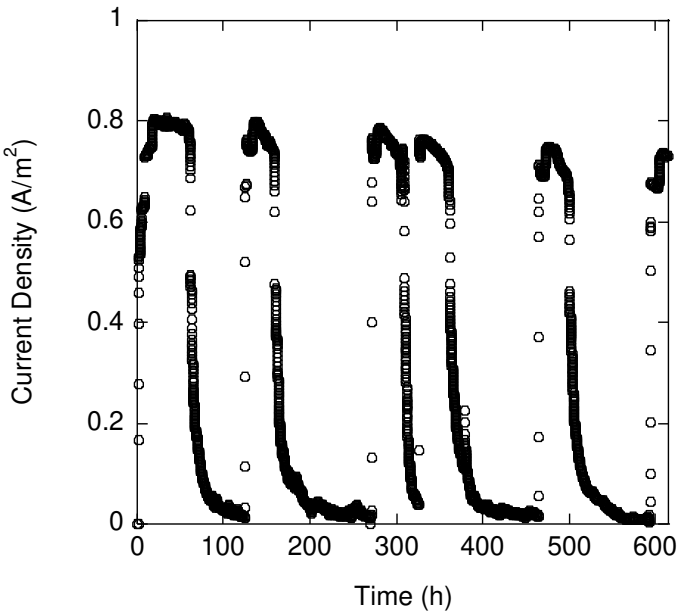

Figure S19**:** Current density of a mature MFC (inoculum originally derived from anaerobic digester sludge) after enrichment for over two years on batches of 30 mM

acetate.

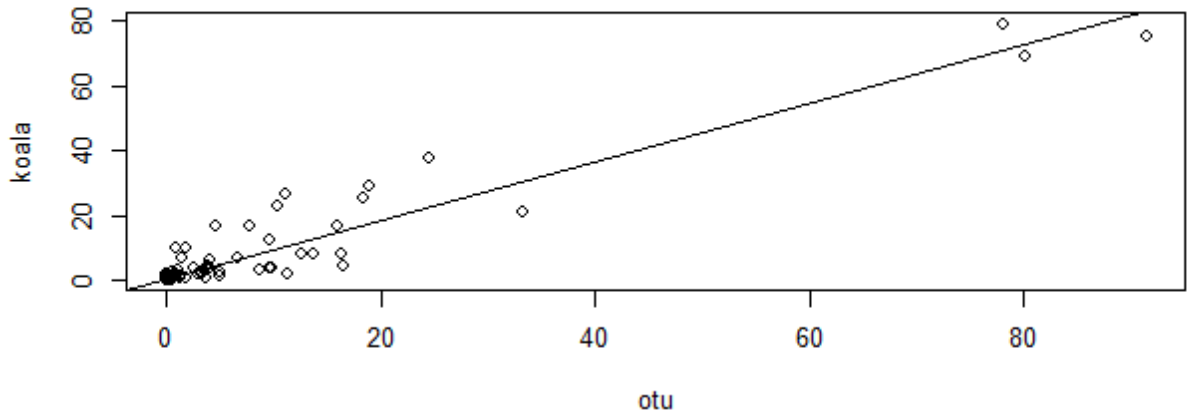

Figure S20: Linear regression of OTUs from MiSeq sequencing of 16S rRNA gene amplicons ("otu") against proteins identified by GhostKOALA ("koala") with respect to relative abundance of taxa. The linear regression was performed in R using the *lm* function on paired relative abundance values for each taxon in each biological replicate anode biofilm, excluding the intercept. Adjusted $R^2 = 0.914$, p-value < $2.2e^{-16}$.

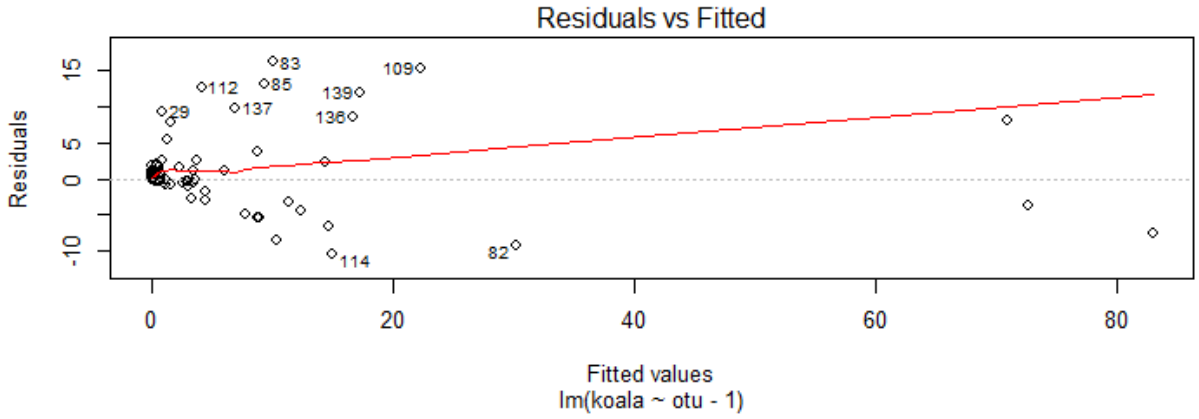

Figure S21: Residuals vs. fitted plots for linear regression of taxon relative abundances, as quantified by GhostKOALA identification of proteins ("koala") and OTUs from MiSeq sequencing of 16S rRNA gene amplicons ("otu"). The ten pairwise comparisons with the greatest positive or negative residuals are labeled.

(A)

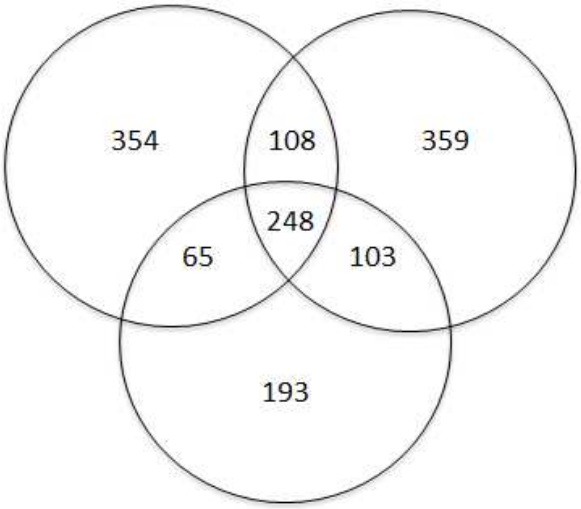

(B)

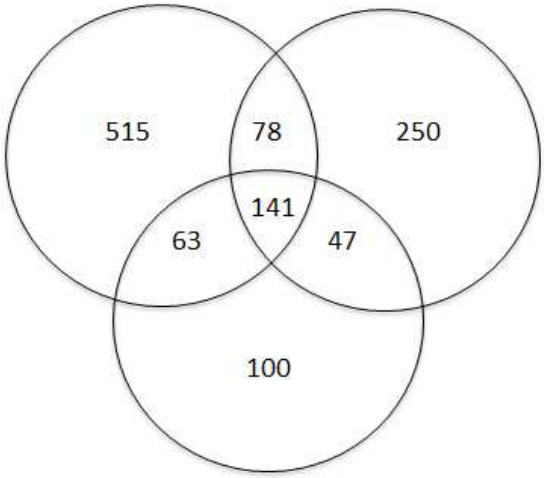

Figure S22**:** Venn diagrams of numbers of protein identifications identified in and shared between three biological replicates of (A) early MFC anodes and (B) intermediate MFC anodes.

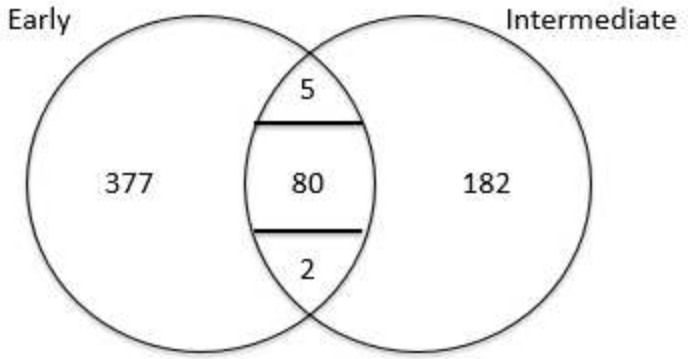

Figure S23**:** Venn diagram of proteins identified in early and intermediate anode development stages. Proteins in the overlapping area were identified in both conditions in at least one technical replicate of at least two biological replicates. The upper section of the overlapping area represents DEPs significantly more abundant in the intermediate condition, while the lower section represents DEPs significantly more abundant in the early condition.

SI 5.4 Supplemental Information References

Al-Shahrour F, Diaz-Uriarte R, Dopazo J. (2010) FATIGO: a web tool for finding significant associations of Gene Ontology terms with groups of genes. Bioinformatics 2010;20:578-580.

Benjamini Y and Hochberg Y. Controlling the false discovery rate: a powerful and practical powerful approach to multiple testing. J Royal Stat. Soc, Series B. 1995;57:289-300.

Buttigieg PL and Ramette A. A guide to statistical analysis in microbial ecology: a community-focused, living review of multivariate data analyses. FEMS Microb. Ecol. 2014;90: 534-550.

Clarke, KR. Non-parametric multivariate analyses of changes in community structure. Austral. Ecol. 1993;18:117-143.

Kuczynski J, Liu Z, Lozupone C, McDonald D, Fierer N, Knight R. Microbial community resemblance methods differ in their ability to detect biologically relevant patterns. Nat. Methods 2010;7:813-819.

Liu H and Logan BE. Electricity generation using an air-cathode single chamber microbial fuel cell in the presence and absence of a proton exchange membrane. Environ. Sci. Tech. 2004;38:4040-4046.

Pascovici D, Handler DCL, Wu JX, Haynes PA. Multiple testing corrections in quantitative proteomics: a useful but blunt tool. Proteomics 2016;16:2448-2453

Qu Y, Feng Y, Wang X, Logan BE. Use of a coculture to enable current production by *Geobacter sulfurreducens*. Appl. Env. Microbiol. 2012;78:3484-3487

Rittman BE and McCarty PL. Environmental Biotechnology: Principles and Applications. New York, NY: McGraw-Hill. 2001

Storey JD. A direct approach to false discovery rates. Stat. Methodol. Ser. B. 2002;64:479-498.

Zhang Y, Wen Z, Washburn MP, Florens L. Refinements to label free proteome quantitation: how to deal with peptides shared by multiple proteins. Anal. Chem. 2010;82:2272-2281.